CHARACTERIZATION FOR EFFECTIVE MANAGEMENT AND UTILIZATION OF RED MUD

Shamshad Alam

Department of Civil Engineering
National Institute of Technology Rourkela

CHARACTERIZATION FOR EFFECTIVE MANAGEMENT AND UTILIZATION OF RED MUD

Dissertation submitted to the

National Institute of Technology Rourkela

in partial fulfillment of the requirements

of the degree of

Doctor of Philosophy

in

Civil Engineering

by

Shamshad Alam

Roll Number: 514CE6024

based on the research carried

out under the supervision of

Prof. Sarat Kumar Das

December 2018

Department of Civil Engineering

National Institute of Technology Rourkela

December 2018

Certificate of Examination

Roll Number: 514CE6024

Name: Shamshad Alam

Title of Dissertation: <u>Characterization for Effective Management and Utilization of Red Mud</u>

We the below signed, after checking the dissertation mentioned above and the official record book (s) of the student, hereby state our approval of the dissertation submitted in partial fulfillment of the requirement of the degree of Doctor of Philosophy in Civil Engineering at National Institute of Technology, Rourkela. We are satisfied with the volume, quality, correctness, and originality of the work.

- - - - - - - - - - - - - - - -
Prof. Sarat Kumar Das

Supervisor

- - - - - - - - - - - - - - - - Prof. Suresh Prasad Singh Member (DSC)	- - - - - - - - - - - - - - - - Prof. Saroj Kumar Patel Member (DSC)
- - - - - - - - - - - - - - - - Prof. Archana Mallik Member (DSC)	- - - - - - - - - - - - - - - - Prof. Sreedeep S. (IIT Guwahati) External Examiner
- - - - - - - - - - - - - - - - Prof. Nagendra Roy Chairman (DSC)	- - - - - - - - - - - - - - - - Prof. Mahabir Panda Head of the Department

Department of Civil Engineering
National Institute of Technology Rourkela

Prof. Sarat Kumar Das   December 2018

Supervisor's Certificate

This is to certify that the work presented in this dissertation entitled *"Characterization for Effective Management and Utilization of Red Mud"* by *"Shamshad Alam"*, Roll Number: 514CE6024, is a record of original research carried out by him under my supervision and guidance in partial fulfillment of the requirements of the degree of *Doctor of Philosophy* in *Civil Engineering*. Neither this dissertation nor any part of it has been submitted for any degree or diploma to any institute or university in India or abroad.

- - - - - - - - - - - - - - - -
Prof. Sarat Kumar Das

Supervisor

Dedicated
To
My Parents and Brother

Declaration of Originality

I, Shamshad Alam, Roll Number: 514CE6024 hereby declare that this dissertation entitled *"Characterization for Effective Management and Utilization of Red Mud"* represents my original work carried out as a doctoral student of NIT Rourkela and, to the best of my knowledge, it contains no material previously published or written by another person, nor any material presented for the award of any degree or diploma of NIT Rourkela or any other institution. Any contribution made to this research by others, with whom I have worked at NIT Rourkela or elsewhere, is explicitly acknowledged in the dissertation. Works of other authors cited in this dissertation have been duly acknowledged under the section "Bibliography". I have also submitted my original research records to the scrutiny committee for evaluation of my dissertation.

I am fully aware that in case of my non-compliance detected in the future, the Senate of NIT Rourkela may withdraw the degree awarded to me on the basis of the present dissertation.

December 2018

NIT Rourkela

Shamshad Alam

Acknowledgement

First of all, I would like to express my heartfelt gratitude to my supervisor Prof. Sarat Kumar Das for his motivation in the successful completion of my research. Prof. Das has always been affable and supportive in every situation during the journey of my Ph.D. He devoted a lot of his time for my research, giving valuable ideas and took great pains to see me through. He dedicated a lot of time and patience to the reading and correction of this thesis.

I am grateful to Prof. N. Roy (DSC chairman) and DSC members Prof. Suresh Prasad Singh, Prof. Saroj Kumar Patel, and Prof. Archana Mallik for sparing their valuable time for examining my research work and providing valuable suggestions. I am thankful to DRC chairman Prof. M. Panda (HOD) and DRC members Prof. K. C. Patra, Prof. S. K. Sahu, Prof. K. C. Biswal, Prof. K. K. Khatua, Prof. K. K. Paul, Prof. Robin Davis P, and Prof. R. N. Behera for being present during the presentations of my research work and providing me with their valuable comments and suggestions.

I am thankful to my Ph. D senior Dr. Lasyamayee Garanayak and Miss. Mahashakti Mahamaya for their technical support throughout my work. I thank Mr. Anshumali Mishra, Mr. Vinay Kumar, Miss Akhila, and Mr. Jonnagiri Chandrasekhar for all their support and encouragement. I would like to thank Mr. A. K. Nanda, Mr. Parmanand Pandit, and Mr. Subrat Pradhan for their technical assistance during my work. I sincerely appreciate the lab staffs Mr. Mohanti and Mr. Harmohan Garnayak for their helping hand during the laboratory work. I would like to thank my research colleagues for being patient with me during all circumstances in the pursuit of my Ph.D.

Last but not least, I am deeply indebted to my parents for their unconditional love, sacrificial giving and support to me. It was impossible to come to this stage without their teachings and blessings. I would like to offer my sincere thanks to my brother Prof. Naushad Alam for all the aid and moral support during my research work. I offer my heartfelt gratitude to the Almighty for giving me the right encouragement at right time, blessing me with all the good prosperities and the surrounding of right people who helped me move towards the goal of life.

December 2018   Shamshad Alam

NIT Rourkela   Roll Number: 514CE6024

Abstract

The bauxite residue or red mud (RM) is generated during the production of alumina. Every year, approximately 120 million tons of RM is generated worldwide. Due to high alkalinity, red mud is a threat to the environment in terms of land and water pollution. Though various attempts has been made to utilize other industrial waste like fly ash and steel slag but the characterization of red mud is very limited and scattered.

The present study aims at the characterization of two Indian red mud from a different type of disposal system as a geotechnical construction material. A detailed study on different physical, chemical, morphological, and geotechnical characterizations of the basic and modified/stabilized red mud were made to correlate the findings. The red mud was found to be dispersive, which could be controlled through stabilization using biopolymer and NaCl. The sedimentation properties improved with the addition of NaCl and phosphogypsum and its impact on red mud pond management is discussed. The stabilization of red mud using other industrial waste like ground granulated blast furnace slag was found to be effective in terms of increase in unconfined compressive strength. But, the durability in terms of alternate wet-dry cycle was found to be depend upon the chemical reaction of the red mud with the stabilizer. The leachate analysis of the stabilized red mud showed an increase in heavy metal, due to high alkaline condition, but the value was within permissible limit. Based on the comparison with Indian standard sand, the coarse fraction ($> 75\mu m$) of red mud can be alternate of fine aggregate replacing natural sand. The findings of the present study can help in proper management and utilization of red mud, thereby helping in the sustainable development of the aluminum industries. However, its compatibility with cement in mortar and concrete need further investigation. The future challenges are in the implementation of the developed methodology as a pilot project to transfer the technology.

Key Words: Red mud, sedimentation, dispersiveness, coarse fraction, stabilization, compressive strength, durability

Contents

List of Figures

List of Tables

List of Abbreviations

AAS	Atomic absorption spectroscopy
AT	Ambient temperature
CBR	California bearing ratio
Cc	Compression indices
c_c	Coefficient of curvature
c_u	Coefficient of uniformity
c_v	Coefficient of consolidation
DFS	Differential free swell
e	Void ratio
EC	Electrical conductivity
EDX	Energy-dispersive X-ray
EGME	Ethylene glycol monoethyl ether
e_{max}	Maximum void ratio
e_{min}	Minimum void ratio
EPA	Environmental protection agency
E_R	Elongation ratio
FTIR	Fourier-transform infrared spectroscopy
F_R	Flakiness ratio
F-TRM	$FeCl_3.6H_2O$ treated red mud
GG	Guar gum
GGBS	Ground granulated blast furnace slag
Gs	Specific gravity
HC	Humidity chamber
HRM	HINDALCO red mud
HRS	HINDALCO red sand
H-TRS	HCl treated red sand
I_c	Collapse potential
ISI	Impact strength index
k	Coefficient of Permeability
LL	Liquid limit

LR	Lime reactivity
L/S	Liquid to Solid Ratio
MDD	Maximum dry density
NRM	NALCO red mud
NRS	NALCO red sand
N-TRM	NaCl treated red mud
OMC	Optimum moisture content
OPC	Ordinary Portland cement
PI	Plasticity index
P-TRM	Phosphogypsum treated red mud
PVC	Polyvinyl chloride
RCC	Reinforced concrete cement
R_i	Roundness index
RM	Red mud
RS	Red sand
R_T	Thermal resistivity
SEM	Scanning electron microscope
SD	Standard deviation
SDI	Slake durability index
S_F	Shape factor
SS	Indian standard sand
SWCC	Soil-water characteristics curve
TCLP	Toxic characteristic leaching procedure
TDS	Total dissolved solids
TRM	Treated red mud
UCS	Unconfined compressive strength
UTRM	Untreated red mud
W-D	Wetting and drying
w/c	Water-cement rato
WHO	World Health organization
XG	Xanthan gum
XRD	X-ray diffraction
XRF	X-ray fluorescence

ϕ	Angle of internal frictional
σ_p	Pre-consolidation Pressure
ζ	Zeta potential
ψ	Sphericity

Chapter 1

Introduction

1.1 Overview

Aluminium is the third most abundant element on the earth behind oxygen and silicon with total sharing of 8.1%. The growing demand for aluminium in different products and industries urges to increase the production. Transportation, packaging products, pharmaceuticals, electronics, and construction are the common industries and products where aluminium is mostly used. In the aluminium production plant, mostly the bauxite is used as the raw material throughout the world. The alumina extraction from bauxite ore may involve either sintered process (Figure 1.1) or leaching process (Figure 1.2).
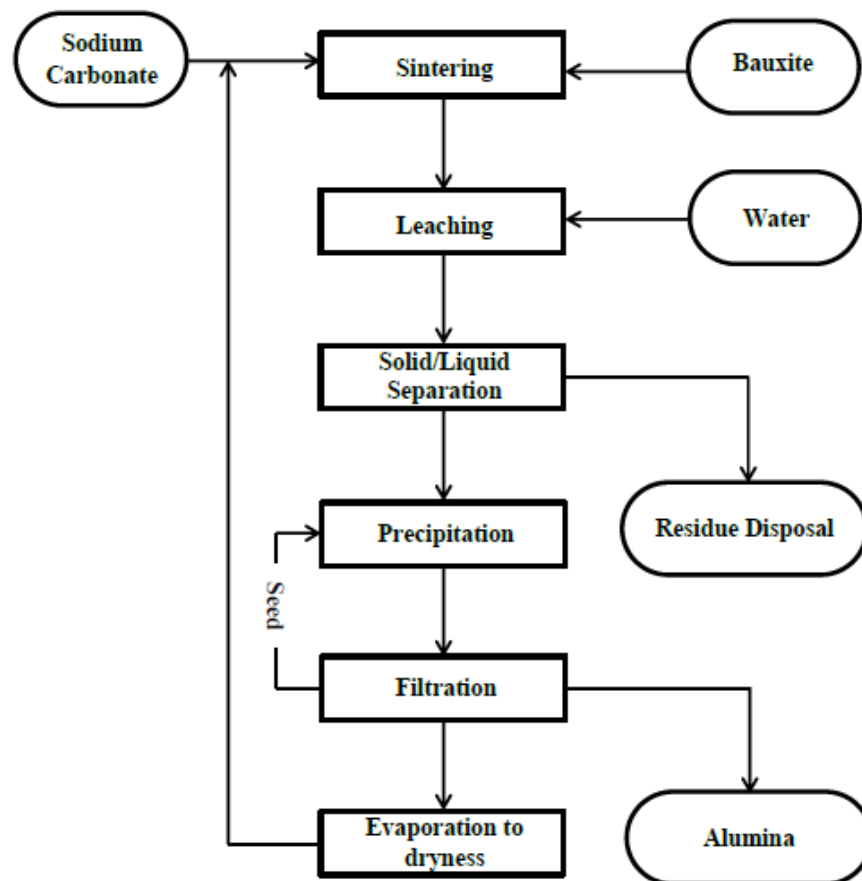
Figure 1.1. Sintered process (Bayer, 1888) (modified from Klauber et al., 2011)
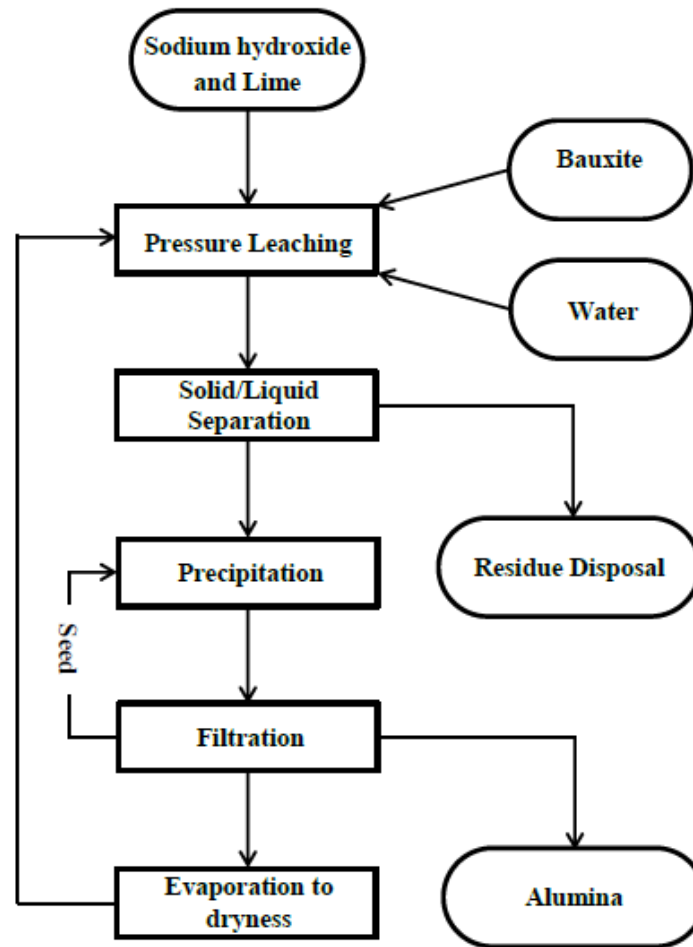
Figure 1.2. Leaching process (Bayer, 1892) (modified from Klauber et al., 2011)

The sintering process is highly effective in breaking down the bauxite ores which contains diasporite (α-AlO(OH)) as the main alumina mineral and rendering them into a soluble form as sodium aluminate but is energy and capital intensive (Klauber et al., 2009). However, nowadays the sintering process is having limited application due to the requirement of high-temperature sintering of the bauxite. The leaching process, commonly known as Bayer's process, is used by around 95% alumina industries and is limited to gibbsitic and boehmitic bauxites (Klauber et al., 2009). In the Bayer's process, the sodium hydroxide (NaOH) is mixed with the bauxite ore and heated at 110°C to 300°C (based on the mineralogy of bauxite) in a pressure chamber until the alumina is dissolved. The overflow (aluminate liquor) is pumped for controlled filtration and underflow containing waste is washed and disposed into the pond.

The waste generated during the process (sintered or leaching process) is called as red mud owing to red colour because of a high percentage of iron oxide. The quantity of red mud generation mostly depends on the oxide/hydroxide of aluminium like gibbsite, boehmite

or diaspore present in the bauxite and the method of extraction. The current methods of managing the red mud are (1) storing the slurry red mud in pond with 15%-40% solid content by volume (Yang and Xiao, 2008), (2) storing the red mud in dry form with more than 65% solid content (Power et al. 2009), or (3) discharging the red mud into the sea (Power et al., 2011). As the disposal into the sea endangers the aquatic life, it is being discouraged. Also, the storage of highly alkaline (pH>11) red mud may cause severe environmental problems due to the presence of several toxic heavy metals (Pb, Cr, Hg, As etc.). In India, slurry disposal system (used by NALCO, Damanjodi) (Figure 1.3) or dry disposal system (HINDALCO, Muri) (Figure 1.4) is commonly used.

Figure 1.3. Slurry disposal system of NALCO, Damanjodi (photo by S. Alam)

Figure 1.4. Dry disposal system of HINDALCO, Muri (photo by S. Alam)

1.2   Research Background

Depending on the quality of bauxite ore and method of extraction (sintered or leaching process) used, around 0.8 – 1.5 tons of red mud (RM) is generated during the production of every ton of aluminium (Nath et al., 2015). Every year, around 120 million tons of red

mud is produced globally (Mayes et al. 2011, Nath et al., 2015; Xue et al., 2015). Table 1.1 represents the red mud generated by major Indian aluminium industries based on the result of Samal et al. (2013). The red mud generation has increased rapidly due to the rapid growth in alumina production as shown in Figure 1.5.

Table 1.1 Red mud generated by major Indian industries (source: Samal et al., 2013)

Aluminium refinery	Red mud generation rate (million tonnes/annum)
NALCO	2.697
HINDALCO	2.062
VEDANTA	1.820
UTKAL	1.950
ADITYA	1.820
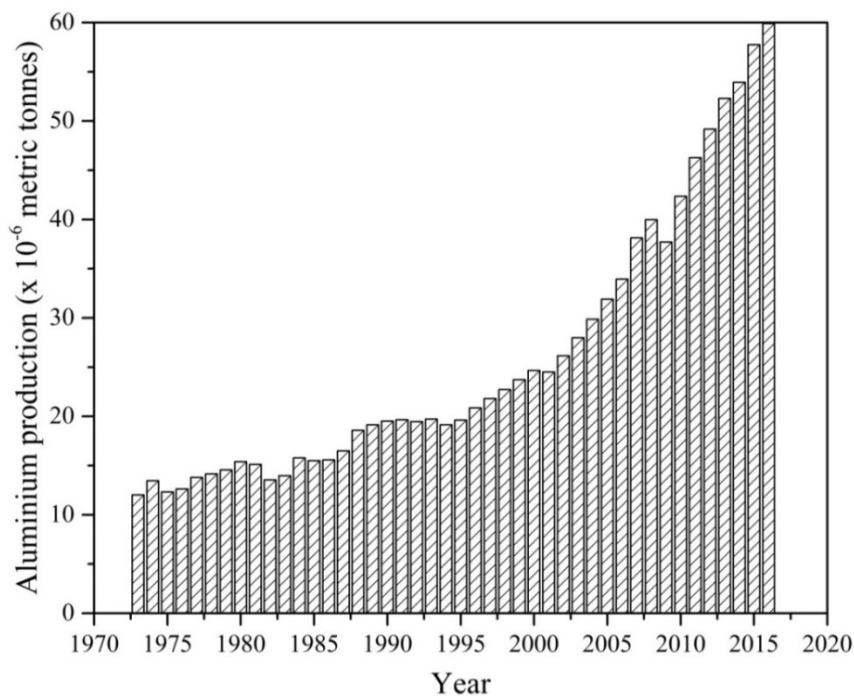
Figure 1.5. Yearly alumina production (Source: http://www.world-aluminium.org)

The high alkalinity (pH >11) of red mud is the most significant barrier to its utilization. Still, various researchers have made studies on low value, medium value and high value utilization of red mud.

The low value utilization of red mud includes its utilization in road construction (Kehagia, 2008), embankment construction (Rout et al., 2012), as filling material (Liu and Wu, 2012), tailing dam construction (Rout et al., 2013). The utilization of red mud for preparation of clay liner (Kalkan, 2006; Yang et al., 2012; Rubinos et al., 2013),

development of bricks (Dass and Malhotra, 1990; Yang and Xiao, 2008; Liu et al., 2009), development of paving blocks (Kumar and Kumar, 2013), partial replacement of cement in concrete (Tsakiridis et al., 2004; Ribeiro et al., 2011; Sawant et al., 2013), preparation of iron rich cement (Singh et al., 1997), and synthesis of inorganic polymeric materials (Dimas et al., 2009; He et al., 2013) comes under the medium value utilization. The utilization volume in high value utilization is very low and includes the making of X-ray radiation-shielding materials (Amritphale et al., 2007), ceramic tiles (Khan et al., 2012), glass ceramic (Yalcin and Sevinc, 2000) along with utilization for removal of toxic metals from aqueous solution (i.e. As, Cr, Pb, Cd) (Pradhan et al., 1998, 1999; Sahu et al., 2001, 2011; Gupta et al., 2001; Kalkan et al., 2013; Cengeloglu et al., 2002, 2006, 2007), wastewater treatment (Lopez et al., 1998; Wang and Tade, 2008; Bhatnagar et al., 2011), catalytic applications (Sushil and Batra, 2008), and extraction of iron (Liu et al., 2009). But in all the above studies, either several aspects were not studied or the utilization rate was very low. Due to the low utilization rate, most of the unutilized red mud remains stored into the pond (Figure 1.3) or at the dump site (Figure 1.4). This stored red mud creates several environmental problems due to the generation of highly alkaline leachate which favours the leaching of heavy toxic metals (Quina et al., 2009). Occasional failure of red mud pond dike as observed in Ajka (Hungary) leaves an adverse impact on greater vicinity due to spreading of red mud particles over a large area (Mayes et al., 2011).

Figure 1.6. Red mud pond dike failure in Ajka, Hungary

(https://aboutenvironment.files.wordpress.com/2010/10/red-mud-pond-hungary.jpg)

1.3   Challenges in Utilizing the Red Mud

The basic challenges associated with the utilization of red mud are the variability in the basic characteristic of red mud as reported by several researchers. The variability in the characteristics is due to the type of bauxite used, the method adopted for the extraction of aluminium, and the method of disposal. Wang and Liu (2012) reported that the Bayer's process red mud is finer and more dispersive compare to sintered process red mud. Somogyi and Gray (1977) and Fahey et al. (2002) presented the permeability of Bayer's process red mud in between $(2\text{-}20) \times 10^{-7}$ cm/s, whereas, Liu and Wu (2012) reported the permeability of sintered process red mud in between $10^{-4}\text{-} 10^{-5}$ cm/s. Miners (1973) reported that majority of the particle in the red mud is in silt range along with 20-30% clay-sized particle, whereas, Li (1998) reported around 50% clay-sized particles. Vick (1990) found that specific gravity (Gs) of red mud lies between 2.8 to 3.3. Fahey et al. (2002) observed the compression indices of red mud vary from 0.27 to 0.39, while the coefficient of consolidation was found to lie in between $(3\text{-}50) \times 10^{-3}$ cm^2/s. Newson et al. (2006) reported the angle of internal friction (φ) of 38° - 42° for Bayer's red mud, whereas, for sintered process red mud, low angle of internal friction ($13.5^o - 21^o$) was reported by Liu and Wu (2012). The plasticity of the red mud varies with LL 25 - 92.5% and PI 2.5 – 60%.

The temperature and the pore fluid is another parameter which alters the property of red mud. Somogyi (1978) and Newson et al. (2006) discussed the effect of temperature exposure and pore fluid on the behaviour of red mud. Their observation shows that the samples preparation method and the pH of the fluid used can greatly affect the behaviour of red mud. Also on the disposal site, the exposer to different weather, the percolation of water into the sediment, and the different physical and chemical reaction may change the property of red mud. Pinnock (1992) and Newson et al. (2006) reported that the exposer to an alternate water and drying leads to cementation in the red mud which is again one of the challenges in utilizing the red mud. This tendency is also observed on the disposal site of NALCO during sample collection (Figure 1.7) but at the HINDALCO disposal site, it was not observed. The hardened layers may be due to the air drying during the short period of time which is followed by subsequent coverage of new layers of red mud slurry (Figure 1.7).
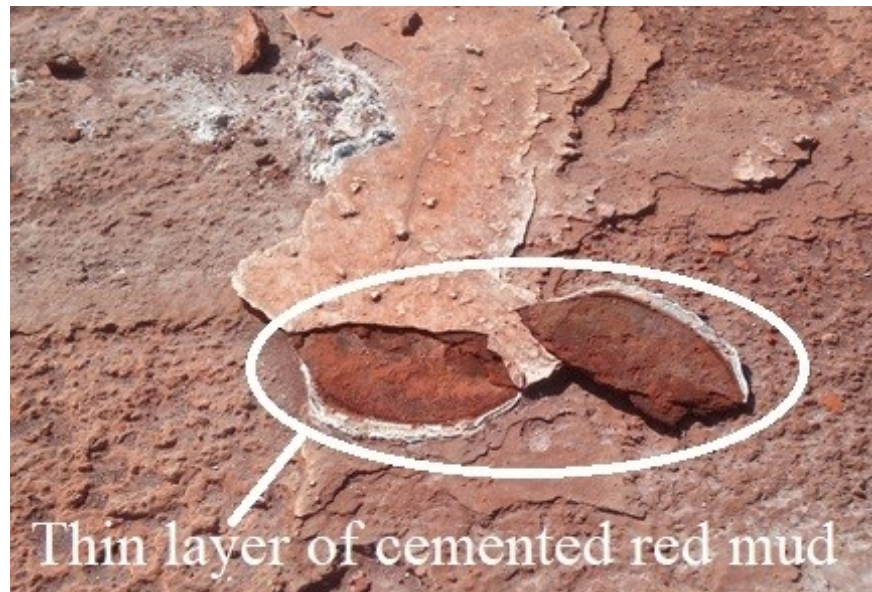
Figure 1.7. Typical photo showing the thin cemented layer (photo by S. Alam)

1.4 Research Gap

Based on the literature survey following observation was made:

1.   Several studied are available regarding the high value (making of ceramic tiles, glass ceramic production, iron extraction etc.) and medium value (making of paving blocks, partial replacement of cement in concrete etc.) utilization of red mud but in all these cases, the utilization rate is very low.

2.   A few studies on characterization of red mud are available but the study on the Indian red mud for bulk utilization is limited and available only after stabilizing by bioremediation. But the study on strength and durability of stabilized red mud is not available. Also, the study on the utilization of coarse fraction of red mud is not available.

3.   As in most of the cases, the red mud is disposed in slurry form and sedimentation characteristic become important, but research on sedimentation characteristic of red mud is limited.

1.5 Aim and Objectives of the Research

The aim of the present study is to develop a better management system for the red mud by considering its low value utilization. The objectives are to study the basic characteristic of red mud along with the dispersiveness, sedimentation, and the strength characteristic of GGBS stabilized red mud.

The research objectives includes the following aspect:

- Complete physical, chemical, mineralogical and geotechnical characterization of red mud in the Indian context.

- Study on the dispersiveness characteristic of both NALCO and HINDALCO red mud and sedimentation characteristics of NALCO red mud using phosphogypsum, sodium salt (NaCl), and biopolymer (guar gum and xanthan gum)

- Characterization of coarse fraction (> 75μm) of red mud as a civil engineering construction material

- Strength and durability characteristic of red mud stabilized with GGBS without and with alkali activation.

1.6   Scope of the Research

The scope of the present study include the chemical, morphological, mineralogical, physical, and geotechnical properties of red mud in general collected from a different source and its comparison with other industrial waste or standard geo-materials. The dispersive nature of the red mud is controlled by using biopolymer and salt solution (NaCl), while the effect of salt solution (NaCl) and phosphogypsum (fertilizer industry waste) on sedimentation behaviour are studied. The coarser fraction (>75μm) of red mud is studied separately and the result is compared with the result of Indian standard sand. The stabilization of red mud using different other industrial waste (ground granulated blast furnace slag) to improve its strength and durability characteristics.

1.7   Thesis Outline

The Chapter 1 discusses the generation of red mud, variability in the geotechnical characteristics, challenges in utilizing the red mud along with the motivation, scope and research approach. The previously published work on the characterization of red mud for its utilization is discussed in Chapter 2. The research gaps found in the previous studies are also discussed in Chapter 2 as a critical review. The basic material characterizations by considering the physical, chemical, mineralogical, morphological, and geotechnical characteristics are discussed in Chapter 3. Chapter 4 discusses the dispersiveness and sedimentation characteristic of red mud and its remediation using the phosphogypsum,

sodium salt (NaCl), and biopolymer. The morphological and chemical changes in red mud due to the treatment are also discussed using SEM, Zeta potential, and concentration of heavy metal in supernatant liquid. The possible utilization of coarser fraction ($75\mu m$) of red mud as civil engineering construction materials are discussed by considering the morphology, mineralogy, chemistry, and thermal resistivity and are presented in Chapter 5. The effect of stabilization of red mud using GGBS in term of unconfined compressive strength, durability characteristic and morphology is discussed in Chapter 6. Chapter 6 also discusses the effect of alkali (Na_2SiO_4) activation on the strength, durability, mineralogy, and morphology of stabilized red mud. In the same chapter, the leachate analysis of the stabilized red mud is discussed for environmental friendly utilization as a structural fill and embankment material. In Chapter 7, the summarized observations and conclusions of the present work are presented. Outline of the thesis is shown in Figure 1.8.

Chapter 1- Introduction

Chapter 2- Literature Review

Chapter 3- Basic Material Characterization

Chapter 4- Dispersive and Sedimentation Characteristic

Chapter 5- Characterization of Coarse Fraction of Red Mud

Chapter 6- Strength Characteristic of Stabilized Red Mud

Chapter 7- Conclusions
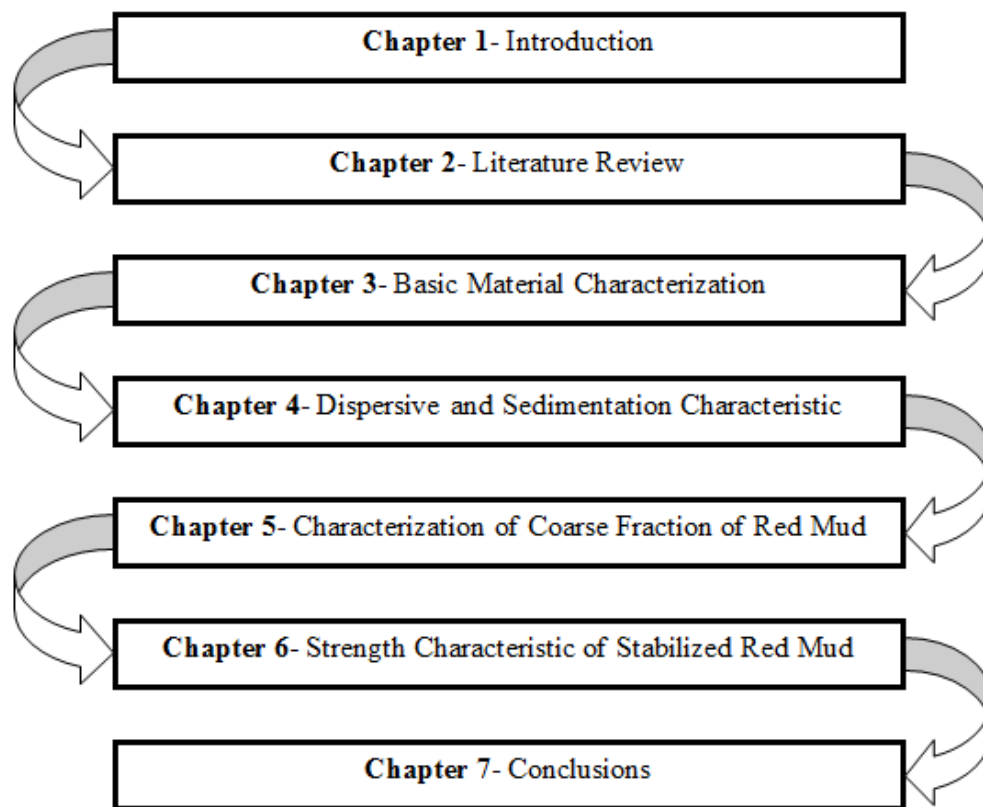
Figure 1.8. Outline of the thesis

Chapter 2

Literature Review

2.1 Introduction

The red mud is disposed off in the slurry form with solid content between 15%-40% by volume in the pond for storage or stored in dry form with solid content >65%. Storage of red mud in either form takes a vast tract of usable land and creates geo-environmental problems like soil contamination, ground and surface water pollution due to high alkalinity and the presence of trace metal. So, to avoid the threat due to storage, it is required to utilize this waste in bulk as an alternate value-added material. There is a large scope of utilizing the red mud in the field of geotechnology. However, deep understanding of its chemical, mineralogical, morphological, physical, and geotechnical properties are needed.

Various efforts have been made regarding the generation and utilization of red mud in different branches of science and engineering. The literature presenting the basic properties and its utilization in different industries and infrastructure development are discussed in the present thesis. As high alkalinity of the red mud is an important issue for bulk utilization of red mud, efforts made in this direction are also discussed.

2.2 Chemistry of Red Mud

The chemical composition of the red mud depends upon several factors like the composition of the raw material, the extraction process, and the additives used during the extraction process. However, irrespective of the source and additives, Fe_2O_3 (12-60%) has been found as major constituent of Bayer process red mud by several researchers (Pratt et al., 1981; Vachon et al., 1994; Kumar et al., 1998; Sglavo et al., 2000; Gupta et al., 2004; Bertocchi et al., 2006; Tsamo et al., 2014). The red mud from NALCO, Koraput, Odisha was also found rich in Fe_2O_3 (51-57%) by Meher (2014), which is also a Bayer's processed red mud. On the other hand, CaO (22-46%) has been found as a major constituent in sintered process red mud (Zhihua et al., 2003; Zhang et al., 2009; Yue et al., 2010; Wang and Liu, 2012). It is observed that the CaO and SiO_2 content in sintered

process red mud are higher than that of Bayer's process red mud (Liu and Wu, 2012). It is also observed that the red mud rich in Fe_2O_3 contain a lower percentage of CaO and vice versa. The Al_2O_3 (7.74-51.07%) has been found as a second major constituent in both (Bayer process and sintered process) red mud (Apak et al., 1998; Cengeloglu et al., 2002; Paramguru et al., 2005). The Bayer process red mud found to have a higher concentration of Na_2O (0.2-23.98%) as compared to sintered process red mud (Kehagia, 2008; Samal et al., 2013). Due to the higher concentration of Na_2O, in general red mud is highly alkaline with pH value ranging from 9.00 to 13.94 (Lopez et al., 1998; Pradhan et al., 1998; Koulikourdis et al., 2005; Gherardi and Rengel, 2001; Sahu et al., 2001; Park et al., 2002; Lombi et al., 2003; Fois et al., 2007; Grafe et al., 2011). The pH of the red mud depends upon the source of origin and the process. The red mud from Birac Alumina Industry, Serbia has a pH value of 12.2 (Cablik, 2007) whereas the pH value of red mud from Konya (Turkey) varies from 12 to 13 (Kalkan et al., 2006; Cengeloglu et al., 2007; Nadaroglu et al., 2010). However, Gok et al. (2007) reported the pH value of red mud from the same source as 10.34. The pH value of red mud from China and USA was reported as 11.00 (Zhang et al., 2008; Zhao et al., 2009; He et al., 2013). Mayes et al. (2011) reported very high pH value (13.10) of red mud from Ajka, Hungary. Yadav et al. (2010) presented very low pH value (7.00-8.00) of Indian red mud from HINDALCO (Renukoot). However, Dubey and Dubey (2011) reported the pH value of 10.5 to 13.00 from the same source. Similarly, the pH value of red mud from NALCO (Damanjodi, Odisha) was found to vary as 11.40 (Rout et al., 2012) and 12-13 (Satayanarayana et al., 2012). The large variations in the pH value of red mud from the same source may be due to the different collection location in the storage pond.

2.3 Mineralogy and Morphology of Red Mud

The alkalinity is highly dependent on the quality and quantity of the chemical/mineral phase present in the red mud (Grafe et al., 2011). Generally, the red mud produced from the raw material with similar chemical composition may have different mineralogical composition depending upon the process of extraction of aluminium (i.e. Bayer or sintering process) and the age of disposal of red mud. Castaldi et al. (2011) studied the mineralogy of the red mud collected from Eurallumina, Italy and found hematite, sodalite, and boehmite as major chemical phase along with cancrinite, anatase, andradite, gibbsite, and quartz. Manfroi et al. (2014) also found chantalite, gibbsite, hematite,

quartz, and calcite in the red mud collected from the state of Minas, Gerais. Similar phase has been observed by Lopez et al. (1998) along with magnetite, and ilmenite in the red mud collected from Alumina-Aluminio of San Ciprian, Spain. Chemical phase like perovskite has also been observed by Dodoo-Arhin et al. (2013), Pontikes et al. (2007), and Zhang et al. (2009) in the red mud collected from the western region of Ghana, Aluminium of Greece and Shandong alumina refinery respectively. Silicates of sodium and calcium along with calcium alumina silicate have been observed in red mud by Yalcin and Sevinc (2000), and Atasoy (2005). Clay mineral like kaolinite has also been observed in the Brazilian red mud (Antunes et al., 2012; Hildebrando et al., 2013). The similar mineralogical composition is found in the Indian red mud collected from Hindalco, Renukoot (Gupta et al., 2001; Yadav et al., 2010) and Nalco, Damanjodi (Sahu et al., 2011; Rout et al. 2013). Several other researchers (Pera et al., 1997; Tsakiridis et al., 2004; Srikanth et al., 2005; Paradis et al., 2007; Ribeiro et al., 2010; Smiljanic et al., 2010; Hai et al., 2014) has also observed the similar mineralogical phase in the red mud from different sources.

The morphology of the red mud was also studied by several researchers and most of the researchers found the poorly crystallized porous and irregular shaped particles in the red mud (Liu et al., 2007; Agatzini-Leonardous et al., 2008; Wang et al., 2008). However, few researchers also reported the spherical and smooth particles in red mud (Gok et al., 2007; Huang et al., 2008). Meher (2014) also found the poorly crystallized hexagonal plate-like particles in Indian red mud collected from Nalco, Damanjodi. But most of the researchers reported the spherical, rounded, cubic, and angular to subangular particles in the Indian red mud (Rai et al., 2013; Rout et al., 2013).

2.4 Neutralization of Red Mud

The high pH value of red mud as found in the previous section may favour the leaching of several toxic heavy metals present in the red mud. Quina et al. (2009) found in their study that the leaching of toxic metals like Zn, Pb, and Cr increases at the acidic and alkaline pH but the leaching of Cd, Ni, and Cu was found to decrease with increase in pH. Komonweeraket et al. (2015) also found the similar result for Al, and Fe while leaching of Mn was found to decrease with increase in pH. The leaching of soluble salt like K, Ca, and Na was found to be independent of pH (Quina et al., 2009). Above studies show that the leaching of most of the heavy toxic metal increases on both acidic and alkaline side.

So, it is required to neutralize the red mud to control the leaching and possible reuse. The following sections deal with the literature regarding the different technique of red mud neutralization.

2.4.1 Sea water neutralization

The neutralization of red mud using sea water was found effective in reducing the pH up to 8.6 (Menzies et al., 2004). The reduction in pH value was due to the precipitation of hydroxide of Mg, Ca, and Al. Hanahan et al. (2004) also found a similar effect of seawater on pH but an increase in settling rate was also reported.

Palmer and Frost (2009) studied the mineralogical changes in red mud due to neutralization by sea water. Slightly reduction in the intensity of hematite peak was observed while a significant change in the peak of gibbsite was observed. The peak of new mineral like hydrotalcite was found after treatment.

2.4.2 Neutralization using gypsum

Several types of research have been reported by researchers to neutralize the red mud using the gypsum. Barrow (1982) found the gypsum was effective in improving the chemical properties of red mud in term of plant growth by reducing the alkalinity. In the recent years, many other researchers (Wong and Ho, 1991; Courtney and Timpson, 2004; Xenidis et al., 2005) also found a similar effect of gypsum on chemical property of red mud. Wong and Ho (1991) found that the gypsum is also effective in replacing the Ca^+ and Na^+, which leads to the flocculation and increases the permeability. Glenister and Thornber (1985) reported an optimum value of gypsum utilization as 50 to 60 g per kilogram of wet red mud as an effective dose of neutralization. Wong and Ho (1993) studied the effectiveness of 2, 5, and 8% (w/w) gypsum as a neutralizing agent of red mud. The gypsum was found effective in reducing the pH and electrical conductivity of red mud. The Na and Al were also found to reduce in red mud while a continuous supply of Ca^{+2} was observed which causes lowering the exchangeable sodium percentage. Woodard et al. (2008) perform a similar study using 7.5% gypsum and found that the pH value of treated red mud dropped below 9.5 while the electrical conductivity was observed to decrease below 10 dS/m. Chauhan and Silori (2011) studied the Indian red mud from Hindalco, Karnataka and found 15% gypsum along with farmyard manure, vegetative dry dust, and bacteria was effective in reducing the pH up to 7.00 and electrical conductivity up to 2.20 dS/m. Other researchers (Courtney et al., 2005; Ippolito

et al., 2005; Xenidis et al., 2005) also reported the similar effect of gypsum on the electrical conductivity and soluble calcium. However, Ho et al. (1989) studied the quality of leachate generated from gypsum neutralized red mud collected from Western Australia alumina refinery. Sodium sulfate was found to release as a major salt. The retention of superphosphate was found over 99% while the Al, Fe, and Cd were found negligible in leachate.

2.4.3 Neutralization using CO_2

Shi et al. (2000) made an attempt to neutralize the red mud slurry by mixing it with liquid CO_2 and found that the pH can be reduced in between 9.0 – 9.5 from 12.5 within 5-15 minute. Sahu et al. (2010) performed a similar study on NALCO red mud collected from Koraput, Odisha and found that the pH of the red mud can be lower down to 8.45 from 11.80 by sequestration of CO_2 thereby reducing the alkalinity from 10789 mg/L to 178 mg/L. Johnston et al. (2010) found that the CO_2 sequestration was effective also in increasing the grain size of the red mud along with reducing the alkalinity.

Further, Rai et al. (2017) reviewed different neutralization techniques of red mud. The study shows that the neutralization of 10g red mud required 100 ml of 0.1M concentrated inorganic acid like HCl and HNO_3, while the quantity of acid can be reduced to half by using H_2SO_4. The calcium was found to dissolve completely along with 35-40% reduction of sodium due to acid treatment, while the iron and titanium remain unchanged. A small quantity (6 ml) of pickling liquor was found effective to neutralize the 100 ml of slurry with 40% solid content and it lowered the pH value to 7.0, while the alkalinity was found to reduce by 80-85%. The pickling liquor was also found to reduce the viscosity of red mud slurry. The sintering of red mud at 1100°C after mixing it with silicate material in the range of 25-50% to 50-75% was found effective in lowering the pH to 8.9. It was also found that the sintering temperature plays an important role in lowering the alkalinity. The sea water was not found effective in eliminating the hydroxide but it was able to convert the strongly alkaline waste into less soluble and weekly alkaline solid.
Patel et al. (2008) carried out a study on neutralization of red mud using mine water to make pollution free environment. Investigation results showed that pH of red mud was decreased to the standard environmental level using mine water and also the red mud was neutralized. The neutralized red mud can be used for other socio-economic and environmental benefits.

2.5 Sedimentation and Dispersiveness of Red Mud

The sedimentation behaviour of soil slurry become important during land reclamation and governed by the gravitational force. Several researchers have studied the sedimentation behaviour of the different type of soil slurry. Based on the theoretical study, Kynch (1952) found that the sedimentation of the particles greatly affected by the nearby particle density. McRoberts and Nixon (1976) made a sedimentation study on the different type of soil like Fort Norman silt, Devon silt, Devon sand, Grit, Bromborough mud and bentonite clay and suggested the maximum water content in the slurry at which hindered sedimentation is not possible. Imai (1980) studied the settling of clay and found that the salt concentration and liquid to solid ratio greatly affect the sedimentation behaviour of clay. Imai (1981) based on the experimental study on clay, found that the sedimentation process generally consists of three stages (flocculation stage, settling stage, and consolidation stage). He et al. (2017) studied the effect of flocculent (polyacrylamide) on the sedimentation characteristic of marine clay. But, the study on bauxite residue (red mud) is limited (Hirosue et al., 1988; Li 2001). However, Hirosue et al. (1988) presented only the effect of concentration of ferric chloride on the pH and Zeta potential of suspension but the rate of sedimentation has not been presented. Although, Li (2001) presented the effect of solid concentration on the settling velocity but the study was made at the elevated temperature of 135, 240, and 250° C. The dispersive characteristic of red mud was found to be limited (Rout et al., 2013; Das et al., 2015) and only based on the crumb test.

2.6 Stabilization of Red Mud

Several studies are conducted on the stabilization of soil without or with alkali activation of industrial waste. Cristelo et al. (2012) studied the effect of alkali (NaOH) activated class C and class F fly ash on the strength of fly ash stabilized soft soil. The soil stabilized with activated class C fly ash was found to show higher strength than class F fly ash. The effect of the type of alkali activator has also been reported by several researchers. Cristelo et al. (2012) stabilized the residual granitic soil by activated fly ash and found that Na_2O is more effective as compared to NaCl. Yi et al. (2015) investigated the unconfined compressive strength and microstructural changes of the marine soft clay stabilized with alkali activated (NaOH, Na_2CO_3) GGBS. Liu et al. (2016) made a

comparative study of the strength of Loess stabilized with KOH and NaOH activated fly ash and reported that KOH is more efficient activator compare to NaOH. Alsafi et al. (2017) observed the similar difference between the KOH and NaOH activated fly ash used to stabilize the gypseous soil. The KOH was also found more effective compare to $Ca(OH)_2$ to activate the volcanic ash for stabilizing the expensive black cotton soil (Miao et al. 2017).

But the study on the stabilization of red mud is found limited. Duchesne and Doye (2005) studied the possibilities of cement kiln dust stabilized red mud as a cover and liner materials for acid mine drainage. Panda et al. (2016) studied the geotechnical characteristics of biopolymer stabilized red mud.

2.7 Application of Red Mud

A number of efforts have been made for effectively utilize the red mud in different industries along with few types of research in geotechnical utilization to reduce the storage. Pera et al. (1977) calcined the red mud in the temperature range of 600 to 800°C to prepare the pozzolanic pigment. The high temperature was found effective in transforming the aluminium hydroxide (goethite and boehmite) and clay minerals into pozzolanic admixtures. The pozzolanic pigment developed from red mud was found to effectively replace 20% ordinary Portland cement (OPC). Now a days, the red mud is being used to manufacture the bricks, tiles, cement etc. and also used as a metal removal agent, and to develop the geopolymer. This section includes the literature review related to the use of red mud for the above purpose and various efforts made in this direction.

2.7.1 Application in construction industry

Various researches are available on the use of red mud as alternate construction materials like bricks, building blocks, cementing materials and as substitute of aggregate in the mortar and concrete.

Dass and Malhotra (1990) studied the development of red mud brick by mixing different percentage of lime (5% and 8%) into Bayer's process red mud. A compressive strength of 3.75 MN/m^2 and 4.22 MN/m^2 was observed after 28 days by stabilizing the red mud by 5% and 8% lime, respectively.

Sglavo et al. (2000) utilized the Bayer's process red mud to make clay-based ceramic and study the effect of red mud content. The addition of red mud was found to cause more

deflocculated soil-water system and an increase in moisture content. It was also observed that below 900°C, red mud can be considered an inert component in mixtures with carbonate-rich clays. Conversely, red mud represents a reactive phase above 950 – 1000°C when mixed with Kaolin. Yalcin and Sevinc (2000) conducted a research to utilize the Bayer's process red mud in ceramic glazes. The chemical strength of glaze in 3% HCl and 3% NaOH was studied.

Zhihua et al. (2003) utilized the sintered process red mud to prepare the red mud-slag base cementitious materials and studied the ultimate strength and resistance towards a chemical attack on the newly developed materials. It was observed that the alkali-activated red mud-slag cement shows a compressive strength of 56 MPa and flexural strength of 8.4 MPa after 28 days which further increases up to 66.5 MPa and 9.9 MPa after 180 days. The alkali-activated red mud-slag cement shows better resistant towards Na_2SO_4, $MgSO_4$, NaCl, simulated seawater, and diluted HCl.

Tsakiridis et al. (2004) studied the effect of red mud addition in raw metal Portland cement clinker production based on the unreacted lime after exposer of 1350, 1400, and 1450°C. The properties like setting time, compressive strength, and expansibility were also presented. The free lime value in the red mud mix was observed to decrease from 2.27% to 1.94% after the exposure to 1450°C temperature. The compressive strength of mortar prepared using Bayer's process red mud was found to increase after 28 days of curing.

Cablik (2007) investigated calcinated Bayer's process red mud as a pigment for use in the building material industry. The test blocks varied in colour depending on the mix and the amount of red mud added. The blocks were tested for compressive strength after having cured for 7, 14 or 28 days at the room temperature (18 to 23°C). Compressive strengths from 14.83 to 27.77 MPa of the blocks that contained red mud from 1 to 32% were observed.

Yang and Xiao (2008) performed a research on the development of bricks using sintered process red mud along with fly ash, sand, lime, gypsum, and cement. Based on the experimental work, an optimum mix proportion (25-40% red mud, 18-28% fly ash, 30-35% sand, 8-10% lime, 1-3% gypsum, and 1% cement) was suggested for red mud brick. The compressive strength of the bricks developed using the optimum mix was found as 19.43 MPa while the flexural strength was found as 5.05 MPa. The bulk density of brick was found as 1620 kg/m^3 and the water absorption capacity was 22.93%.

Zhang et al. (2009) studied the possibilities of utilizing the sintered process red mud along with coal gangue (a solid waste left after process of coal mining) to develop cementitious material. The flexural and compressive strength of cementitious material developed by red mud (RGC) was compared with OPC. The 28 days strength of RGC was found 2 MPa higher than that of OPC. However, a large difference in initial setting time (160 min) and final setting time (225 min) of RGC was observed as compare to OPC.

Desai and Herkal (2010) effectively utilized the Bayer's process red mud in making burnt and unburnt bricks in pressed and unpressed conditions. Red mud bricks with additives like lime, sand, fibers of 6 mm and 12 mm length were prepared and tested. Unpressed bricks with recron fibers give good strength but just pressing the bricks to proctor density, almost doubles the strength. The result showed that the 4.5% red mud in the brick increases the compressive strength by 12.9%.

Ribeiro et al. (2010) studied on the replacement of cement in mortar by Bayer's process red mud. It was observed that the increase in red mud content lowers down the compressive strength from 20.1 MPa at zero percentage of red mud to 12.75 MPa at 50 % red mud.

Khan et al. (2012) utilized the Bayer's process red mud in the production of ceramic tiles. Pyrophyllite mineral was added to the red mud to improve the strength properties. The tiles were produced at a lower temperature (950-1000°C) than the conventional process of making ceramic tiles and without the addition of phosphatic binders. The structural features of red mud was studied using scanning electron microscope, exhibiting the presence of calcium aluminum silicate crystal which provide reinforcement to the ceramic tiles matrix.

Dodoo-Arhin et al. (2013) studied the effect of clay content (20%, 30%, 40%, and 50%) in Bayer's process red mud bricks. Based on the experimental work, the clay content of 50% was suggested as optimum which gave the flexural strength of about 16.67 MPa after burning it at 1100°C.

He et al. (2013) utilized the Bayer's process red mud to develop the rice husk ash based geopolymer composites and reported the mechanical property in term of compressive strength. It was found that the longtime curing increases the compressive strength and Young's modulus with a decrease in ductility. The high ratio of rice husk ash to red mud

ratio gave higher strength. The influence of composition, like rice husk ash to red mud ratio and concertation of NaOH was studied. The Si/Al ratio of the end product was varied from 0.3, 0.4, 0.5, to 0.6 while the concentration of NaOH was varied from 2 M to 6 M. The rice husk ash to red mud ratio of 0.5 was found to give maximum compressive strength (20.46MPa) along with maximum Young's modulus (1.89GPa).

Kumar and Kumar (2013) studied the possibilities of making a paving block using Bayer's process red mud and fly ash by geopolymerization technique. It was found that the introduction of red mud upto 10% increased the compressive strength and further increase in red mud content caused the reduction in strength. The red mud upto 25% showed higher 3 days strength as compared to 100% fly ash but 28 days strength with 25% red mud was found less than that of 100% fly ash.

Pontikes and Angelopoulos (2013) conducted a review on the utilization of Bayer's process red mud as raw material for OPC, calcium sulfoaluminate based cement, and calcium, iron-rich cement.

The red mud is also being used for the manufacturing of cement and cementitious materials. Yao et al. (2013) conducted a study on the possibilities of partial replacement of cement by 15% coal refuse, 15% red mud, 15% fly ash, and 2% gypsum based on mechanical property, durability property, and the leachate property of reinforced concrete cement (RCC). The compressive and flexural strength was observed to decrease initially but after 90 days of curing, it was observed to increase. After 180 and 360 days of curing, the compressive strength was found as 47.5MPa and 48.7MPa, respectively. The freeze-thaw resistance of newly develops cementing material was observed higher than that of OPC. The RCC showed strong binding ability on heavy toxic metal like Pb, Zn, Cr, Mn, and As.

Liu and Poon (2016) studied the effect of fly ash replacement by different percentage of Bayer's process red mud in self-compacting concrete. The study was made by incorporating 25%, 50%, 75% and 100% red mud by weight and the result were compared with the concrete made with 100% fly ash. The fluidity and the hardened density of concrete were found to decrease with increase in the percentage of red mud with an increase of water absorption and permeable voids. An improvement in compressive and flexural strength was observed for the sample prepared with red mud at 50% of replacement ratio. The dry shrinkage value was found to increase with an increase in red mud content.

Krivenko et al. (2017) made an investigation on alkali-activated cement and concrete using the Bayer's process red mud. The possibilities of using up to 90% red mud in concrete road base observed a compressive strength of 30-60MPa.

Lemougna et al (2017) studied the effect of 25, 50 and 75% replacement of slag by Bayer's process red mud in the mortar and light-weight materials. The test specimens were prepared using sodium silicate solutions from 1.6 to 2.2 mole and then cured at 25, 40 and 60°C. A 7 days compressive strength of 54 MPa was observed for a mixture of 50% red mud with 50% slag.

Yang et al. (2017) studied the mechanical property of mortar prepared by replacing the cement by Bayer's process red mud (3%, 6%, and 9%). The fresh mortars with red mud showed 25% higher plastic viscosity and increase in flow time but reduce the slump flow. The mortar with red mud was observed to have higher air content but it is eligible to adjust the decorative mortar colour. The 6% red mud was found as optimum value based on the 28 days compressive strength.

Nikbin et al. (2018) studied the effect of 25% replacement of cement in lightweight concrete by Bayer's process red mud in terms of mechanical properties, global warming potential, cumulative energy demand, and major criteria for air pollutants (CO, NO_X, Pb, SO_2). The density of the newly developed materials was found to vary in between 1685–1789 kg/m^3. It was also observed that incorporating 25% red mud reduces CO, NO_X, Pb and SO_2 in the air.

The impact of utilizing red mud as building materials on human health has also been investigated by few researchers. Based on which, it was suggested the maximum percentage of red mud which can be used to replace the conventional building materials. Gu et al. (2012) studied the effect of using red mud as main building materials on human health. The internal and external exposure index was calculated and was found to lie between 1.1-2.4 and 2.3-3.5, respectively. Less than 28-44% red mud was suggested to use as main building materials. Croymans et al. (2017) studied the radiological effect of utilizing the red mud in concrete. The concrete with 30, 40, 50, 60, 75, 85, and 95% red mud was studied for activity concentrations of radionuclides from the ^{238}U, ^{232}Th decay series and ^{40}K using gamma-ray spectrometry with an HPGE detector. Based on the experimental result, less than 75% (by mass) red mud was suggested to use. Table 2.1 summarizes observation on the application of red mud as a construction material.

Table 2.1. Summary of previous work on medium value utilization of red mud

Researchers	Major finding
Pera et al. (1977)	Production of Portland cement clinker with the addition of alkaline leaching waste.
Dass and Malhotra (1990)	Development of red mud brick by mixing 5% and 8% lime into red mud
Yalcin and Sevinc (2000)	Red mud can be used to produce the ceramic glaze.
Sglavo et al. (2000)	Red mud can be used to manufacture of clay-based ceramic.
Zhihua et al. (2003)	Develop the red mud-slag cementitious material.
Tsakiridis et al. (2004)	Preparation of Portland cement clinker using red mud.
Cablik (2007)	Characterization of pigment building blocks.
Patel et al. (2008)	Neutralization of red mud using mine water.
Yang and Xiao (2008)	Development of brick using the red mud along with fly ash, sand, lime, gypsum, and cement.
Zhang et al. (2009)	Development of cementitious material using red mud along with coal gangue.
Desai and Herkal (2010)	Manufacturing of bricks.
Ribeiro et al. (2010)	Replaced the cement with red mud in a mortar.
Gu et al. (2012)	Based on the calculated exposure index, less than 28-44% red mud was suggested to use as main building materials based on exposure index.
Dodoo-Arhin et al. (2013)	Development of red mud-clay brick.
He et al. (2013)	Developed red mud-rice husk ash based geopolymer.
Kumar and Kumar (2013)	Developed paving block using red mud- fly ash based geopolymer.
Yao et al. (2013)	Cement can be replaced by 15% red mud along with coal refuse, fly ash, and gypsum.
Liu and Poon (2016)	Replacement of fly ash by red mud in self-compacting mortar.
Croymans et al. (2017)	Less than 75% red mud was suggested to use in building construction material based on the radiological

	study.
Krivenko et al. (2017)	A large volume of red mud can be used in concrete road base.
Lemougna et al. (2017)	Effectively replaced the 50% slag by red mud in a mortar and light-weight materials.
Yang et al. (2017)	Feasibility of replacing the cement with red mud in a mortar.
Nikbin et al. (2018)	Replacement of cement in lightweight concrete by 25% red mud.

2.7.2 Characterization and Application as Geotechnical Materials

In order to use red mud (RM) in bulk quantity, several attempts have been made for geotechnical characterization of red mud. Miners (1973) found that majority of the particle in RM is in silt range along with 20-30% clay-sized particle. However, Li (1998) observed that some RM contains around 50% clay-sized particles. Wang and Liu (2012) found that Bayer's process red mud is finer and more dispersive as compare to sintered process red mud. Vick (1990) found that specific gravity (G_s) of RM lies between 2.8 to 3.3 and has a low liquid limit (LL = 45%) and plasticity index (PL = 10%). Somogyi and Gray (1977) and Fahey et al. (2002) studied the permeability characteristics of remolded RM sample and found that Bayer's process red mud has very low permeability (k) ranging between $(2\text{-}20) \times 10^{-7}$ cm/s, whereas, the remolded sintered RM has higher permeability with k value of $10^{-4}\text{-}10^{-5}$ cm/s (Liu and Wu, 2012). The compression indices (C_c) of red mud lies in between $0.27 - 0.39$ and coefficient of consolidation (c_v) in between $(3\text{-}50) \times 10^{-3}$ cm^2/s (Fahey et al., 2002). Vogt (1974) and Newson et al. (2006) found that the RM has a high angle of internal frictional (φ) of $38^o\text{-}42^o$, which is very similar to sandy soil, though its particle size corresponds to a fine fraction. But Liu and Wu (2012) found that the sintered process RM has a low angle of internal friction ($13.5^o - 21.0^o$), while it contains 65% particles in the range of 0.1-0.02mm. Kehagia (2008) studied the feasibility of red mud as an embankment material by mixing with local soil.

Mymrin and Vazauez-Vaamonde (2001) studied the possible use of red mud in the road, airfield base, levee core, dumps, foundation etc. based on its strength. It was observed that the addition of 4% ferrous slag in red mud causes an increase in the strength up to almost 9 MPa after 360 days of curing. The addition of a small amount (< 2%) of

traditional binders like CaO or Portland cement increases the strength further by 1.5 to 4 times.

Duchesne and Doye (2005) studied the possibilities of cement kiln dust stabilized red mud for cover or liner materials for acid mine waste based on the leachate analysis. Kalkan (2006) studied the suitability of Bayer's process red mud as a stabilizer material for clay liner and reported an increase in compressive strength and a decrease in permeability of the stabilized material. Rout et al. (2013) found the red mud suitable as embankment material but with a soil cover at the top is required to protect the red mud from erosion based on their finite element analysis.

Kalkan (2006) examined the effects of red mud on the unconfined compressive strength, hydraulic conductivity, and swelling percentage of compacted clay liners as a hydraulic barrier. The test results showed that compacted clay samples containing red mud and cement–red mud additives had a high compressive strength with decreases in the hydraulic conductivity and swelling percentage as compared to natural clay samples. The addition of these additives changed the soil groups from high-plasticity soil group (CH) to low-plasticity soil group (MH). Consequently, it was concluded that red mud and cement–red mud materials can be successfully used as a clay liner in geotechnical applications.

Sundaram and Gupta (2010) found that red mud slurry behaves like soft clay and conducted an in-situ investigation after stabilizing it by stone column. The investigation on red mud showed that it is highly alkaline (9.3-10.2) with a liquid limit of 39-45 %, plastic limit of 27-29% and shrinkage limit of 19-22%. The undrained shear strength was observed to lie in between 39.22 to 137.29 kN/m^2, specific gravity in between 2.85-2.97, and cohesion in between 9.8 to 19.61 kN/m^2. The angle of internal friction was observed to vary from 26-28°.

Yang et al. (2012) used red mud in different percentage with fly ash and bentonite for the preparation of liner material. The result was presented in term of permeability of red mud-bentonite mixture and red mud-fly ash-bentonite mixture. The addition of 5% bentonite decreases the permeability of red mud from 10^{-6} cm/s to 10^{-7} cm/s. The hydraulic conductivity of 65% red mud, 20% fly ash, and 15% tailings mixture was observed as 1.76×10^{-6} cm/s which is less than the desired value (10^{-7} cm/s)

Satayanarayana et al. (2012) studied the possible use of lime stabilized red mud in road

construction. The lime (2, 4, 6, 8, 10, and 12%) was mixed with red mud and after 1, 3, 7, and 28 days of curing, the unconfined compressive strength, split tensile strength, and CBR were studied. An optimum percentage of lime as 10% was found to show maximum strength.

Rubinos et al. (2013) studied the suitability of RM as a liner material for the waste disposal facility in term of permeability.

Rubinos et al. (2016) studied the chemical and environmental compatibility of using the red mud as liner materials for hazardous waste and presented the result in term of permeability and effluent characteristic. The red mud was found to show good resistance towards the flow of chemicals like methanol, acetic acid, n-heptane, trichloroethylene, and calcium chloride. The permeability was also found to reduce from 1.18×10^{-7} cm/s in case of deionized water to 1.00×10^{-7} cm/s in case of seawater. The concentration of Si and Fe in the leachate was found to increase, while the concentration of Al, and Cr was found to reduce when acetic acid was used as permeant.

Panda et al. (2017) characterize the Indian red mud as a geotechnical material using bioremediation and found that the bioremediation is effective in lowering the pH value along with increasing the unconfined compressive strength. A decrease in the permeability was reported along with the decrease in specific gravity after bioremediation of red mud. The liquid limit was found to decrease after bioremediation but the negligible change in plasticity index was observed. Table 2.2 summarizes observation on the geotechnical engineering application of the red mud.

Table 2.2. Summary of previous work on geotechnical engineering application of red mud

Researchers	Major finding
Miners (1973)	Found that the red mud contains around 20-30% clay-sized particles along with the majority of silt-sized particles
Vogt (1974)	The friction angle was found to vary from 38°-42°.
Somogyi and Gray (1977)	Observed that the Bayer's process RM has a very low permeability (k) ranging between (2-20) $\times 10^{-7}$ cm/s.
Vick (1990)	The specific gravity (Gs) of red mud was found to lies in between 2.8 to 3.3. The red mud shows a liquid limit of 45% with plasticity index value of 10%.
Li (1998)	The red mud was found to contain 3.71% to 8.88% sand-sized particle

	along with 8.90% to 18.58% silt-sized particles. The specific gravity of the red mud was found to vary from 2.91 to 4.22 and the surface was found to vary from 19.2 - 51.7 m^2/g.
Mymrin and Vazauez-Vaamonde (2001)	It was found that the red mud content increases the strength up to 9 MPa after 360 days. Further introduction of a small amount of CaO or Portland cement increases the strength by 1.5 to 4 times.
Fahey et al. (2002)	The compression indices (Cc) was found to lie in between 0.27-0.39 and the coefficient of consolidation (Cv) in between $3 - 50 \times 10^{-3}$ cm^2/s.
Duchesne and Doye (2005)	The pH value of the leachate was measured as 7 and the concentration of Fe, SO_4, Cu, and Zn in leachate was observed to decrease.
Kalkan et al. (2006)	Addition of 20% red mud was found to improve the UCS value by 79.10% and it decreases the permeability up to 1.58×10^{-7} cm/s.
Newson et al. (2006)	Observed that the red mud showed very high friction angle (42°) and a cohesion value of 10-20kPa.
Kehagia (2008)	An increase in CBR value by 25% was observed by mixing 40% red mud in the soil while the modulus of deformation was observed to increase by 8%.
Sundaram and Gupta (2010)	pH value of red mud was found to vary from 9.3-10.2 with a liquid limit in between 39-45 %, and plastic limit in between 27-29%. The shrinkage limit of 19-22% was observed. The undrained shear strength was found to vary from 39.22 to 137.29 kN/m^2, specific gravity in between 2.85-2.97, cohesion from 9.8 to 19.61 kN/m^2, and angle of internal friction from $26-28^0$.
Liu and Wu (2012)	It was found that the sintered process red mud has a low angle of internal friction (13.5^o - 21.0^o), although it contains 65% particles in the range of 0.1-0.02 mm
Satayanarayana et al. (2012)	10% lime was found to give maximum unconfined compressive strength, split tensile strength and CBR value.
Wang and Liu (2012)	Found that the sintered red mud shows higher cohesion (287 kPa) as compared to Bayer's process red mud (14.60 kPa). Although, the particles of Bayer's red mud was found finer than sintered red mud; negligible difference in the friction angle was observed. For the same

	water content, hydraulic conductivity of Bayer's red mud was found lower than that of sintered red mud.
Rout et al. (2013)	Perform finite element analysis on the embankment made up of red mud. The minimum factor of safety of 1.49 was observed during vibratory loading. However, a soil cover is required at the top to protect the embankment from erosion.
Rubinos et al. (2013)	Studied the permeability characteristic of red mud and achieved the minimum value as 9×10^{-8} cm/s at 1.3% higher moisture content then optimum moisture content.
Yang et al. (2012)	The permeability of red mud decreases to 10^{-7} cm/s from 10^{-6} cm/s after addition of 5% bentonite.
Rubinos et al. (2016)	The effectiveness of red mud as liner material based on permeability and leachate characteristic.
Panda et al. (2017)	The unconfined compressive strength was observed to increase by 1.18% and pH was also found to get reduced to 7.5 from 10.06.

2.8 Summary of Critical Review

Based on literature survey the following observations were made:

1. Several studies are available regarding the high value (making of ceramic tiles, glass ceramic production, iron extraction etc.) and medium value (making of paving blocks, partial replacement of cement in concrete etc.) utilization of red mud but in all these cases, the utilization rate is very low.

2. A few studies on characterization of red mud are available but the study on the Indian red mud for bulk utilization is limited and available only after stabilizing by bioremediation. But the study on strength and durability of stabilized red mud is not available. Also, the study on the utilization of coarse fraction of red mud is not available.

3. As in most of the cases, the red mud is disposed in slurry form and sedimentation characteristic become important, but research on sedimentation characteristic of red mud is scarce.

Chapter **3**

Material Characterization

3.1 Introduction

It is observed during the literature survey that the red mud is highly alkaline and is stored in the pond. Various attempts have been made worldwide to characterize the red mud for bulk utilization. However, large variability in the physical, chemical and geotechnical properties is observed based on the source of generation. These variations in the property show need of characterizations of red mud from different sources for getting confidence in the utilization of red mud. In this chapter, oven dried Indian red mud from two different sources (NALCO, Odisha and HINDALCO, Jharkhand) are studied for their chemical, mineralogical, morphological, physical and geotechnical property.

3.2 Material Collection

The raw materials like red mud (RM), ground granulated blast furnace slag (GGBS), red sand (RS), and standard sand (SS) was used in the present research. The materials were dried in the oven at $100^{o} - 110^{o}$C to evaporate the natural moisture content. The raw materials were considered as dry when no evaporable water remains in the material at the temperature $100^{o} - 110^{o}$C. The RM was grounded to make it finer than 425μm, while the GGBS finer than 150 μm was used in the present study. The characteristic of RS and SS are discussed in Chapter 5 while the detail about GGBS is discussed in Chapter 6.

3.3 Red Mud

Red mud (RM) for the present research was collected from two different Indian aluminium industries (i.e NALCO and HINDALCO). The NALCO RM (NRM) was collected from the Damanjodi in the state of Odisha (Figure 3.1), while the HINDALCO RM (HRM) collected from the Muri in the state of Jharkhand (Figure 3.2). Type of RM (Bayer or sintered type) is discussed in Section 3.4.2 based on their chemical composition.
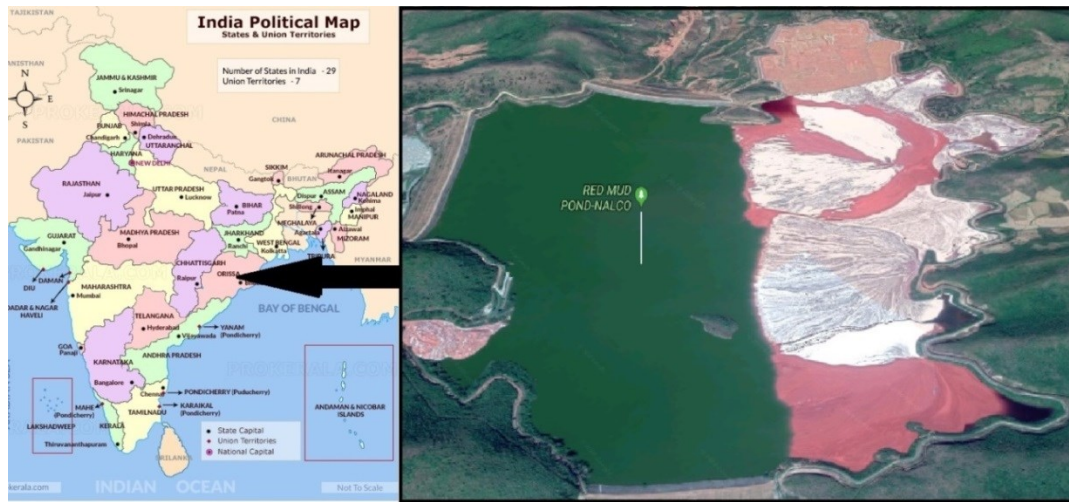
Figure 3.1. NRM disposal pond, Damanjodi, Odisha (Source: google image)

Figure 3.2. HRM disposal site, Muri, Jharkhand (Source: google image)

The NRM is disposed of in a slurry form with 40% (by volume) solid content using a pipeline as shown in Figure 3.3. The water available in the RM gets descended over a period of time and the RM starts drying. The descended liquid is used back in the aluminium refinery for different purposes but the solid part (RM) remains unutilized. During the drying period, the unstable $Ca(OH)_2$ comes at the surface and react with CO_2 to form stable calcium carbonate ($CaCO_3$). This stable calcium carbonate deposited at the surface of RM is transported to the nearby area by the wind in the form of dust. To avoid the stable $CaCO_3$ in the RM sample used for present research, the top layer was removed before the collection of RM.

The HRM is subjected to a filter press to make the RM cake with solid content more than 65% before disposal (Figure 3.4). Due to the low water content during the disposal, the trace of formation of calcium carbonate was not observed at the surface of HRM dump.

The fresh HRM was collected just after the unloading from the truck to avoid any physical and chemical alteration due to storage.
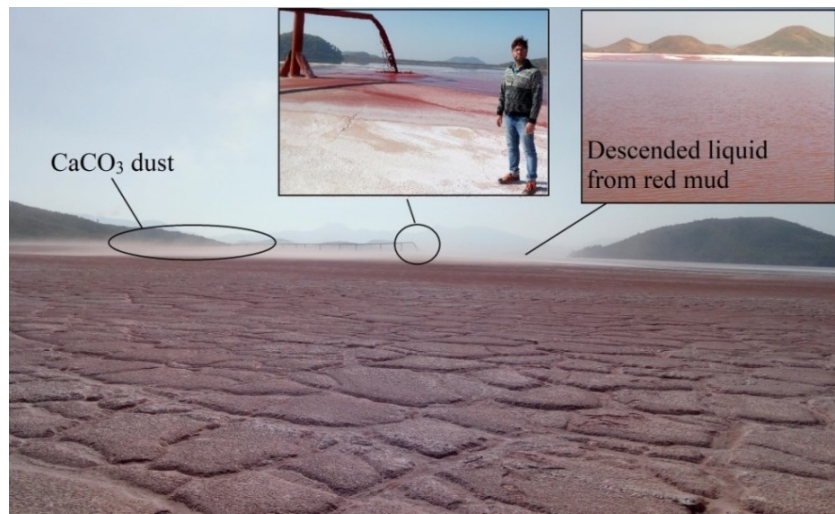
Figure 3.3. Slurry disposal of RM in NALCO, Damanjodi, Odisha

Figure 3.4. RM disposal area of HINDALCO, Muri, Jharkhand

3.4 Characterization of Red Mud

3.4.1 Morphology and Mineralogy

Particles morphology and chemistry were studied using scanning electron microscope (SEM) (JEOL-JSM-6480 LV model) fitted with energy-dispersive X-ray (EDX) micro analyzer at 20 kV acceleration voltage and spot size of 60. The platinum coating was applied on RM at 30 mA for 90 seconds before loading the sample for analysis. The mineralogical composition of the RM studied using the X-ray diffraction (XRD) analysis

which performed using Rigaku Japan/Ultima-IV model with Cu Kα radiation at 40 kV and 40 mA over the range of 10° to 60° at a scanning rate of 4°/minute with step size of 0.05^o.

The SEM micrographs of NRM and HRM showing microstructure presented in Figures 3.5 (a) and (b). The SEM image shows that RM contains some spherical particle along with the majority of angular to a subangular agglomerated particle of different sizes.
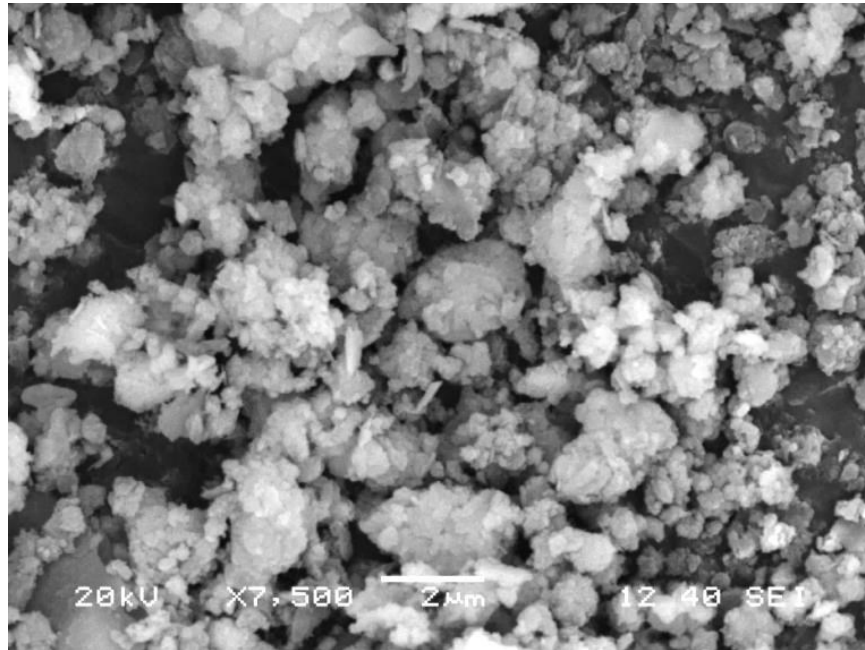
(a)
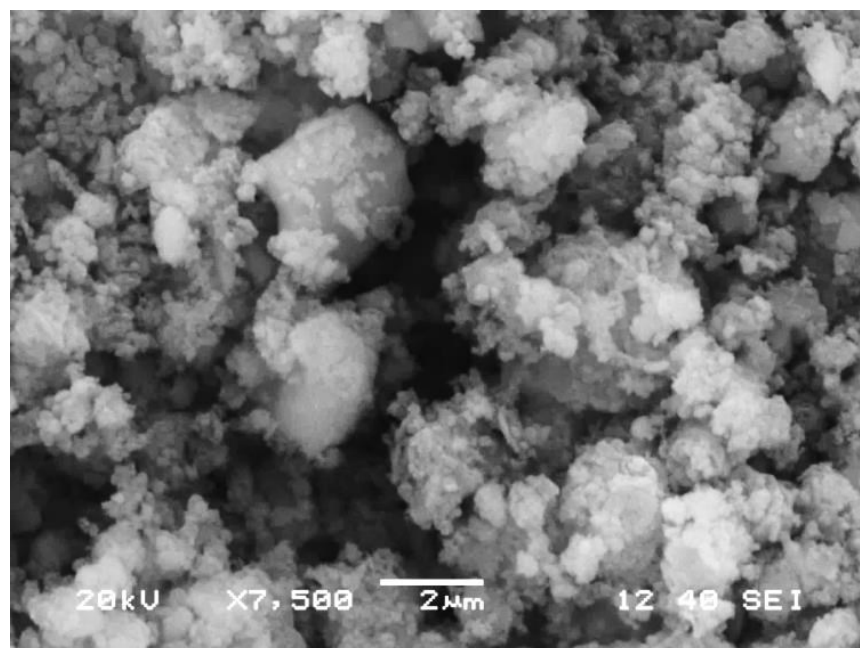
(b)

Figure 3.5. SEM image of (a) NRM (b) HRM

It can be seen that HRM contains more agglomerated particles than NRM. Rout et al. (2013) also reported that the NALCO RM contains angular to sub-angular particles, however, Meher (2014) reported poorly crystallized, hexagonal plate like structure for the same RM. But the tetragonal, hexagonal, spherical, and orthorhombic particles were observed in the RM collected from HINDALCO, Renukoot (Amritphale et. al. 2007). The difference in particle morphology of RM from HINDALCO, Renukoot ((Amritphale et. al. 2007) and HINDALCO, Muri (present study) may be due to the difference in source of bauxite and production process.

1=Hematite 2=Goethite 3=Gibbsite 4=Boehmite 5=Rutile
6=Quartz 7=Kaolinite 8=Sodalite 9=Calcite
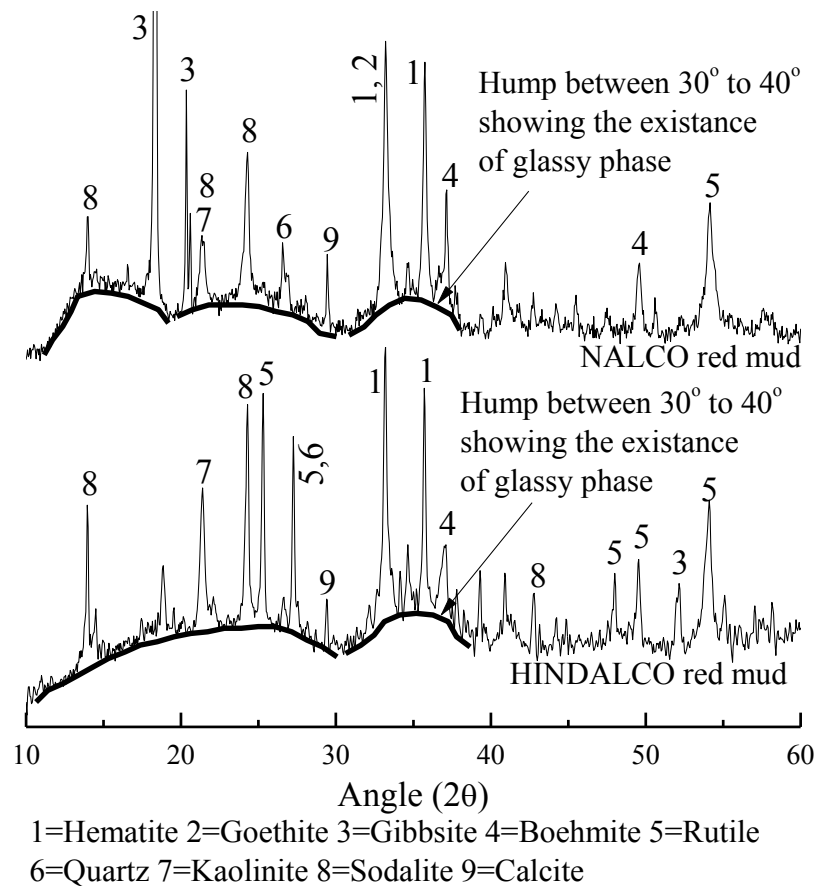
Figure 3.6. XRD graph of NRM and HRM

The XRD graph of both the RM (NRM and HRM) are presented in Figure 3.6. Both RM show the major peak corresponding to iron compound like hematite (Fe_2O_3), goethite ($FeO(OH)$) and aluminium compound like gibbsite ($Al_2O_3.3H_2O$) along with kaolinite ($Al_2Si_2O_5(OH)_4$), sodalite ($Na_8(Al_6Si_6O_{24})Cl_2$) and rutile (TiO_2). Duchesne and Doye (2005) also found similar mineral phases present in Bayer's RM. Along with the iron and

aluminium bearing minerals as the major minerals, RM also contains clay minerals like kaolinite which is responsible for the cohesive property of RM (Alhassan et al., 2012). The XRD pattern (Figure 3.6) shows several humps at a 2θ value of 25º and 35º in HRM and at 15º, 25º, and 35º in NRM which shows the existence of amorphous phases. Diamond (1983) and Das and Yudhbir (2006) have discussed glassy content in term of hump position (2θ) for fly ash. Yalcin and Sevinc (2000), Sglavo et al. (2000) also found similar XRD pattern of RM with several humps. Castaldi et al. (2008) found similar XRD pattern for RM and also found that 15-20% by weight of the RM consists of amorphous oxides. Kani et al. (2012) observed a similar pattern of XRD with humps position (2θ) between 25º-30º for natural pozzolanic material.

3.4.2 Chemical Characteristics

The particles chemistry plays an important role in the pozzolanic activity of the materials. Chemical reactions depend on the overall chemistry along with the surface chemistry. In the present research, the chemistry of the raw materials is presented in term of chemical composition and pH value of the materials.

The relative quantitative element concentration at the surface of both RMs (NRM and HRM) were studied using EDX (JEOL-JSM-6480 LV model) at a 20 kV acceleration voltage and spot size of 60. The analysis was performed at five spots and the average concentration of element with their standard deviation (SD) is presented in Table 3.1. However, it is to be noted the EDX was limited to element heavier than the carbon (C), so the element lighter than carbon could not be detected. The result shows that the surface of NRM is abundant in sodium and iron while the surface of HRM contains a trace amount of sodium which may be due to the difference in disposal system. As mentioned earlier, NRM is disposed in slurry form but HRM is disposed through dry disposal system. In dry disposal system, RM passes through filter press system to reduce water content and it is also washed for caustic recovery (Power et al., 2009), which may reduce the concentration of Na_2O at the surface of HRM. EDX only describes the surface chemistry of the particles. Hence, the total chemistry of both RM was studied using X-ray fluorescence (XRF). The quantification of chemicals in NRM and HRM was done using X-ray fluorescence (XRF) analysis using Axios PANalytical with scintillation type detector at 20 kV and 10 mA

available at Indian Institute of Technology, Kharagpur. The chemical composition of NRM and HRM is presented in Table 3.2.

Table 3.1. Surface chemistry of RM (% by weight)

Element	NALCO		HINDALCO	
	% weight of chemicals	SD	% weight of chemicals	SD
O	46.70	3.08	51.78	13.29
Na	23.98	0.95	7.33	2.90
Al	7.74	1.33	7.38	0.85
Si	3.65	1.03	3.96	2.00
Ti	1.07	0.11	4.84	4.68
Fe	16.86	4.24	13.57	12.84
Ca	-	-	0.96	0.78
Total	100		100	

Table 3.2. Chemical composition of NRM, and HRA

Chemicals	Weight percentage (%)		Typical range (based on literature review)
	NRM	HRM	
Fe_2O_3	51.04	35.54	7.15-65
Al_2O_3	17.57	16.80	7.74-51.07
SiO_2	8.65	15.63	1.2-33.44
Na_2O	8.03	13.56	0.2-23.98
TiO_2	3.24	7.73	1.07-28
CaO	1.64	1.24	0.06-26.63
MgO	0.21	0.10	0.01-4.31
K_2O	0.19	0.06	0.01-2.57
P_2O_5	0.20	0.34	-
SO_3	0.29	0.23	-

Both the RMs are rich in Fe_2O_3, however, NRM (51.04%) contains a higher percentage of Fe_2O_3 as compare to HRM (35.54). Meher (2014) found that the NRM contains 53.75% of Fe_2O_3. Li (1998) also found Fe_2O_3 (24.34% - 64.21%) as a major constituent of Bayer's process RM. Along with Fe_2O_3, NRM contains Al_2O_3 (17.57%) as the second major constituent while HRM contains 16.80% Al_2O_3. The HRM found to have a higher

Na_2O percentage (13.56%) compare to NRM (8.03%). However, the CaO percentage is almost same in both NRM (1.64%) and HRM (1.24%).

A graph has been plotted by considering maximum and minimum limit Fe_2O_3, Al_2O_3, SiO_2, CaO, and Na_2O based on the chemical composition data collected from the literature for Bayer's process (Figure 3.7) and sintered process (Figure 3.8) RM.
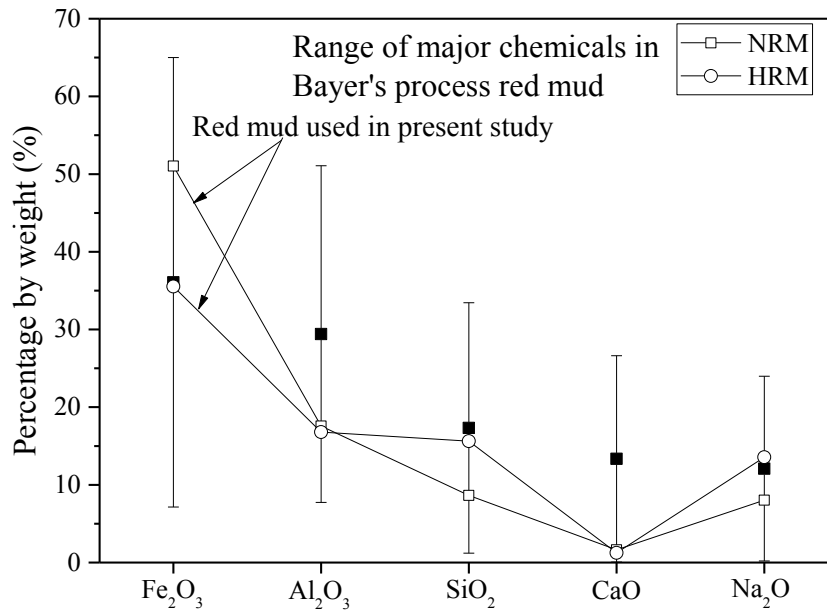
Figure 3.7. Variation of the major chemical in Bayer's process RM
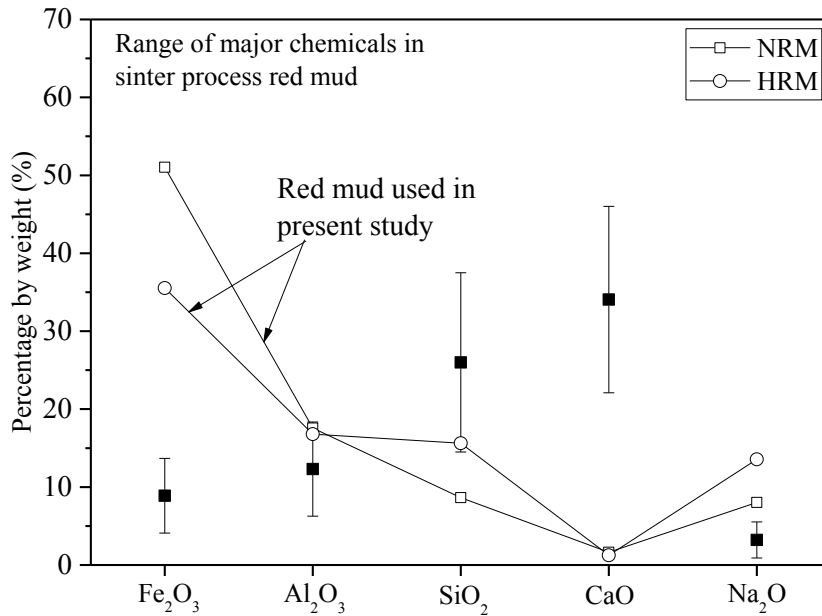
Figure 3.8. Variation of the major chemical in sintered process RM

On the same plot, the chemical composition of the NRM and HRM has also been plotted.

It can be seen that the percentage of the chemicals like Fe_2O_3, Al_2O_3, SiO_2, CaO, and Na_2O falls within the maximum and minimum limits of Bayer's process RM (Figure 3.7). But the above chemicals falls beyond either maximum or minimum limit of sintered process RM (Figure 3.8). NRM and HRM found to have an approximately similar percentage of Al_2O_3 and CaO (Figure 3.7).

A triangular plot by considering the percentage of Fe_2O_3, CaO, and Al_2O_3 in the Bayer's process and sintered process RM along with the percentage available in NRM and HRM is plotted (Figure 3.9). It is found that the plot can be divided into two different zones for Bayer's process RM (with high Fe_2O_3 and low CaO percentage) and sintered process RM (with low Fe_2O_3 and high CaO percentage). It is found that the NRM and HRM fall within the Bayer's process RM zone. It can be seen in Figure 3.9 that the Bayer's process RM contains relatively higher percentage of Fe_2O_3 and relatively lower percentage of CaO which can also be observed in Table 3.2
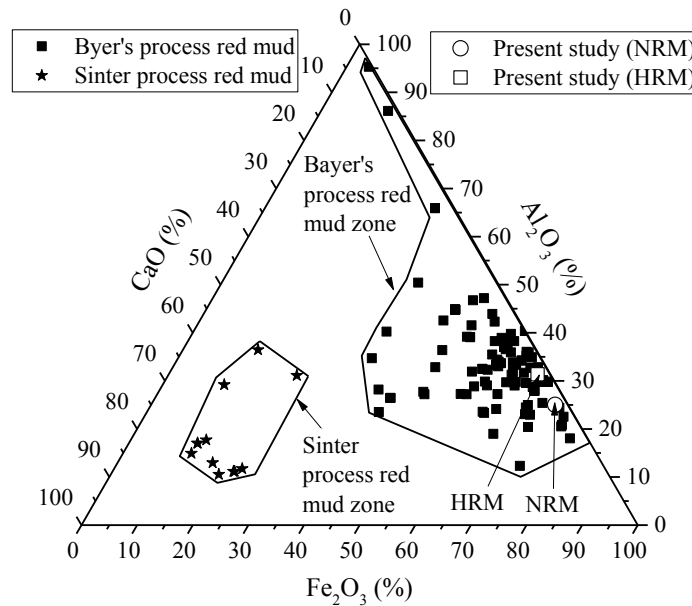
Figure 3.9. Triangular plot to differentiate the Bayer's and sintered process RM

As the main difference between Bayer's and sintered process is lime content, an attempt has also been made to differentiate the Bayer's process and sintered process RM based on the lime index. The lime index for each data collected from the literature has been calculated using the Equation 3.1 and is plotted against CaO (%) as shown in Figure 3.10. It has been divided into two zones i.e. zone I and zone II base on the CaO percentage and lime index.

$$Lime\ index = \frac{CaO\ (\%)}{Fe_2O_3\ (\%) + Al_2O_3\ (\%) + SiO_2\ (\%)} \tag{3.1}$$

The RM having more than 25% CaO and lime index greater than 0.5 has been identified as sintered process RM. But the Bayer's process RM is found to have less than 25% CaO and lime index less than 0.5. Figures 3.9 and 3.10 can be used to differentiate the Bayer's process and sintered process RM based on the Fe_2O_3, Al_2O_3, CaO and SiO_2 percentage.
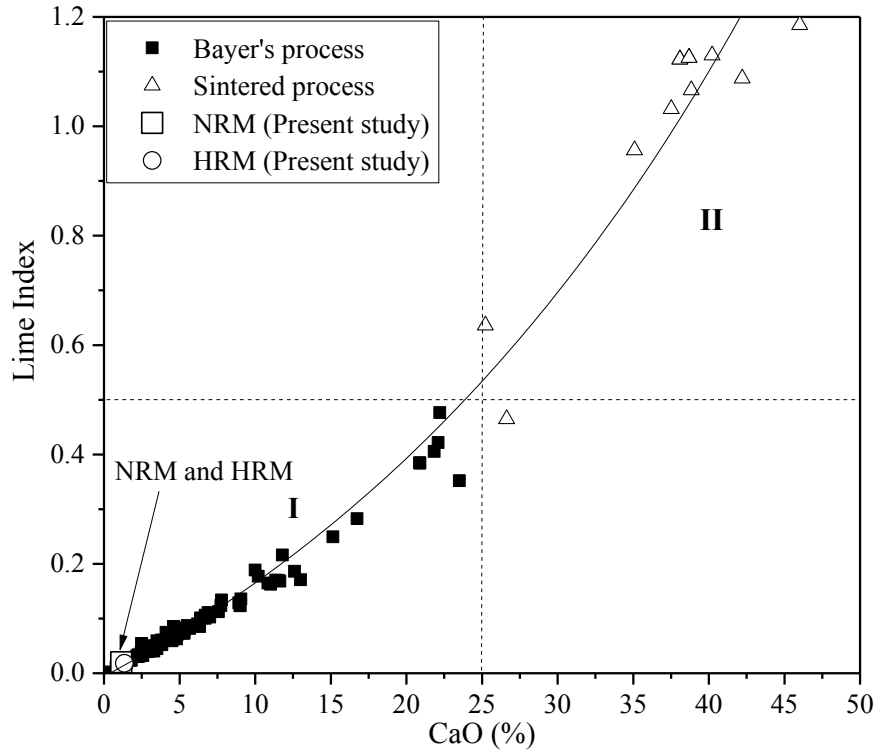
Figure 3.10. Variation of the lime index with CaO percentage

To demonstrate the overall chemistry of RM, pH test was performed using the HACH HQ40D pH meter and it was found that pH value of NRM and HRM are 11.40 and 11.53, respectively. Grafe et al. (2011) also found that the pH of RM lies within the range of 9.2-12.8. Sutar et al. (2014) reported that the pH value of NALCO (Damanjodi) RM varies from 10.00 to 12.50. But the pH value of HINDALCO (Renukoot) was found to vary from 10.50 to 13.00 (Dubey and Dubey, 2011). The high pH value shows that the RM is highly alkaline in nature. The pH of RM varies with alkalinity, CaO and Na_2O, Figure 3.11 shows the variation of pH with CaO and Na_2O for the present study and data available in the literature. Based on the CaO and Na_2O content, the pH of RM can be estimated from the presented diagram.
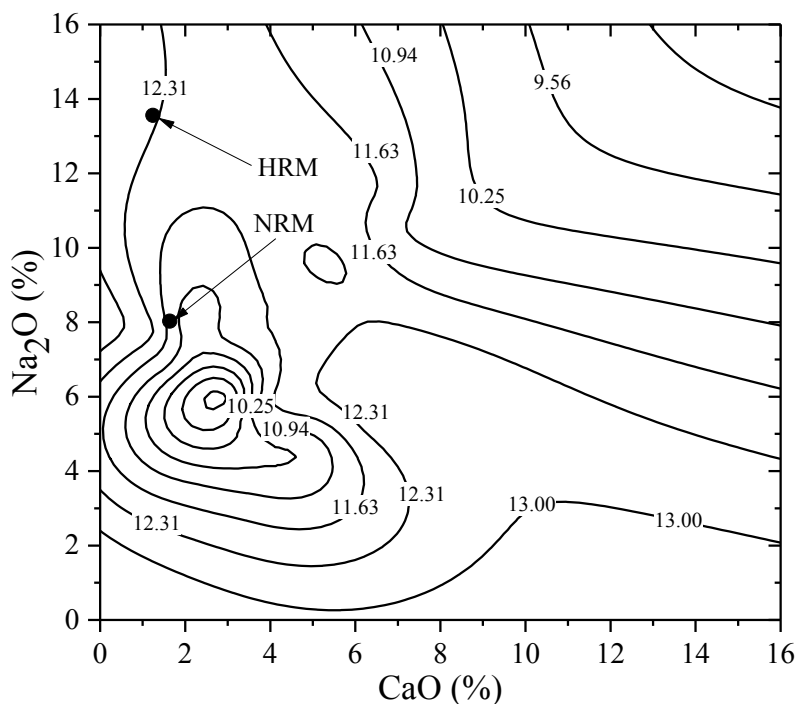
Figure 3.11. Variation of pH value corresponding to Na_2O and CaO

As the RM found highly alkaline with pH value greater than 11 which may be due to the addition of NaOH during the Bayer's process, the alkalinity in the RM due to the concentration of hydroxyl ion (OH^-) was also studied. The descended water was collected from the NALCO RM pond (Figure 3.12) for the chemical analysis in terms of the concentration of hydroxyl ions.

Figure 3.12. Collection of descended water from NALCO RM pond

The water collected was titrated with a strong acid (HCl) in the presence of phenolphthalein and methyl orange indication (Figure 3.13). It was found that the

alkalinity present in the water was due to the presence of hydroxyl and carbonate ions in which the concentration of hydroxyl found as 5.47 g/l. By considering that all hydroxyl ions present are associated with either Na^+ or K^+, the molarity of NaOH/ KOH in the descended water was calculated as 0.32 moles. However, further in-depth study is required to find out the exact molarity of NaOH and KOH as the descended liquid contains both K and Na. The presence of alkalinity in form of OH^- in the RM can be used to activate the pozzolanic material.

Figure 3.13. Typical photo showing the titration of descended water

3.4.3 Fourier-Transform Infrared Spectroscopy

As the X-ray diffraction is limited to the crystalline materials, the Fourier-Transform Infrared (FTIR) spectroscopy is performed to identify the functional group and hence the possible chemical composition. The FTIR sample prepared by grounding RM with potassium bromide (KBr) and the mixture pressed at 10 ton load to get about 1 mm thick pallet with 13 mm diameter. FTIR spectrum of empty KBr pallet was subtracted from the spectrum of the mixture to get the RM spectrum. The FTIR spectra of NRM and HRM are shown in Figure 3.14.

In both RMs, the strong broadband is present in the range of 3400-3500 cm^{-1} due to the stretching of OH group, H_2O molecule is indicated by the deformation vibration at 1639.35 cm^{-1} and 1637.09 cm^{-1} in NRM and HRM, respectively. The peak at 1478.10 cm^{-1} in NRM and 1453.25cm^{-1} in HRM indicates the presence of Ca-O, which signifies the

presence of $CaCO_3$. The stretching vibration of Si-O-Si is indicated by the band at 994.85 cm^{-1} and 995.27 cm^{-1} in NRM and HRM, respectively. The peak between 500 and 600 cm^{-1} indicates the vibration of SiO_4 or AlO_4 tetrahedral while peak ranging 400-500 cm^{-1} indicates the Si-O or Al-O bend. The peak at 474.64 cm^{-1} in NRM and peak at 460.24 cm^{-1} in HRM show the stretching vibration of the Fe-O bond which confirms the presence of iron oxide in RM as observed in XRF and XRD analysis. Similar result has been reported by previous researchers (Ruan et al., 2001; Alp and Goral, 2003; Gok et al., 2007; Castaldi et al., 2010; Luo et al., 2010; Liu et al., 2011; Bernal et al., 2012; Kaya and Soyer-Uzun, 2016; Ye et al. 2016).
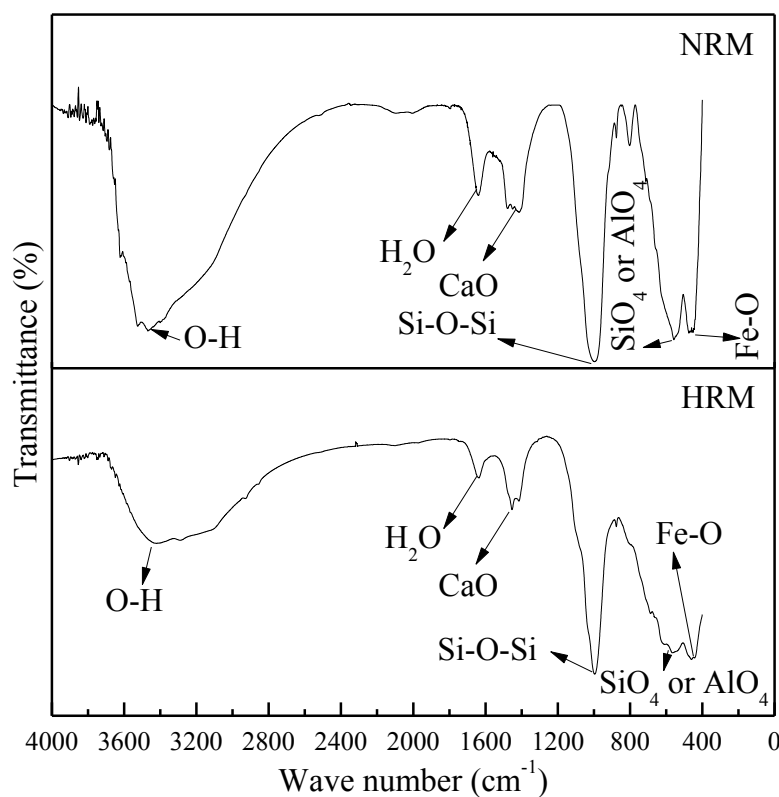
Figure 3.14. FTIR spectra of RM

3.4.4 Particle Size Analysis, Atterberg's Limits and Specific Gravity

Grain size distribution, consistency test (Atterberg's limits) and specific gravity tests were performed as per Indian Standard (SP-36 (1) - 1987). Grain size distribution curve of RM obtained by combining the result of sieve analysis (for particle greater than 0.075mm) and hydrometer method (for particle smaller than 0.075mm) is shown in Figure 3.15. It can be seen that the majority of the particle (around 60%) in NRM having a size ranging 50-

75μm with 5% fine sand size particle. On the other hand, HRM contains 17% fine sand-sized particle. It can also be observed that NRM contains around 81% silt-sized particle while the percentage of silt-sized particle in HRM is around 51%. HRM contains a higher percentage of the clay-sized particle (32%) than NRM which contains 14 % clay-sized particle. Miners (1973) also observed 20-30% clay-sized particle in RM. Li (1998) observed up to 50% clay-sized particle in some RM. It may also be noted from Figure 3.15 that the fine percentage in the RM is varying from 83-95%. He et al. (2013) also found the similar result (76%). A sudden jump can also be observed in NRM at 0.075 mm which indicate that the NRM is gap graded.
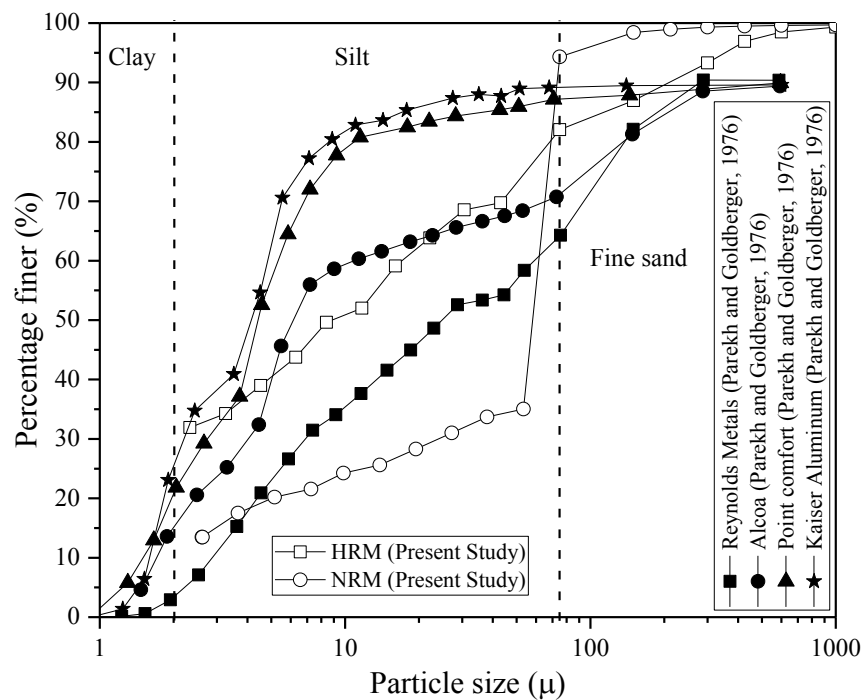
Figure 3.15. Grain size distribution of RM

Atterberg's limits test was conducted using the Casagrande device. Liquid limit (LL) of NRM is 30.75% while the plastic limit (PL) is 27.56% along with the plasticity index (PI) value of 3.19%. The LL and PI of NRM found in the present study are slightly different from the value (LL=24.75%, PI=7.25%) reported by Rout et al. (2012). The difference in the result may be due to the different collection location in the disposal pond. The LL of HRM found as 39.89% while the PI 3.81%. Figure 3.16 shows the plasticity chart drawn as per the IS1498 (1970). It can be seen that both NRM and HRM and mud fall below the

A-Line because RM shows high LL in relation to its PI. The high LL may be due to ineffective water within the RM, which raises the LL and PL but the PI remains ineffective (Dumbleton and West, 1966). NRM has low plasticity, which may be due to the presence of kaolin group like kaolinite (Bain, 1971; Alhassan et al., 2012). Higher LL and PI value of HRM as compared to NRM may be due to higher clay content and mineral type. It has been found that both NRM and mud are inorganic silt with low plasticity (ML) while HRM and mud both are inorganic silt with medium plasticity (MI). It can also be seen that other RM in the literature (Vick, 1990; Rout et al., 2013) are also either ML or MI.
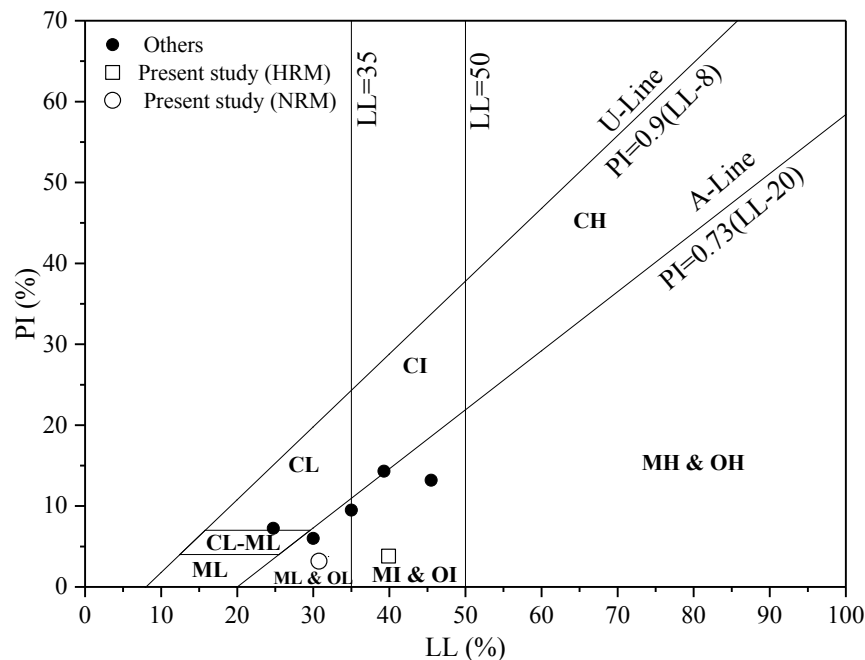
Figure 3.16. Plasticity chart (Modified from IS1498, 1970)

Specific gravity (G_s) of NRM and HRM were found to be 3.33 and 3.27, respectively. The higher specific gravity of RM is due to the presence of iron rich mineral. A large variation in the specific gravity of the RM was found in the literature. Kehagia (2008) reported a higher G_s of RM (3.95) from Aluminum of Greece, whereas, Wang and Liu (2012) reported a lower G_s value (2.47) of the RM from China. Vick (1990) also observed a wide variation in specific gravity of RM (2.8 - 3.3) due to the particle heterogeneity. Variation of the specific gravity of RM and fly ash with Fe_2O_3 has been shown in Figure 3.17. As both geotechnical and chemical studies on RM are limited, a few data represented in the literature was used. It can be seen that in comparison to fly ash, with the same iron

41

content, G_s value is more for RM. This may be due to fact that fly ash contains hollow spheres like cenospheres and plerospheres (Das and Yudhbir, 2005), but RM contains solid and angular/subangular particles.
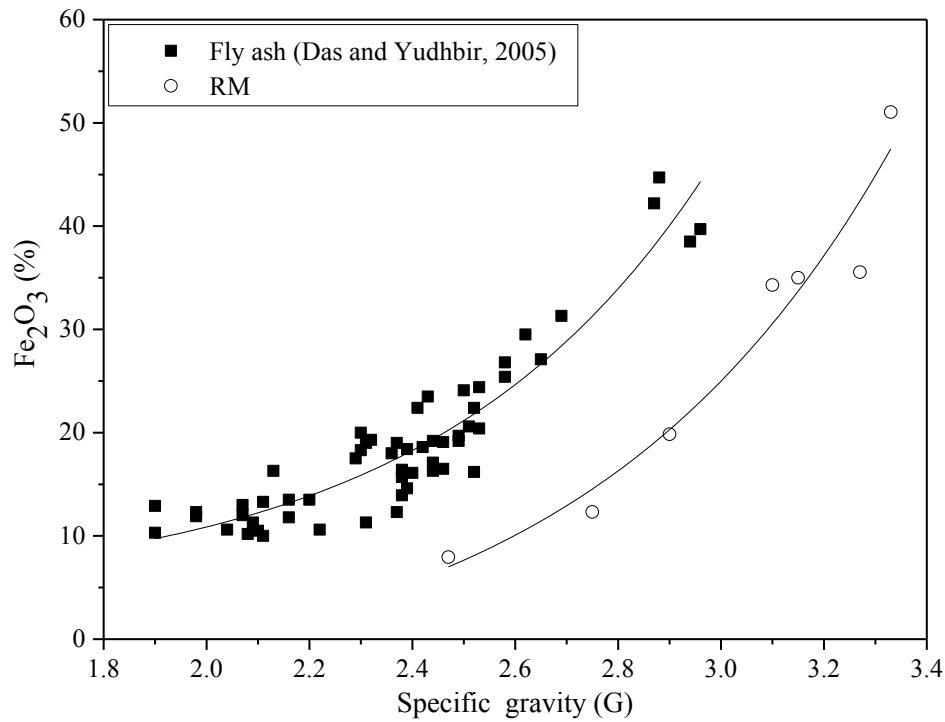
Figure 3.17. Variation of specific gravity with Fe_2O_3

3.4.5 Compaction Characteristic

The compaction characteristics under light and heavy compaction test as per Indian standard (SP-36 (1) - 1987) of the NRM and HRM are presented in Figure 3.18. It can be seen that NRM shows the higher maximum dry unit weight (MDD) (16.5 kN/m³) than HRM (15.2 kN/m³). The MDD values of NRM and HRM under heavy compaction are 17.7 kN/m³ and 15.9 kN/m³, respectively. Rout et al. (2012) also reported the MDD value of NRM (Damanjodi) as 19.84 kN/m³ and 13.93 kN/m³ respectively. Desai and Herkal (2010) found the MDD value of HRM (Renukoot) as 14.00 kN/m³. However, this type of result on HRM (Muri) is not found. It may be due to the fact that NRM has higher specific gravity due to higher iron content. The optimum moisture content (OMC) of NRM is lower than the HRM under both light and heavy compaction.
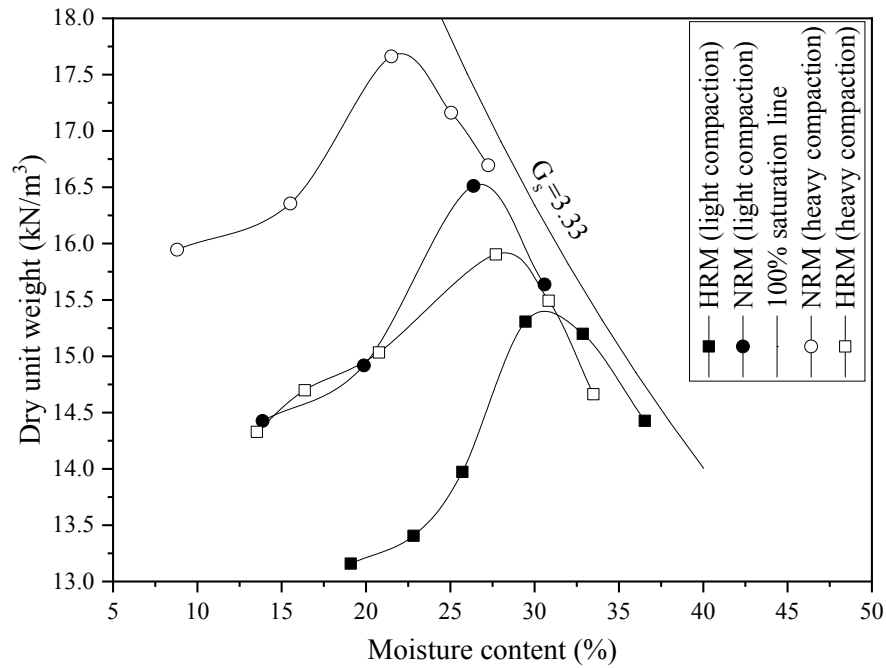
Figure 3.18. Compaction characteristic of RM
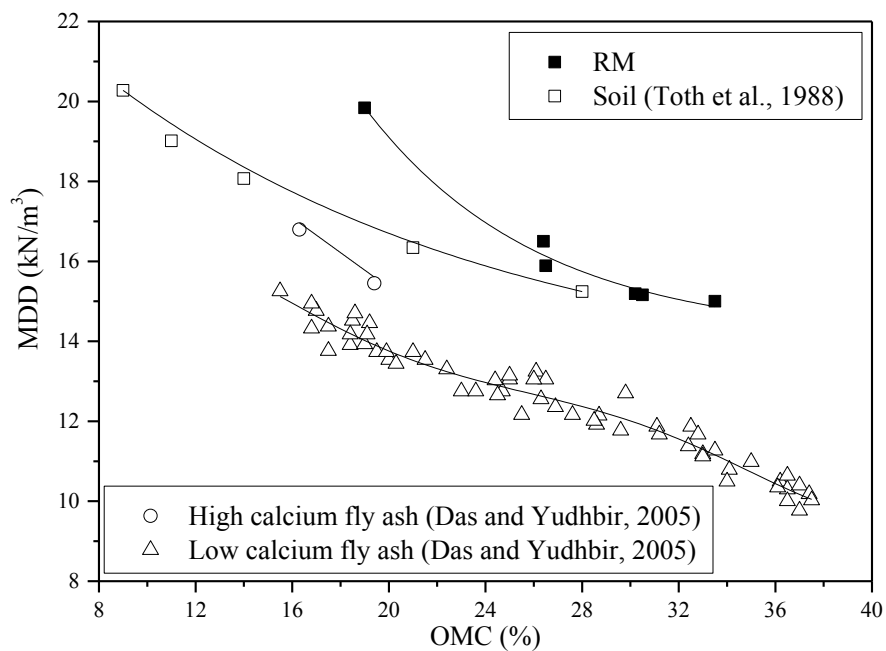
Figure 3.19. Variation of MDD with OMC

Figure 3.19 shows the variation of MDD with OMC, where MDD decreases with increase in OMC value. The variation of MDD with OMC of present study RM along with other RM (from literature), fly ash (Das and Yudhbir, 2005) and soil (Toth et al., 1988) is shown here. It can be seen that similar trend was observed for all the materials. But, the quantitative difference in the trend is due to the variation in G_s values. Higher G_s value has higher MDD value corresponding to same OMC value.

3.4.6 Hydraulic Characteristics

The hydraulic characteristic of both the RM (NRM and HRM) has been presented in term of permeability characteristic and soil-water characteristic curve. The permeability characteristics of both RM (NRM and HRM) with distilled water at different confining stress (100kPa, 300kPa, and 500kPa) are conducted using the flexible wall permeameter (Figure 3.20).

Figure 3.20. Photo of flexible wall permeameter

The remoulded samples with an aspect ratio of 2 are prepared at different moisture content to study the effect of moulding moisture content on the permeability. The effect of salt solution on the permeability characteristics of RM samples compacted at OMC was also studied at above mentioned confining stress. For all confining stresses, the permeability was found to decrease with the increase in moisture content and reached its minimum value at OMC in case of NRM (Figure 3.21a), while HRM shows its minimum permeability at the moisture content approximately 3% higher than OMC (Figure 3.1ba). The permeability of both NRM (Figure 3.21a) and HRM (Figure 3.21b) was found to decrease with the increase in confining stress, which may be due to the decrease in voids at higher confining stress. However, negligible difference in minimum achieved permeability was observed at any confining stresses. In order to study the effect of a different permeant, the permeability of RM with salt solution (10% NaCl) was also studied and the result is presented in Figure 3.21.

(a)

(b)
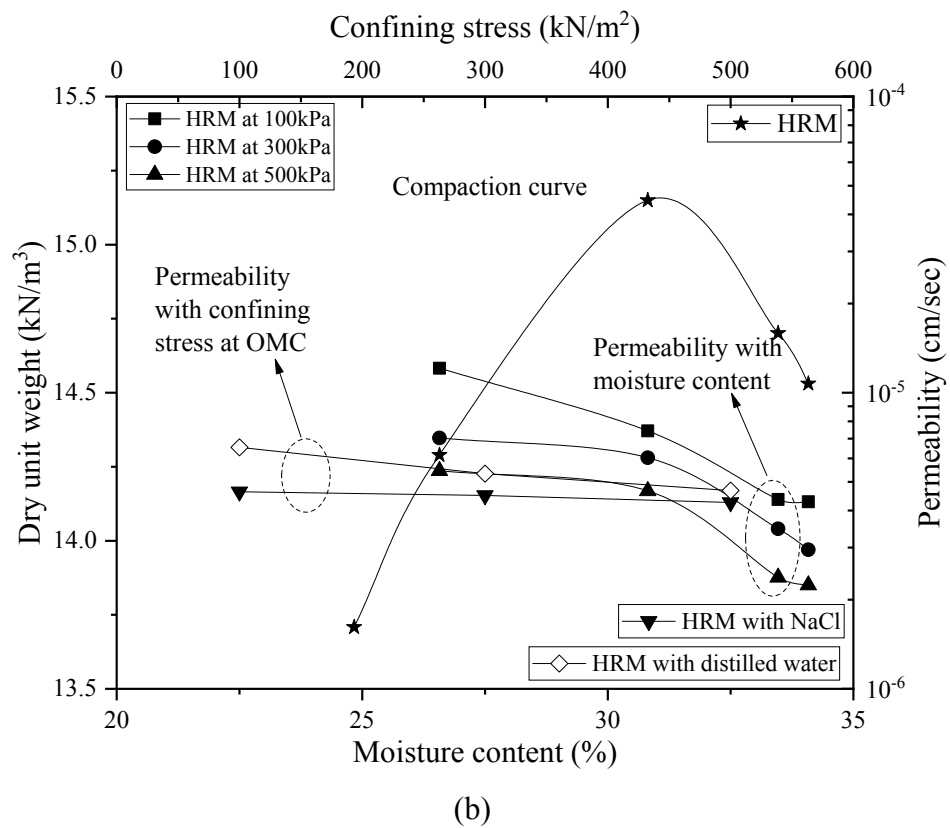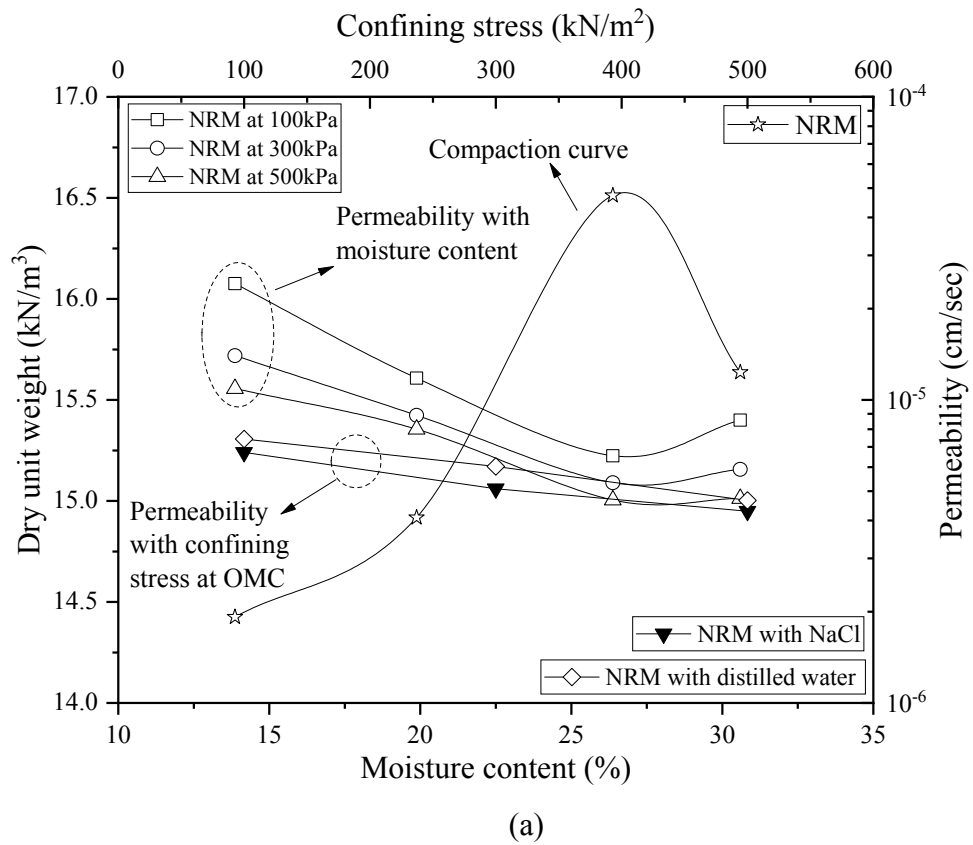
Figure 3.21. Variation of permeability with moisture content, confining stress and type of permeant for (a) NRM (b) HRM

It is observed that both the RM (NRM and HRM) compacted at OMC shows higher permeability towards the distilled water as compared to the salt solution. The lower permeability towards the salt solution may be due to the change in soil structure. Although Na^+ is poor flocculater, it changes the disperse structure into flocculated one and offer the resistant towards the flow of permeant (Spagnoli et al., 2010). Rubinos et al. (2016) reported similar permeability characteristic of ALCOA-San Cibrao bauxite refinery RM in case of $CaCl_2$ and seawater as permeant fluids. The low permeability is having an advantage of ex-situ utilization as liner/barrier materials but the strength requirement must be studied before using the RM. However, the low permeability of RM lowers the dewatering rate of the RM slurry in the pond.

The soil-water characteristics curve (SWCC) plays a significant role in understanding the characteristics of unsaturated soil (Fredlund and Xing, 1994). SWCC can be used to determine the hydraulic permeability, shear parameters, chemical diffusivity etc. (Fredlund et al., 1998). In the present study, the pressure plate apparatus fabricated in the laboratory (Figure 3.22) was used to measure the matric suction in the range of 0.05 MPa to 1.5 MPa, while the Dewpoint Potentiometer was used for the matric suction beyond 1.5 MPa (Campbell et al., 2007).

Figure 3.22. Typical photo of pressure plate apparatus with a pressure cell

A graph of matric suction and volumetric water content using the experimental data is shown in Figure 3.23. The different theoretical models like Brooks and Corey (1964), van Genuchten (1980), Fredlund and Xing (1994), and Kosugi (1996) were used to draw SWCC and it was found that the Fredlund and Xing (1994) model gave the best fit line and has been shown in Figure 3.23. On the same figure (Figure 3.23), a typical SWCC for clayey, silty and sandy soils are also plotted by extracting data from the literature

(Fredlund and Xing, 1994). When comparing the SWCC of NRM and HRM with the typical SWCC of different soil, it can be seen that the SWCC of the RM is very similar to that of silty soil. The SWCC of NRM and HRM lies in between silty soil and clayey soil. It is observed that the SWCC of HRM behave similar to that of clayey soil as HRM contains higher percentage of clay (32%) compare to 14% in NRM (Figure 3.15). It need to be pointed out here that the RM contains less amount of clay minerals.
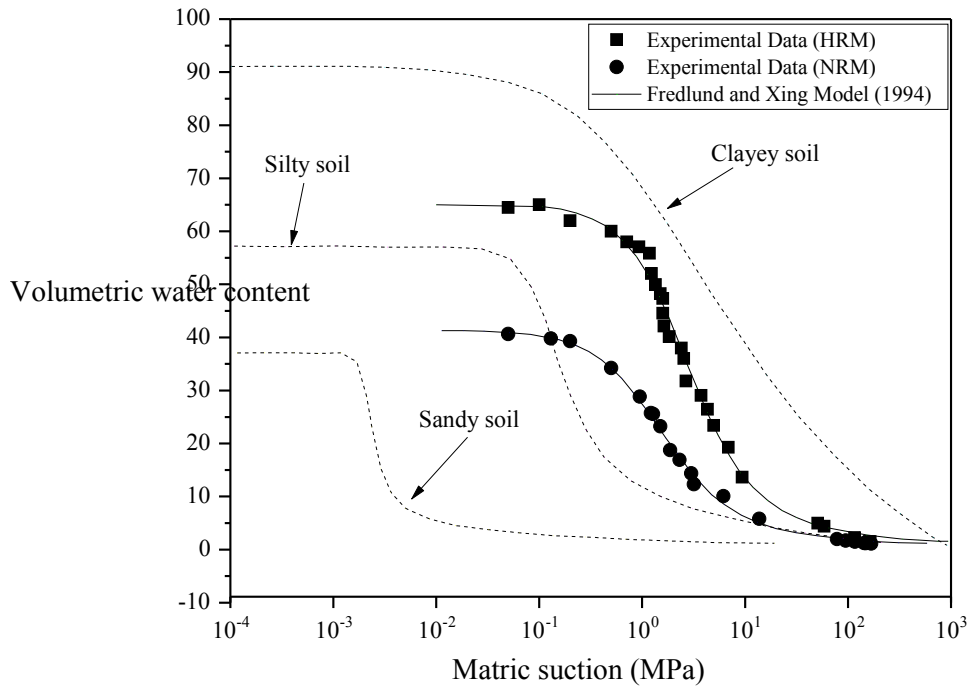
Figure 3.23. SWCC of NRM and HRM along with clayey, silty and sandy soil

3.4.7 Free swell index and dispersion characteristic

As the RM contain mostly fine particles along with the considerable amount of clay fraction, it also becomes important to study the swell behaviour of RM. In the present study, differential free swell (DFS) was considered to find the swell index of RM as per the method described by Sivapullaiah et al. (1987). It was observed that RM is non-expansive with negative DFS value of -26.67% and -14.71% for NRM and HRM, respectively. Sivapullaiah et al. (1987) studied several clay soils and found that the dispersive soil shows the negative DFS. Hence, negative DFS value of RM indicates that it may be dispersive in nature. The NRM is classified as highly dispersive (D1) while HRM is classified as dispersive (D2) based on the pinhole test result. The detail of the dispersive nature of the RM is discussed in Chapter 4.

3.4.8 Unconfined Compressive Strength

The unconfined compressive strength (UCS) tests on both, NRM and HRM were performed as per ASTM D2166. The remoulded samples (5 cm x 10 cm) were prepared at different moisture content. The variation of UCS with different moisture contents is shown in Figure 3.24. It can be seen that the UCS increases with the increase in moisture content up to a maximum value of 564.08 kPa (NRM) and 441.45 kPa (HRM) at their OMC and then decreases.
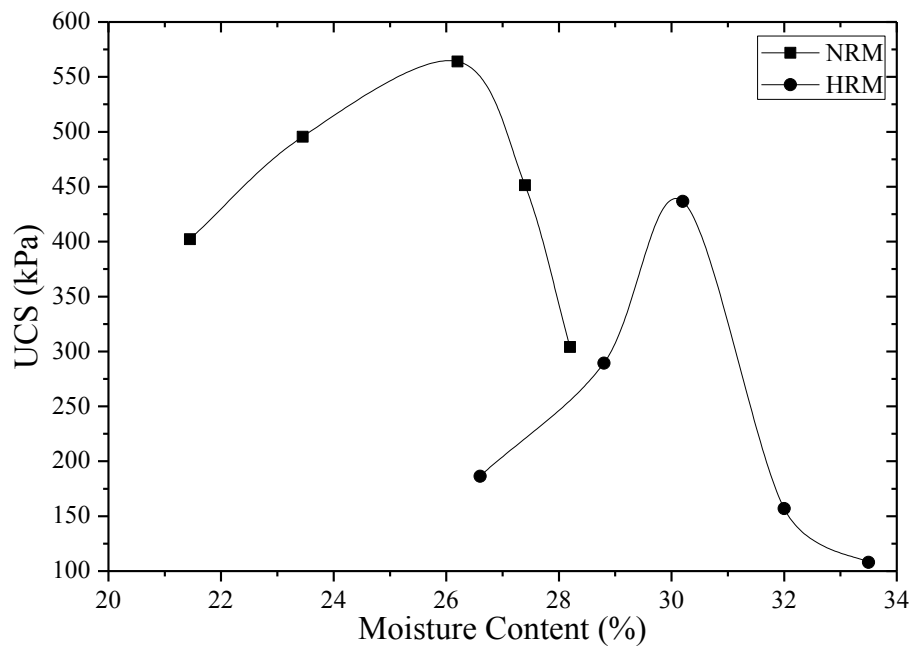
Figure 3.24. Variation of unconfined compressive strength of RM

3.4.9 Laboratory Shear Test

The direct shear test was performed on both the RM (NRM and HRM) as per Indian standard (SP -36 (1), 1987) at their OMC to study the shear strength of RM. It was found that HRM possesses a higher angle of internal friction (ϕ) (37.96°) than NRM (31.11°), which may be due to the higher percentage of angular particles in a coarse fraction of HRM. Nikraz et al. (2007) have also found higher ϕ value of Bayer's process RM varying from 37° to 45°. The higher friction angle of HRM may be due to the presence of a higher percentage of the sand-sized particle (17%) as compared to NRM (5%) as shown in Figure 3.15. On the other hand, cohesion value of NRM (35.93 kPa) is much higher than HRM (5.57 kPa) as the total fine content is more in NRM (95%) though HRM contains a higher percentage of clay (32%) than NRM (14%). In overall, it may be also mentioned here that the ϕ value of both RMs is comparatively high, though, they contain mostly clay-sized

particle. Similar observations have been made by Newson et al. (2006) for Bayer's process RM.

3.4.10 California Bearing Ratio

California bearing ratio (CBR) test is very commonly used for the design of flexible pavements. To characterize the RM as a subgrade material, un-soaked and soaked CBR test of both the RM (NRM and HRM) at OMC were performed according to ASTM D1883-16. It was observed that the unsoaked and soaked CBR value of RM is 15.53% and 2.00%, respectively. As the CBR value of the RM is very low, the RM may be treated before its use as subgrade material to improve its CBR value in order to reduce the thickness of pavement (IRC: 37-2001).

3.4.11 Consolidation

The consolidation behaviour of both the RM (NRM and HRM) was studied as per Indian standard (IS 2720:15 2002). The slurry sample of NRM and HRM was filled into the mould with an initial void ratio of 0.91 and 1.13, respectively. The RM slurry was prepared by adding an arbitrary amount of water which was 29.35% and 37.30% for NRM and HRM, respectively. The consolidation curve for NRM and HRM are shown in Figure 3.25 and Figure 3.26, respectively.
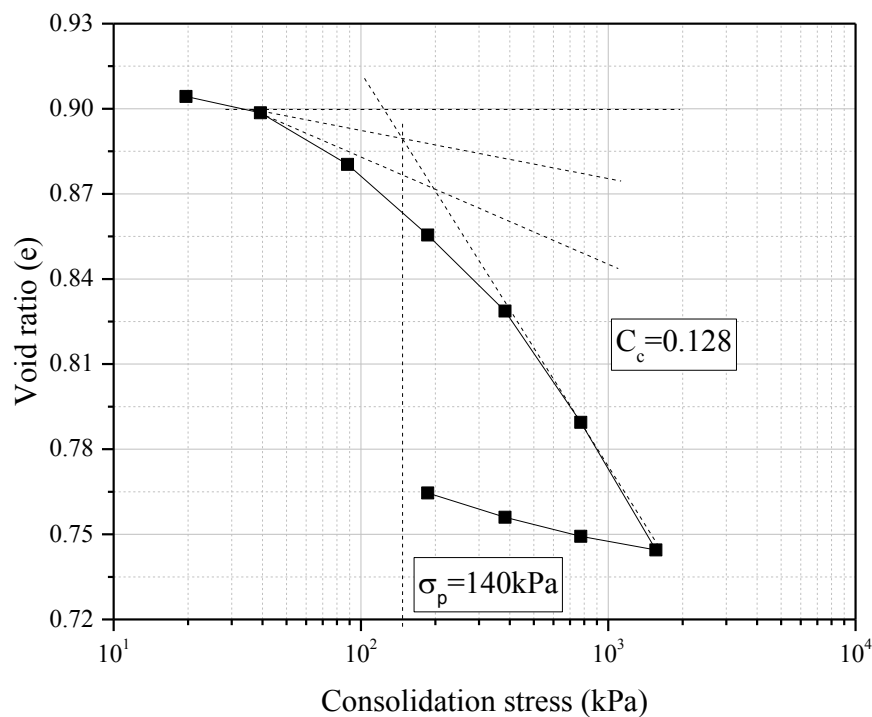
Figure 3.25. Consolidation characteristic of NRM
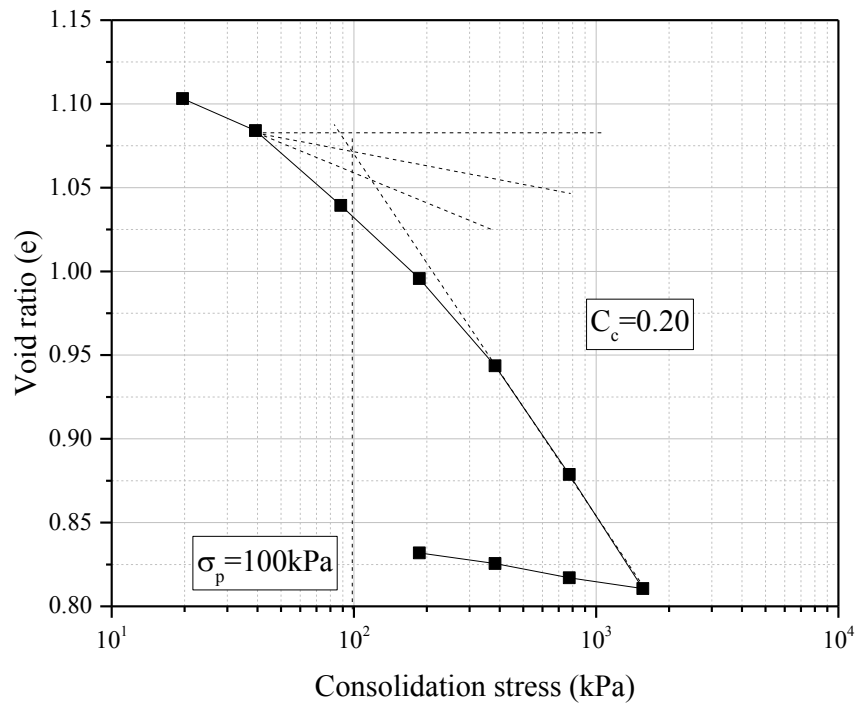
Figure 3.26. Consolidation characteristic of HRM

3.4.12 Collapse Behaviour

One of the important geotechnical problem associated with partially saturated compacted soil is their collapse behaviour under inundation pressure. The unsaturated collapsible soil may withstand relatively higher vertical stress with a small settlement, but large settlement takes place at the same vertical stress when it is flooded. For the construction of infrastructure on abandoned RM pond, collapse potential is important. Collapse behaviour of the RM investigated as per ASTM D5333-03. Three number of the unsaturated samples with same initial moisture content and dry density were prepared in oedometer test apparatus and studied for the collapse behaviour. The vertical stress applied to the soil sample. The first sample flooded at the vertical stress of 160 kPa, the second sample flooded at the vertical stress of 320 kPa and the third sample flooded at the vertical stresses of 640 kPa. The pressure vs void ratio curve of all three soil samples are shown in Figure 3.27 and Figure 3.28 for NRM and HRM, respectively. It is observed that NRM is moderately to severe collapsible with collapse potential (I_c) value of 7.8 at lower inundation pressure, while, at higher inundation pressure, it is moderately collapsible with I_c value of 2.73. Similarly, HRM is moderately collapsible (I_c = 3.46) at lower inundation pressure and slightly collapsible (I_c = 1.97) at higher inundation pressure. It may be due to the fact that low pressure is not effective in compaction of

unsaturated RM; hence large settlement was observed after inundation. But, high compaction pressure was found to be effective and reduced the collapsibility of RM as small settlement observed after inundation. Further, for the same inundation pressure, NRM is more collapsible than HRM.
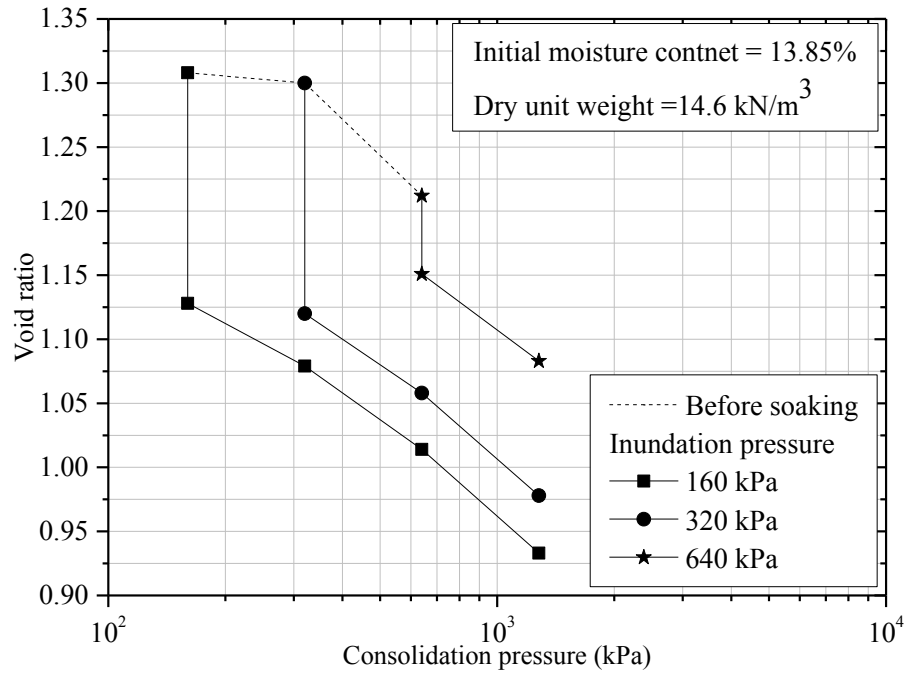
Figure 3.27. Collapse behaviour of NRM
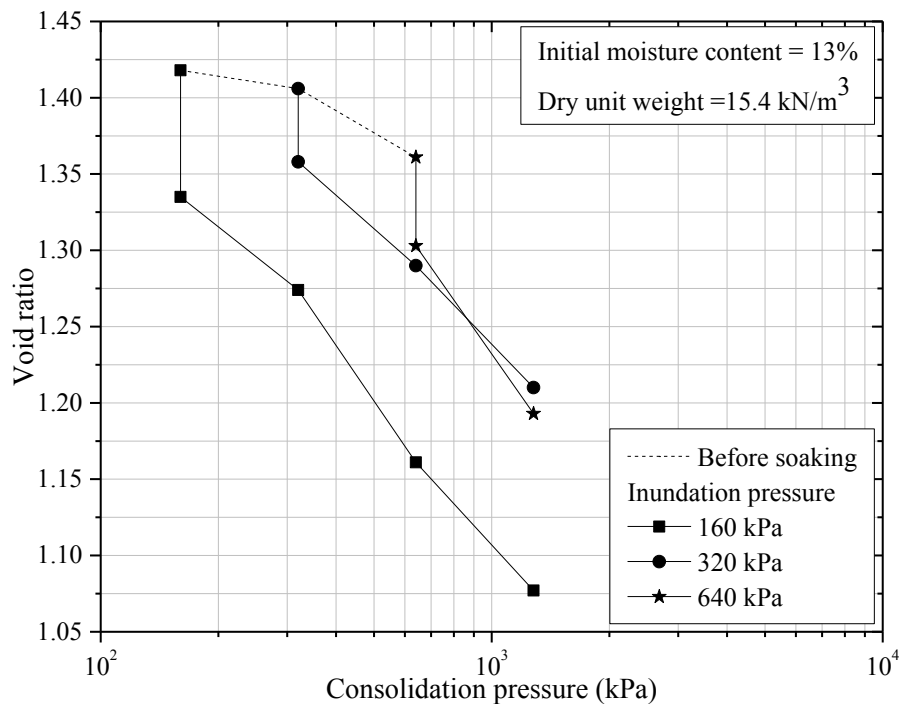
Figure 3.28. Collapse behaviour of HRM

51

3.4.13 Leachate Analysis

The samples for leachate analysis were prepared as per EPA test method 1311. The leachate separated from solution using 0.45μm filter paper was analyzed using atomic absorption spectroscopy and the concentration (average of three replicas) of different heavy toxic metal in leachate is presented in Table 3.3.

Table 3.3 The concentration of heavy metal in RM detected using AAS.

Heavy metals	Concentration (ppm)			
	NRM	HRM	Regulatory level for toxicity characteristic as per EPA, United State	Acceptable limit in drinking water as per WHO
As	0.002	0.032	5.00	0.010
Cr	1.832	2.590	5.00	0.050
Pb	-	-	5.00	0.010
Hg	0.004	0.002	0.20	0.006
Ni	0.019	0.009	-	0.070
Cu	0.004	-	-	2.000
Zn	0.005	0.007	-	0.01-0.05

It is observed that the concentration of toxic heavy metals as identified by United State EPA (As, Cr, Pb and Hg) is at a regulatory level in both NRM and HRM. The concentration of Cr in NRM and HRM is found as 1.832 ppm and 2.59 ppm respectively, which is very similar to Cr (3.97 ppm) concentration as observed in RM from Spain (Rubinos et al. 2016). Yao et al. (2013) found higher Cr (11.89 ppm) concentration along with Zn (0.019 ppm), and Pb (0.002 ppm) in the RM from Texas. It may also be mentioned here that the chromium present in the RM is in the form of Cr^{+3} (Burke et al. 2012). The leachate from HRM is found to have As (0.032 ppm) similar to the value reported by Yao et al. (2013) (0.034 ppm), while NRM shows the lower concentration of As (0.002 ppm). The Pb was not detected in the leachate of either RM. Although the concentration of heavy metals As, Cr, and Hg in leachate are within the EPA toxicity regulatory limits, but it is above the regulatory limit in drinking water as suggested by WHO. So the chemical analysis of drinking water is required as the ex-situ utilization of RM may contaminate the nearby drinking water sources.

3.5 Conclusion

Laboratory investigations have been performed for geotechnical characterization of two Indian RM and based on that, following conclusions can be drawn.

1. Based on the morphological study, it was found that RM contains the majority of angular to a subangular agglomerated particle of different sizes. The XRF analysis reveals that the RM contains Fe_2O_3 as the major constituent. Based on the hump position in XRD plot, the RM was also found to contain the amorphous oxides.

2. The RM was found highly alkaline and the pH value depends upon the percentage of CaO and Na_2O. The Bayer's process RM was identified with lime index < 0.5 and CaO < 25%.

3. The HRM contains higher clay fraction (~32%) as compared to NRM (~14%). The liquid limit of HRM (39.89%) also found higher than that of NRM (30.75%), which may be due to the higher clay content and low LL due to the presence of low clay minerals.

4. The permeability of both the RM show higher resistant to the flow of salt solution as compared to distilled water due to change in soil structure.

5. The RM is found to have negative DFS value which shows that RM is dispersive in nature. Based on pinhole test NRM is found highly dispersive and HRM is found dispersive in nature.

6. Based on AAS result, the heavy toxic metals as identified by United State EPA were found within toxicity level in leachate generated from RM.

7. Though the angle of internal friction of both the RM was found very near to each other, the remarkable difference in the cohesion was observed. This may be due to the difference in fine content.

As very few studies are available regarding the geotechnical characterization and application of Indian RM and the international status showed a large variability in properties of RM depending upon the source, this chapter discussed mainly the basic geotechnical characteristic of Indian RM from two different sources. As the RM shows the negative differential free swelling index, which indicates that the RM may be dispersive in nature. Also, high pH of RM may hinder the sedimentation, the dispersive and sedimentation characteristic of RM are discussed in Chapter 4.

Chapter 4

Dispersive and Sedimentation Characteristic

4.1 Introduction

Various attempts have been made to characterize and utilize the RM but due to the low utilization rate, a large volume of unutilized RM remains in the pond. Also, the occasional collapse of RM reservoir dam like Ajka (Hungary) left an adverse impact on the nearby area by flooding (Mayes et al., 2016). As the RM is dispersive (Rout et al., 2013), so, on-site stabilization/management of RM is one of the important aspects to prevent its spreading into the nearby area due to erosion and during occasional failure of the dam. Hence, this chapter covers the dispersiveness and sedimentation characteristics of Indian RM, from two different sources with different types of the disposal system. The pin-hole test and cylindrical dispersive test along with morphology, chemistry, and mineralogy are investigated to correlate the dispersive properties of RM with its basic properties. Another aspect of RM management is accelerating the sedimentation rate of the RM slurry to reduce the sedimentation time. So an attempt has also been made to study the sedimentation behaviour of bauxite residue at the ambient condition and the effect of different additives (phosphogypsum and salt solution) on the rate of sedimentation.

4.2 Stabilizing Materials and Methodology

The phosphogypsum used in the present study were collected from the Paradeep Phosphates Limited, Odisha while the NaCl powder was supplied by Merck Life Science Private Limited. The biopolymer (Guar gum and Xanthan gum) were supplied by HiMedia Laboratories Private Limited.

The laboratory investigation on dispersive and sedimentation properties along with morphology, chemistry, and mineralogy of the RM is presented. The RM was stabilized using biopolymer (Guar gum and Xanthan gum) and salt (NaCl) to control the dispersiveness. Phosphogypsum and salt solution (NaCl) were used to accelerate the rate

of sedimentation of NRM slurry. The dispersiveness and sedimentation tests were performed according to relevant Indian standards (SP-36(1), 1987) and ASTM standards (D4647). Dispersive characteristics were studied using pin-hole test and cylindrical dispersive test with different fluids (i.e., distilled water and salt solution). To simulate the field condition, the column sedimentation test of RM slurry was conducted with 40% solid content. The X-ray fluorescence (XRF) analysis was performed using Axios PANalytical with scintillation type detector at 20kV and 10mA for detailed chemical analysis. The particle morphology and chemistry were studied using scanning electron microscope (SEM) (JEOL-JSM-6480 LV model) fitted with energy-dispersive X-ray (EDX) micro analyzer at 20kV acceleration voltage and spot size of 60. The platinum coating was applied on RM at 30mA for 90 seconds before loading the sample for analysis. The chemical analysis of supernatant liquid was performed using atomic absorption spectroscopy (AAS) along with pH, Zeta potential, total dissolved solids (TDS), and electrical conductivity (EC) measurement for its possible reuse. The pH was measured using HACH HQ40d model pH meter and TDS, EC and Zeta potential were measured through Nano Zetasizer.

4.3   Result and Discussion

4.3.1 Chemistry of Stabilizing Agent

The chemistry of the phosphogypsum was studied using the XRF and was found that the phosphogypsum is rich in SO_3 (54.38%) and CaO (35.77%) along with 7.15% SiO_2 (Table 4.1).

Table 4.1. Chemical composition of phosphogypsum

Chemicals	Na_2O	MgO	Al_2O_3	SiO_2	P_2O_5	SO_3	K_2O	CaO	Fe_2O_3
Conc. (%)	0.05	0.02	0.23	7.15	0.79	54.38	0.26	35.77	0.47

4.3.2 Dispersive Test

During the sample collection from NRM pond, channel formation at the surface of dry RM (Figure 4.1) due to the flow of water was observed. This channel formation indicates the susceptibility of RM towards water erosion due to dispersive nature. The dispersive nature is also confirmed by negative differential free swelling of RM as discussed in Chapter 3. The RM due to its high alkalinity can be favourable for leachate transport

(Dijkstra et al., 2004) and may pollute the groundwater and the nearby aquatic lives, hence, it is important to know and control the dispersiveness. In the present study double hydrometer test, crumb test, turbidity test, sodium absorption ratio (SAR) (Rout et al., 2013), pinhole test (ASTM D 4647-13 2006), and cylindrical dispersive (Atkinson et al., 1990) test were conducted to know the extent of dispersiveness. As true cohesion is the governing factor that affects the internal erosion (Atkinson et al., 1990), which in turn is affected by pore pressure. During crumb and pinhole test, the sample may not be saturated, and negative pore pressure may generate, which may affect the result.

Figure 4.1. A typical picture showing the susceptibility of RM towards water erosion in a RM pond
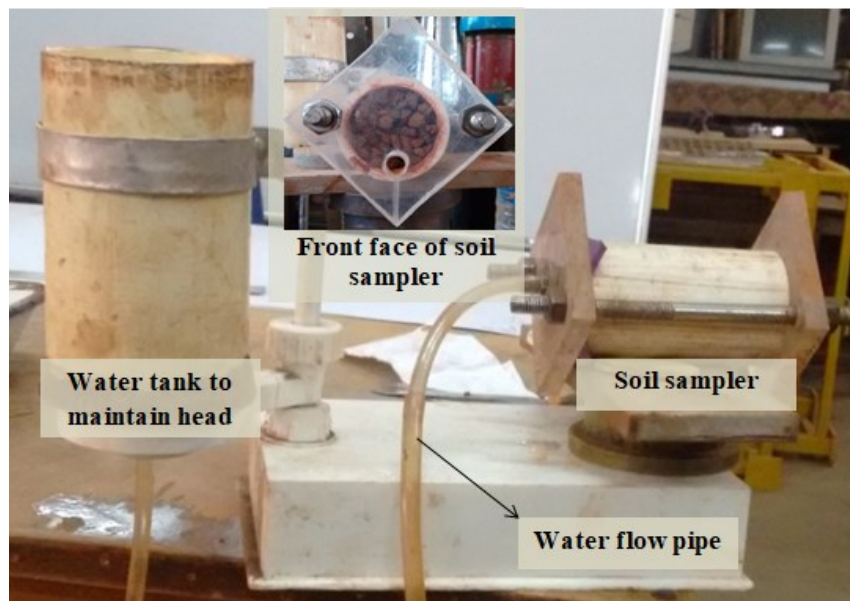
Figure 4.2. Typical photo of pinhole test setup

Hence, in the present study, pinhole test as per the ASTM D 4647-13 and the cylindrical dispersive test as per method reported by Atkinson et al. (1990) has been performed. Based on the pin-hole test (Figure 4.2) with collected water quality (Figure 4.3) and the enlarged diameter of the hole (Figure 4.4) during the test, NRM is classified as highly dispersive (D1) while HRM is classified as dispersive (D2) as per the ASTM D4647-13 (2013). Rout et al. (2013) also found the NRM as highly to extremely dispersive based on double hydrometer test, crumb test and turbidity test.
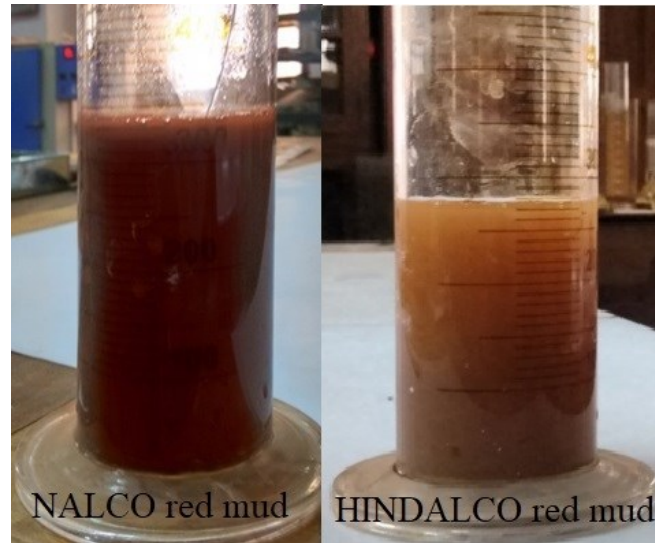
Figure 4.3. Water collected during pinhole test
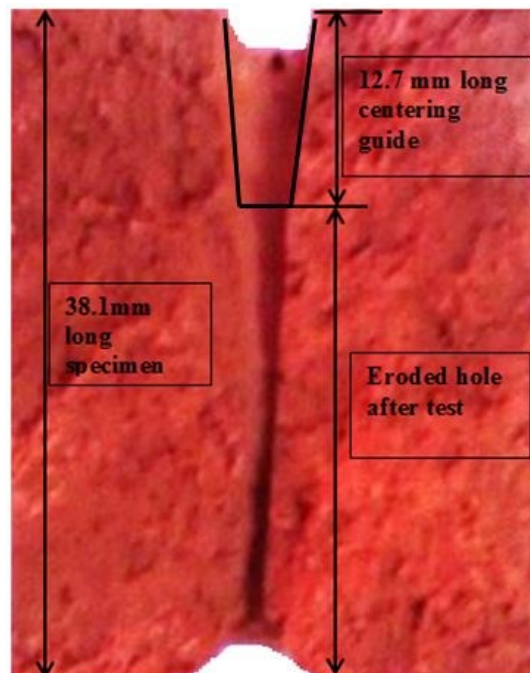
Figure 4.4. Specimen showing the enlargement of hole diameter inside RM sample after pinhole test.

There are different stabilization methods to control the dispersiveness of soil; alum (Ouhadi and Goodarzi, 2006), pozzolana (Vakili et al., 2013) and ZELIAC (a mixture of zeolite, activated carbon, limestone, rice husk and Portland cement) (Vakili et al., 2017). However, chemical stabilization methods have their limitation in terms of environmental sustainability. Hence in the present study, an attempt has been made to control the dispersiveness of the RM using two natural gums (biopolymer); guar gum (GG) and xanthan gum (XG) and also using salt solution (NaCl). Recently, Chen et al. (2013) used the GG and XG to stabilize the mine tailings. The results of the cylindrical dispersive test of un-stabilized RM conducted according to the method reported by Atkinson et al. (1990) is shown in Figure 4.5. It can be seen that the surrounding water become muddy after submerging the un-stabilized sample into it (Figure 4.5). After getting submerged into the water, the highly negatively charged RM particles from un-stabilized sample starts detaching from each other and remains suspended due to strong intraparticle repulsive force (Abel and Stangle, 1994; Martinez, 2012).

Figure 4.5. Cylindrical dispersive test of un-stabilized NRM (present study)

The Figure 4.6 shows the cylindrical dispersive test (Atkinson et al., 1990) of 0.5% GG and XG stabilized RM. It is observed that the 0.5% biopolymer as a pore fluid is effective in binding together the RM particles by overcoming the intraparticle repulsive force; thereby controlling the dispersiveness (Figure 4.6). The binding action of biopolymers arises due to the formation of hydrogen bond in case of GG (naturally charged

polysaccharide) and ionic bond in case of XG (anionic polysaccharide) (Chen et al., 2013).
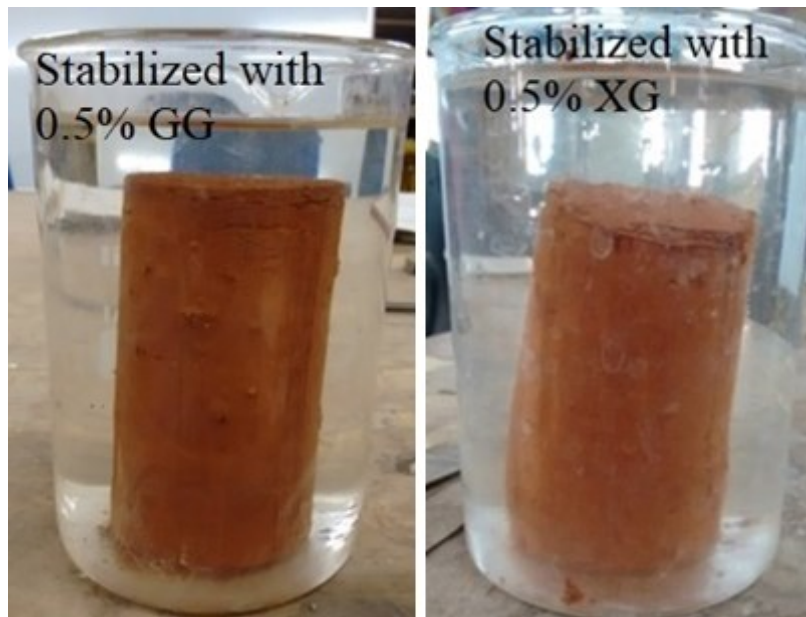
Figure 4.6. Cylindrical dispersive test of GG and XG stabilized RM

The SEM images of NRM stabilized with 0.5% GG and 0.5% XG solution is shown in Figure 4.7 (a) and (b) respectively. It is found that the XG (Figure 4.7b) causes a higher level of aggregation as compared to GG (Figure 4.7a).
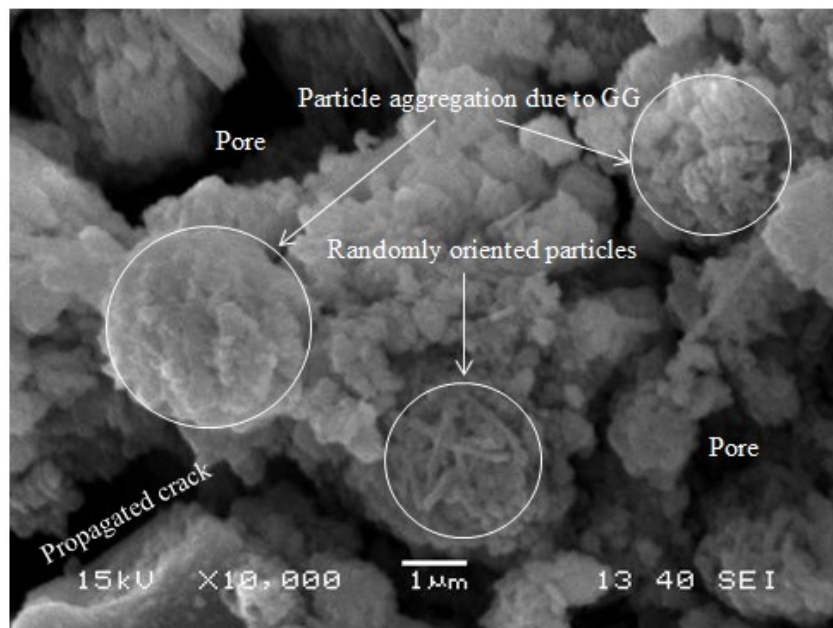
(a)
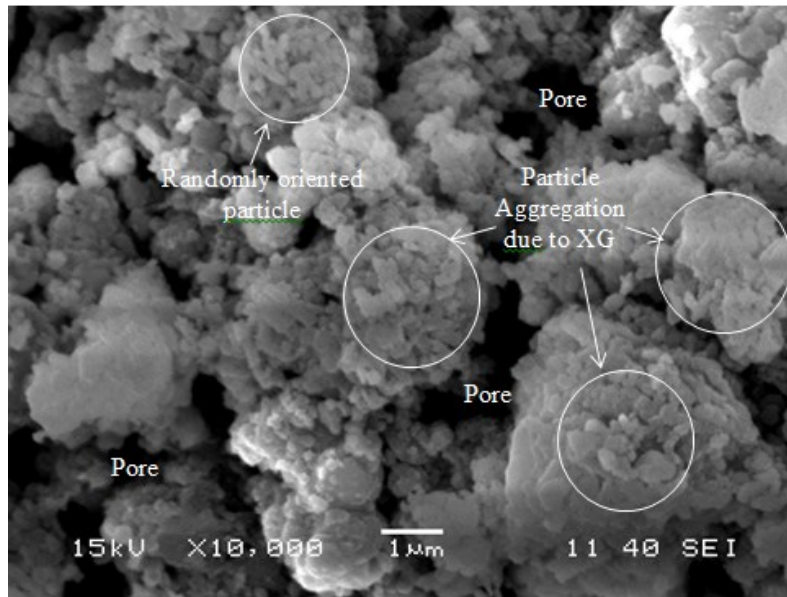
(b)

Figure 4.7. SEM image of (a) GG stabilized RM (b) XG stabilized RM

The higher level of aggregation is due to the formation of the ionic bond during the reaction of XG with cations (Fe^{2+}, Cu^{2+}, Na^{1+}) present in the RM. In contrast, stabilization of RM using GG solution induce less aggregation due to the formation of hydrogen bonding between the GG and RM particles (Chen et al., 2013) with randomly oriented particles (Figure 4.7a). Along with the high level of aggregation, it is also found that the stabilization with XG makes a denser matrix (Figure 4.7b) with low void space as compared to the RM stabilized with GG (Figure 4.7a). In field condition, biopolymer can be applied at the discharge point of RM when it is disposed of in slurry form, whereas in case of dry disposal, biopolymer can be mixed in RM before filter press. The mixing of biopolymer will reduce the surface erosion of stored RM due to the flow of water; thereby reducing the leachate effect of RM. However, a system for the proper mixing of the biopolymer with RM needs to be explored further.

The effect of the salt solution with varying NaCl concentration (1% to 9%) as a pore or as surrounding fluid on the dispersive characteristic of RM was also studied. The salt solution was prepared in the laboratory by mixing the different percentage of NaCl in distilled water. Two samples, one with salt solution and other with distilled water was prepared. The former is submerged into the distilled water while the latter is submerged into the salt solution. It was found that the salt solution with 7% or higher NaCl concentration is effective in controlling the dispersiveness when used as pore fluid. However, when used as surrounding fluid, a salt solution with 3% or more NaCl

concentration is found effective (Figure 4.8).
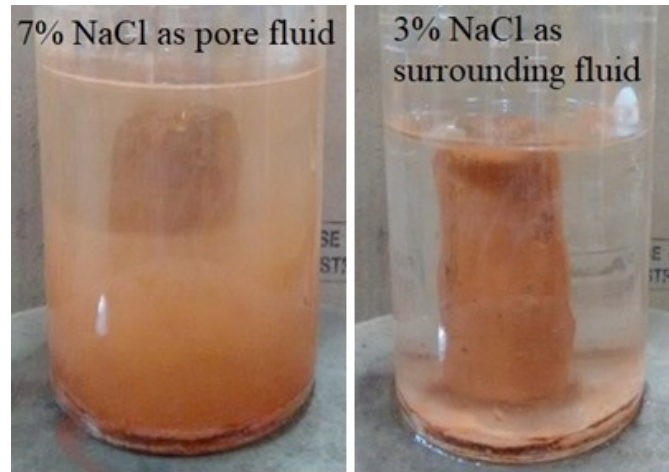
Figure 4.8. Cylindrical dispersive test of NaCl stabilized RM

Based on the above result, a salt solution with 3% or more NaCl concentration can be suggested to sprinkle on abandoned RM pond which will have another advantage of controlling the water erosion. The sea water can also be used to sprinkle as it contains high NaCl concentration but the present study is based on the solution prepared by mixing 99% pure NaCl into distilled water.

4.3.3 Column Sedimentation Test

The disposal of RM in slurry form contains low solid content (15%-40% by volume) (Yang and Xiao, 2008). Due to the dispersive nature of the RM as discussed in the previous section with high pH value, the sedimentation rate is very low. In the present research, phosphogypsum, a fertilizer industry waste, and commercially available NaCl are used to treat the RM; thereby accelerate the rate of sedimentation. The RM slurry with 40% solid content was prepared in the laboratory and treated with different percentages (5%, 10%, and 15 % by weight of RM) of phosphogypsum powder or with 1%, 3% and 5% (by volume of solvent) NaCl solution. In the column sedimentation test as described by Jaditager and Sivakugan (2017), the treated RM slurry is poured into the transparent glass cylinder up to a height of 24cm and allowed to settle under gravity. The height of RM-water interface was measured at different time interval with the help of ruler as shown in Figure 4.9. Sedimentation characteristic observed during column sedimentation test is presented in terms of changes in interface height with times in Figure 4.9 for untreated RM (UTRM). It should be mentioned here that the interface height refers the height of supernatant liquid. It is found that the particles in the untreated RM slurry do not flocculate and settles freely without any mutual interaction. So the

settling behaviour of the RM slurry can be designated as dispersed free settling (settling type I) as discussed by Imai (1980). The sedimentation curve can be divided into three different zones, i.e., flocculation zone, settling zone, and consolidation zone (Imai, 1981). The sedimentation process of the RM slurry (Figure 4.10) consists of all the three zones. After the disposal of untreated RM (UTRM) slurry, the particles remain in flocculation stage for the long duration as denoted by flocculation zone in Figure 4.10.
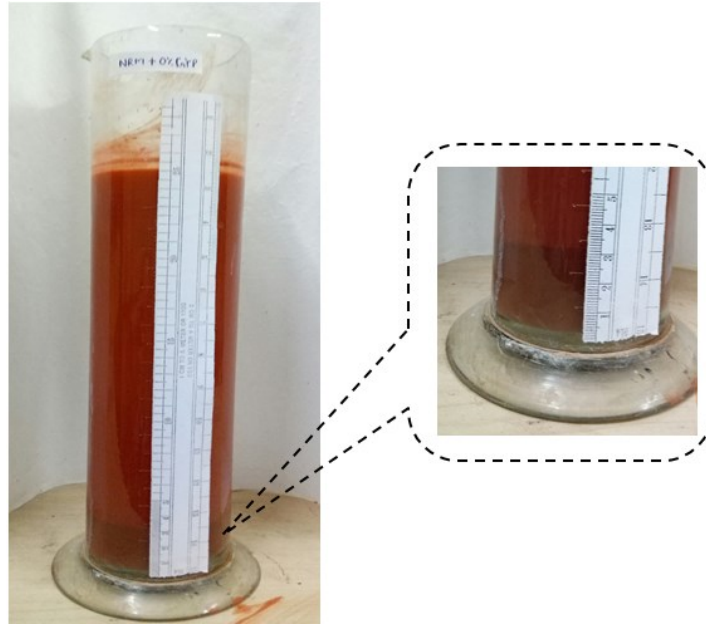
Figure 4.9. Column sedimentation test setup of untreated RM (UTRM) slurry
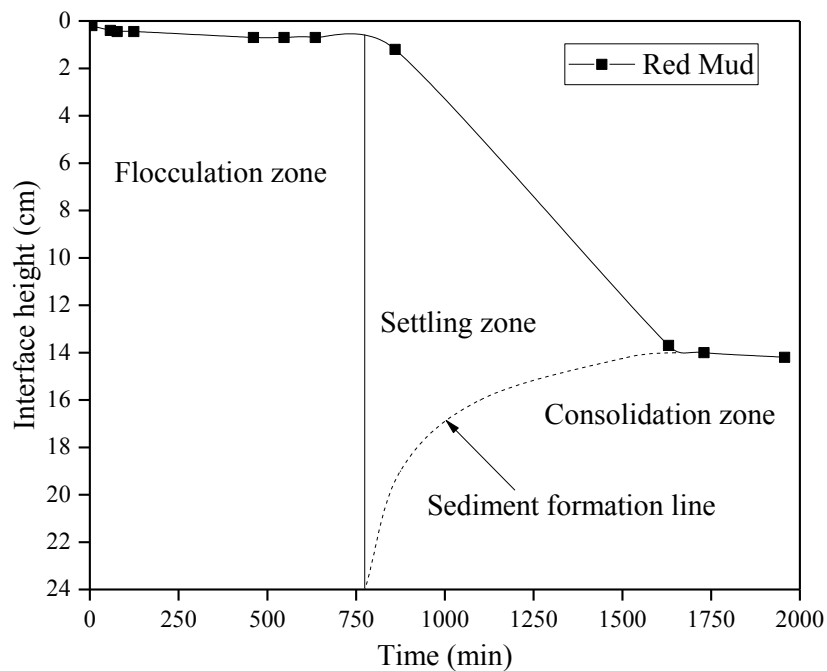
Figure 4.10. Sedimentation characteristics of untreated RM (UTRM) slurry

At the end of flocculation stage, settling of heavier particles, mostly iron oxide, which is in majority (Chapter 3), start under gravity and it also takes long duration before going into the consolidation stage. In overall, it can be said that the sedimentation process of RM slurry is very slow. The stable suspension of RM slurry is due to the high magnitude of Zeta potential (37.1 mV) of negatively charged particles (Table 4.2) at the corresponding pH value of 11.4 (Abel and Stangle, 1994). The Zeta potential and corresponding pH value along with electrical conductivity (EC) and total dissolved solids (TDS) of untreated and treated RM slurry are presented in Table 4.2. Hirosue et al. (1988) reported that fine particles of RM can be coagulated by lowering the magnitude of Zeta potential below 13 mV, which can be achieved by maintaining the pH in between 7 to 8.

Table 4.2. Zeta Potential, pH, EC, and TDS value of untreated and treated RM slurry

Basic material	Percentage of additives		Zeta potential (mV)	pH	EC (mS/cm)	TDS (ppm)
	Phosphogypsum	Salt				
Red Mud	0	0	-37.10	11.40	1.50	757.96
	5	0	-7.32	7.61	7.64	3860.54
	10	0	-9.93	7.64	7.41	3744.32
	15	0	-9.81	7.42	7.39	3734.21
	0	1	-10.96	8.44	88.77	44854.30
	0	2	-13.87	8.68	36.03	18207.85
	0	3	-21.27	8.24	10.12	5112.01

Hence, in the present study, phosphogypsum and salt solution (NaCl) was used to reduce the Zeta potential (ζ) of RM slurry by reducing the pH and thereby accelerating the rate of sedimentation by agglomeration of the particles. It was found that the treatment of RM slurry with phosphogypsum reduces the magnitude of Zeta potential to 7 mV (5% phosphogypsum) to 10 mV (15% phosphogypsum) from 37.1 mV but the particles remain negatively charged. Similarly, the pH value reduces to 7.42 (5% phosphogypsum) - 7.61 (15% phosphogypsum) from 11.4. The treatment of RM slurry using salt (NaCl) solution is also found effective in lowering the magnitude of Zeta potential from 37.1 mV to in between 10.96 mV (1% NaCl) and 21.27 mV (5% NaCl) while the pH gets reduced to in between 8.24 (1% NaCl) and 8.44 (5% NaCl). The lower magnitude of Zeta potential lowers down the repulsive force between the adjacent particles causing coagulation, thereby accelerating the sedimentation rate (Yukselen and Kaya, 2003). The column sedimentation test setup (Jaditager and Sivakugan, 2017) of RM slurry treated

with phosphogypsum and NaCl is shown in Figure 4.11 and Figure 4.12 respectively.
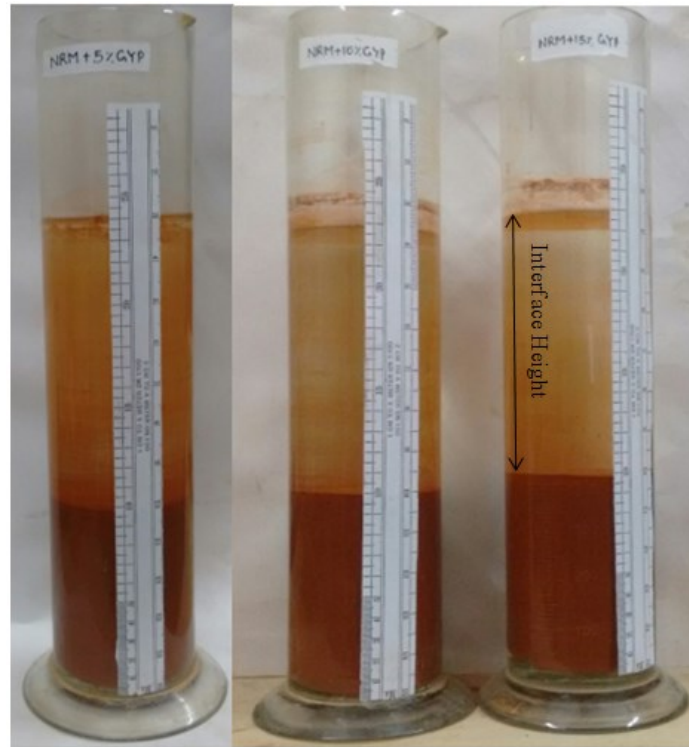
Figure 4.11. Column sedimentation test setup of phosphogypsum treated RM (P-TRM) slurry
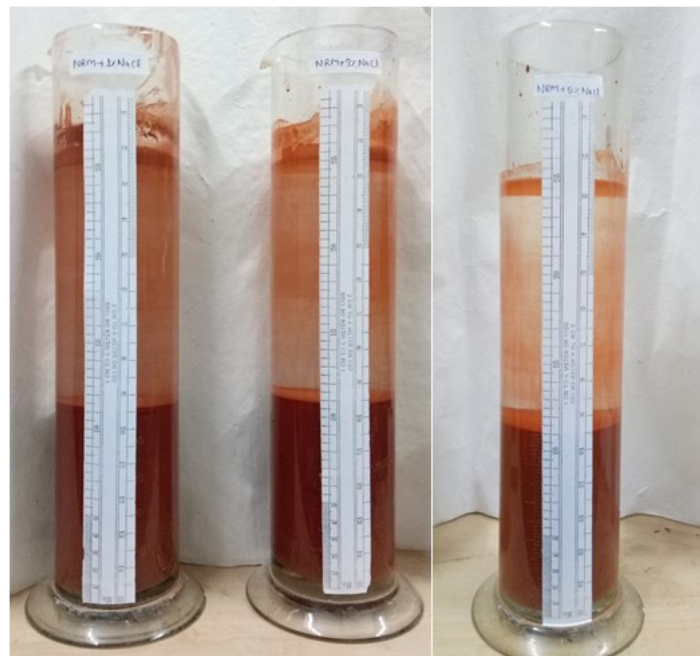
Figure 4.12. Column sedimentation test setup of NaCl treated RM (N-TRM) slurry

The sedimentation characteristics of the RM treated with phosphogypsum and NaCl is compared in Figures 4.14a and 4.14b respectively. The shape of settling curve of treated

RM is found similar trend without flocculation zone but different settling rate (Jaditager and Sivakugan, 2017). The final sediment thickness decreases with the increase in the percentage of phosphogypsum or NaCl concentration, but still higher than that of UTRM.
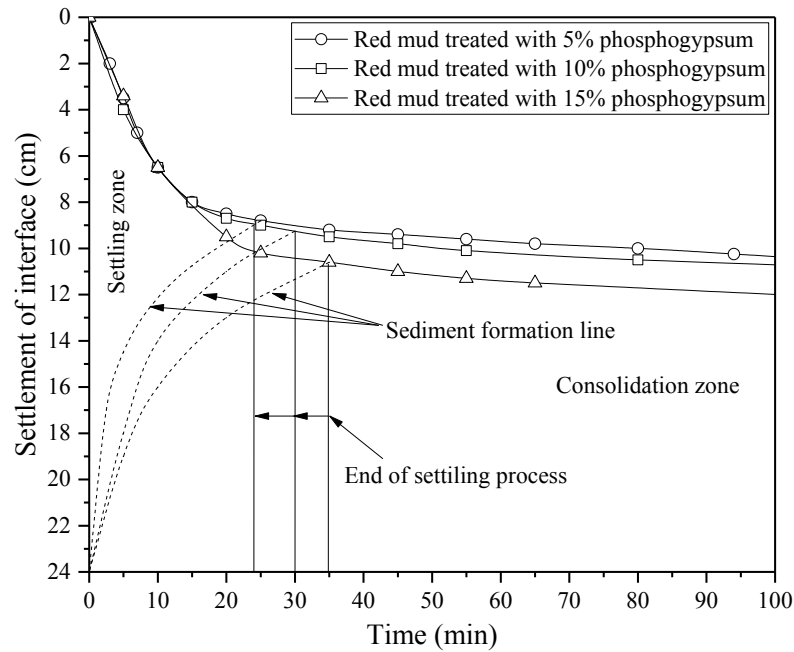
(a)
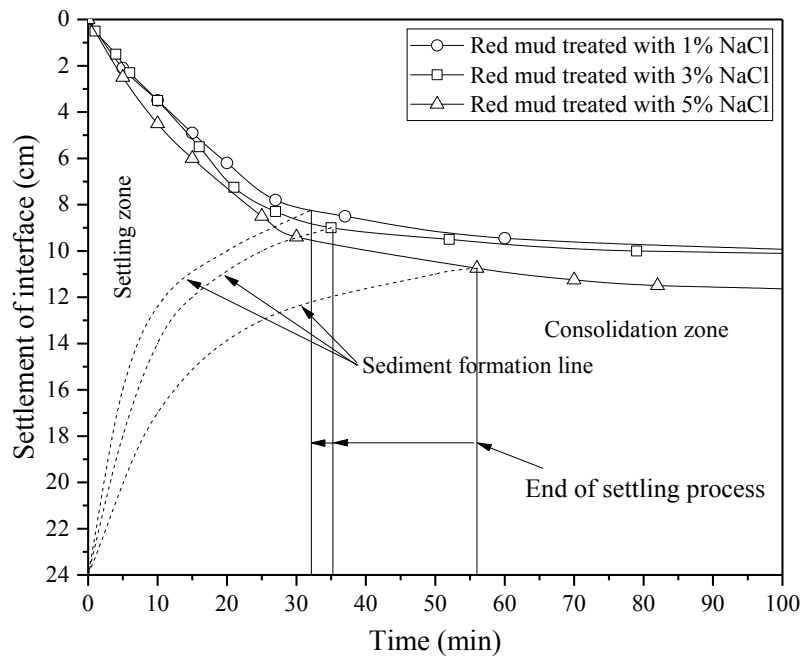
(b)

Figure 4.13. Sedimentation characteristics of (a) P-TRM (b) N-TRM

It was observed that the RM slurry treated with phosphogypsum or NaCl solution undergoes flocculation and settles with the strong mutual interaction between them. Imai

(1980) described this settling behaviour as zone settling (settling type III). The thickness of final sediment depends upon the formation of flocculates in the suspension, which in turn depends on the Zeta potential. It can be seen in Figures 4.14a and 4.14b that the RM treated with 5% phosphogypsum and 1% NaCl makes thicker sediment as compared to higher concentration as flocculated fabric occupies the higher volume and makes thicker sediment (Mitchell 1956; Salehi 2009). The magnitude of the Zeta potential of RM treated with 5% phosphogypsum is found as 7.32 mV, which is less than that of 10% (9.93 mV) and 15% (9.81 mV) phosphogypsum (Table 4.2). Also, the magnitude of Zeta potential of RM treated with 1% NaCl is 10.96 mV which is less than that of 3% NaCl (13.87 mV) and 5% NaCl (21.27 mV). As more flocculated fabrics are formed at the low magnitude of Zeta potential, the slurry occupies larger volume (Mitchell, 1956; Salehi, 2009). But the formation of thicker sediment for the same volume of solid content in the slurry may make the sediment collapsible, and further study is required in this regard. But, untreated RM slurry takes longer duration for sedimentation and makes denser sediment as compared to the treated RM slurry. The sediment formation line is drawn to separate the settling zone and consolidation zone as described by Imai (1981). The zone above the sediment formation line is called as settling zone while the zone below the sediment formation line is termed as consolidation zone. Initially, the volume change is governed only by settling, but as the time passes, the combined effect of settling and consolidation causes the volume change. The settling process is complete when the sediment formation line touches the time vs. interface height curve. After that, the volume change is fully governed by consolidation process. It was found that unlike untreated RM slurry, the RM treated with phosphogypsum or salt shows only two zones (Figure 4.13) due to the simultaneous occurrence of flocculation and settling process. Comparing Figures 4.13 (a) and 4.13 (b), it can be noticed that the settling process of NaCl treated RM (N-TRM) slurry takes longer than that of the phosphogypsum treated RM (P-TRM) slurry. It is due to the low magnitude of the Zeta potential of the phosphogypsum treated RM slurry as compared to the NaCl treated RM slurry which flocculates the particle rapidly, and hence settlement takes place quickly. Droppo and Ongley (1989) in their study on the suspended solids (mostly silt and clay) from Ontario rivers found the degree of flocculation as a major parameter for the rate of sedimentation. It was also found that the settling process of RM slurry treated with a lower concentration of phosphogypsum (Figure 4.13a) or NaCl (Figure 4.13b) completed earlier than that of higher concentration of phosphogypsum or NaCl due to low magnitude of Zeta potential. However, the rapid settlement will make the loose sediment and may undergo large volume change under

external loading, which can be ascertained by volume change behaviour under external loading.

The microstructure analysis of the treated RM sediment performed and the SEM image is shown in Figure 4.14. A distinguished difference between the SEM image of phosphogypsum treated RM (Figure 4.14a) and NaCl treated RM (Figure 4.14b) is observed.
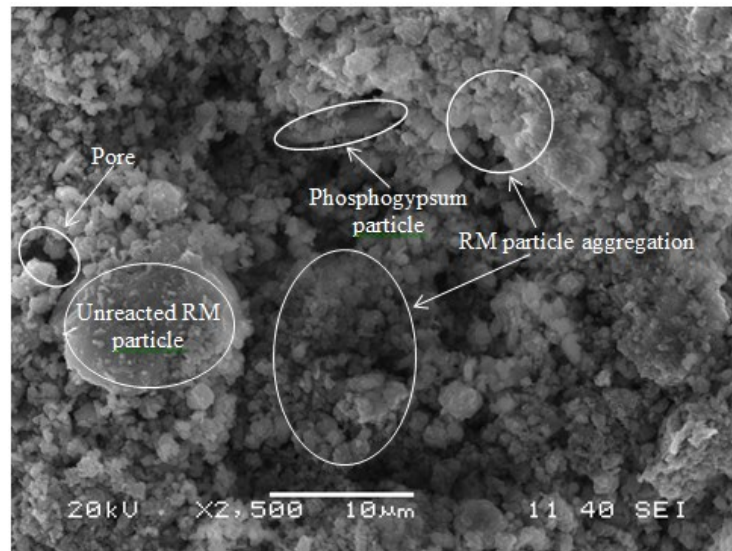
(a)
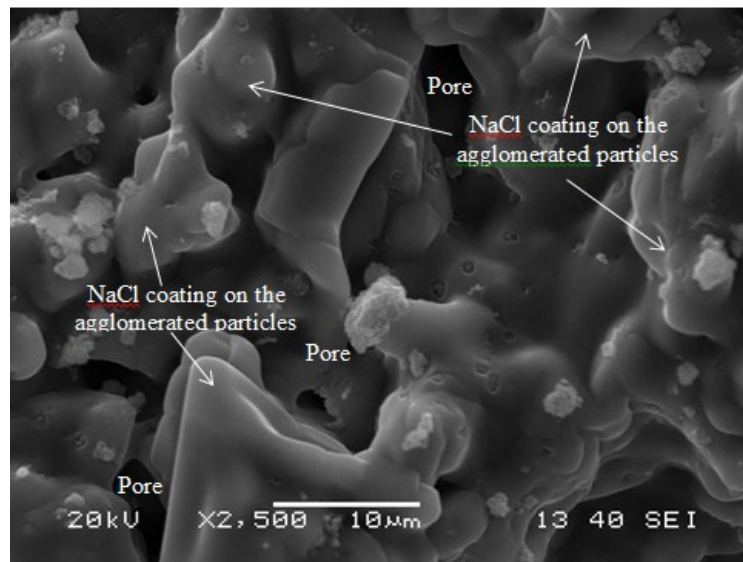
(b)

Figure 4.14. SEM image of sediment (a) P-TRM (b) N-TRM

It was found that the treatment of RM slurry using phosphogypsum makes the agglomerates RM particles which control the sedimentation process (Figure 4.14a),

though few unreacted RM and phosphogypsum particles are also observed along with the pores and cavity. The pore space is attributed to the loose packing of bigger size agglomerates (Abdullah et al. 2012). While the SEM image of NaCl treated RM shows a smooth coating over the RM particle binding a number of particles together (Figure 15b) with very few pore spaces. Mirzababaei et al. (2009) made a similar observation for the clay treated with aluminosilicate geopolymer.

As discussed earlier, the sedimentation rate depends on the Zeta potential which is attributed to the pH value (Hirosue et al., 1988).The variation of pH and Zeta potential using the present study results for untreated RM (UTRM), phosphogypsum treated RM (P-TRM) and NaCl treated RM (N-TRM) is presented in Figure 4.15.
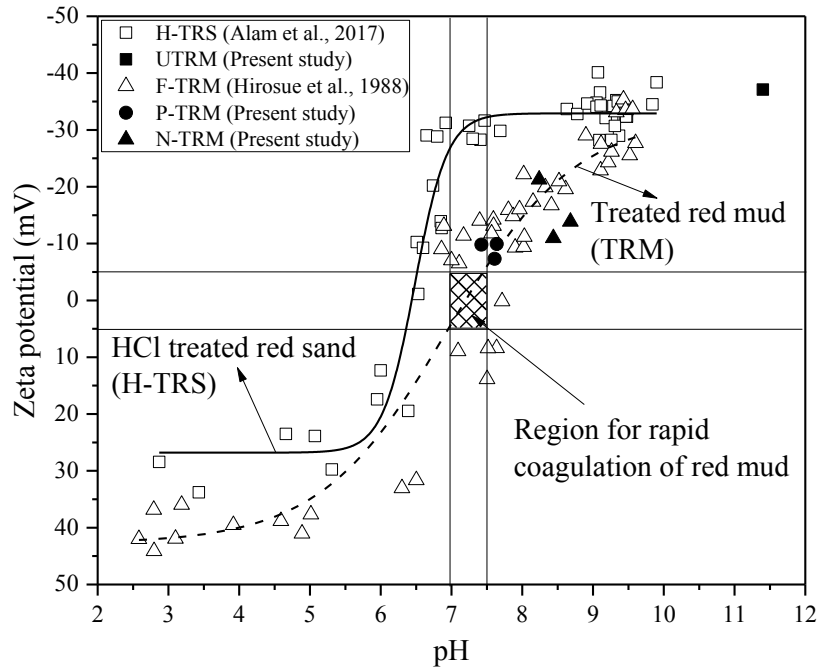
Figure 4.15. Variation of Zeta potential with pH value for RM and red sand

The results of data collected from Hirosue et al. (1988) for $FeCl_3.6H_2O$ treated RM (F-TRM) and HCl treated red sand (H-TRS) is also presented. The two separate best fit lines are drawn for HCl treated red sand and salt (phosphogypsum, NaCl or $FeCl_3.6H_2O$) treated RM. Sharpe change in Zeta potential value is observed between the pH values of 6 to 7 when the red sand is treated with HCl. The quick change in Zeta potential may be due to the release of H^+ ions which makes the negatively charged red sand particles neutral. However, in the case of phosphogypsum, NaCl or $FeCl_3.6H_2O$ treated RM slurry, gradual change in Zeta potential is observed between comparatively large ranges of pH value (5.5 - 9). It was also observed that for the pH value more than 6, at a particular pH,

phosphogypsum, NaCl and $FeCl_3.6H_2O$ was more effective in reducing the Zeta potential as compared to HCl. But, below the pH value of 6, HCl was found more effective. Figure 4.15 also reveals that the Zeta potential of RM is directly dependent on the pH value irrespective of the salts used for the treatment. So, instead of treating the RM with commercially available chemicals, phosphogypsum (fertilizer industry waste) can be used. However, it may also be seen that for a particular pH, the Zeta potential of RM and red sand is different, which may be due to the difference in surface charge density (Wnek, 1977). As for the rapid coagulation of the particles, the Zeta potential should lie in between 0 mV to ±5 mV (Duman and Tunc, 2009), a region in the Figure 4.15 has been marked. It can be seen that to achieve the rapid coagulation of the RM, the pH value needs to lower down in between 7.0 to 7.5. But in the present study, neither phosphogypsum nor NaCl were able to lower the pH value in between 7-7.5. However, the suspension remains unstable in between the Zeta potential value of 0 mV to ±30 mV and the particle can coagulate (Duman and Tunc, 2009), which can be achieved in the wide pH range for the present study. It was observed that both phosphogypsum and NaCl were able to maintain the pH value required to lower the Zeta potential in between 0 mV to -30 mV.

4.3.4 Table Flow Test

As discussed in the previous section, during the failure of RM pond dam, the RM particles spread over a large area due to the dispersive nature of RM. A small-scale flow test on the untreated and treated RM slurry is performed in the laboratory. The flow test setup is shown in Figure 4.16.
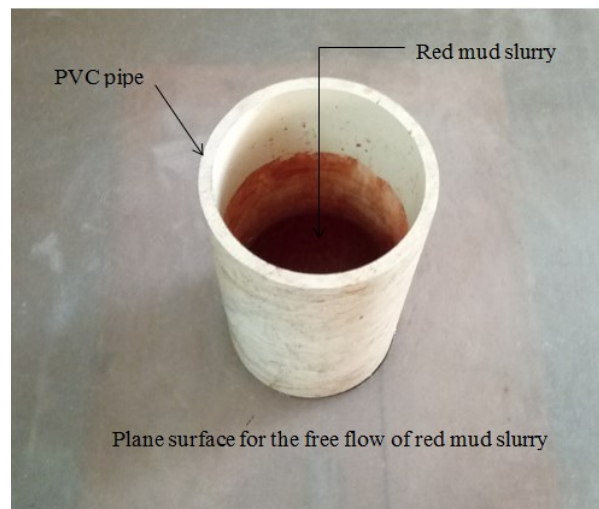
Figure 4.16. Laboratory flow test setup used in the present study

The setup consists of one 10 cm diameter PVC pipe fixed on the smooth horizontal plane. The slurry is poured into the PVC pipe and allowed to settle under gravity for 24 h and then the supernatant liquid is decanted through suction.

The PVC pipe then lifted up and the slurry is allowed to spread freely over the plane area as shown in Figure 4.17. It can be seen in the Figure 4.17 (a) that the untreated RM slurry spread over a large area as compared to phosphogypsum or salt solution treated RM slurry (Figure 4.17 b).
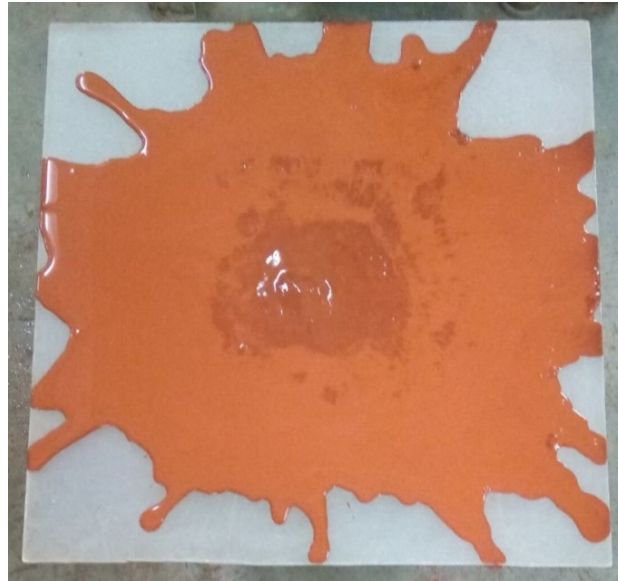
(a)

(b)

Figure 4.17. Top view of RM slurry after flow (a) untreated (b) treated RM

The spreading of treated RM over the relatively smaller area can be attributed to the agglomeration of particles (Droppo and Ongley, 1989; Mirzababaei et al., 2009). It was found that the treated RM

slurry spread over an average diameter of 29.5 cm while untreated RM slurry spread over an average diameter of 60 cm. However, the large-scale flow test is required for the understanding of actual flow behaviour of RM slurry. A hump at the centre of the spread slurry can be observed (Figure 4.18), which shows that the coarser particles of RM are not transported by water.
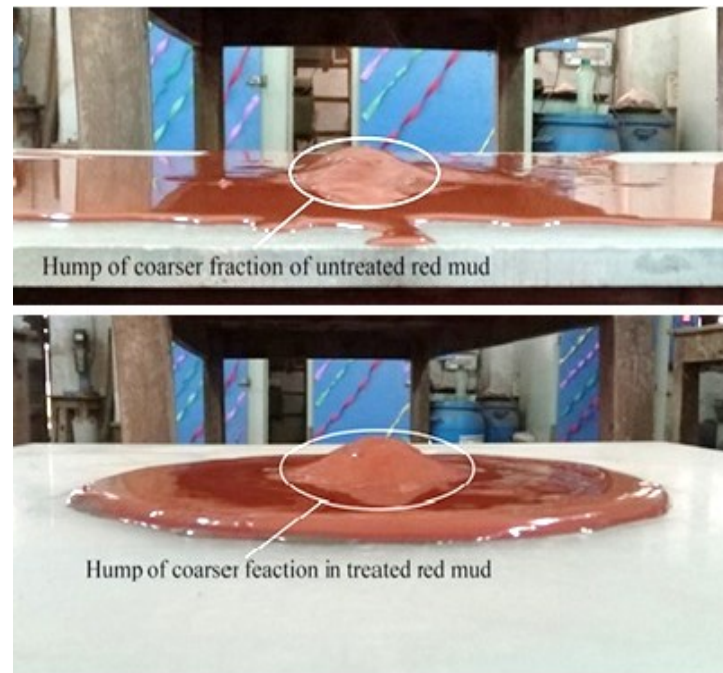
Figure 4.18. Side view of untreated and treated RM slurry after flow test showing a hump of coarser fraction

4.3.5 Chemical Analysis of Supernatant Liquid

The chemical analysis result of the supernatant liquid collected from UTRM, P-TRM, and N-TRM is presented in term of the concentration of toxic metals (As, Hg, Pb, and Cr) as identified by EPA, USA and presented in Table 4.3.

Table 4.3. Concentration of toxic heavy metals in untreated and treated RM

Element	Concentration (mg/L)				Remark
	UTRM	P-TRM	N-TRM	Acceptable limit	
As	0.002	-	-	5.00	Acceptable limit as per
Hg	0.004	-	-	0.20	EPA, USA for toxicity
Pb	-	0.135	1.039	5.00	characteristic.
Cr	1.707	1.706	1.731	5.00	

It was found that the toxic metals like As, Hg, and Cr are below the threshold limit for toxicity characteristic in UTRM, however, the trash of Pb was not found in the untreated RM. The trace of As and Hg were not found in the phosphogypsum or salt (NaCl) treated RM but a very small increase in the Cr concentration was observed in N-TRM, which is in the form of Cr^{+3} (Burke et al. 2012) and is within permissible limit. Although, the treatment of RM with the phosphogypsum or NaCl increases the leaching of Pb; it is within the permissible limit. Hence, the supernatant liquid can be used or disposed of without any environmental hazards.

4.4 Conclusion

In order to understand and reduce the impact of RM on the environment, laboratory investigations were conducted on the dispersive and sedimentation characteristics of RM. Two different type of RM based on the disposal system was considered for the present study and based on the results and discussion thereof following conclusions can be drawn.

1. Based on the pinhole test and cylindrical dispersive tests, RM was found highly dispersive, hence another reason for environmental hazard.

2. Addition of 0.5% of biopolymer (GG and XG) was found to be effective in controlling the dispersiveness of RM, due to the formation of the ionic bond (XG) and hydrogen bond (GG) with cations of RM particles. The dispersion also reduced with 3% NaCl solution as a surrounding fluid and 7% as a pore fluid.

3. The sedimentation of NRM was slow due to high magnitude of Zeta potential (37.1 mV) at pH value of 11.4. Phosphogypsum and NaCl found to be effective in reducing the magnitude of Zeta potential of RM slurry; thereby accelerating the rate of sedimentation. The pH value reduced to the range of 7.42-7.61 and 8.24-8.44 due to phosphogypsum and NaCl respectively, with a higher rate of sedimentation with phosphogypsum. But the high rate of sedimentation may become susceptible to collapse, which requires further detail study in this regard. It was also observed that phosphogypsum is more effective in controlling the leaching of toxic material from RM.

4   The flow test showed that the spreading of RM suspension over a large area can be controlled by treating the RM slurry using phosphogypsum or NaCl solution. The

present laboratory study may help in developing a better management system for smooth and effective disposal and storage of RM.

This chapter discussed the dispersive and sedimentation behaviour of RM and the remediation of the same to prevent the hazard due to spreading of RM over large vicinity due to dispersive nature of RM. But the stored RM needs to utilize in bulk to reduce the storage. So, to reduce the storage by utilizing the RM, the coarse fraction (>75µm) of RM is characterized as a civil engineering construction materials and discussed in Chapter 5.

Chapter 5

Characterization of Coarse Fraction of Red Mud

5.1 Introduction

Several studies have been conducted to replace natural sand by manufactured sand (Goncalves et al., 2007; Cortes et al., 2008), fly ash and blast furnace slag (Ali and Fiaz, 2009) in cement mortar. But, the sole study on red mud as a substitute of natural sand by Liu and Poon (2016) is limited to physical properties of self- compacting concrete with red mud as a whole. The detailed studies related to physical, morphological, mineralogical, chemical and thermal characteristics of coarse fraction (> 75 μm) of red mud (red sand) as a construction material is not available. Another important parameter of a construction material is its shear strength, which solely depends on the angle of internal friction (ϕ) of granular material (Negussey et al., 1988). The angle of internal friction (ϕ) of aggregates is greatly affected by the size and the shape of the particles (Alias et al., 2014; Stark et al., 2014). Jerves et al. (2016) studied the effect of morphology on the critical state friction angle and found that critical state friction angle decreases with increase in angularity. Shape of particle also affects the shear modulus and damping ratio (Tong and Wang, 2015) and the compression behaviour of granular materials (Zhuang et al., 2014). Studies have been undertaken on the size, shape and morphological properties of the aggregates (Janoo, 1998; Mora and Kwan, 2000). However, all the available studies are for coarse aggregate except Yudhbir and Rahim's (1991) in which the particle shape and angularity of river sand were studied.

Hence, the present chapter discusses the characteristic of non-cohesive coarse fraction (> 75 μm) of the red mud (red sand) as a civil engineering construction material. Its engineering properties such as specific gravity, grain size analysis, zeta potential, shear strength parameter, thermal conductivity, lime reactivity and leachate analysis are studied along with morphology, mineralogy and the chemistry of the red sand (RS). The relationship between these parameters is also discussed and compared with Indian standard sand of Grade I (size 1 mm – 2 mm) and Grade II (size 0.5 mm – 1 mm) (IS

650:1991). The effect of the use of red sand on the environment is discussed with the help of leachate analysis as the high pH of the red sand may cause the leaching of heavy metal (Chaabane et al., 2016). The characterization of the red sand considering all above parameters will help the professional engineers to use it as a substitute for natural sand.

5.2   Physical Characteristics

5.2.1   Grain Size Distribution

The grain size distribution curves of the sands used for the present study are shown in Figure 5.1. In the same figure, grain size distribution curve of other river sand has been shown by collecting data from the literature. From the grain size distribution curve, it can be observed that both NRS and HRS are finer than standard sands and also RSs do not contain coarser sand particle i.e. 4.75 mm passing and 2 mm retaining (ASTM D2487-11).
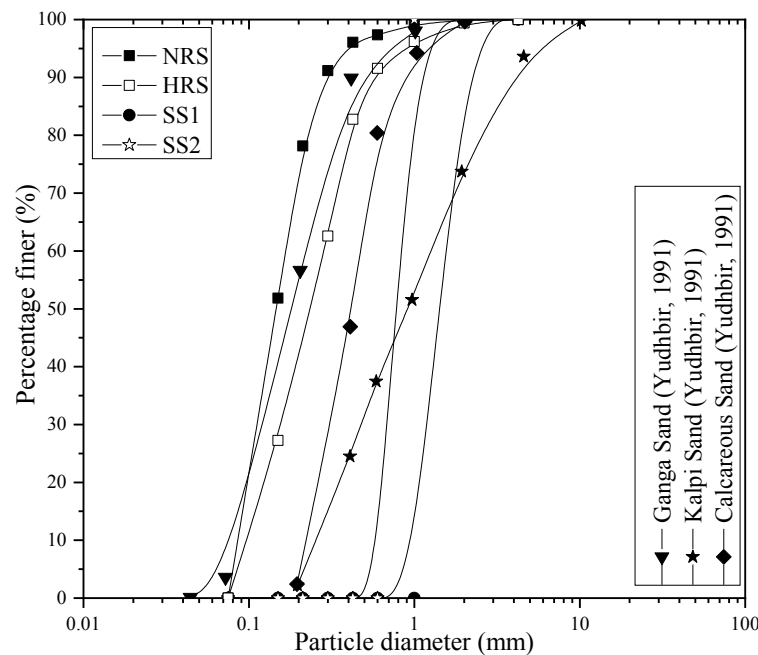
Figure 5.1. Grain size distribution of red sand

It can also be seen from Figure 5.1 that the NRS contains around 96% fine sand while HRS contains around 82.5% fine sand (0.075 mm - 0.425 mm) and the remaining percentage is medium sand (0.425 mm – 2 mm) (ASTM D2487-11). Xue et al. (2016) also found that particle size of RM lies between 2 μm to 2 mm with 80-90% mud and remaining sand sized particles. Based on the coefficient of uniformity (c_u) and coefficient

of curvature (c_c) as listed in Table 5.1, the RSs and standard sands can be classified as poorly graded sand (SP) (ASTM D2487, 2011). It may be mentioned here that the grading of RS may vary depending on the grinding of the bauxite during Bayer's process. Also, fineness modulus of NRS and HRS are calculated as per IS 383-1970 and found to as 1.86 and 2.40 respectively.

Table 5.1. Physical characteristics of RSs and SSs

Parameter	Value			
	NRS	HRS	SS1	SS2
G_s	3.18	3.21	2.62	2.49
e_{min}	0.96	1.05	0.76	0.66
e_{max}	1.27	1.46	1.03	0.96
γ_{dmax} (kN/m^3)	15.89	15.30	14.62	14.72
γ_{dmin} (kN/m^3)	13.73	12.85	12.65	12.46
D_{10} (mm)	0.085	0.095	0.950	0.575
D_{30} (mm)	0.110	0.160	1.250	0.675
D_{60} (mm)	0.170	0.275	1.700	0.840
c_u	2.00	2.89	1.79	1.46
c_c	0.84	0.98	0.97	0.94

5.2.2   Specific Gravity

Specific gravity (G_s) of the sand samples was determined as per ASTM standard (D854, 2014). For each sand sample, six tests were conducted and the average of six values is taken as G_s. It was found that the G_s value of NRS (3.18) and HRS (3.21) is higher than the SS1 (2.62) and SS2 (2.49) due to the presence of iron compound (Fe_2O_3 and Fe_3O_4) in RS. The G_s value of HRS (3.21) and NRS (3.18) is comparable as shown in Table 5.1. Vick (1990) found high G_s value of red mud which lies between 2.8 to 3.3.

5.2.3   Void Ratio and Porosity

The maximum dry density (γ_{dmax}) and the minimum dry density (γ_{dmin}) of the sand samples are determined as per ASTM standard (D4253, 2016; D4254, 2016). Ten trials for each sand sample were undertaken and the minimum value was taken as the γ_{dmin} and listed in Table 5.1. For the determination of maximum dry density, the sand samples are poured into the mould and a surcharge weight was applied to the sample and the mould

was subjected to vibration. The maximum and minimum void ratios (e_{max} and e_{min}) corresponding to the minimum and maximum density were calculated and are also presented in Table 5.1. The maximum variation in void ratio was observed for HRS (0.41) and least variation for SS1 (0.27). The difference in void ratio determines the compatibility of the material and also the shear parameter, though as determined earlier, all four sands are poorly graded sand. Particle shape analysis of RSs was performed as it greatly affects the packing density, stiffness and the strength of construction materials (Cho et al., 2006). Hence particle morphological study was made to discuss this aspect.

5.3 Particle Shape Analysis Using Optical Microscope

The shear parameter of red sands is correlated with shape parameters like roundness index (Ri), flakiness ratio (F_R), elongation ratio (E_R), sphericity (ψ) and shape factor (S_F) (Yudhbir and Rahim, 1991). The shape analysis of particles was performed with the help of particles dimensions (largest, intermediate and shortest dimension) and the results are presented in terms of their angularity, sphericity and shape factor. For measuring the largest and intermediate dimension of the particles, 2D images of representative particles as shown in Figure 5.2 were captured with the help of optical microscope fitted with particle size analyzer. The representative sample from each sand sample was spread on a glass slide and by tapping the slide, the sand was made to rest on its maximum projected area. The smallest dimension of each sand particle was measured by focusing alternately on the glass plate and the top of the grain measuring the differential deviation by using the Vernier reading of the optical microscope (Yudhbir and Rahim, 1991).

After measuring the dimensions, calculations for different shape parameters were performed. The angularity of the particle is presented in term of roundness index (Ri), which was calculated using the Equation (5.1) (Wadell, 1932).

$$R_i = \frac{\dfrac{\sum\limits_{i=1}^{N} r_i}{N}}{R} \qquad (5.1)$$

Where,

r_i is the radius of corners of sand grain, N is the number of the corner, R is the radius of the inscribed circle as shown in Figure 5.2. It describes the way of measurement of the radius of the corner and the radius of the inscribed circle.
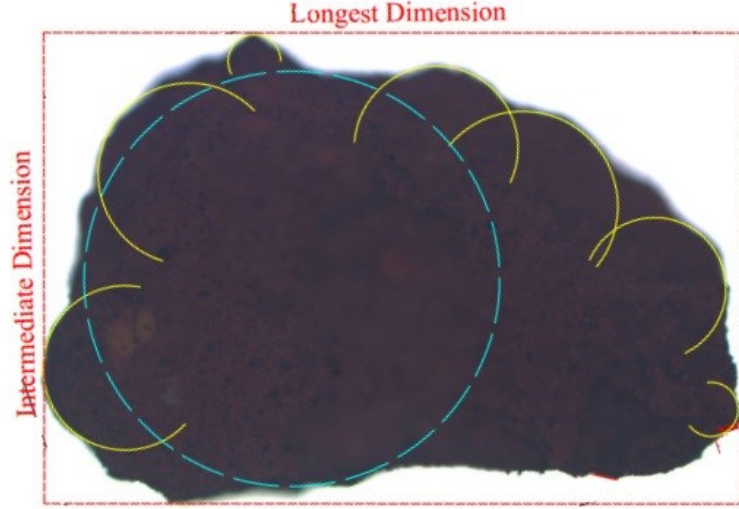
Figure 5.2. Measurement of different dimensions

Sphericity (ψ) and shape factor (S_F) were calculated with the help of particle's dimension using the Equation (5.2) and Equation (5.3), respectively (Yudhbir and Rahim, 1991).

$$\Psi = \sqrt[3]{\frac{d_S \times d_i}{d_L^2}} \qquad (5.2)$$

$$S_F = \frac{d_S}{\sqrt{d_L \times d_i}} \qquad (5.3)$$

Where,

d_S is the smallest dimension of sand grain, d_i is the intermediate dimension of sand grain, d_L is the largest dimension of sand grain.

On an average, 75 particles from each sieve fraction were randomly chosen for particle shape analysis in comparison to 25-30 particles for each sieve fraction by Yudhbir and Rahim (1991). Persson (1998) performed his study on the total of 400 particles, while Barksdale et al. (1991) studied a total of 250 particles. However, in the present study, 75 particles from each sieve fraction and a total of 600 particles were studied. The total number of the particles was also selected based on the statistical analysis with 95% confidence level. The margin of error (ME) was calculated using the Equation (5.4) as discussed by Lohr (1999) and was found as 1%.

$$ME = z \times \sqrt{\frac{p \times (1-p)}{n}} \qquad (5.4)$$

Where,

z is based on confidence level, p is the percentage of the sample and n is the sample size.

The morphology and surface chemistry of the sand samples are studied using Japan

Electron Optics Laboratory SEM fitted with EDX at 20 kV acceleration voltage. Before loading the sample for analysis, the platinum coating was applied at 30 mA current for 90 seconds. X-ray diffraction (XRD) test is performed to investigate the mineralogical composition of sand samples using Rigaku Japan/Ultima-IV model with C_uK_β radiation at 40 kV and 40 mA. The chemical characteristics of the material used are presented in terms of pH, electrical conductivity, total dissolved solids (TDS), zeta potential, lime reactivity and leachate analysis. The thermal resistivity (R_T) of red sand was also studied for its thermal property.

Images of few particles of each RSs and SSs are shown in Figure 5.3 and Figure 5.4, respectively. It is found that the NRS (Figure 5.3) contains the majority of the particles with a rounded edge with few angular edged particles while the HRS contain spherical, elongated particles with a sharper edge and rough surface. Both standard sands (Figure 5.4) are found to contain spherical particles with mostly rounded with few angular edged particles.

The shape analysis of RS and SS was performed using the Equations 5.1 to 5.3 and the range of values of each parameter is listed in Table 5.2. The large variation of R_i is observed for NRS (0.12 – 0.72) and HRS (0.12 – 0.55) in comparison to R_i of SS1 (0.25 - 0.50) and SS2 (0.16 - 0.50). The R_i value greater than 0.7 shows the presence of well-rounded particles while less than or equal to 0.25 shows the presence of angular particles (Yudhbir and Rahim, 1991).
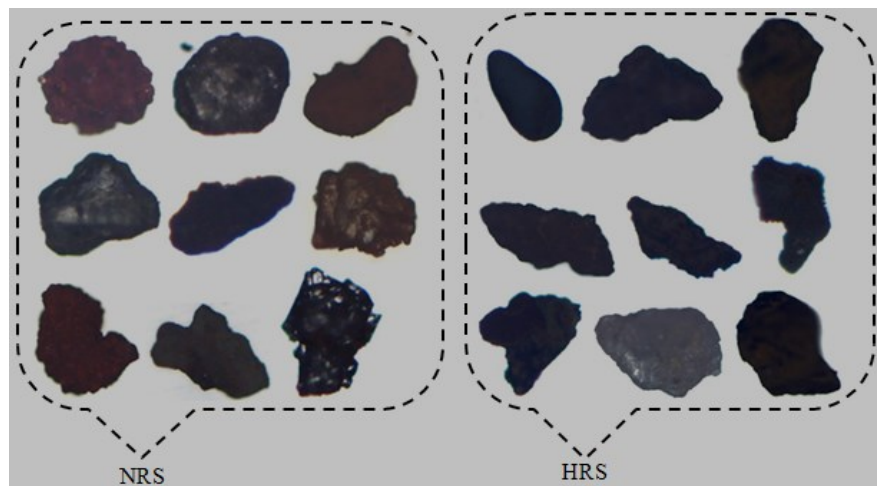
Figure 5.3. Optical microscopic image of NRS and HRS used for image analysis
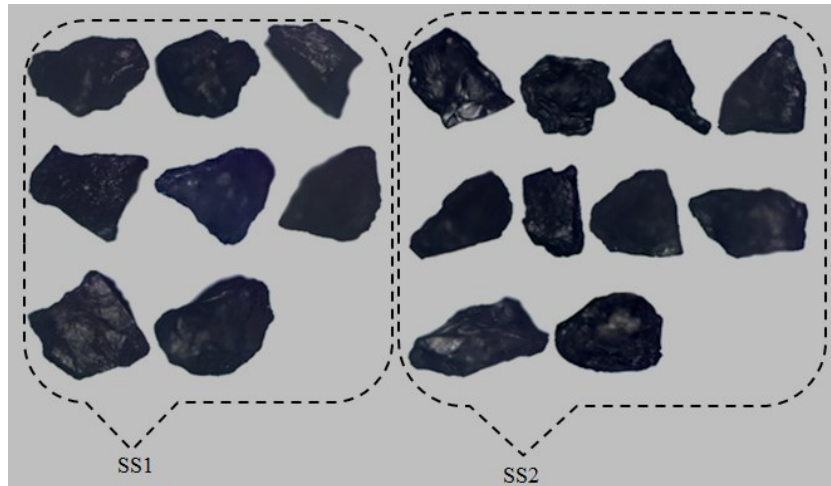
Figure 5.4. Optical microscopic image of SS1 and SS1 used for image analysis

Table 5.2 Particle shape parameters of NRS, HRS, SS1 and SS2

Sand type	R_i	F_R	E_R	ψ	S_F
NRS	0.12 – 0.72	0.03 – 0.99	1.00 – 2.50	0.26 – 0.96	0.06 – 0.93
HRS	0.12 – 0.55	0.18 – 0.99	1.01 – 2.00	0.44 – 0.97	0.15 – 0.93
SS1	0.25 – 0.50	0.13 – 0.38	1.14 – 1.59	0.47 – 0.55	0.13 – 0.32
SS2	0.16 – 0.50	0.12 – 0.49	1.03 – 1.92	0.36 – 0.66	0.09 – 0.40

Based on the roundness index, percentages of different types of particle present in the sand sample were calculated and are presented in Figure 5.5. It can be seen that the total angular particle in NRS is 71.65% along with 28.35% of rounded particles in comparison to 91.23% of angular particles along with 8.77% of rounded particles in HRS.

The total angular particles of NRS (71.65%) is the sum of 26.87% very angular, 22.39% of each angular and sub-angular particles, while the total angular particles of HRS (91.23%) is the sum of 22.80% very angular, 42.11% angular and 26.32% sub-angular particles. It may be mentioned here that ϕ value of granular soil depends on percentage of total angular (i.e sum of very angular, angular and sub-angular) particles (Janoo, 1998). However, there are many more factors which control the angle of internal friction, so the direct shear test was performed (Section 5.7) to find the angle of internal friction of different sand.
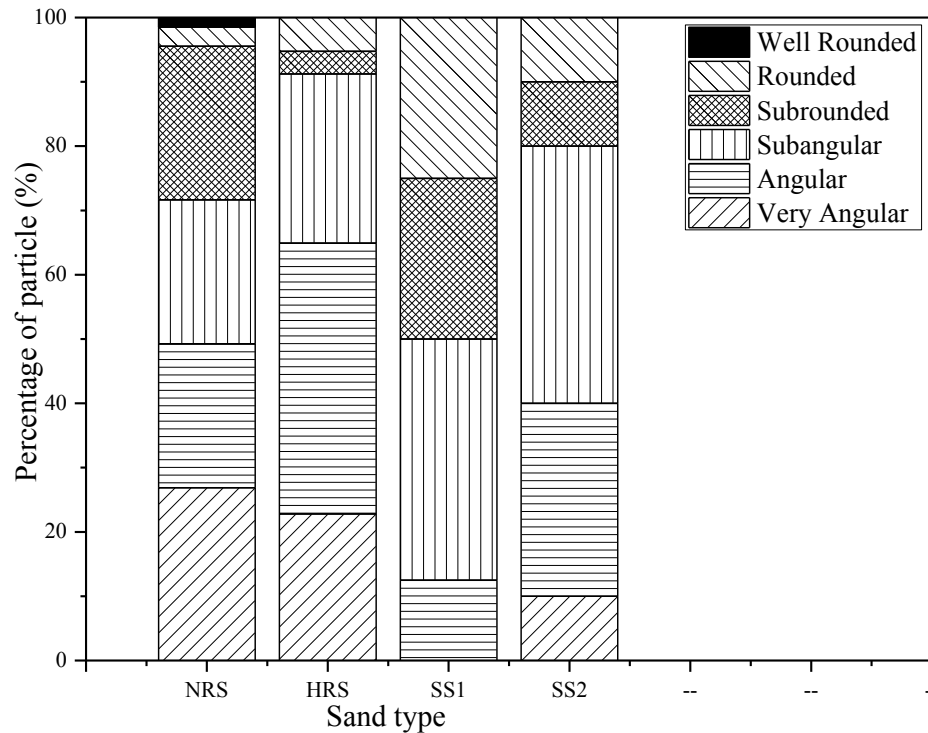
Figure 5.5. Percentage of different shaped particle present in NRS, HRS, SS1 and SS2

The average roundness index of RSs was found higher than that of standard sand. Cortes et al. (2008) studied the effect of roundness index on the flowability of fresh mortar and found that for the same water to cement ratio and fine aggregate to cement ratio, the aggregate having a higher value of R_i gives higher flowability. The sphericity of the red sands (NRS and HRS) was found to be higher than that of standard sand (SS1 and SS2) (Table 2). However, HRS shows the higher value of sphericity as compared to NRS. Goncalves et al. (2007) studied the effect of particle shape on cement mortar and found that at lower water to cement ratio (0.4), particles with higher ψ gives better workability.

Flowability of the mortar prepared using RS and SS with sand to cement ratio of 2 and at a different water-cement ratio (w/c), was studied. It was found that for a particular water-cement ratio; the mortar prepared using SS is more flowable compared to RS as shown in Figure 5.6. The study reveals that along with the angularity of the fine aggregate, there are some other factors which affect the flowability of mortar.

One of the factors may be the specific surface area of the fine aggregate. So, the surface area of sands was investigated using ethylene glycol monoethyl ether (EGME) method (Cerato and Lutenegger, 2002). It was found that the surface area of SS1 and SS2 are 0.847m^2/g and 0.866m^2/g respectively while the surface area of NRS and HRS are 23.45m^2/g and 20.40m^2/g respectively. For same water-cement ratio, the lower

flowability of the RS may be due to its higher surface area as compared to standard sand. However, the effect of water to cement ratio on the strength properties of mortar prepared using RS needs to be investigated.
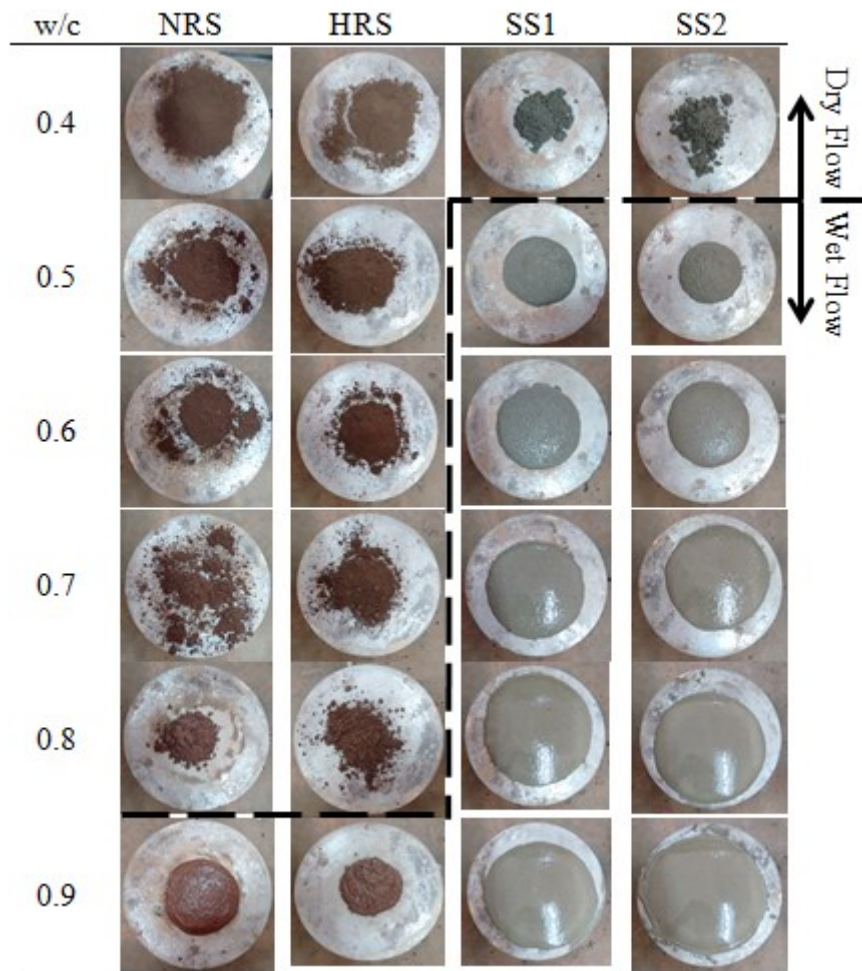
Figure 5.6. Flowability of RS and SS at different water-cement (w/c) ratio

Particle shape analysis of sand particles were performed based on their length, width and thickness. A plot between flatness (d_s/d_i) and elongation (d_i/d_L) of particles has been drawn which is known as Zingg diagram (Yudhbir and Rahim, 1991) and is shown in Figure 5.7. From Zingg diagram, it was found that NRS contains 41.79% disk shaped particles followed by 31.34% of spherical, 19.40% of roller and 7.46% of blade shaped particles.
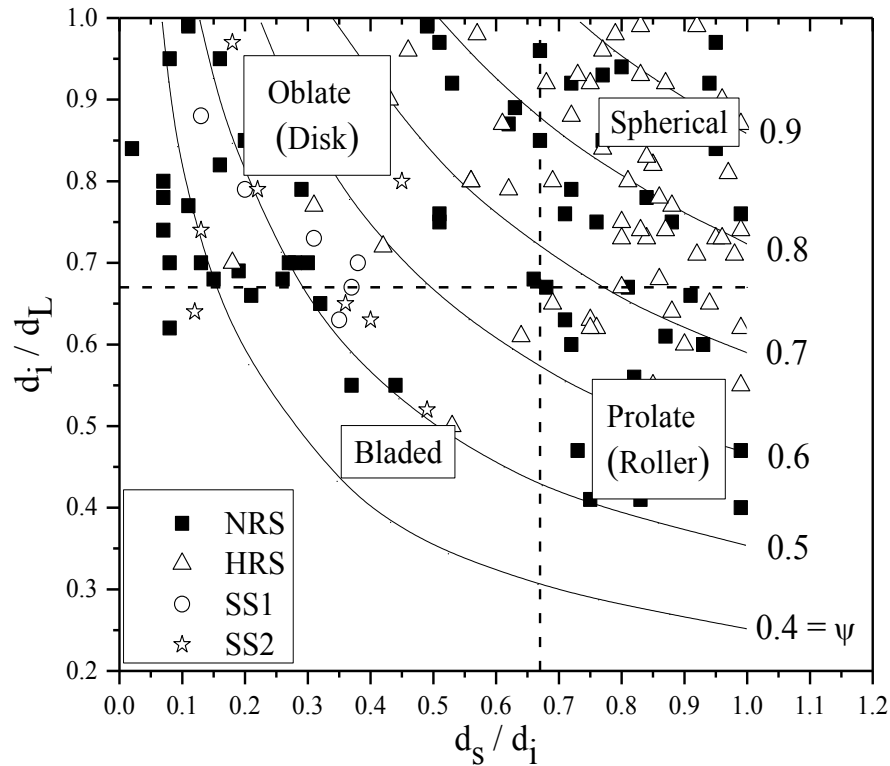
Figure 5.7. Zingg diagram showing the distribution of particles present in RSs and SSs

The HRS contains the majority of spherical particles (61.40%) along with 19.96% roller, 15.25% disk shaped and 3.39% blade shaped particles. It needs to be mentioned here that the high frictional angle of the RS may be due to the presence of the majority of red disk shaped particle (Stark et al., 2014). From the Zingg diagram, it can also be seen that most of the disk shaped particles of NRS are having sphericity value less than 0.6. The HRS contains the majority of the particles having sphericity value more than 0.7. Higher disk shaped particle results in a higher crushing value. Janoo (1998) studied the effect of sphericity on ϕ value and found that the ϕ value increases with the decrease in sphericity. This aspect has been discussed later in the direct shear test section.

The effect of roundness index (R_i) on the void ratio (e) has been studied and the relation between them is presented in graphical form in Figure 5.8. The graph is plotted between the average roundness index and the maximum and minimum void ratio of the sand. The best fit line shows that there is a linear relationship between R_i and e. It found that void ratio increases with a decrease in roundness index. Holubec and Appolonia (1973) also found a similar pattern for the coarse aggregate. However, the present relationship is based on limited data points and needs further study. It was also observed that the increase in the maximum void ratio (e_{max}) is more, compared to increase in the minimum

void ratio (e_{min}) with a decrease in R_i.
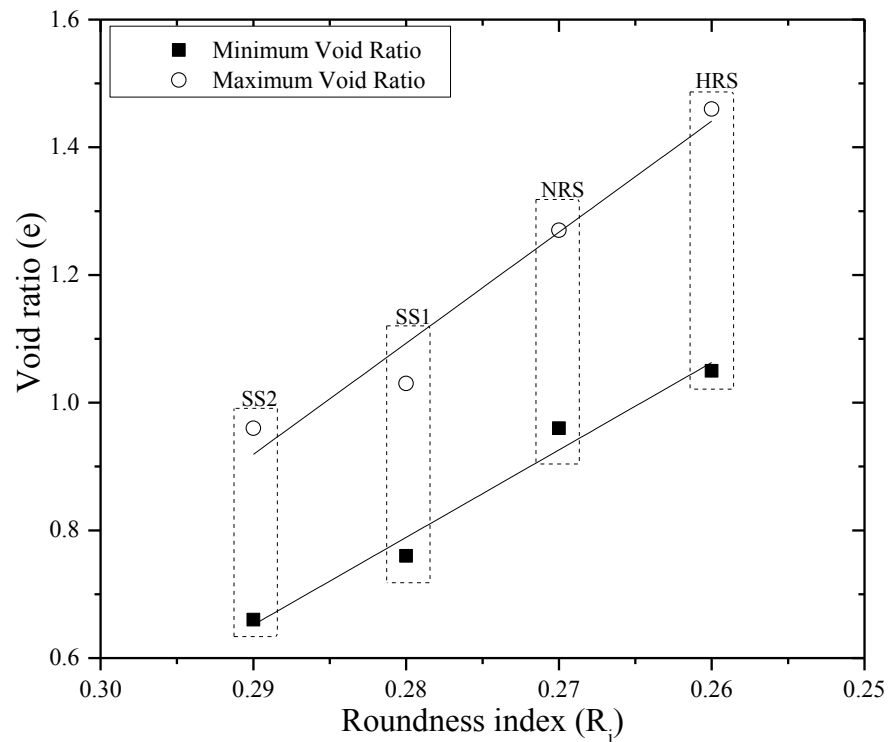
Figure 5.8. Effect of roundness index on void ratio

5.4 Surface Chemistry

The pozzolanic reaction is significantly controlled by the chemicals present at the surface of particles, so the chemistry of the surface in this research was studied using EDX (Yousuf et al., 1995). The EDX spectrum of the sand samples used in the present study are shown in Figures 5.9 to 5.12 for NRS, HRS, SS1 and SS2 respectively.
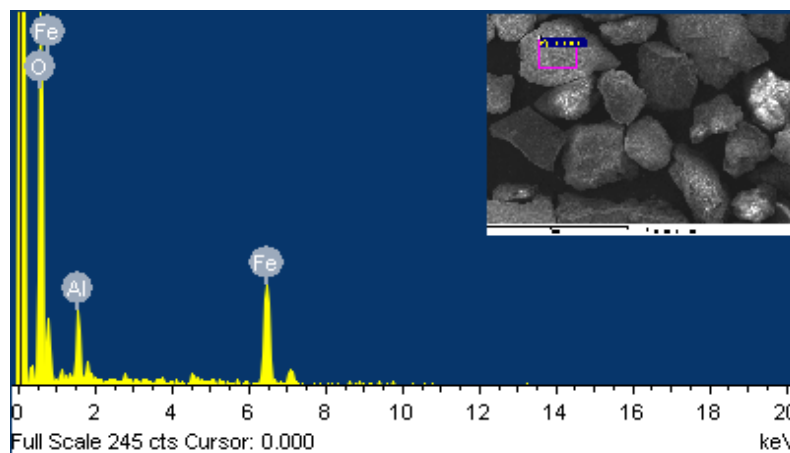
Figure 5.9. EDX spectrum of NRS showing the surface chemistry
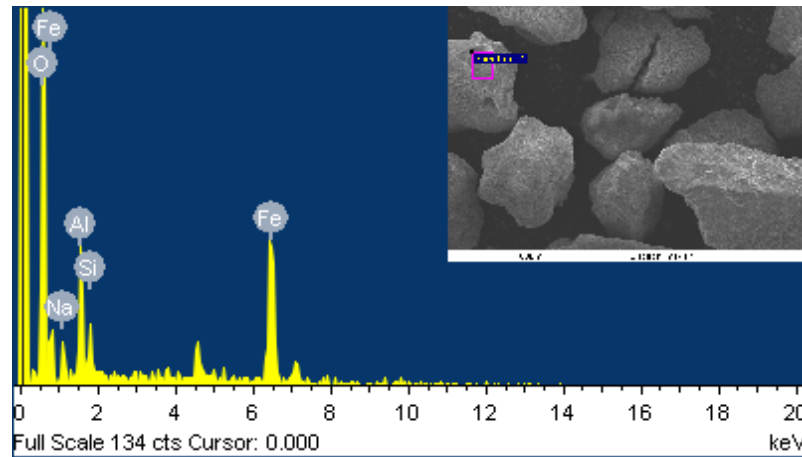
Figure 5.10. EDX spectrum of HRS showing the surface chemistry
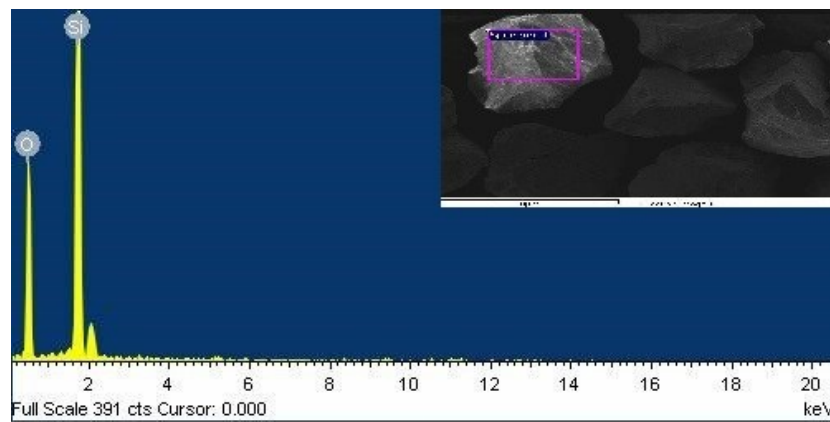
Figure 5.11. EDX spectrum of SS1 showing the surface chemistry
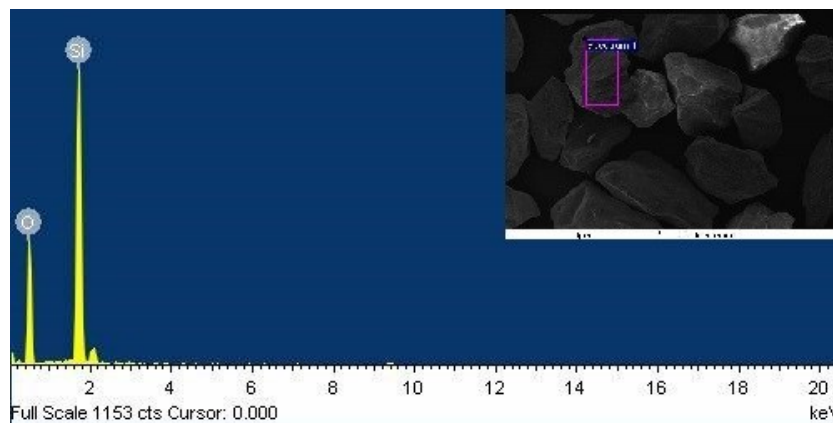
Figure 5.12. EDX spectrum of SS2 showing the surface chemistry

The chemical compositions of sand samples are listed in Table 5.3. It can be seen that the SS1 and SS2 are rich in silica while NRS and HRS contain iron as a major portion with a trace amount of silica. Nath et al. (2015) found that Fe and Al is a main chemical constituent in RM. Rubinos et al. (2013) found that 70% of the total constituent of RM is the oxide of Fe, Al and Ti. It may be mentioned here that all these studies are related to

red mud, while the present study deals with RS.

Table 5.3 Surface chemistry of the sand sample

	Weight (%)			
Element	NRS	HRS	SS1	SS2
O	41.99	32.41	48.61	53.44
Si	-	2.87	51.39	46.56
Fe	51.89	52.77	-	-
Al	6.12	8.25	-	-
Na	-	3.70	-	-
Total	100	100	100	100

The bright and dark particles of the sand samples were also studied to know the difference in surface chemistry. It was found that there is no difference in chemical composition but the difference in the brightness may be due to the different shape and size of the particles.

5.5 Surface Texture Analysis

The surface texture of the RS and SS studied using the using SEM image. The SEM image of different sand samples is shown in Figure 5.13. The SEM image of NRS (Figure 5.13a) shows that it contains spherical particles with rounded to the angular edge and almost smooth surface while the HRS (Figure 5.13b) contains mostly sharp edged particles with a rough surface. The SEM image of both the Indian standard sand (SS1 and SS2) shows mostly rounded to few angular edged particles (Figure 5.13c and 5.13d). The SEM micrograph of sand samples at higher magnification is also shown at the right top corner. On the higher magnification, the NRS particles (Figure 5.13a) shows smooth surface while the surface of HRS particles (Figure 5.13b) seems to be rough. The roughness of HRS surface may also be a reason for high friction angle as discussed later. The surface of standard sand shows textures like cleavage plates, upturned plates and conchoidal fracture pattern due to the presence of oxide of silica (Figure 5.13c and 5.13d).
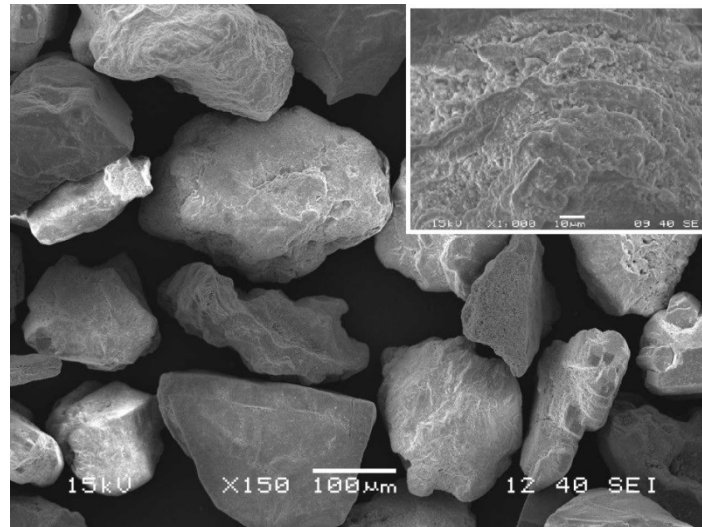
(a)
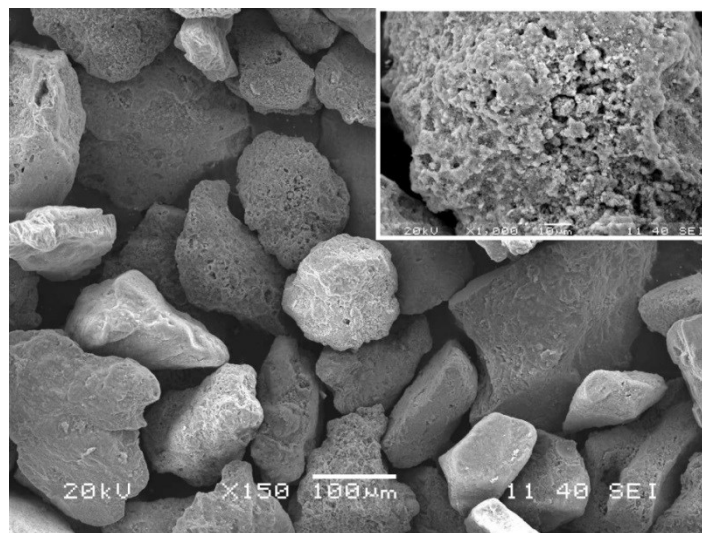
(b)
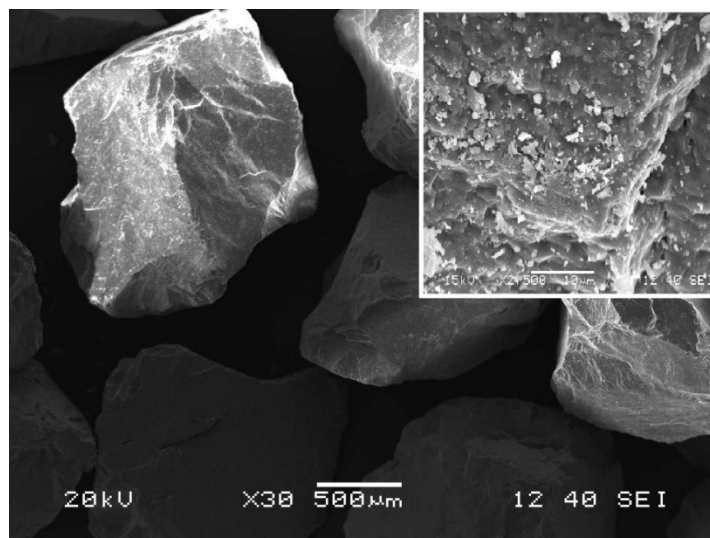
(c)
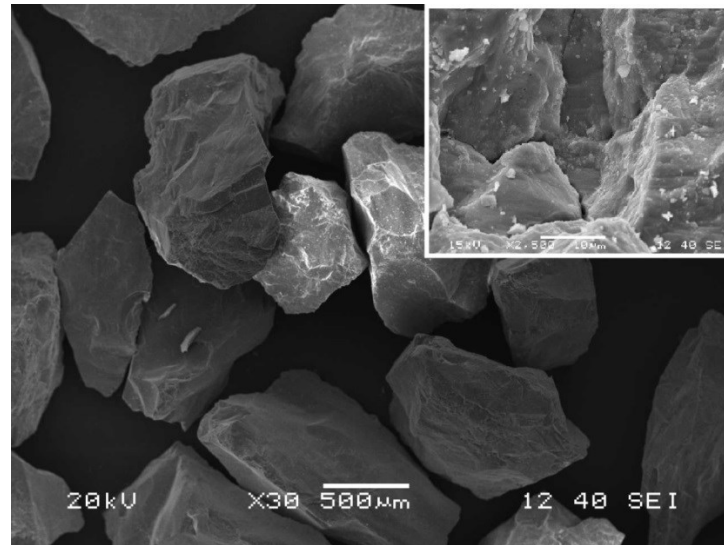
(d)

Figure 5.13. SEM image of (a) NRS, (b) HRS, (c) SS1, and (SS2)

5.6 Mineralogy

The XRD pattern of RSs and SSs is presented in Figures 5.14 and 5.15 respectively. The mineral phases of NRS and HRS consist of iron and aluminium compounds like magnetite (Fe_3O_4), hematite (Fe_2O_3), gibbsite, pyrite as shown in Figure 5.14, with quartz found only in HRS.
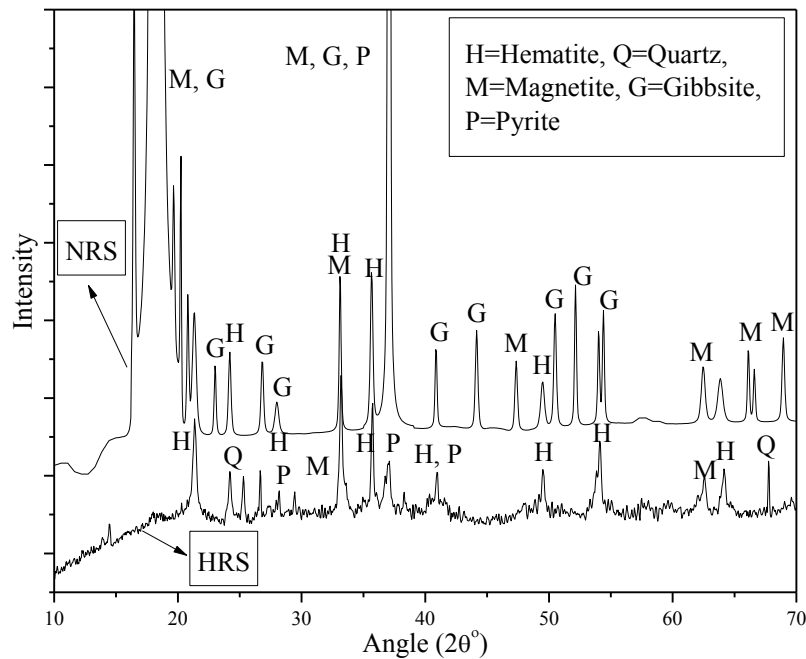
Figure 5.14. XRD pattern showing the minerals present in NRS and HRS
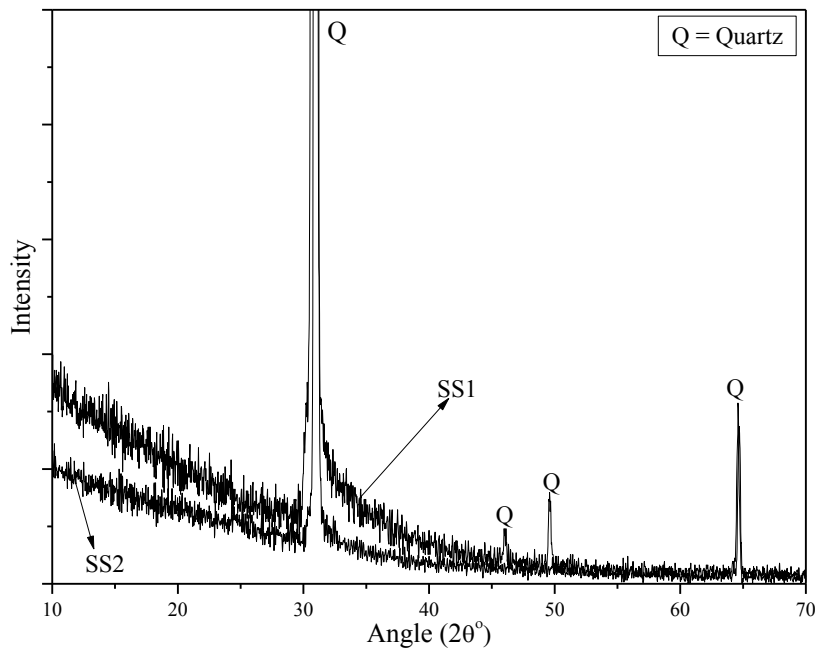
Figure 5.15. XRD pattern showing the minerals present in SS1 and SS2

Nath et al. (2015) and Liu et al. (2014) found the hematite and gibbsite as the main mineral phase in red mud and Rubinos et al. (2013) also found magnetite along with hematite as the main mineral phase in red mud. The standard sands (SS1 and SS2) predominantly contain quartz (Figure 5.15) and a similar result has been presented by Padmakumar et al. (2012). The glassy phase in NRS and HRS with the help of hump position has also been identified (Figure 5.14), which shows the existence of glassy phase. Castaldi et al. (2010) found similar XRD pattern for RM.

5.7 Laboratory Shear Test

The shearing response of the dry sand samples (NRS, HRS, SS1 and SS2) was studied by performing the direct shear test as per ASTM standard (D3080, 2011). To study the effect of relative density on the shearing response, tests were conducted at a minimum (0.0%), average (50%) and maximum (100%) relative densities. The desired relative density of sand sample was achieved using rainfall technique. The sand was allowed to fall through a funnel from a particular height which was decided after several trials. The test was performed by applying four normal stresses (50kPa, 100kPa, 150kPa and 200kPa). A typical result of NRS at its maximum and minimum relative density under normal stress of 200 kPa is shown in Figure 5.16 whereas the Figure 5.17 shows the plot between normal stress and shear stress of NRS at different relative density. From the normal stress

– shear stress plot, the angle of internal friction of different sand (NRS, HRS, SS1, and SS2) was calculated.
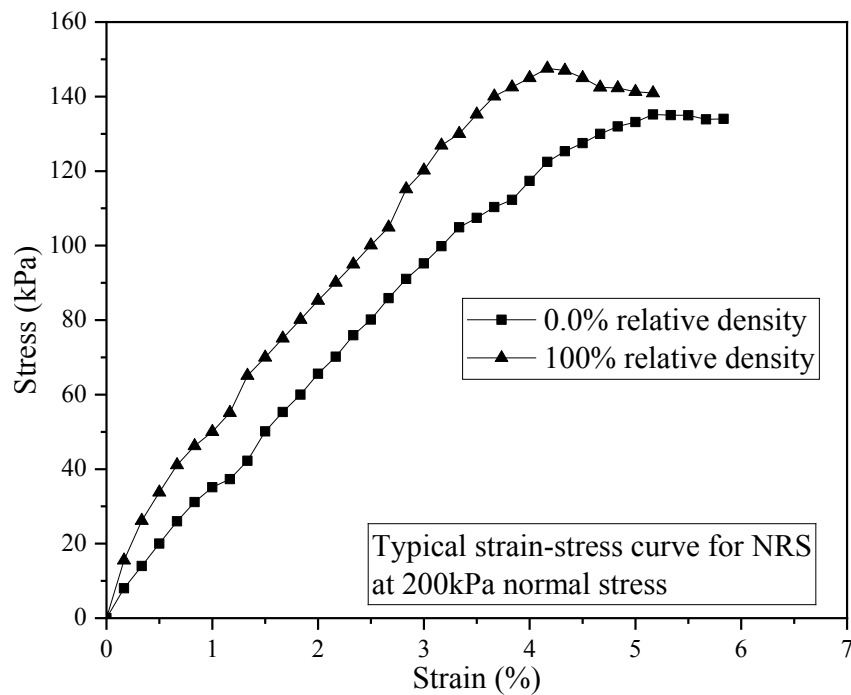
Figure 5.16. Strain-Stress curve of NRS
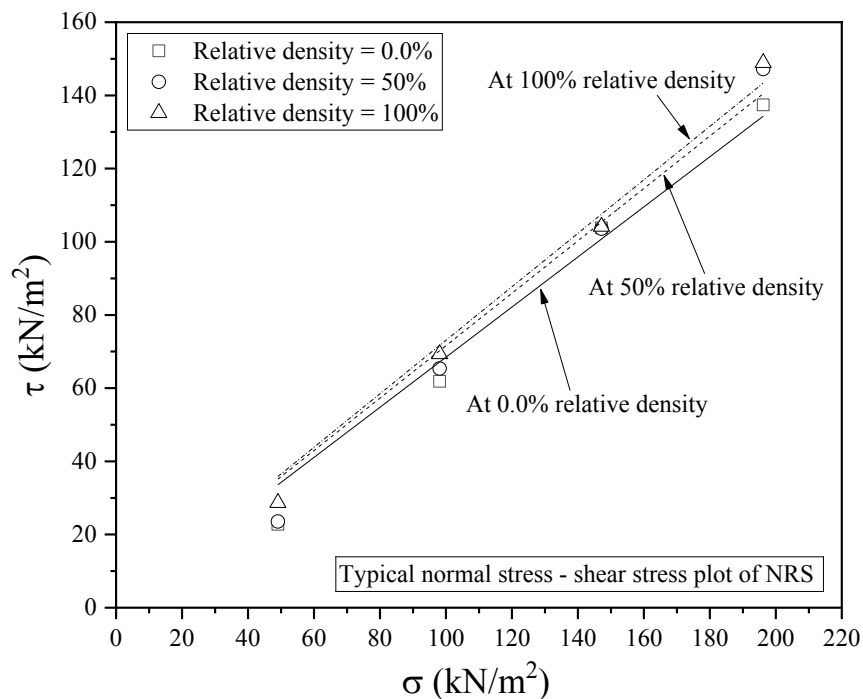
Figure 5.17. Normal stress vs shear stress response of NRS

It was found that the ϕ value of NRS varied from 38.19° to 39.91° while for HRS it varied from 35.38° to 44° at their minimum and maximum relative density respectively.

Newson et al. (2006) found high ϕ value of the red mud varying from 38° to 42° using consolidated undrain test. Rubinos et al. (2013), using direct shear test, found high ϕ value of red mud as 38°. It was found that HRS possesses a maximum ϕ value (44°) at its maximum relative density and a minimum ϕ value 35.38° at its minimum relative density. The higher ϕ value may be due to the fact that the HRS contains a high amount of angular particles (Janoo, 1998). However, there are many more factors which may affect the angle of internal friction and further study is required in this regard. The ϕ values of SS1 and SS2 are varying from 40.04° to 41.57° and 36.36° to 42.78° respectively. Koloski et al. (1989) found a similar range of angle of internal friction (30°-40°) for poorly graded medium to coarse outwash. Padmakumar et al. (2012) also found the angle of internal friction as 40° for Aeolian sand from Indian desert. It was also found that the variation of friction angle corresponding to maximum and minimum density depends upon the percentage of angular particles. The maximum variation of friction angle (35.38°- 44°) for HRS corresponds to 91.23% of angular particles and the least variation (40.04° to 41.57°) for SS1 corresponds 51% of angular particles. However, this relationship is based on the limited data used in the present study; more data may shed more light in this regard. The advantage of the high friction angle of RSs is that it can be used as fine aggregate in cement mortar. The high friction angle increases the yield stress of mortar and also increases the plastic viscosity (Westerholm et al., 2008; Nanthagopalan and Santhanam, 2011). The present study deals with red sand of medium to fine grain at their maximum dry density.

Further study was performed in term of the angle of repose using laboratory developed box with acrylic glass on the front and a 1 cm wide slot at the bottom of the box. A set square (protractor) is fixed at the outer surface of the acrylic glass to measure the angle (Figure 5.18). Initially, the slot was closed and the sand was filled into the box at their minimum density using rainfall technique. After filing the sand the slot was opened and the sand was allowed to fall through the slot under self-weight. When the sand reached to stable condition, the angle of repose (angle of inclination) was measured using the protractor. An average angle of repose of standard sand was found as 40°, which is very similar to the angle of internal friction found using direct shear test, while the angle of repose of NRS and HRS was found to vary from 35° to 40°. However, friction between the sand and acrylic glass may induce a minor error.
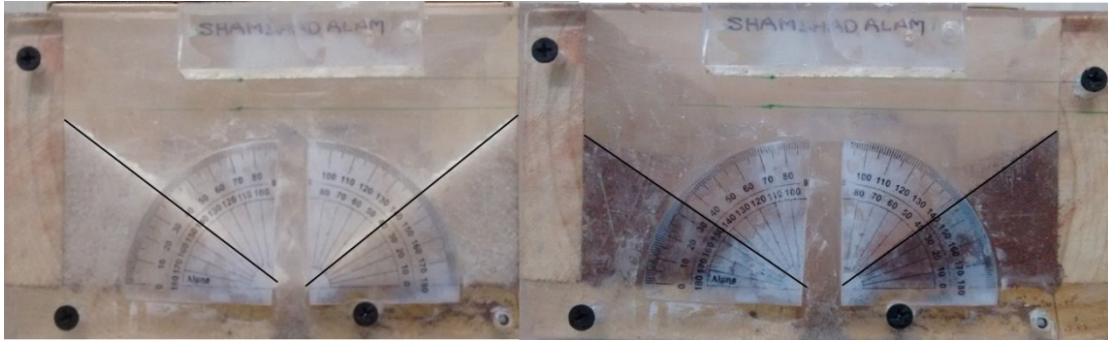
Figure 5.18. Typical photo showing the angle of repose of different sand

The effect of sphericity on ϕ value was studied and the plot is shown in Figure 5.19. The ϕ value increases with the decrease in sphericity of the particles. Janoo (1998) also studied the effect on base course materials (100% passing the 75 mm and 65% passing the 25 mm sieve) and found the similar pattern. Though the trend is similar, the relationship is different as the present study is based on fine grain aggregate (size < 4.75 mm), RS and Indian SS.
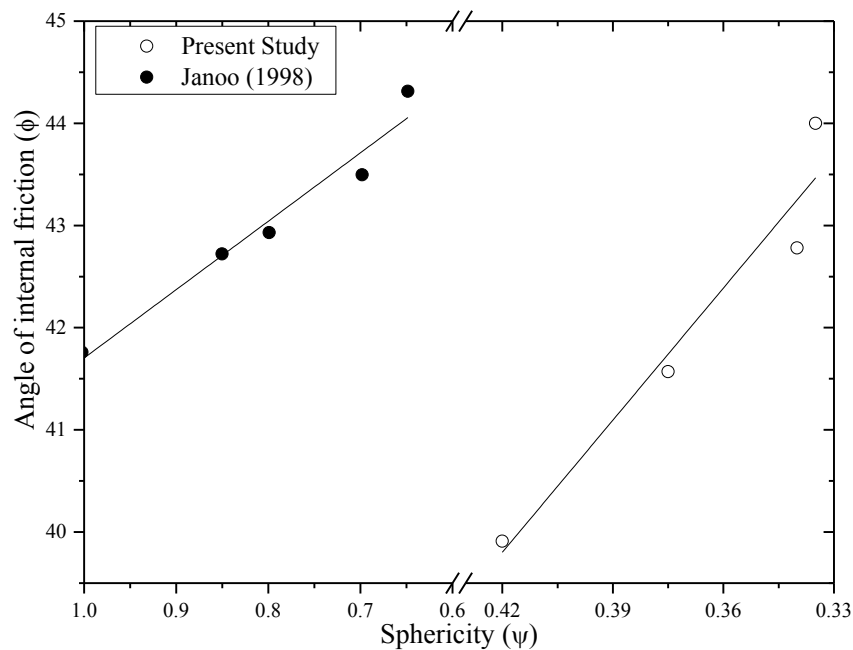
Figure 5.19. Relation between sphericity and angle of internal friction (ϕ)

5.8 Chemical Characteristics

5.8.1 pH, Electrical Conductivity, and Total Dissolved Solid

The pH of the sand sample (NRS, HRS, SS1 and SS2) was determined using digital pH meter (HACH HQ40d). To investigate the effect of liquid to solid ratio (L/S) on pH

value, a sample with different L/S, varying between 2 to 10 with an increment of 1 was prepared using distilled water. The variation of pH with L/S is shown in Figure 5.20.
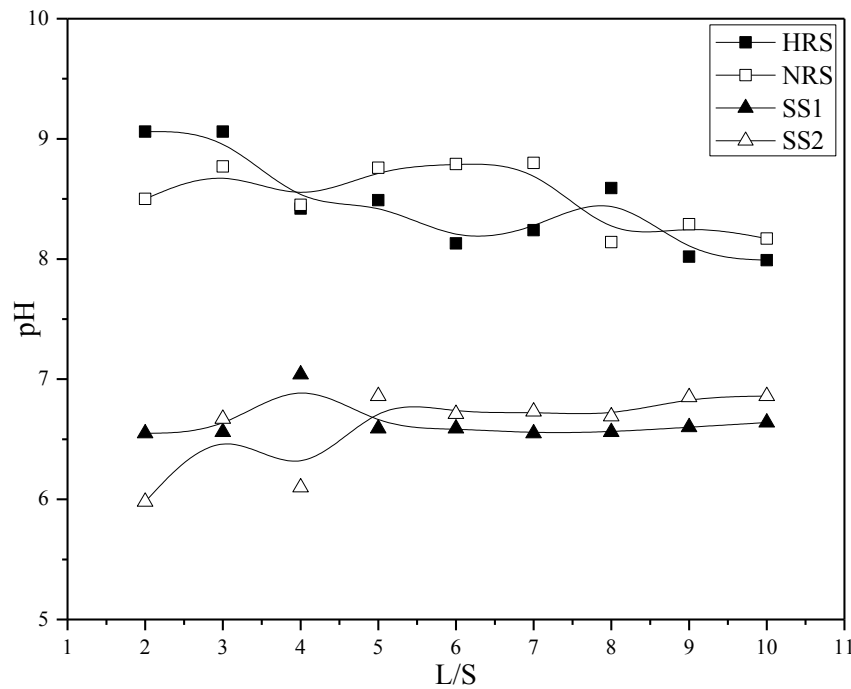
Figure 5.20. Variation of pH of NRS, HRS, SS1 and SS2 with liquid to solid ratio (L/S)

It can be seen that there is no regular pattern of pH variation with L/S ratio. Padmakumar et al. (2012) also found a similar results for Aeolian sand. Figure 5.20 also reveals that the NRS and HRS are more basic in nature than SS1 and SS2, which make them suitable for lean concreting work (Padmakumar et al., 2012). However, the high pH value may cause the leaching of heavy metal (Chaabane et al., 2016), so the leachate generated from mortar or concrete prepared using RS needs to be investigated.

The electrical conductivity (EC) and total dissolved solids (TDS) of RS were also studied at different L/S using HACH HQ40d and shown in Figures 5.21 and 5.22, respectively. It can be seen that both EC and TDS of RSs decrease as the L/S increases. A similar pattern was also observed for SS. The maximum TDS value of HRS and NRS is 700 ppm and 500 ppm respectively at L/D of 2 and the value decreases with the increase in L/S ratio. The World Health Organization (WHO) recognizes the water quality as fair if the TDS value lies between 600-900 ppm and the water is unacceptable if the TDS is higher than 1200 ppm. However, for the same L/S value, red sands show the higher value of EC and TDS than SSs. As the mineralogical study reveals that the RSs contain the majority of metallic oxides (iron and aluminium oxide), so the higher EC of the RS as compared to

SSs may be due to the presence of dissolved metallic ions.
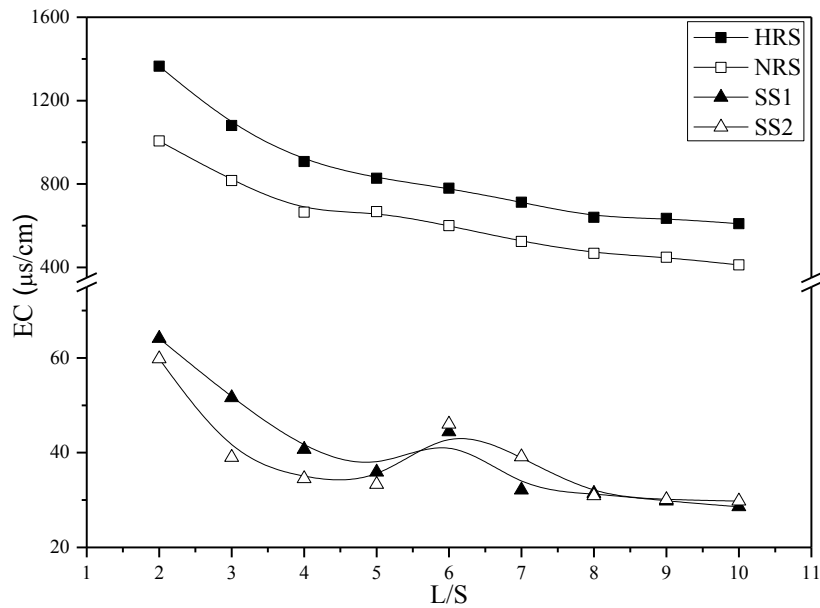
Figure 5.21. Variation of EC of NRS, HRS, SS1 and SS2 with liquid to solid ratio (L/S)
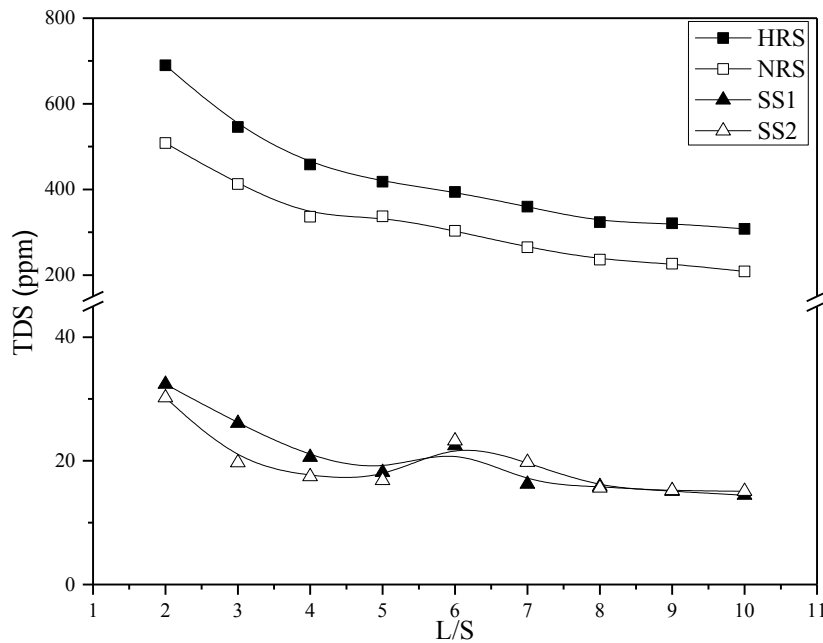
Figure 5.22. Variation of TDS of NRS, HRS, SS1 and SS2 with liquid to solid ratio (L/S)

5.8.2 Lime Reactivity

Pozzolanic activity is an important parameter which makes a material suitable as a construction material. To investigate the pozzolanic activity of the RSs and SSs, its lime reactivity (LR) was determined using Equation (5.5) (Dalinaidu et al., 2007).

$$LR = 0.25 \times \Delta EC - 2.5 \qquad\qquad (5.5)$$

Where ΔEC (mS/m) is the drop in electrical conductivity when the pozzolanic material is added to the lime solution.

The drop in electrical conductivity of the lime solution is due to the decrease in Ca^+ ions in solution as the Ca^+ ion get adsorbed at the surface of pozzolanic materials. The adsorption of Ca^+ ions at the surface of pozzolanic material forms hydration gel which results in the development of strength.

The LR of the NRS and HRS was found to be 13.7 MPa and 11.1 MPa respectively. Similarly, the LR of the SS1 and SS2 was obtained as 13 MPa and 12 MPa respectively. Hence the LR of RS is similar to that of SS. It may also be mentioned here that as the LR value of red sands is more than the standard value of 4 MPa (ASTM C593, 2011), the materials can be used in cement and concrete.

5.8.3 Leachate Analysis

To study the concentration of heavy metal in the leachate generated from RS, leachate analysis was performed using atomic absorption spectroscopy (AAS). PerkinElmer AAnalyst 200 atomic absorption spectrometer is used for the leachate analysis. The sample for the analysis prepared as per the ASTM D4793-09. Reagent water, conforming ASTM D1193, mixed with RS in 1:1 ratio and the mixture agitated continuously using magnetic stirrer for 18 h. Then the sample filtered on 0.45μm filter paper and analyzed using AAS. Before measuring the concentration of a particular element, the equipment calibrated using 1, 2 and 3 ppm standard solution of that element. The concentration of water leachable heavy metals present in the RS is shown in Table 5.4.

Table 5.4 Concentration of water leachable heavy metals in red sand

Heavy metal	Concentration (mg/L)			
	NRS	HRS	Acceptable limit	Remark
Cu	0.011	0.011	2.0	Acceptable limit is as per
Fe	3.359	1.832	1.0-3.0	guidelines for drinking
Zn	0.021	0.023	0.01-0.05	water quality, World
Ni	0.002	0.018	0.07	Health Organization.
Ca	0.793	0.364	75.00	Acceptable limit is as per
Mg	2.197	2.217	30.00	IS 10500:2012
Al	12.750	6.555	0.03	

It is found from the analysis that the heavy metals like Cu, Zn, and Ni are within acceptable limits as suggested by World Health Organization (WHO). The iron content in HRS is within acceptable limit but in NRS, it is 11.96% higher than that of permissible limit. There is no acceptable limit for Al is suggested by WHO but the Indian standard (IS 10500:2012) has fixed the acceptable limit as 0.03 mg/L. The acceptable limit for Ca and Mg in drinking water is fixed as 75.00 mg/L and 30.00 mg/L, respectively, by IS 10500:2012. From leachate analysis, it was found that the concentration of Ca and Mg is within the permissible limit in both RS. It may be mentioned here that in this research, leachate analysis of only RS was performed. However, the chemical analysis of leachate generated from mortar prepared using red sand may give different results.

5.9 Thermal Resistivity

Understanding of soil thermal characteristics is important to understand the effect of change of temperature on the soil. The thickness of soil cover above water drain, warm oil pipeline, power cable etc. is generally decided based on the thermal characteristics of soil (Farouki, 1981). Thermal characteristics of sand samples in the present study were investigated in terms of thermal resistivity (R_T) using the thermal needle probe (ASTM D5334, 2014), which works on the principle of "Transient heat method" (Naidu and Singh, 2004). The indigenously developed probe was calibrated by measuring the thermal conductivity of glycerol solution at different voltages (Naidu and Singh, 2004, Mishra et al., 2016). The measured value is then compared with the standard thermal conductivity of glycerol solution (0.287 W/m-^{o}C) and it was found that the developed probe gave the most accurate result at an applied voltage of 1V.

The R_T (in °C-cm/W) of the sand was measured at its maximum and minimum density. To measure the RT, sand was poured into the mould which used to calibrate the probe and then the probe inserted into the sample. The sample with a probe inserted into it was left for some time to bring the temperature of sand and probe in equilibrium. After that, a constant voltage of 1V applied with the help of DC power supply unit and temperature (in ^{o}C) of the probe recorded as a function of time (minute). The slope of the linear portion of the plot is calculated and Equation (5.6) (Krishnaiah and Singh, 2004) was used to calculate R_T.

$$R_T = s \times \left[\frac{Q}{4\pi} \right]^{-1} \qquad (5.6)$$

Where "s" is the slope of the linear portion of curve and "Q" is the heat input per unit length (= $I^2.R$). Here "I" is the current applied and "R" is the resistance (in Ω/cm) of nichrome wire used in the probe.

The thermal resistivity of sand at their minimum and maximum dry density is shown in Figure 5.23. From this study, it was found that the thermal resistivity of the NRS at the dry density of 15.89 kN/m^3 and 13.73 kN/m^3 are 258.25 ^{o}C-cm/W and 346.40 ^{o}C-cm/W, respectively which is lower than that of aeolin sand at the same dry density (303 ^{o}C-cm/W and 368 ^{o}C-cm/W) (Padmakumar et al., 2012). The thermal resistivity of HRS at the dry density of 14.32 kN/m^3 is 135.40 ^{o}C-cm/W, which is lower than that of aeolian sand (340 ^{o}C-cm/W) at same dry density.

The lower value of thermal resistivity of RS as compared to aeolian sand (Padmakumar et al., 2012) at same dry density may be due to composition and structure of sand particles (Farouki, 1981). It can be seen that as the density decreases, R_T increases for all sand sample. This may be due to the fact that higher density results in higher grain to grain contact area and less air void within the sand mass. Padmakumar et al. (2012) also found a similar pattern for aeolian sand deposit from Indian desert. It is found that the HRS shows lesser RT value as compared to other sand which may be due to the presence of angular particles (Abdel-Mottal, 2014). Low RT values of RSs reveal that they can dissipate the heat more efficiently as compared to the SS. So it may be used as a construction material where the heat dissipation is required like power cable trench.
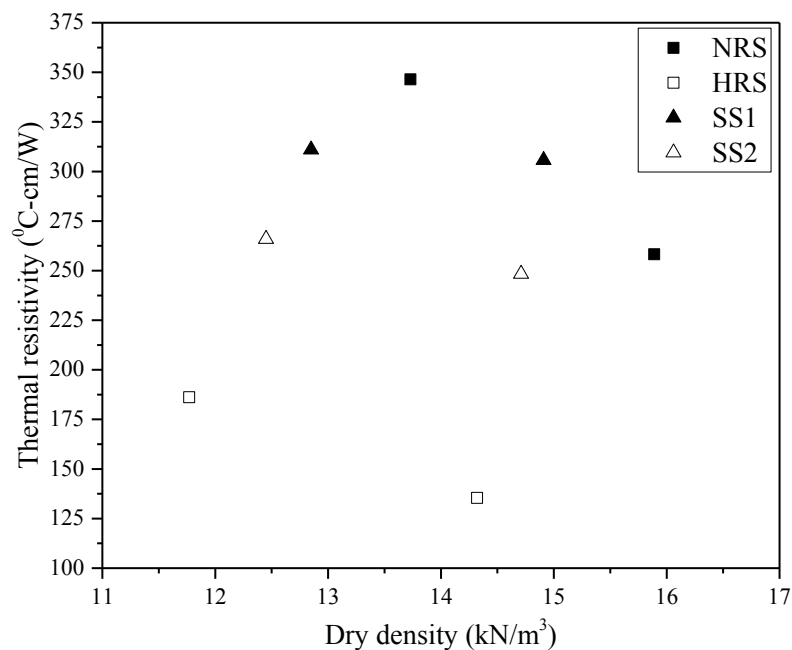
Figure 5.23. Variation of thermal resistivity with dry density

5.10 Conclusions

Based on the laboratory investigation on two Indian red sands, NALCO red sand (NRS) and HINDALCO red sand (HRS), following conclusions can be drawn.

1. The average roundness index and sphericity of RSs are found to be higher than that of SSs. But, for the same water to cement ratio, flowability of red sand is less than that of SS due to the higher specific surface area of RS. The maximum and minimum void ratios of the sands are found to depend upon the roundness index. It was also found that the variation of friction angle corresponding to maximum and minimum density depends upon the percentage of angular particles.

2. Though the sphericity of the RS is higher than SS, but for a particular water-cement ratio, the mortar prepared using SS is more flowable compared to RS. One of the reasons for the same was found due to the low specific surface area of red sands.

3. Both NRS and HRS contain an oxide of iron in form of hematite (Fe_2O_3) and magnetite (Fe_3O_4) as a major constituent along with SiO_2 and Al_2O_3. It was also observed that HRS and NRS contain amorphous phase, which can take part in the pozzolanic activity.

4. As the angle of internal friction of RS is higher than that of Indian SS, RS in mortar will increase its yield stress and plastic viscosity. However, the proper strength test of the mortar prepared using RS needs to be conducted.

5. The zeta potential values of RS at high pH values are similar to that of standard sand, hence, can be used in cement mortar/concrete.

6. As the LR value of NRS and HRS is more than the standard value (4 MPa), the material can be used in cement and concrete. However, it is suggested to conduct necessary strength test on the concrete prepared using RS.

7. As the RS shows lower thermal resistivity as compared to SS, it can be used as a construction material where the heat dissipation is required.

8. Though, the total dissolved solids in both NRS and HRS is more than that of SS but falls within the acceptable limit as suggested by WHO. However, the chemical analysis of leachate generated from mortar and concrete prepared using RS may give different results.

9. The major difficulty is the recovery of RS from RM as Indian RM contains only 10-20% of RS by weight. Also as the gradation of RS depends on the process of

grinding of bauxite during Bayer's process, RS collected from different sources may have different gradation and particle shape.

In this chapter, the characterization of coarse fraction (>75µm) of RM as a civil engineering construction materials has been discussed. But it is found that the utilization rate is very low as RM contain less percentage (10-20%) of sand sized particles. Chapter 6 discusses the stabilization of RM as a whole using ground granulated blast furnace slag (GGBS) and alkali activated GGBS for its bulk utilization.

Chapter 6

Strength and Durability Characteristic of Stabilized Red Mud

6.1 Introduction

Several studies are available on the stabilization of soil without or with alkali activation of industrial waste but the study on the stabilization of red mud is limited (Duchesne and Doye, 2005; Panda et al., 2016) and particularly using geopolymer is not reported. It is also observed that in most of the cases, KOH or NaOH are used as an activator.

So, in the present study, the Indian red mud collected from two different sources is stabilized using ground granulated blast furnace slag (GGBS) to improve the strength and durability characteristic of red mud. The effect of alkali (Na_2SiO_3) activation of GGBS blended red mud on strength, durability, and microstructural property have been studied for its possible use as geotechnical materials. The durability study under alternate wetting and drying was studied along with the slake durability to understand the effect of flowing water on particle integrity. Although utilizing the industrial waste helps in the reduction of storage and minimizing the use of natural resources, however it can have a negative impact on a human in terms of dusting, leaching, and radiations (Gidley and Sack 1983). So, the chemical analysis of leachate in term of water-leachable heavy toxic metals (Hg, As, Pb, and Cr) as identified by EPA were studied in the present research.

6.2 Stabilizing Materials Used

Ground granulated blast furnace slag (GGBS) was used to stabilize the red mud to improve its strength and durability characteristics. The GGBS collected from Rourkela steel plant (RSP), Rourkela in the state of Odisha. An extra pure sodium silicate (Na_2SiO_3) was used as an alkali activator in the present research and was purchased from Loba Chemie Pvt. Ltd.

6.3   Experimental Result and Discussion

6.3.1 Morphology and Mineralogy of GGBS

The morphology of the GGBS studied using the SEM image (Figure 6.1) and shows that it contains solid particles of different shapes with a very sharp edge and smooth surface. The GGBS particles also found to have a few cavities at the surface as can be seen in the magnified image.
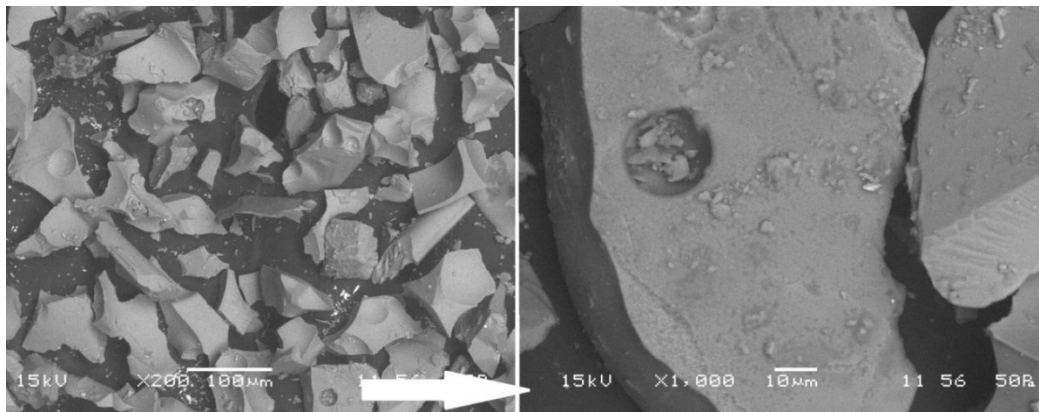
Figure 6.1. SEM image of GGBS
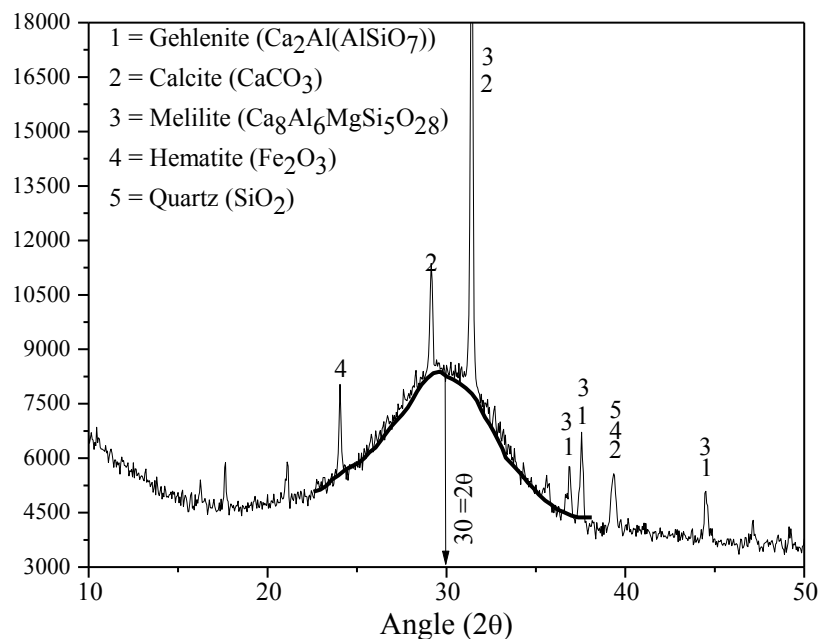
Figure 6.2. XRD graph of GGBS

Figure 6.2 shows the XRD micrograph of GGBS used in the present study. It is to be noted that calcium compound like calcite ($CaCO_3$) and melilite ($Ca_8Al_6MgSi_5O_{28}$) are present in the majority, which was also found by XRF and FTIR (Section 6.3.2 and

101

6.3.3). Along with the peak of quartz, the GGBS also shows the peak of haematite (Fe_2O_3), quartz (SiO_2), and gehlenite ($Ca_2Al(AlSiO_7)$). The mineral peak observed in the XRD micrograph also confirmed by the XRF analysis (Section 6.3.2).

6.3.2 Chemical Characteristic of GGBS

Chemical composition of the GGBS studied using the X-ray fluorescence (XRF) analysis using Axios PANalytical with scintillation type detector at 20kV and 10mA available at Indian Institute of Technology, Kharagpur and is presented in Table 6.1. Major portion of GGBS (95.83%) contains Al_2O_3, SiO_2, CaO, and MgO in which CaO is 34.92% and SiO_2 is 32.56%. Along with CaO and SiO_2 as major chemical, the GGBS also contains considerable percentage of Al_2O_3 (17.11%) and MgO (11.24%).

Table 6.1 Chemical composition of GGBS

Chemicals	Weight percentage (%)	
	GGBS	Typical range
Fe_2O_3	0.41	0.00- 5.80
Al_2O_3	17.11	5.74- 21.60
SiO_2	32.56	21.00- 41.86
CaO	34.92	33.50- 56.10
MgO	11.24	0.00- 12.09
Na_2O	0.24	0.00- 1.06
TiO_2	0.49	0.00- 1.90
K_2O	0.94	0.00- 1.47
P_2O_5	0.01	-
SO_3	1.80	-

6.3.3 Fourier Transform Infrared (FTIR) Analysis of GGBS

The FTIR spectra of GGBS are shown in Figure 6.3. The smooth, symmetrical band at 1639 cm^{-1} is due to the water molecule adsorbed at the surface. The sharp band at 1419 cm^{-1} denotes the carbonate ion stretching of anhydrous $CaCO_3$ which confirm the presence of calcite in the GGBS. The band at 981 cm^{-1} and 709 cm^{-1} indicate the stretching of silicate ions which also confirm the presence of quartz in GGBS (Castaldi et al., 2010).
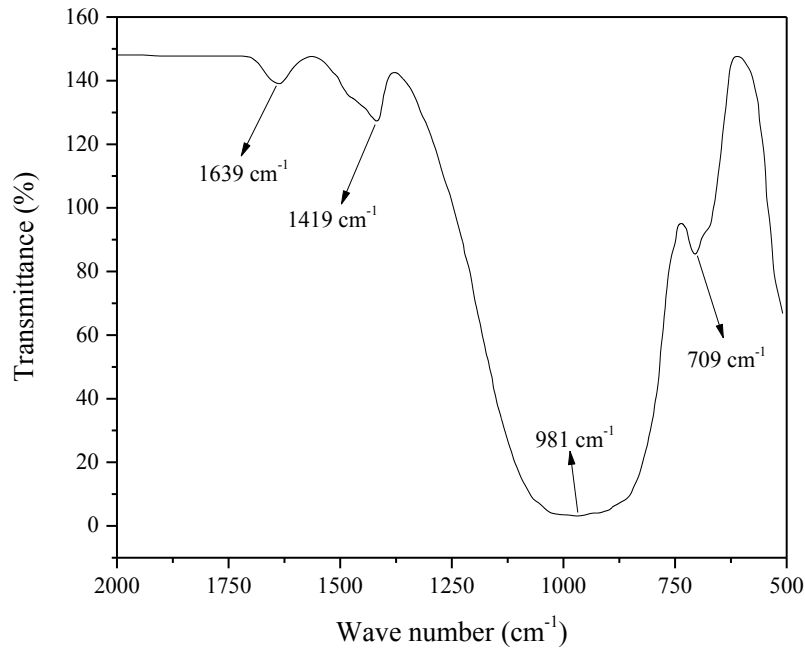
Figure 6.3. FTIR spectra of GGBS

6.3.4 Particle Size Analysis and Specific Gravity

The particle size analysis of the raw materials (NRM, HRM, and GGBS) along with NRM/HRM-GGBS mix is performed using sieve analysis (ASTM D7928) for a fraction above 75 µm and sedimentation method (ASTM D6913) for the particle below 75 µm and is presented in Figure 6.4. The NRM/HRM-GGBS mixture is prepared by mixing 5%, 15%, and 25% GGBS by weight in NRM and HRM (Table 6.2).
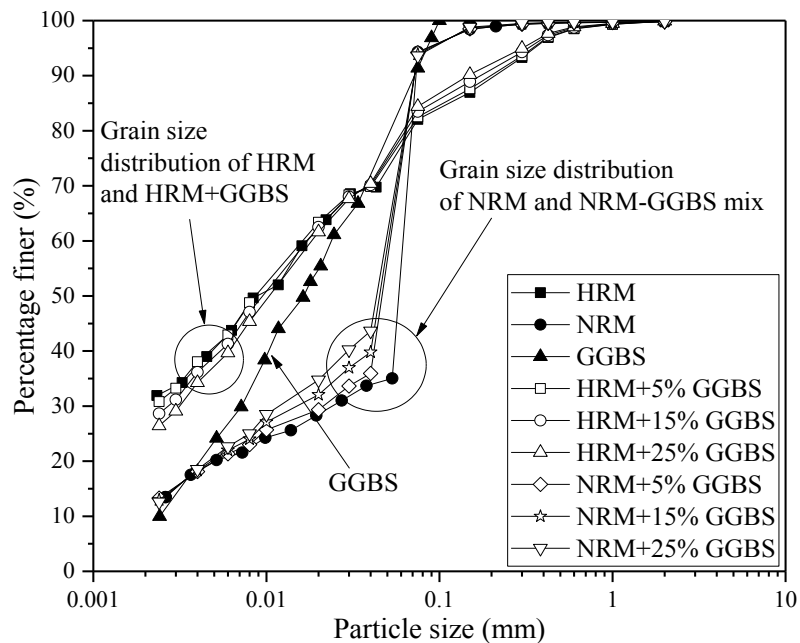
Figure 6.4. Particle size analysis of RM, GGBS and RM-GGBS mix

Using the particle size distribution curve, the coefficient of uniformity (c_u) and coefficient of curvature (c_c) of NRM, HRM, GGBS, and NRM/HRM-GGBS mixture has been calculated and presented in Table 6.2.

Table 6.2 Physical characteristic of RM, GGBS, and RM-GGBS mix

	c_u	c_c	Clay fraction (%)	Silt fraction (%)	Sand fraction (%)	G_s	MDD kN/m^3
GGBS	10.00	1.11	10.00	82.50	7.50	2.80	-
NRM	27.27	3.34	14.00	81.00	5.00	3.33	16.50
HRM	8.09	0.12	32.00	51.00	17.00	3.27	15.35
95% NRM+5% GGBS	24.05	3.77	13.40	80.80	5.80	3.17	16.70
85%NRM+15%GGBS	23.81	1.60	13.00	80.80	6.20	2.98	17.15
75%NRM+25%GGBS	23.81	1.05	12.50	81.10	6.40	2.92	17.55
95% HRM+5% GGBS	7.61	0.13	30.85	51.65	17.50	3.24	15.65
85%HRM+15%GGBS	8.09	0.14	28.60	54.90	16.50	2.91	16.00
75%HRM+25%GGBS	9.05	0.23	26.50	58.00	15.50	2.87	16.30

The c_u value of NRM, HRM, GGBS, and NRM/HRM-GGBS mix are greater than 6. GGBS is well graded with c_u and c_c value of 10.00 and 1.11 respectively but the NRM and HRM are poorly graded with c_c value of 3.34 and 0.12 respectively. The mixture of 5% GGBS and 95% NRM remains poorly graded with c_c value (3.77) greater than 3. However, a higher percentage of GGBS (15% and 25%) makes the NRM-GGBS mixture well graded with c_c value of 1.60 and 1.05 for 15% and 25% GGBS respectively. The addition of GGBS in HRM increases the c_c value of HRM-GGBS mixture from 0.12 at zero percent to 0.23 at 25% GGBS, but the mixture remains poorly graded. GGBS has 82.50% silt fraction followed by 10.00% clay fraction and 7.50% sand fraction. NRM contains 81.00% silt fraction along with 14.00% clay fraction while HRM contains 51.00% silt fraction along with 32.00% clay fraction. Miners (1973) also observed 20-30% clay-sized particle in RM. Li (1998) observed up to 50% clay-sized particle in some red mud. Although both the red mud (NRM and HRM) contain a higher percentage of clay fractions compare to GGBS; the total fine content in GGBS (92.50%) is very similar to NRM (95.00%) and higher than that of HRM (83%).

Specific gravity (G_s) of the GGBS and RM-GGBS mixture studied according to ASTM D854 and are presented in Table 6.2. The GGBS has G_s value of 2.80, which is very similar to the value (2.79) reported by Li and Zhao (2003). However, the G_s of NRM (3.33) and HRM (3.27) is higher than that of GGBS (2.80). Vick (1990) also reported that the specific gravity (G_s) of RM lies between 2.8 to 3.3. Higher G_s of RM compare to GGBS may be due to the higher percentage of iron oxide (Fe_2O_3) in RM as reported in Table 6.2. The G_s of NRM/HRM mix with 5, 15, and 15% GGBS decreases with increase in GGBS (Table 6.2).

6.3.5 Compaction Characteristics

Moisture content and dry unit weight obtained under standard effort for the RM and red mud blended with 5, 15, and 25% GGBS are presented in Figure 6.5. NRM shows higher maximum dry density (MDD) (16.50 kN/m^3) compare to HRM (15.35 kN/m^3) which may be due to the higher G_s of NRM (Table 6.2).
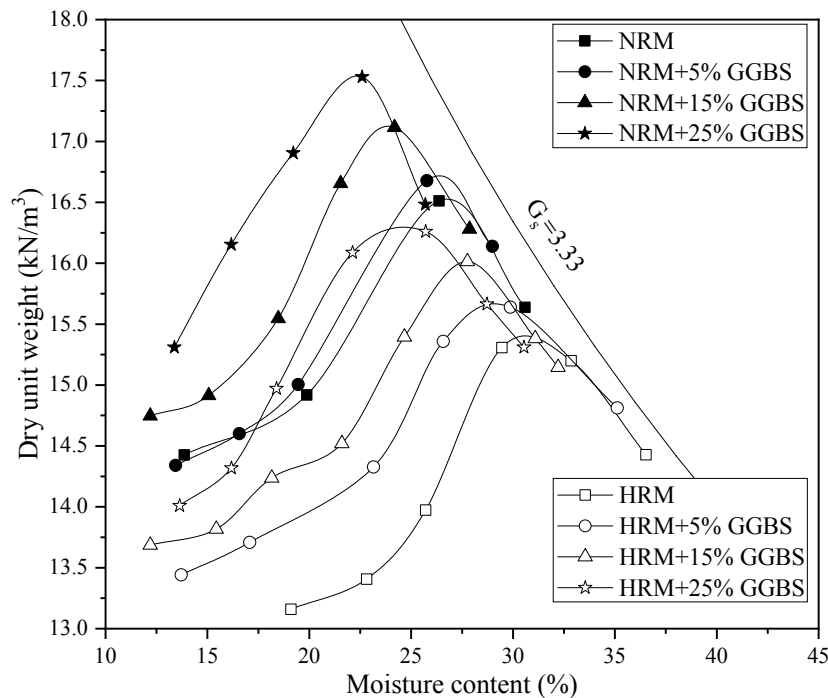
Figure 6.5. Compaction characteristic of red mud and red mud-GGBS mix

As listed in Table 6.2, the addition of 5, 15, and 25% GGBS increases MDD value of NRM-GGBS mixture by 1.21, 3.93, and 6.36% respectively, whereas MDD value of HRM-GGBS mixture increases by 1.95, 4.23, and 6.19% due to addition of 5, 15, and 25% GGBS respectively. It is observed that although the specific gravity decreases with

the increasing percentage of GGBS; the MDD value of the mixture increases till 25% GGBS. The increase in MDD value may be attributed to the decrease in clay fraction (Table 6.2) which reduces the resistance towards the particle movement during compaction (Phanikumar et al., 2007). However, a further increase in GGBS may show different compaction behaviour and further study is required in this regard. It is worth to mention here that GGBS used in the present study is finer than 150μm and the effect of particle size of GGBS on the compaction characteristics needs further study.

6.3.6 Unconfined Compressive Strength

The unconfined compressive strength (UCS) test performed on the cylindrical samples (5 cm diameter and 10 cm height) compacted at their respective optimum moisture content (OMC). The samples stabilized with different percentage of GGBS (5, 15, and 25%) were cured at ambient temperature (AT) for 3, 7, and 28 days. The samples were also prepared using 0.25, 0.50, and 1.00M sodium silicate (Na$_2$SiO$_3$) solution in place of water to study the effect of alkali activation.

A typical strain-stress curve of NRM and HRM is shown in Figure 6.6. The UCS of the NRM and HRM is 564.08 kPa and 441.45 kPa respectively. The post peak behaviour of NRM indicates brittle rupture (Das and Yudhbir, 2005).
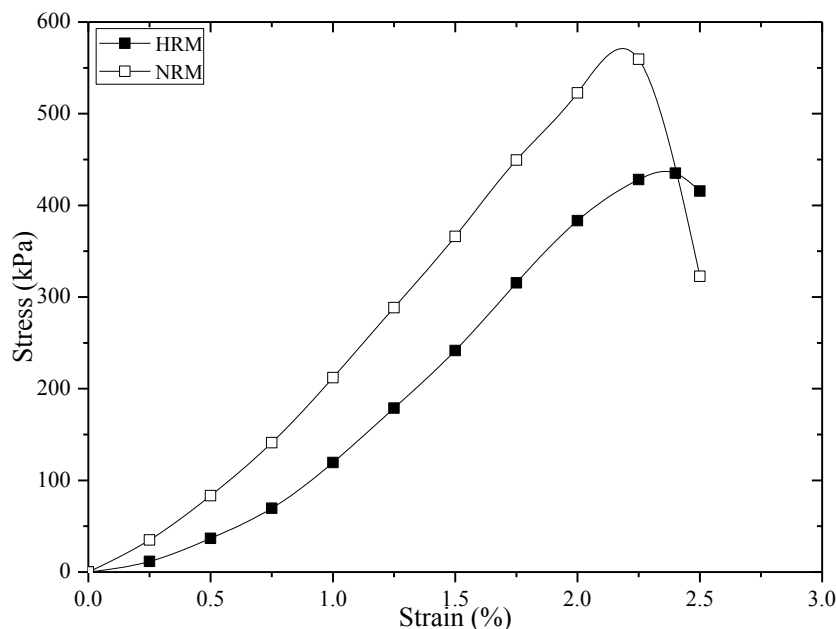
Figure 6.6. Typical strain-stress plot of red mud

106

The curing period and the percentage of GGBS are found to have a positive effect on the UCS of both (NRM and HRM) as shown in the Figure 6.7 and 6.8. The stabilization of either red mud using GGBS increases its unconfined compressive strength and the brittle failure was observed for both the stabilized red mud. The addition of 5, 15, and 25% GGBS in NRM increases the UCS by 26.52, 66.42, and 82.99% after 3 days curing period, while the UCS value increases by 87.60, 172.76, and 290.63% after the curing period of 28 days as presented in Figure 6.7. However, the increase in UCS value after addition of 5, 15, and 25% GGBS in HRM was observed as 1.20, 64.90, and 91.59% after 3 days curing period, while after 28 days curing period, an increase of 143.72, 179.67, and 241.45% of UCS value is observed (Figure 6.8). The increase in UCS value may be attributed to the physical binding of NRM with GGBS during the curing period.
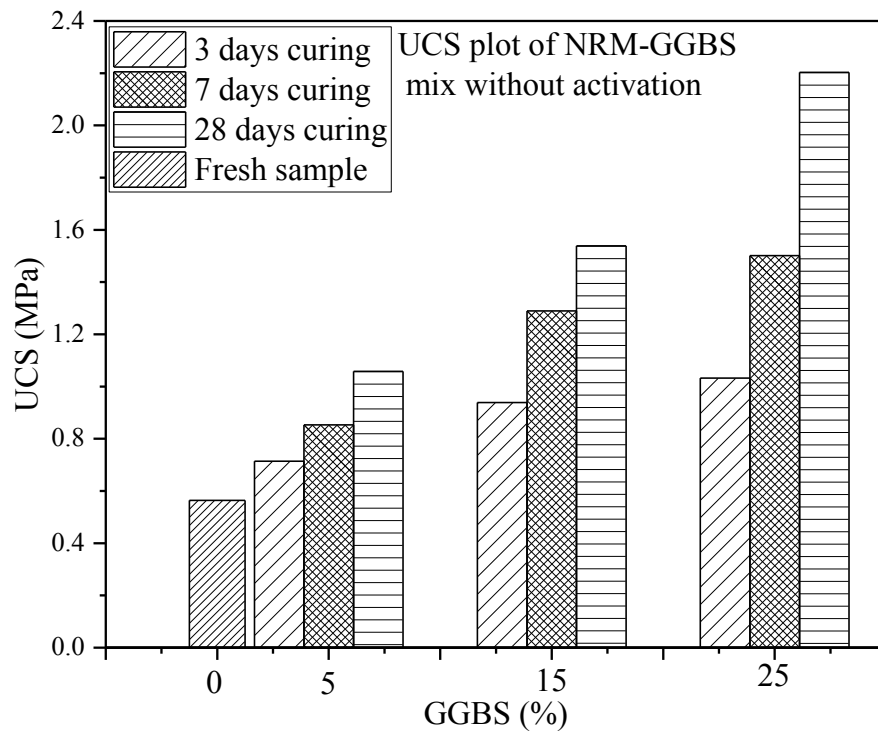
Figure 6.7. Effect of curing period and percentage of GGBS on the UCS of NRM
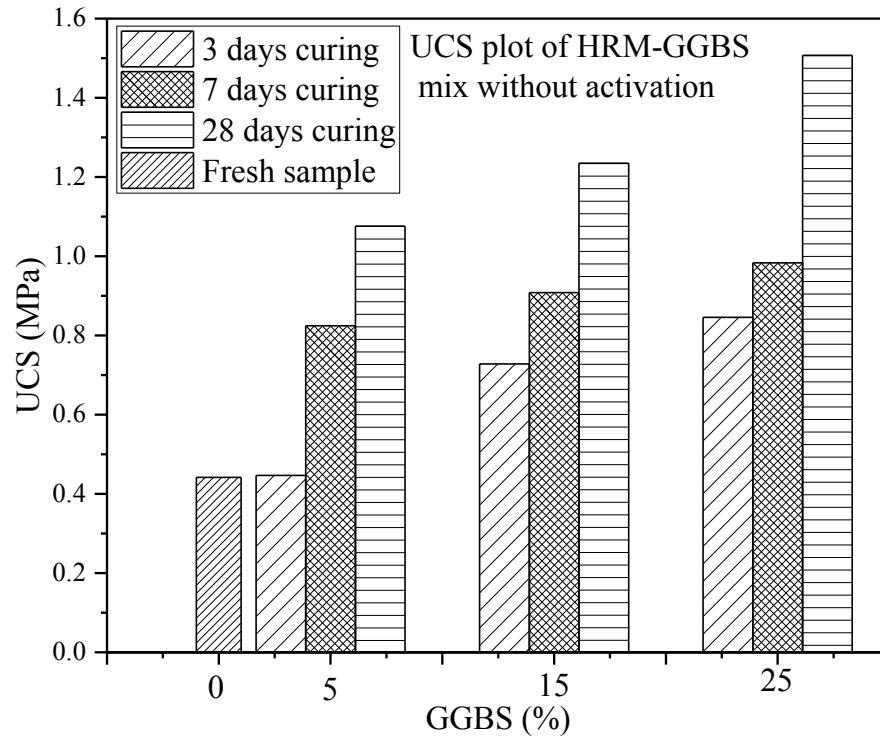
Figure 6.8. Effect of curing period and percentage of GGBS on the UCS of HRM

Although stabilization with GGBS increases the UCS, the stabilized was not found durable under alternate wet-dry cycle and also does not show sufficient resistance towards particle disintegration under flowing water condition.

To improve the durability under alternate wet-dry, GGBS-NRM mixture was stabilized by using Na_2SiO_3 (0.25, 0.50, and 1.00M) as an alkali activator. The unconfined compressive strength of NRM and HRM stabilized with activated GGBS is plotted against percentage GGBS for different molarity of Na_2SiO_3 are shown in Figures 6.9 and 6.10 respectively. The very minor difference in the UCS value of NRM stabilized with alkali activated 5% GGBS is observed while the difference is found to increase with increasing percentage of GGBS. The difference in UCS of GGBS-NRM activated with 0.25 M and 0.5 M Na_2SiO_3 is found marginal after 3 days curing and found to increase with curing period. An abrupt increase in the UCS of NRM stabilized with 25% GGBS activated by 1M Na_2SiO_3 can be observed for any curing period (Figure 6.9). The NRM stabilized with 25% GGBS and activated with 1M Na_2SiO_3 gives the maximum UCS (approximately 11 MPa) after the curing period of 28 days.

(a)

(b)

(c)
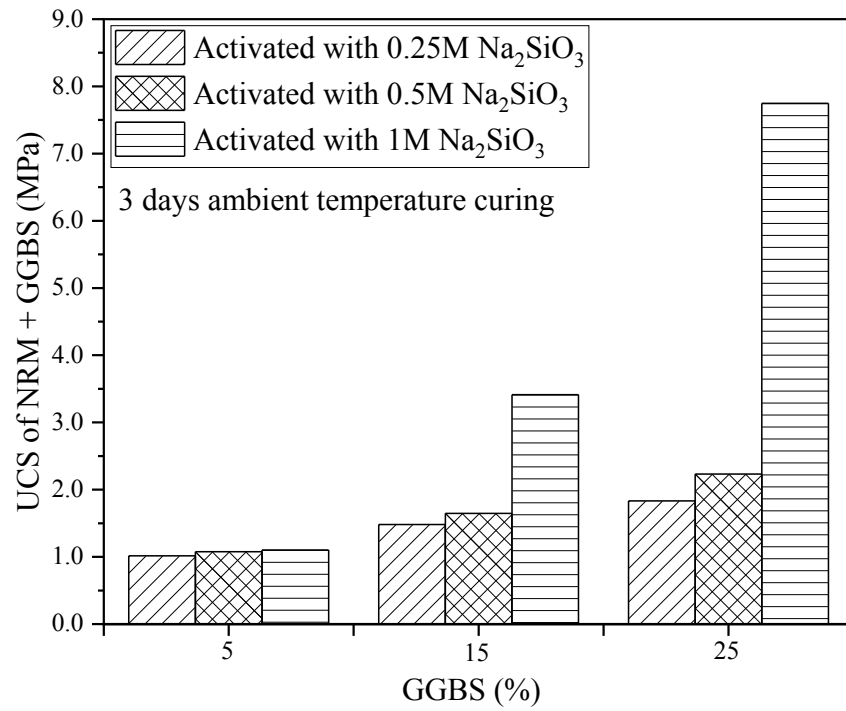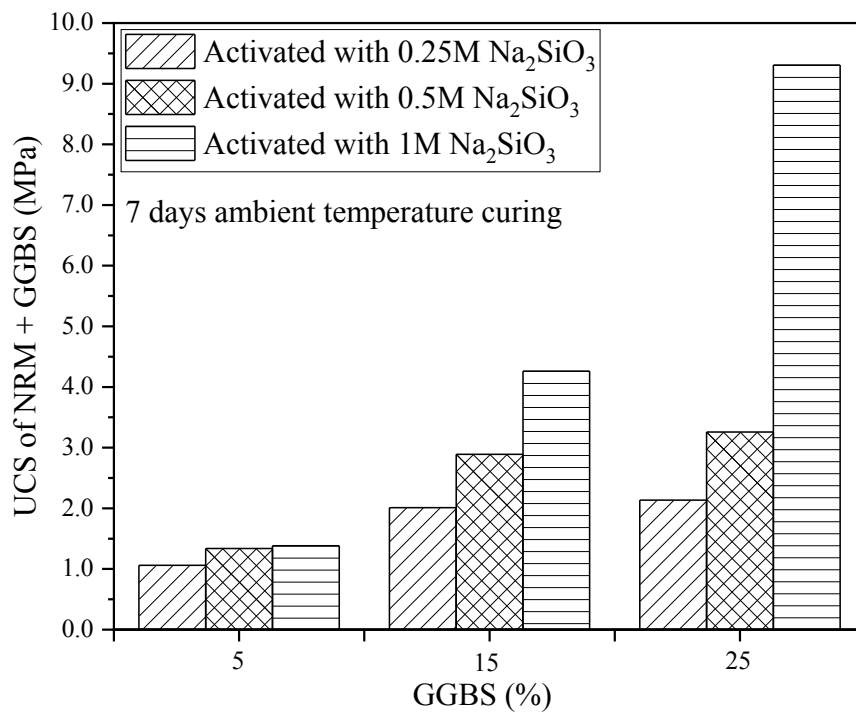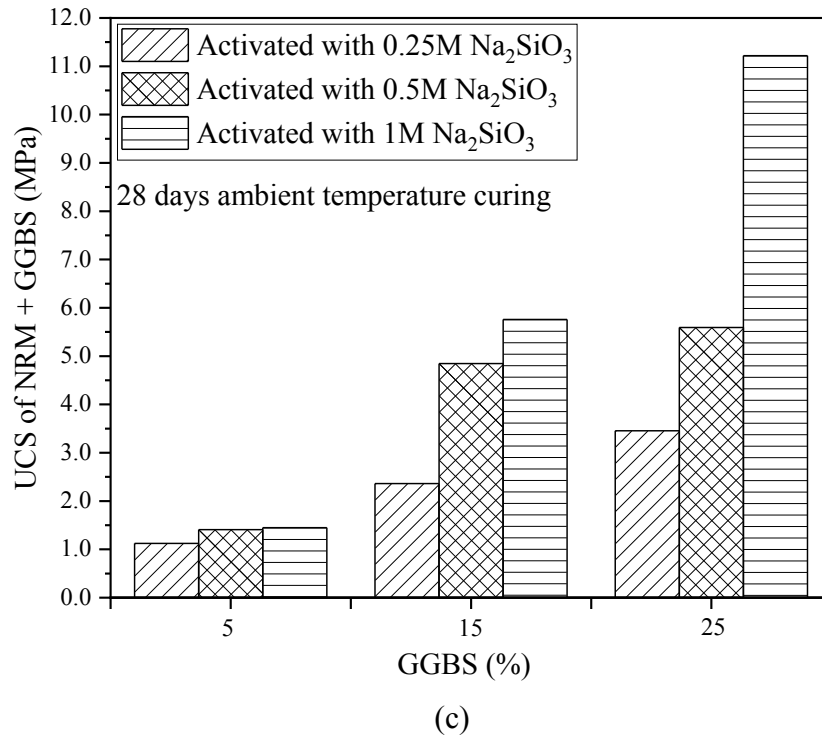
Figure 6.9. Variation of UCS value of GGBS-NRM with molarity of Na_2SiO_3 after (a) 3 days curing (b) 7 days curing, and (c) 28 days curing period

The similar effect of alkali activation is observed in the GGBS stabilized HRM (Figure 6.10), however, unlike NRM, the considerable difference in the UCS is observed in case of activation with 0.25M and 0.5M Na_2SiO_3 for any percentage of GGBS and number of curing days.

(a)
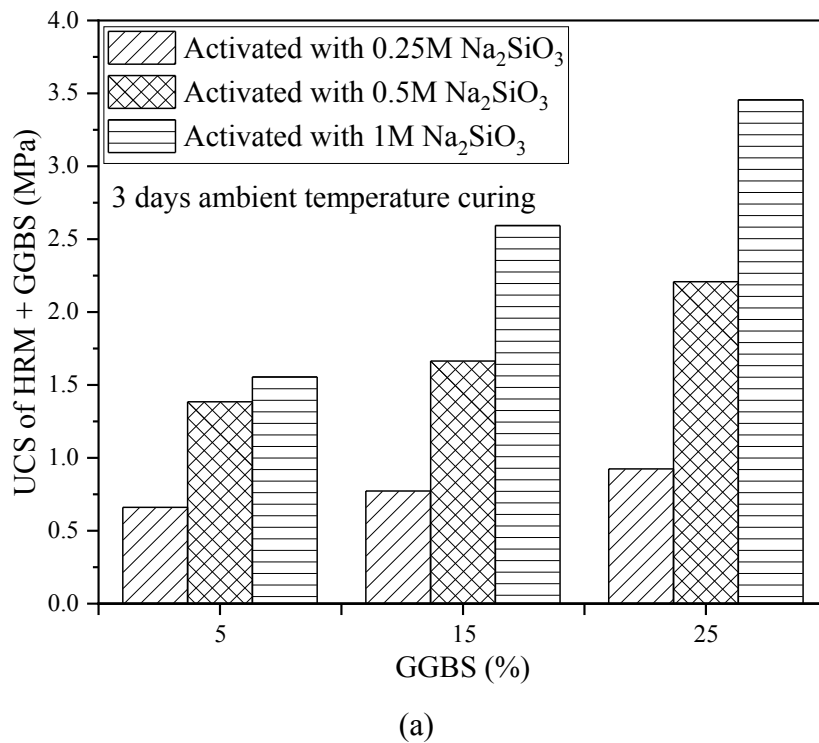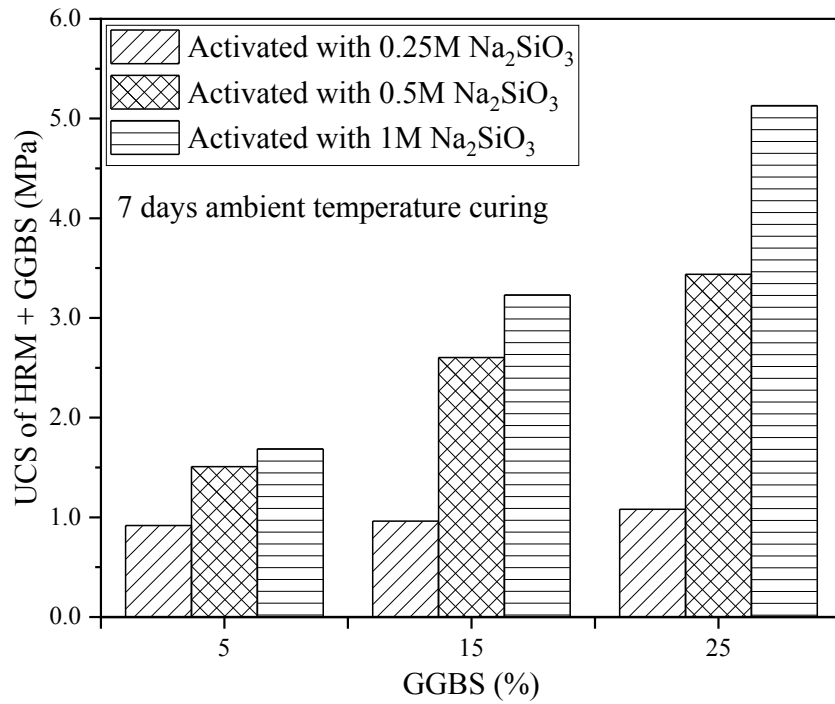
(b)
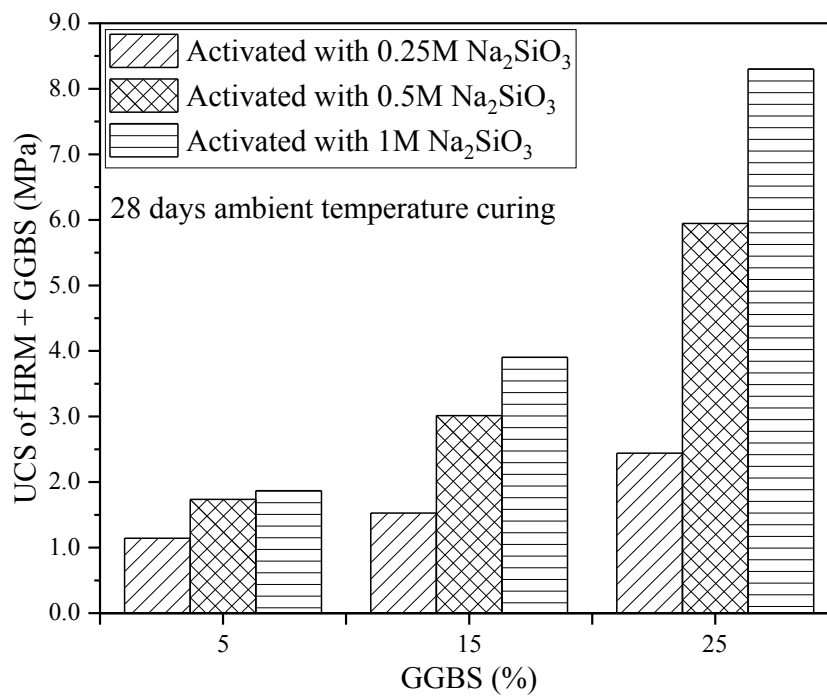
(c)

Figure 6.10. Variation of UCS value of GGBS-HRM with molarity of Na_2SiO_3 after (a) 3 days curing (b) 7 days curing, and (c) 28 days curing period

Similar to the NRM, the maximum UCS is observed in case of HRM stabilized with 25% GGBS and activated with 1M Na_2SiO_3. But the maximum strength observed in case of HRM (approximately 8 MPa) is lower than that of NRM (approximately 11MPa).

The effect of curing period on the UCS of alkali activated red mud stabilized with GGBS is studied and presented in Figure 6.11 for NRM and Figure 6.12 for HRM. An abrupt increase in UCS of NRM stabilized with 25% GGBS and activated with 0.25M Na_2SiO_3 is observed after 28 days curing and the same behaviour is observed after 28 days when the NRM is stabilized with 15% GGBS and activated with 0.5M Na_2SiO_3.
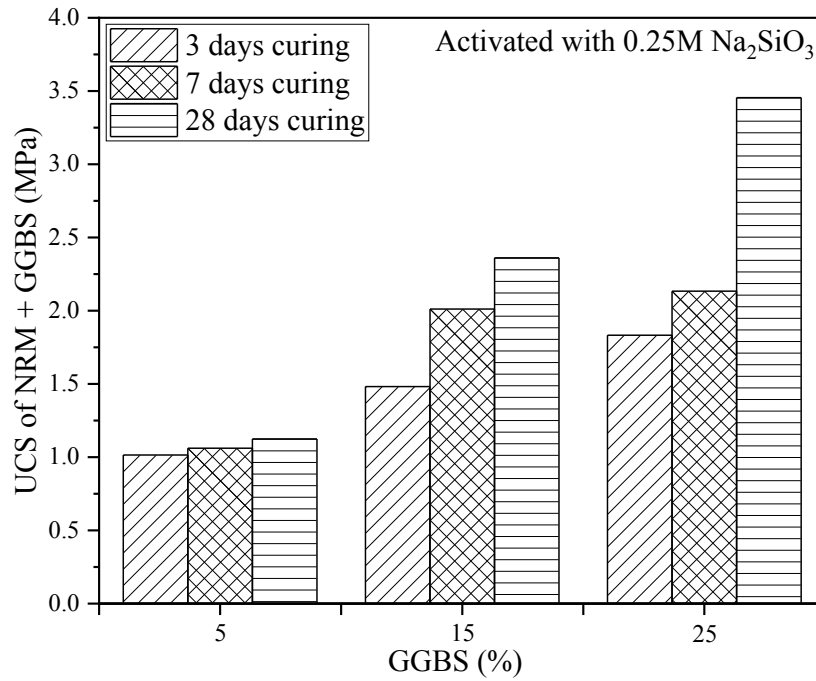
(a)
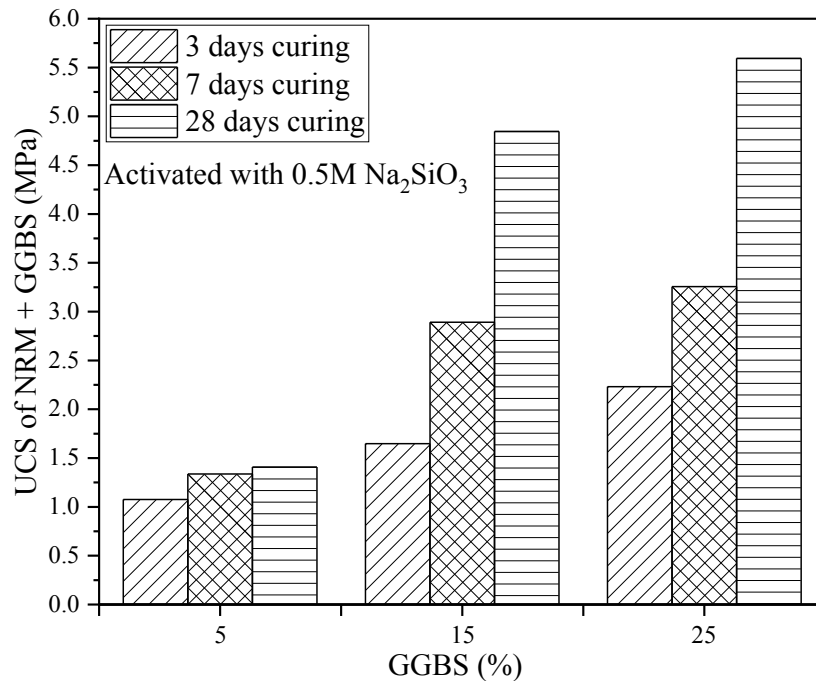
(b)
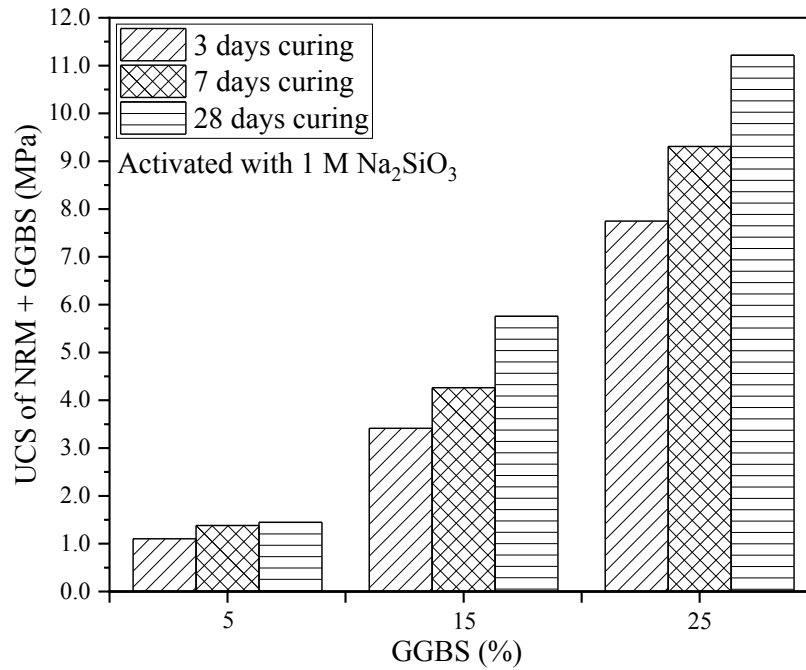
(c)

Figure 6.11. Variation of UCS with different percentage of activated GGBS-NRM mixture

However, when 1M Na_2SiO_3 is used for the activation, a gradual increase in the UCS is observed but it gives the maximum UCS of approximately 11 MPa for NRM-25%GGBS after 28 days curing. The effect of curing period on the UCS of alkali activated HRM stabilized with GGBS is presented in Figure 6.12.

(a)

113

(b)

(c)
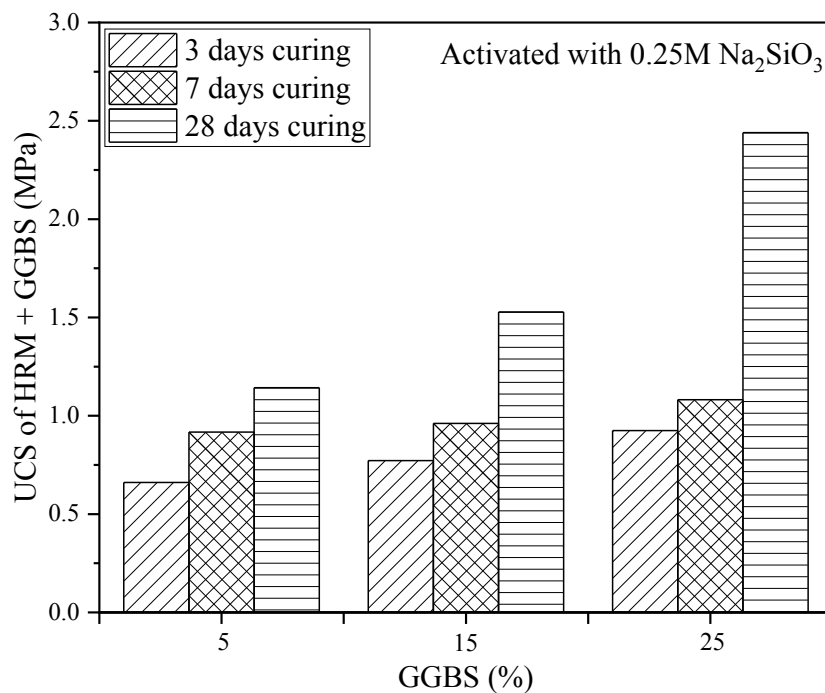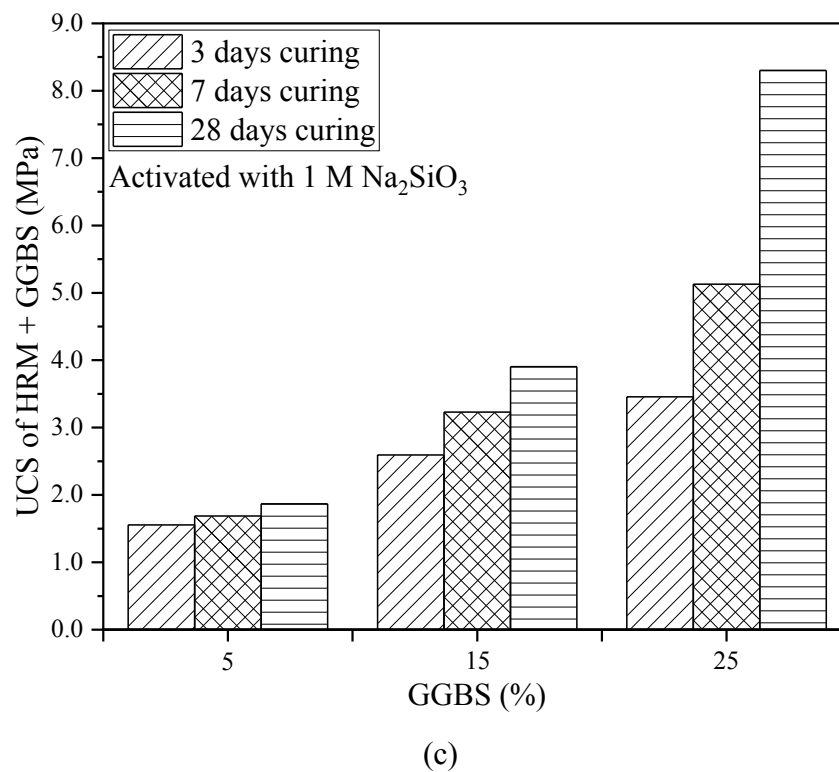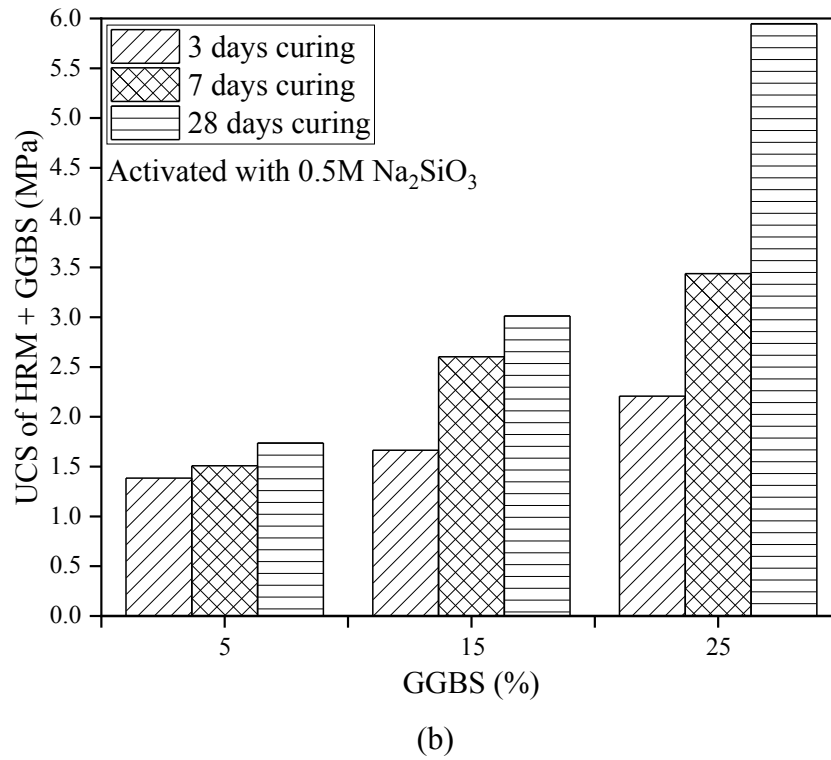
Figure 6.12. Variation of UCS with different percentage of activated GGBS-HRM mixture

The curing period is found to play an important role in increasing the UCS of alkali activated HRM-GGBS (Figure 6.12). As the percentage of GGBS is increased, the difference between the 7 days and 28 days UCS is increased for 0.25M Na$_2$SiO$_3$.

However, the similar observation is made in case of 0.5M and 1M Na_2SiO_3 but for the 25% GGBS.

A comparative study between the UCS of 1M Na_2SiO_3 activated GGBS stabilized red mud after different curing period is presented in the Figure 6.13. It is found that the HRM stabilized with 5% activated GGBS shows the higher value of UCS as compare to NRM stabilized with 5% GGBS irrespective of the curing period.
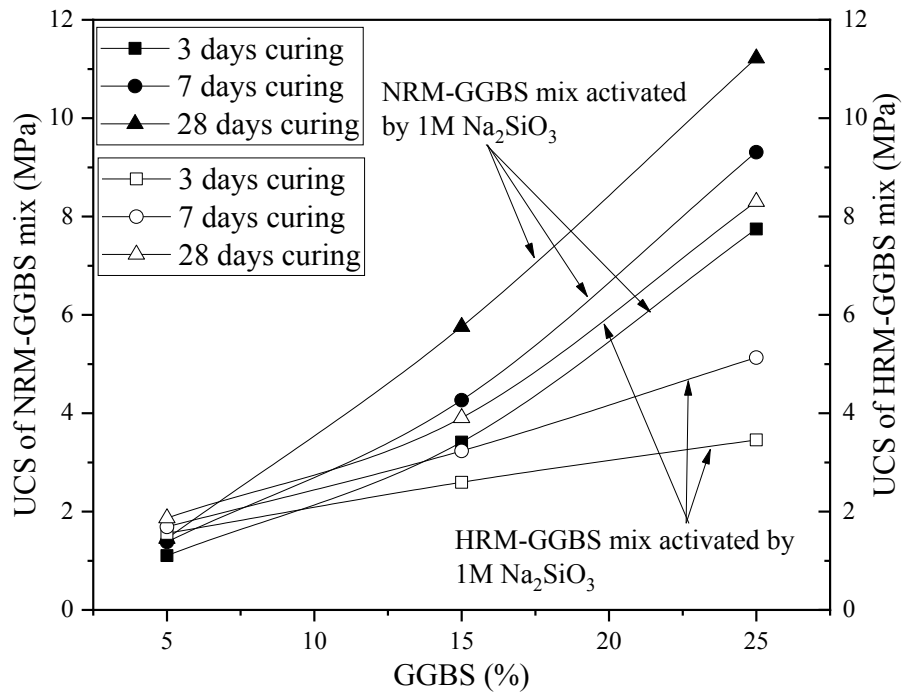
Figure 6.13. Comparative representation of UCS of NRM/HRM-GGBS activated with 1M Na_2SiO_3

However, at the higher percentage of GGBS (15% and 25%) the NRM-GGBS gives the higher UCS and the difference in UCS increases with the increase in GGBS percentage. This difference is found to decrease with the increase in curing period for 25% GGBS but for the 15% GGBS, the difference is maximum after 28 days curing.

6.3.7 Durability Study of Stabilized Red Mud

The stabilized red mud must have the capability to retain its strength and integrity under service environment. To simulate the real field environment, different test conditions like freezing and thawing, heating and cooling, and wetting and drying are used. However, for the tropical area, heating and cooling and wetting and drying conditions are relevant. In the present research, the durability under alternate wetting and drying (W-D) was studied along with the slake durability test.

6.3.7.1 Durability study under alternate wetting and drying

The cylindrical samples of 5 cm diameter and 10 cm height were prepared with GGBS blended RM by compacting at their OMC. The stabilized compacted samples were used to perform the durability study according to ASTM D559 (2015). Samples were placed in humidity chamber and protected from direct contact of free water for seven days. After that, the samples were submerged in portable water for a period of 5 h followed by 42 h oven drying at $71^{o}C$ which completed on cycle of wetting and drying. Figure 6.14 shows the samples submerged in the water during the durability test.
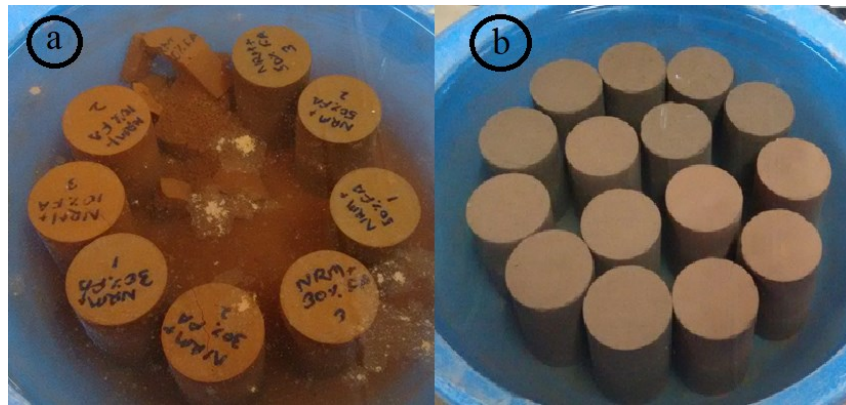
Figure 6.14. Typical photo of stabilized sample for durability test

The samples stabilized with GGBS without activation collapsed when submerged in the water (Figure 6.14a).
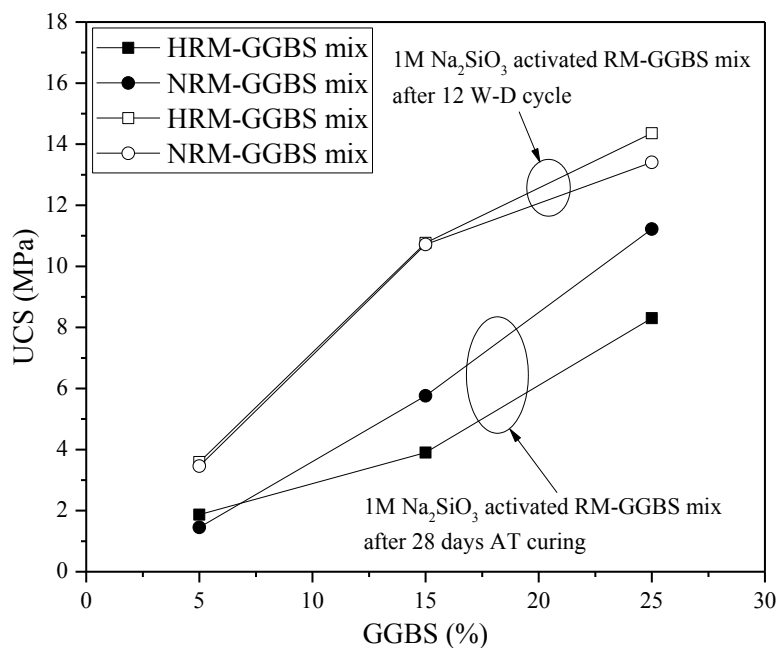
Figure 6.15. A comparison between the UCS value after 28 days UCS and after 12 wet-dry cycle

The effect of alternate wetting and drying on the stabilized RM studied and the results are presented in term of unconfined compressive strength (UCS) and the mineralogical changes. The results are also compared with the 28 days strength of the NRM/HRM stabilized with 5, 15, and 25% activated GGBS (Figure 6.15).

6.3.7.2   Slake durability test

The slake durability test is important to understand the disintegration of the particles due to alternate drying and wetting with the flow of water. In the present research, the test is performed on irregular samples of red mud stabilized with 5, 15, and 25% GGBS and activated with 1.00M sodium silicate (SS) solution as suggested by ASTM D4644 (2016). Figure 6.16 showing the stabilized red mud samples in the rotating drum. The samples were subjected to 4 cycles to understand the effect of a number of the cycle on the slake durability index (Figure 6.17). The test samples before the test and after the fourth cycle are shown in Table 6.3 which shows the appearance of the samples before slaking and after the fourth cycle of slaking. It can be observed that the initially the samples were irregularly shaped but after the fourth cycle, the rounded edge can be observed. It can also be observed that for any molarity of Na_2SiO_3, the alkali activated GGBS-HRM samples shows more rounded edge which shows lower resistant towards the part disintegration as compared to alkali activated GGBS-NRM samples.

Figure 6.16. Typical photo showing the sample during slake durability test

Also, the GGBS-NRM mixture activated by 1M Na_2SiO_3 shows a very small change in the shape after the fourth cycle (Table 6.3) which shows the high resistant toward particle disintegration with SDI value of more than 97% (Figure 6.17).

Table 6.3 Typical pictorial view of samples before slaking and after four cycles

Molarity (M) of sodium silicate	Before cycle	After four cycle
NRM+25% GGBS+0.25M Na$_2$SiO$_3$		
NRM+25% GGBS+0.50M Na$_2$SiO$_3$		
NRM+25% GGBS+1M Na$_2$SiO$_3$		

Figure 6.17 shows the variation of slake durability index with the number of cycles. It is found that the NRM stabilized with 25% GGBS and activated with 1.00M sodium silicate (Na$_2$SiO$_4$) shows the maximum resistance towards the disintegration of particles with 97.86% slake durability index (SDI) after the first cycle and 97.51% after the second cycle which reduced to 95.85% after the fourth cycle. Similarly, the HRM stabilized with 25% GGBS and activated with 1.00M sodium silicate (Na$_2$SiO$_4$) shows the SDI value of 96.91% after the first cycle and 94.11% after the second cycle. Based on the Gamble's slake durability classification, NRM/HRM stabilized with 15, and 25% GGBS and activated with 1.00M sodium silicate can be classified as medium-high durable material (Goodman 1989). Similarly, based on the SDI after the first cycle, the NRM/HRM stabilized with 5% GGBS and activated with 1M of sodium silicate can be classified as medium durable. The variation of the SDI with UCS value of the samples cured for 28

days is presented in Figure 6.18. On the same figure, the UCS vs SDI for different rock samples are also plotted (Sharma and Singh, 2008).
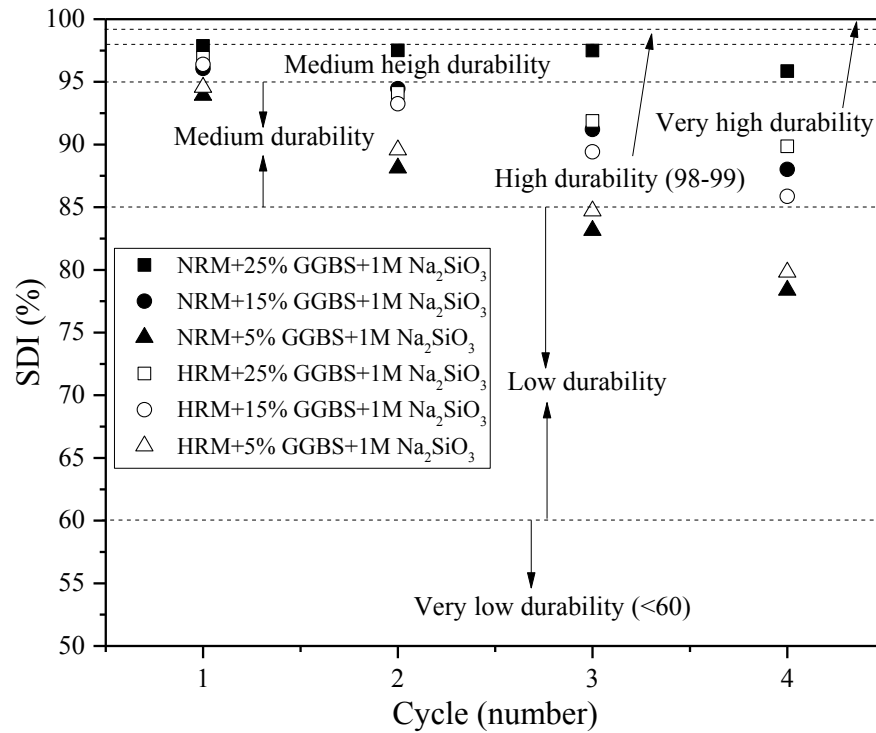
Figure 6.17. Variation of slake durability index with number of cycle
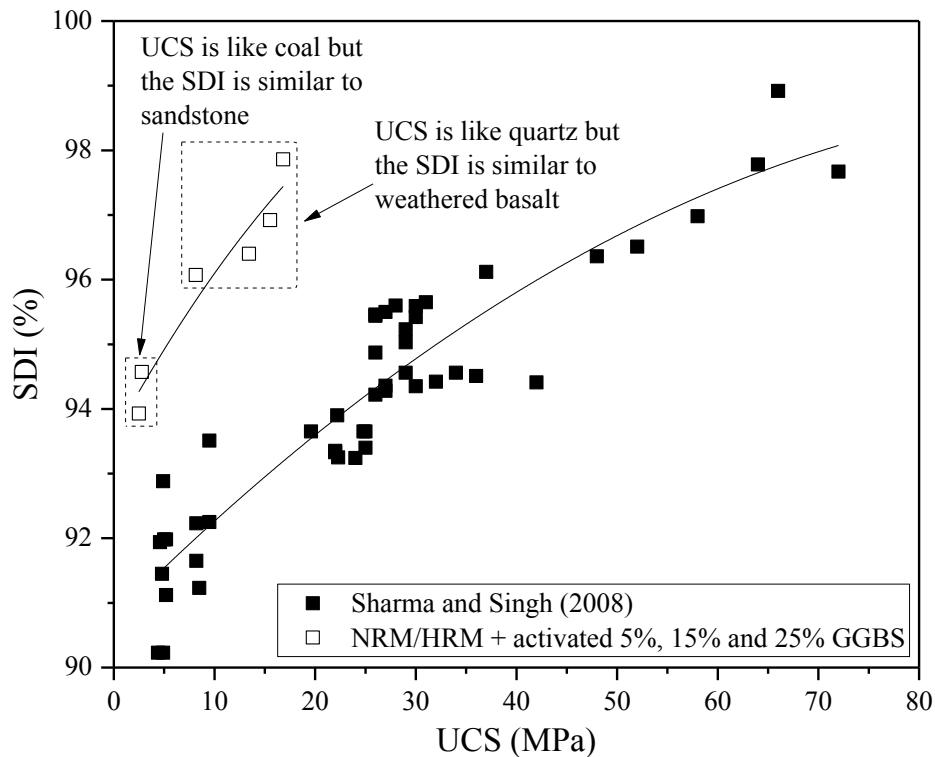
Figure 6.18. Variation of SDI with UCS

119

The similar variation of the SDI with UCS is observed for the stabilized red mud (Figure 6.18) but for the particular UCS value, SDI of the stabilized red mud is observed higher than that of rock samples. The difference in UCS value may be due to the difference in material type and samples size (Sharma and Singh, 2008). The difference observed in Figure 6.18 may also due to the shape of the samples used for slake durability test (Ankara et al., 2015).

6.3.8 Impact Strength Study

The crushability of rock or other materials is studied in term of impact strength index (ISI) by several researchers (Lindqvist, 2008; Su et al., 2010; Toraman et al., 2010). However, this type of study is not available on the stabilized soils in the best knowledge of the authors. So in the present research, the impact strength of red mud NRM/HRM stabilized with 1.00M sodium silicate (Na_2SiO_3) activated GGBS under impact loading was studied and the result is presented in term of ISI. Based on the test result, the variation of ISI of RM stabilized with 5, 15, and 25% GGBS activated by 1M Na_2SiO_3 is presented in the Figure 6.19.
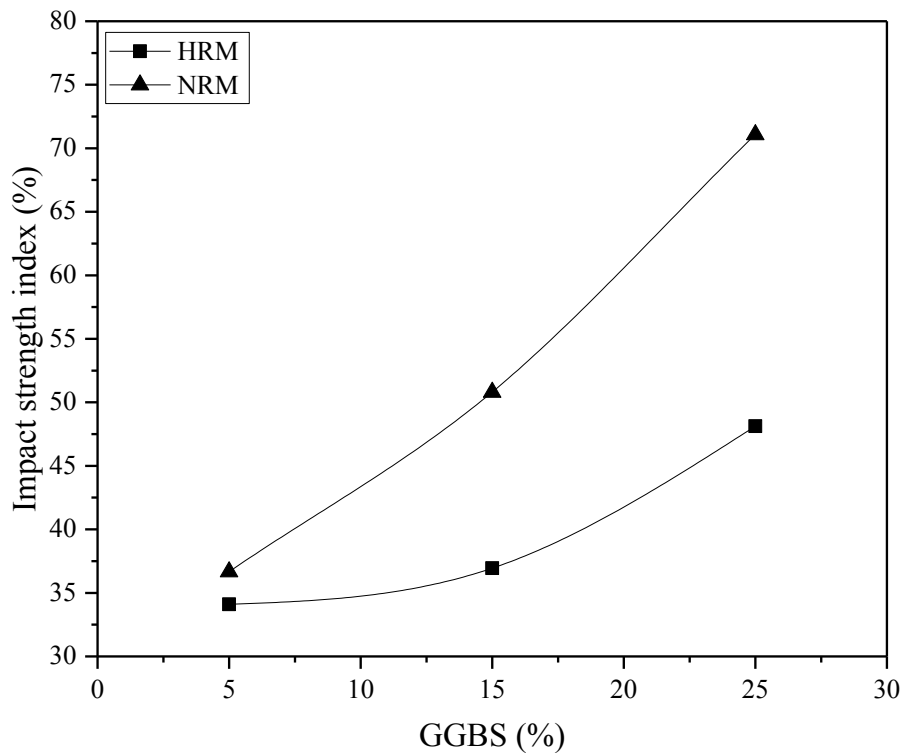
Figure 6.19. Variation of impact strength index with percentage of GGBS

It is found that the alkali-activated NRM-25%GGBS mix shows the higher ISI value as compared to alkali activated HRM-25%GGBS mixture. Further, the ISI of both the stabilized RM increases with the increase in the molarity of sodium silicate but NRM-GGBS shows a higher rate of increment as compared to HRM-GGBS. It may be mentioned here that most of the particles in the consideration are angular in shape (Figure 6.19), however, the effect of particles on ISI needs further investigations.

6.3.9 Microstructure Analysis

The microstructural images of the NRM/HRM-GGBS mix and alkali activated NRM/HRM-GGBS mixes along with the alkali-activated NRM/HRM-GGBS mix subjected to 12 wet-dry cycles were obtained using SEM and are shown in Figures 6.20 and 6.21 for NRM and HRM respectively.
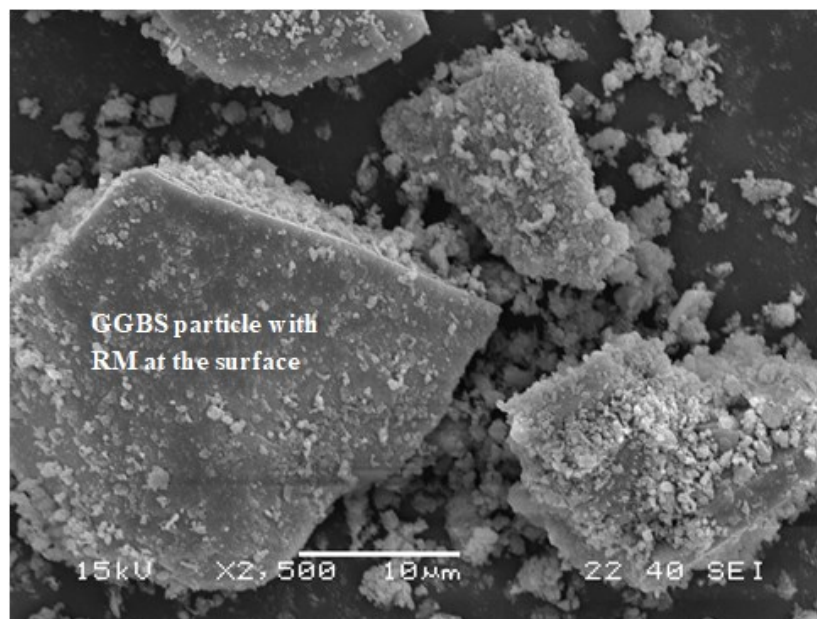
(a)
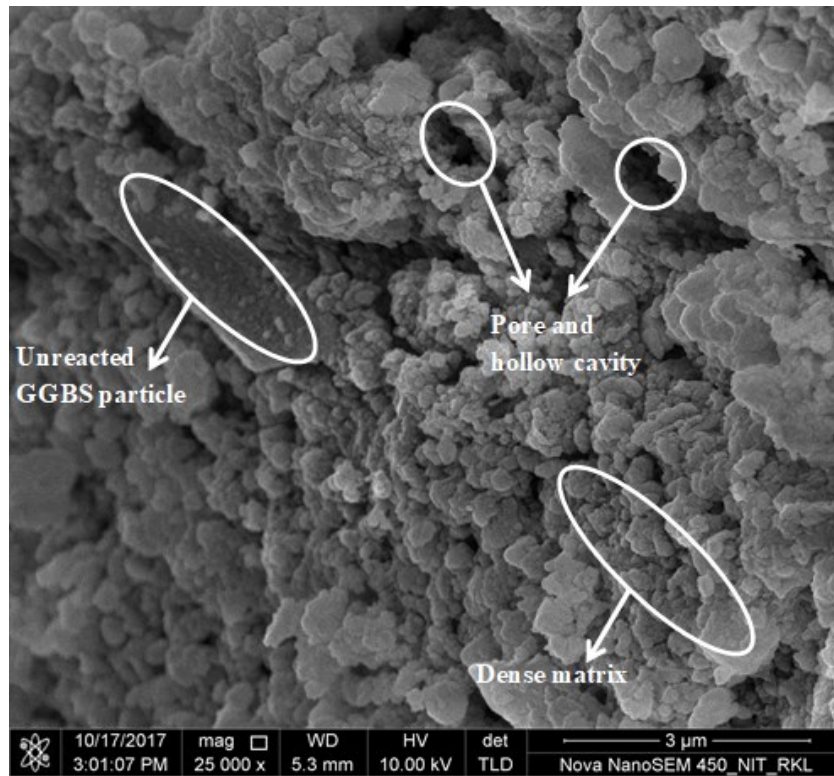
(b)
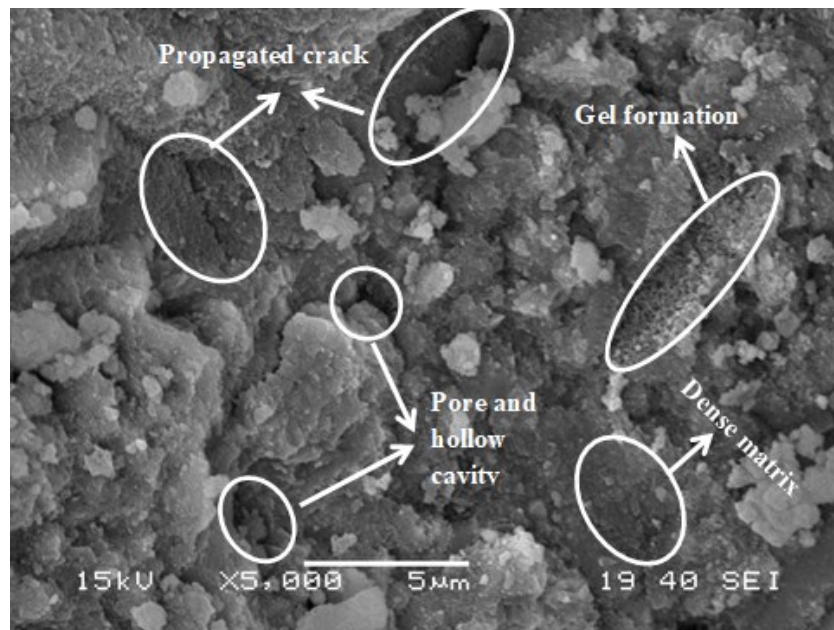
(c)

Figure 6.20. SEM image of (a) NRM-25%GGBS mix (b) NRM-25%GGBS mix activate by 1M Na$_2$SiO$_3$ (c) 1M Na$_2$SiO$_3$ activated NRM-25%GGBS mix after 12 W-D cycle
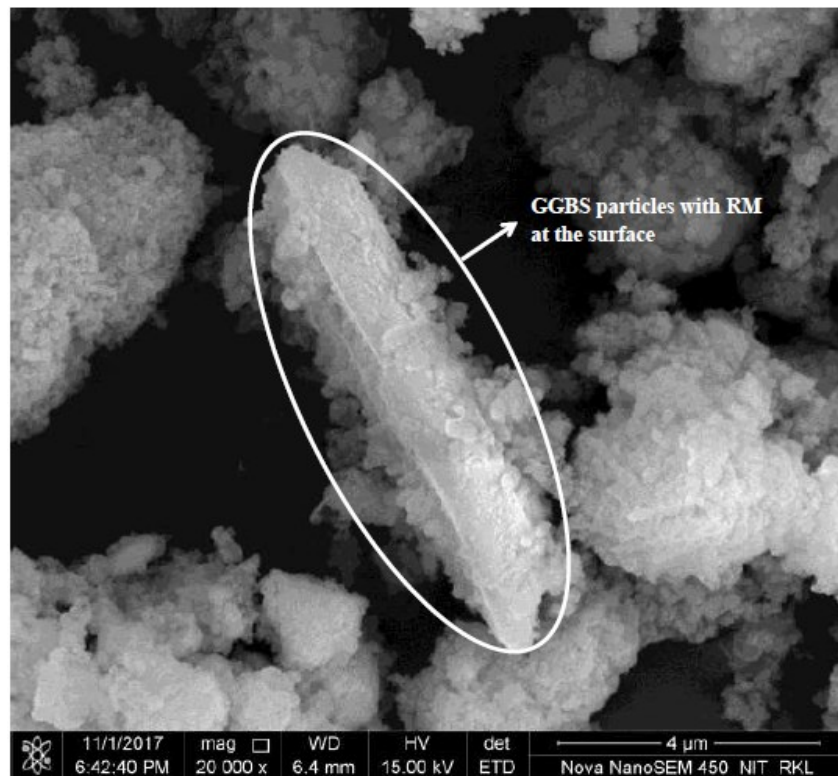
(a)
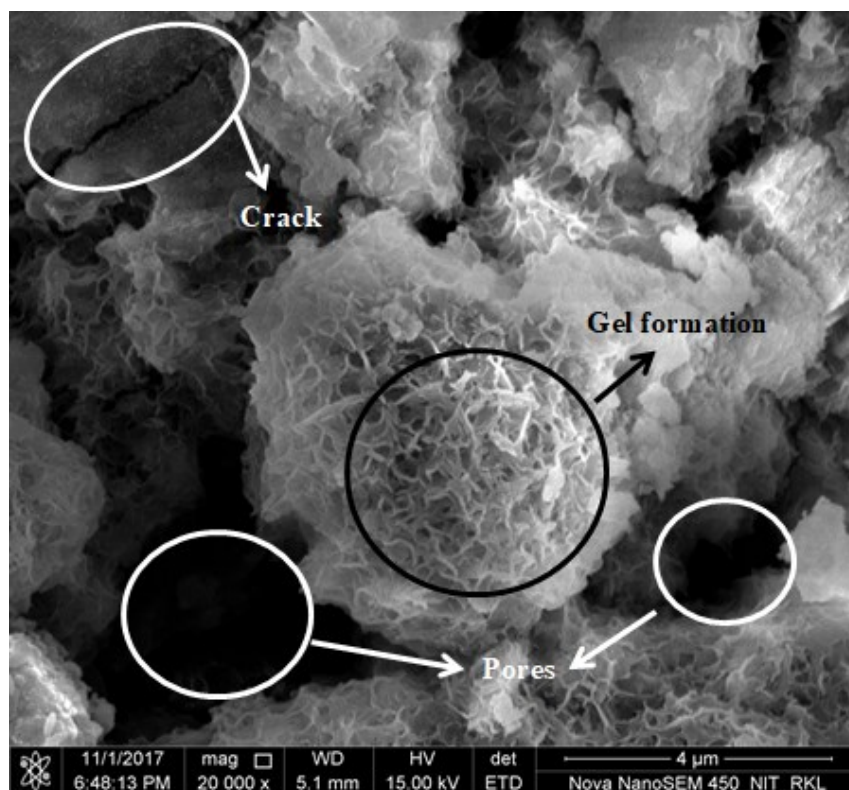
(b)
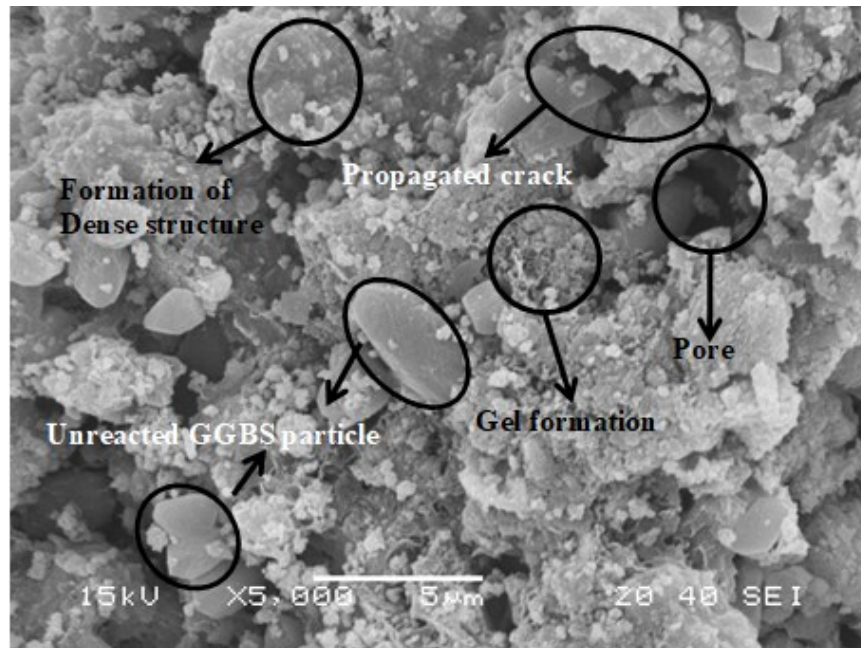
(c)

Figure 6.21. SEM image of (a) HRM-25%GGBS mix (b) HRM-25%GGBS mix activated by 1M Na$_2$SiO$_3$ (c) 1M Na$_2$SiO$_3$ activated HRM-25%GGBS mix after 12 W-D cycle

The SEM image of the NRM-25%GGBS mix is shown in Figure 6.20. The NRM particles are observed to stick at the surface of GGBS particle but the cementing product is not observed (Figure 6.20a). However, a dense matrix due to alkali activation of the NRM-25%GGBS mix can be observed in Figure 6.20b and Figure 6.20c, which indicates the proper gel formation. It can also be seen that the alkali-activated NRM-25%GGBS subjected to 12 W-D cycle shows the denser structure (Figure 6.20c) as compared to the alkali-activated NRM-25%GGBS samples cured for 28 days (Figure 6.20b). The loose honeycomb structure can be seen in the Figure 6.21b and Figure 6.21c, which reveals the incomplete gel formation in the HRM-25% GGBS mix activated with 1M Na$_2$SiO$_3$ after 28 days and after 12 W-D cycles respectively. The effect of microstructural changes due to alkali activation on compressive strength is discussed in the next section.

The XRD micrograph of NRM and alkali activated NRM-GGBS mix cured for 28 days at ambient temperature (AT) and in a humidity chamber (HC) along with the activated sample undergone through 12 W-D cycles are shown in Figure 6.22. The difference in the XRD graph can be seen in term of cancrinite, chantalite, sodalite, and zemkornite. The NRM contains all these minerals but in the micrograph of the alkali-activated NRM-GGBS mix, these minerals are not observed which may be due to the phase transformation due to alkali activation. The peak intensity of cancrinite in between 2θ value of 20°-25° is found to increase, which may be due to the transformation of chantalite (CaAl$_2$SiO$_4$(OH)$_4$)

into the sodium alumina silicate compound (cancrinite) due to activation with sodium silicate (Na_2SiO_4).

1=Cancrinite $Na_8(Al_6Si_6O_{24})(OH)_{2.04}(H_2O)_{2.66}$ 2=Gibbsite $Al(OH)_3$ 3=Hematite Fe_2O_3
4=Goethite $FeO(OH)$ 5=Chantalite $CaAl_2SiO_4(OH)_4$ 6=Calcite $CaCO_3$ 7=Sodalite $Na_4Al_3Si_3O_{12}Cl$
8=Sodium Hydroxide $NaOH$ 9=Zemkorite $Na_2Ca(CO3)_2$
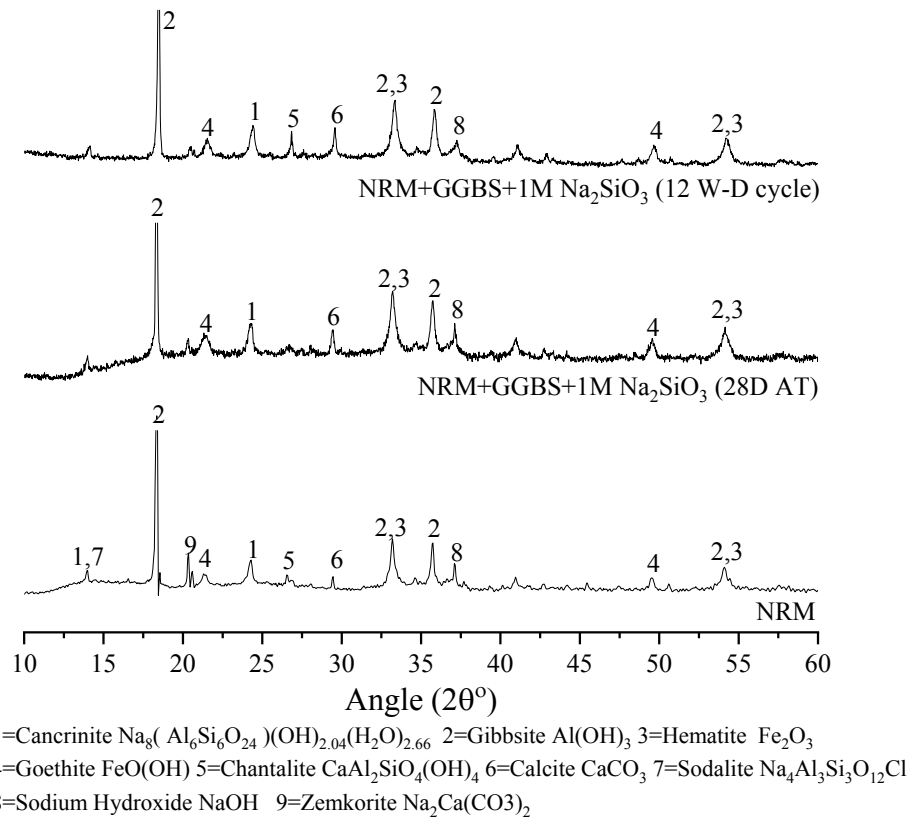
Figure 6.22. XRD graph of NRM and alkali activated GGBS stabilized NRM

The XRD micrograph of HRM and alkali activated HRM-GGBS mix with the same curing condition as NRM-GGBS mix has been shown in Figure 6.23. The difference in the micrograph can be observed in term of cancrinite, chantalite, calcite, and sodalite. A decrease in the peak intensity of cancrinite and sodalite (both are sodium aluminosilicate compound) is observed in-between the 2θ value of 10°-15°, however, the peaks of cancrinite between the 2θ value of 25°-30° and 50°-55° are observed to disappear in the alkali-activated HRM-GGBS mix. The peak intensity of calcite (a calcium-bearing mineral) is observed to increase in the 2θ range of 25°-30°.

125

1= Cancrinite $Na_8(Al_6Si_6O_{24})(OH)_{2.04}(H_2O)_{2.66}$ 2=Gibbsite $Al(OH)_3$ 3=Hematite Fe_2O_3 4= Goethite $FeO(OH)$
5=Chantalite $CaAl_2(OH)_4SiO_4$ 6=Calcite $CaCO_3$ 7=Muscovite $KAl_3Si_3O_{10}(OH)_2$ 8=Sodalite $Na_4Al_3Si_3O_{12}Cl$
9=Sodium Hydroxide Hydrate $NaOH \cdot H_2O$
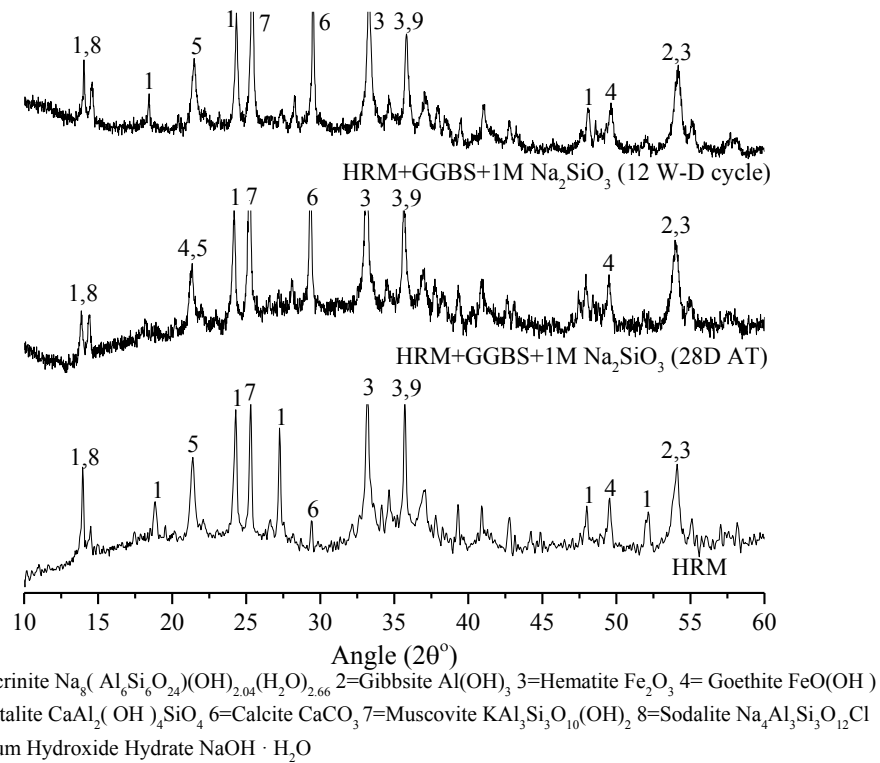
Figure 6.23. XRD graph of HRM and alkali activated GGBS stabilized HRM

The infrared (IR) spectra of the alkali activated GGBS stabilized NRM and HRM after 28 days curing at ambient temperature (AT) and after 12 wet-dry cycle are shown in Figures 6.24 and 6.25 respectively.
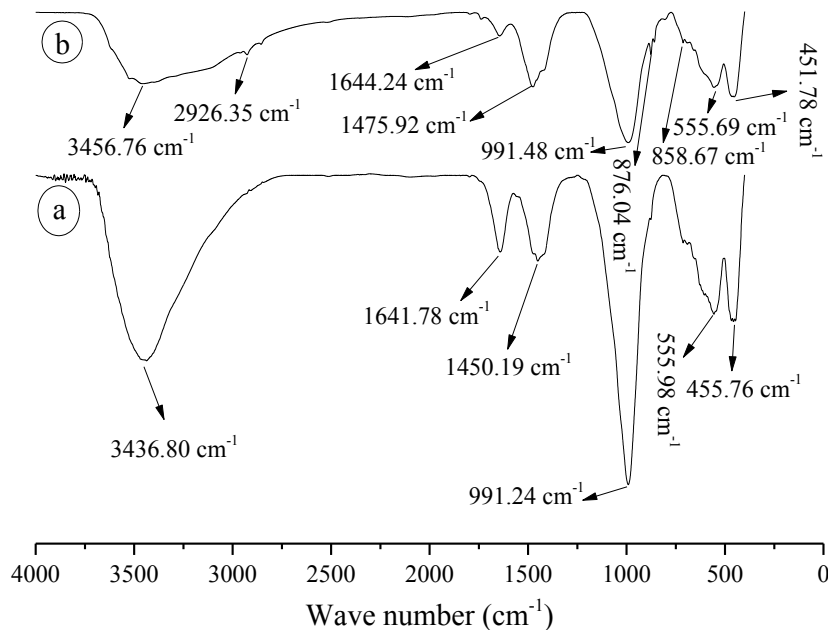
Figure 6.24. FTIR spectrum of alkali activated GGBS stabilized NRM after (a) 28 days curing (b) 12 wet-dry cycle
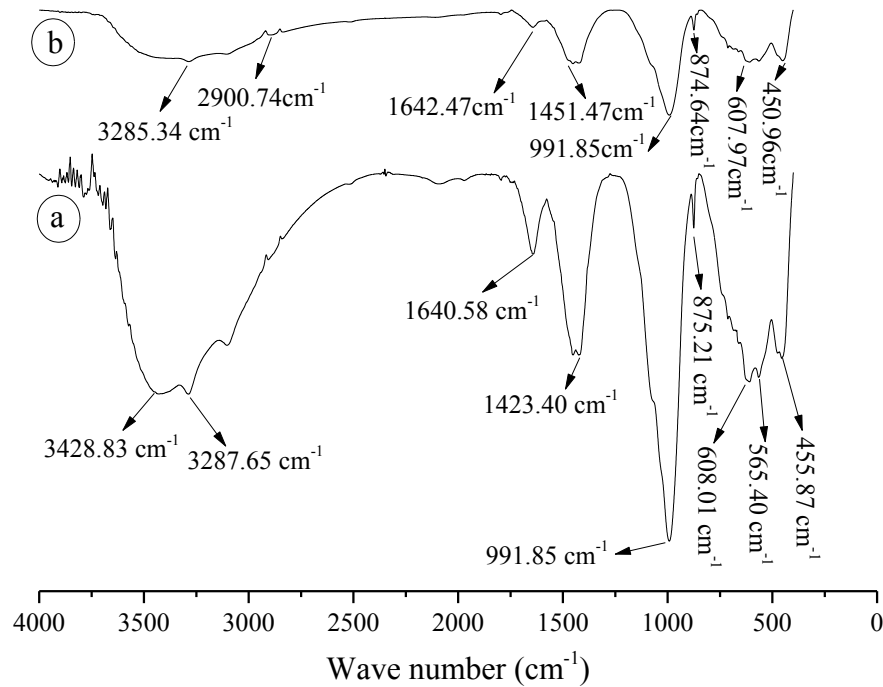
Figure 6.25. FTIR spectrum of alkali activated GGBS stabilized HRM after (a) 28 days curing (b) 12 wet-dry cycle

The band between 3500-3200 cm^{-1} in Figure 6.24 and Figure 6.25 indicate the O-H stretching band of Si-OH. The peak at 2926.35 cm^{-1} (Figure 6.24b) and 2900.74cm^{-1} (Figure 6.25b) indicate the formation of silica based polymer which causes the increase in strength after wet-dry cycle. The band at 1641.78 cm^{-1} and 1644.24 cm^{-1} in Figure 6.24 and at 1640.58 cm^{-1} and 1642.47 cm^{-1} in Figure 6.25 indicate the water molecule incorporated in the lattice structure of the crystalline molecule (Gok et al., 2007). The stretch between 1500 to 1400 cm^{-1} in Figure 6.24 and Figure 6.25 indicates the presence of Ca-O which signify the presence of $CaCO_3$ (Alp and Goral, 2003; Liu et al., 2011; Ye et al. 2016). The stretching vibration of Si-O-Si is indicated by the band in between 1000 cm^{-1} - 900 cm^{-1} in both the figures (Luo et al., 2010; Bernal et al., 2012; Kaya and Soyer-Uzun, 2016). The band at 876.04 cm^{-1} and 858.67 cm^{-1} in Figure 6.24 and at 875.12 cm^{-1} and 874.64 cm^{-1} in Figure 6.25 indicate the presence of carbonate (CO_3^{-2}) ions which may be in for of sodium or calcium carbonate. The peak at 555.98 cm^{-1}, 555.69 cm^{-1} (Figure 6.24), and at 608.01 cm^{-1}, 607.97 cm^{-1} (Figure 6.25) indicate the vibration of SiO_4 or AlO_4 tetrahedral (Castaldi et al., 2010). The peak at 455.76 cm^{-1} and 451.78 cm^{-1} in Figure 6.24 and at 455.87 cm^{-1} and 450.96 cm^{-1} in Figure 6.25 show the stretching vibration of the Fe-O bond (Ruan et al., 2001).

6.3.10 Leachate Analysis

The batch leaching procedure as suggested by EPA test method 1311 was used for sample preparation. The leachate is separated from solution using a 0.45μm filter and analyzed using AAS. The average concertation of three replicas was considered as the actual concentration and presented in Table 6.4.

Table 6.4 Heavy metal concentration in the leachate of alkali activated GGBS stabilized red mud

Element	NRM	NRM+25%GGBS activated with 1.00M Na_2SiO_3	HRM	HRM+25%GGBS activated with 1.00M Na_2SiO_3	GGBS	Regulatory level as per EPA
Ni	0.019	0.092	0.009	0.173	-	-
Zn	0.005	0.051	0.007	0.054	0.031	-
Cr	1.832	4.995	2.59	3.418	0.036	5.00
Cu	0.004	0.174	-	0.13	-	-
Pb	-	-	-	-	-	5.00
Hg	0.004	-	0.002	-	-	0.20
As	0.002	0.026	0.032	0.059	-	5.00
pH	11.40	12.96	11.53	13.09	-	

The toxic heavy metals (As, Cr, Pb and Hg) as identified by EPA for toxicity characteristics are found within acceptable limits in the leachate. It is found that the stabilization of either red mud using activated GGBS is able to arrest the leaching of Hg. However, the leaching of other heavy metals is found to increase after stabilization but remains within the permissible limits. However, Burke et al. (2012) reported that the chromium in the red mud is present as Cr^{+3} which is not considered as a health hazard. The increase in the leaching may be attributed to the slight increase in pH due to use of Na_2SiO_3 as an activator (Quina et al., 2009; Gwiazda, 2014). Although the concertation of heavy metals is within the permissible limit for toxicity characteristics, it is above the acceptable limits in the drinking water as suggested by WHO. So, whenever this material will be used as a geotechnical material, the water quality of nearby drinking water source needs to study.

6.4   Conclusions

Based on the laboratory findings of stabilized red mud and alkali activated red mud,

following conclusions can be drawn:

1. The un-stabilized NRM shows higher unconfined compressive strength with brittle failure as compare to un-stabilized HRM which shows ductile failure.

2. The mixing of GGBS in the NRM makes the GGBS-NRM mixture well graded while the HRM-GGBS mixture remains poorly graded.

3. The stabilization of either red mud (NRM or HRM) with GGBS increases the UCS and the NRM-GGBS mix gives comparatively higher strength than HRM-GGBS but the failure mode become brittle for the both (NRM/HRM-GGBS). The GGBS stabilized red mud was not found durable under alternate wet-dry cycle and slake durability test. So, the alkali activator is used to improve the durability characteristic.

4. The alkali activation was found effective in increasing the UCS and 1M Na_2SiO_3 activated NRM-25%GGBS giving a maximum UCS value as 11 MPa after 28 days.

5. The alkali activation was also found effective in improving the durability under alternate wet-dry cycle and the NRM/HRM-25% GGBS activated with 1M Na_2SiO_3 gives an UCS of more than 13 MPa after 12 wet-dry cycles.

6. Based on the Gamble's slake durability classification, NRM/HRM stabilized with 15, and 25% GGBS and activated with 1M Na_2SiO_3 can be classified as medium-high durable material and the NRM/HRM stabilized with 5% GGBS and activated with 1M Na_2SiO_3 can be classified as medium durable.

7. The alkali-activated NRM-25%GGBS mix was found to have higher ISI value as compared to alkali activated HRM-25%GGBS mixture. Further, the ISI of both the stabilized red mud increases with the increase in the molarity of Na_2SiO_3 but NRM-GGBS shows a higher rate of increment as compared to HRM-GGBS.

8. The toxic heavy metals (As, Cr, Pb and Hg) as identified by EPA for toxicity characteristics are found within acceptable limits in the leachate of red mud. However, the leaching of heavy metals is found to increase after stabilization except for Hg but falls within the permissible limits.

9. Although the concertation of heavy metals is within the permissible limit for toxicity characteristics, it is above the acceptable limits in the drinking water as

suggested by WHO. So, whenever this material will be used as a geotechnical material, the water quality of nearby drinking water source needs to study.

The Chapter 6 discussed strength and durability characteristic of GGBS stabilized red mud along with the alkali activated GGBS stabilized red mud for its bulk utilization as geo-material. Chapter 7 summarizes the observations based on the laboratory experiments discussed in Chapter 3, Chapter 4, Chapter 5, and Chapter 6.

Chapter 7

Conclusions and Scope of Future Work

7.1 Summary

The management of industrial waste is becoming challenging nowadays due to high generation rate and variability in chemical and physical properties. In most of the cases, these wastes are stored, which creates a geo-environmental problem in long run. The bauxite residue (red mud) is one of the major industrial waste generated by an aluminum industry whose storage is challenging due to its high alkalinity. Several studied has been made to utilize the industrial waste like fly ash, blast furnace slag, cement kiln dust, marble dust to reduce the storage but the investigation on red mud has received very less attention. Although several studies for the high value utilization of red mud has been performed but due to the low utilization rate, a large volume of the red mud remain stored in the pond. Though various attempts have also been made for geotechnical characterization, large variability was observed in the geotechnical characteristics due to the difference in the mineralogy of bauxite, the difference in the process adopted for aluminium extraction, and the difference in disposal method. Hence, there is a need to characterize the Indian red mud to gain confidence in utilization. Hence, the primary focus of the present study was to characterize the red mud from Indian aluminium industry (NALCO, Odisha and HINDALCO, Jharkhand) with different disposal method (slurry disposal and dry disposal) for their physical, chemical, mineralogical and geotechnical properties. The sedimentation and dispersive characteristic of red mud were studied by stabilizing it with phosphogypsum (fertilizer industry waste), sodium salt (NaCl) and biopolymer. The coarse fraction (> 75 μm) of the red mud was characterized for its utilization as construction materials. The red mud is stabilized with Na_2SiO_3 to improve the durability under alternate wetting-drying and slake durability.

7.2 General Observations and Conclusions

In general, the outcome of the present research was found useful for proper management of red mud thereby reducing its storage. The main results are outlined here:

7.2.1 Material Characterization

1. Based on the morphological study, it was found that red mud contains the majority of angular to a subangular agglomerated particle of different sizes. The XRF analysis reveals that the red mud contains Fe_2O_3 as the major constituent. Based on the hump position in XRD plot, the red mud is also found to contain the amorphous oxides.

2. The red mud is found highly alkaline and the pH value depends upon the percentage of CaO and Na_2O. The Bayer's process red mud is identified with lime index < 0.5 and CaO < 25%.

3. The HRM contains higher clay fraction (~32%) as compared to NRM (~14%). The liquid limit of HRM (39.89%) is also found higher than that of NRM (30.75%), which may be due to the higher clay content and low LL is due to the presence of low clay minerals.

4. The NRM shows higher maximum dry unit weight (16.5 kN/m^3) as compared to HRM (15.2 kN/m^3) under standard Proctor effort. Under the modified Proctor effort, the maximum dry unit weight of NRM and HRM is found as 17.7 kN/m^3 and 15.9 kN/m^3, respectively. The higher maximum dry unit weight of NRM is due to the higher specific gravity of NRM (3.33) as compared to HRM (3.27).

5. The permeability of both the red mud is found of the order of 10^{-6} cm/s and show higher resistant to the flow of salt solution as compared to distilled water due to change in soil structure. The soil-water characteristic curve of both the red mud is found very similar to that of silty soil.

6. The red mud is found to have negative DFS value which shows that red mud is dispersive in nature. The unconfined compressive strength is observed to vary with moulding moisture content and found maximum at OMC for both NRM (564.08 kPa) and HRM (441.45 kPa).

7. Though the angle of internal friction of both the red mud is found very near to each other, the remarkable difference in the cohesion is observed. This may be due to the difference in fine content.

8. The NRM is found moderately severe collapsible with collapse potential (Ic) value of 7.8 at lower inundation pressure, while, at higher inundation pressure, it is

moderately collapsible with Ic value of 2.73. Similarly, HRM is found as moderately collapsible (Ic = 3.46) at lower inundation pressure and slightly collapsible (Ic = 1.97) at higher inundation pressure.

9. Based on AAS result, the heavy toxic metals as identified by United State EPA are found within toxicity level in leachate generated from red mud.

7.2.2 Dispersive and Sedimentation Characteristic

In this study, an attempt has been made to control the dispersiveness of red mud using biopolymer and phosphogypsum (fertilizer industry waste). The effect of salt (NaCl) solution and phosphogypsum on the sedimentation rate have been studied. The conclusion drawn from this studies are as follow:

1. Based on the pinhole test and cylindrical dispersive tests, red mud is found highly dispersive, hence another reason for environmental hazard.

2. Addition of 0.5% of biopolymer (GG and XG) was found to be effective in controlling the dispersiveness of red mud, due to the formation of the ionic bond (XG) and hydrogen bond (GG) with cations of red mud particles. The dispersion also reduced with 3% NaCl solution as a surrounding fluid and 7% as a pore fluid.

3. The sedimentation of NRM slurry is slow due to high magnitude of Zeta potential (37.1 mV) at pH value of 11.4. Phosphogypsum and NaCl found to be effective in reducing the magnitude of Zeta potential of red mud slurry; thereby accelerating the rate of sedimentation. The pH value reduced to the range of 7.42-7.61 and 8.24-8.44 due to phosphogypsum and NaCl respectively, with a higher rate of sedimentation with phosphogypsum. But the high rate of sedimentation may become susceptible to collapse, which requires further detail study in this regard. It was also observed that phosphogypsum is more effective in controlling the leaching of toxic material from red mud.

4. The flow test shows that the spreading of red mud suspension over a large area can be controlled by treating the red mud slurry using phosphogypsum or NaCl solution. The present laboratory study may help in developing a better management system for smooth and effective disposal and storage of red mud.

7.2.3 Characterization of Coarse Fraction of Red Mud

In this study, the coarser fraction (75 mm) of red mud (red sand) was characterized for its

utilization as construction materials and the result is compared with the result of Indian standard sand. The conclusion drawn from this studies are as follow:

1. The average roundness index and sphericity of red sands are found to be higher than that of standard sands. But, for the same water to cement ratio, the flowability of red sand is less than that of standard sand due to the higher specific surface area of red sand. The maximum and minimum void ratios of the sands are found to depend upon the roundness index. It was also found that the variation of friction angle corresponding to maximum and minimum density depends upon the percentage of angular particles.

2. Though the sphericity of the red sands is higher than standard sand, but for a particular water-cement ratio, the mortar prepared using standard sand is more flowable compared to red sand. One of the reasons for the same was found due to the low specific surface area of red sands.

3. Both NRS and HRS contain an oxide of iron in form of hematite (Fe_2O_3) and magnetite (Fe_3O_4) as a major constituent along with SiO_2 and Al_2O_3. It is also observed that HRS and NRS contain amorphous phase, which can take part in the pozzolanic activity.

4. As the angle of internal friction of red sand is higher than that of Indian standard sand, red sand in mortar will increase its yield stress and plastic viscosity. However, the proper strength test of the mortar prepared using red sand needs to be conducted.

5. The zeta potential values of red sands at high pH values are similar to that of standard sand, hence, can be used in cement mortar/concrete.

6. As the LR value of NRS and HRS is more than the standard value (4 MPa), the material can be used in cement and concrete. However, it is suggested to conduct necessary strength test on the concrete prepared using red sand.

7. As the red sand shows lower thermal resistivity as compared to standard sand, it can be used as a construction material where the heat dissipation is required.

8. Though, the total dissolved solids in both NRS and HRS is more than that of standard sand but falls within the acceptable limit as suggested by WHO. However, the chemical analysis of leachate generated from mortar and concrete

prepared using red sand may give different results.

9. The major difficulty is the recovery of red sand from red mud as Indian red mud contains only 10-20% of red sand by weight. Also as the gradation of red sand depends on the process of grinding of bauxite during Bayer's process, red sand collected from different sources may have different gradation and particle shape.

7.2.4 Strength and Durability Characteristic of Stabilized Red Mud

In this study, the strength and durability characteristic of GGBS stabilized red mud was studied and the alkali activation of GGBS is used to improve the durability characteristic of stabilized red mud. The conclusion drawn from this studies are as follow:

1. The un-stabilized NRM shows higher unconfined compressive strength with brittle failure as compare to un-stabilized HRM which shows ductile failure.

2. The mixing of GGBS in the NRM makes the GGBS-NRM mixture well graded while the HRM-GGBS mixture remains poorly graded.

3. The stabilization of either red mud (NRM or HRM) with GGBS increases the UCS and the NRM-GGBS mix gives comparatively higher strength than HRM-GGBS but the failure mode become brittle for the both (NRM/HRM-GGBS). The GGBS stabilized red mud was not found durable under alternate wet-dry cycle and slake durability test. So, the alkali activator is used to improve the strength and durability characteristic.

4. The alkali activation is found effective in increasing the UCS and 1M Na_2SiO_3 activated NRM-25%GGBS giving a maximum UCS value as 11 MPa after 28 days.

5. The alkali activation is also found effective in improving the durability under alternate wet-dry cycle and the NRM/HRM-25% GGBS activated with 1 M Na_2SiO_3 gives an UCS of more than 13 MPa after 12 wet-dry cycles.

6. Based on the Gamble's slake durability classification, NRM/HRM stabilized with 15, and 25% GGBS and activated with 1 M Na_2SiO_3 can be classified as medium-high durable material and the NRM/HRM stabilized with 5% GGBS and activated with 1M Na_2SiO_3 can be classified as medium durable.

7. The alkali-activated NRM-25%GGBS mix is found to have higher ISI value as compared to alkali activated HRM-25%GGBS mixture. Further, the ISI of both the stabilized red mud increases with the increase in the molarity of Na_2SiO_3 but

NRM-GGBS shows a higher rate of increment as compared to HRM-GGBS.

8. The toxic heavy metals (As, Cr, Pb and Hg) as identified by EPA for toxicity characteristics are found within acceptable limits in the leachate of red mud. However, the leaching of heavy metals is found to increase after stabilization except for Hg but remains within the permissible limits.

9. Although the concertation of heavy metals is within the permissible limit for toxicity characteristics, it is above the acceptable limits in the drinking water as suggested by WHO. So, whenever this material will be used as a geotechnical material, the water quality of nearby drinking water source needs to study.

This is the extensive work on characterization for effective utilization and management of red mud based on which, following points can be suggested:

1. The biopolymer like guar gum and xanthan gum can be used to control the dispersive characteristic of red mud. The phophogypsum can be used to accelerate the rate of sedimentation of red mud disposed in slurry form.

2. The coarse fraction of red mud can be an alternate of fine aggregate in mortar and concrete.

3. The alkali activated GGBS stabilized red mud can be used as a geotechnical material by keeping in mind the strength and durability criteria.

7.3 Future Scope

The present study is a beginning in the new direction of RM utilization in geotechnical engineering and a few preliminary problems have been solved. Based on the present study it was observed that there is a vast scope for application of the red mud to geotechnical engineering, however following problems are needed to sort out.

1. The red mud can be used to develop the controlled low strength material with other industrial waste.

2. The suitable method is needed to develop for the proper mixing of the additives before the discharge point to control the dispersiveness and accelerate the sedimentation rate.

3. Although the red sand is found suitable for cement concrete based on the angularity criteria; the strength parameter of the concrete prepared using the red sand needs to be studied for getting confidence in use.

4. The strength and durability characteristic of red mud stabilized with other industrial waste need to be studied.

References

Abdel-Mottal (2014). "Improvement of sand fill thermal conductivity using sand-oil mixture (Experimental study)." *World Applied Sciences Journal*, 32(5), 807-817.

Abel, J. S., and Stangle, G. C. (1994). "Sedimentation in flocculating colloidal suspensions." *Journal of Materials Research*, 9 (2), 451-461.

Agatzini-Leonardous, S., Oustadakis, P., Tsakiridis, P. E., and Markopoulos, C. (2008). "Titanium leaching from red mud by diluted sulfuric acid at atmospheric pressure." *Journal of Hazardous Materials*, 157, 579-586.

Agrawal, A., Sahu, K. K., and Pandey, B. D. (2004). "Solid waste management in non-ferrous industries in India." *Resources, Conservation and Recycling,* 42, 99-120.

Alhassan, M., Mesaiyete, E., and Mustapha, A. M. (2012). "Clay mineralogy of lateritic soils derived from granite basement – A case study of Minna lateritic soils." *EJGE*, 17, 1897-1903.

Ali, L., and Fiaz, A. (2009). "Use of fly ash along with blast furnace slag as partial replacement of fine aggregate and mineral filler in asphalt mix at high temperature." *Material Design, Construction, Maintenance, and Testing of Pavements*, doi: 10.1061/41045(352)18.

Alias, R., Kasa, A., and Taha, M. R. (2014). "Particle size effect on shear strength of granular materials in direct shear test." *International Journal of Civil, Environmental, Structural, Construction and Architectural Engineering*, 8(11), 1144-1147.

Alp, A., and Goral, S. (2003). "The influence of soda additive on the thermal properties of red mud." *Journal of Thermal Analysis and Calorimetry*, 73, 201-207.

Alsafi, S., Farzadnia, N., Asadi, A., and Huat, B. K. (2017). "Collapsibility potential of gypseous soil stabilized with fly ash geopolymer; characterization and assessment." *Construction and Building Materials*, 137, 390-709.

Amritphale, S. S., Anshul, A., Chandra, N., and Ramakrishnan, N. (2007). "A novel process for making radiopaque materials using bauxite—Red mud.*" Journal of the European Ceramic Society*, 27, 1945-1991.

Ankara, H., Kandemir, S. Y., and Cicek, F. (2015). "Comparison of slake durability index (SDI) value of sphere and rounded marl samples." *Procedia Earth and Planetary Science*, 15, 93-98.

Antunes, M. L. P., Couperthwaite, S. J., Tomazini da Conceicao, F., Costa de Jesus, C. P., Kiyohara, P. K., Coelho, A. C. V., and Frost, R. L. (2012). "Red Mud from Brazil: Thermal Behavior and Physical Properties." *Industrial and Engineering Chemistry Research*, 51, 775-779.

Apak, R., Guclu, K., and Turgut, M. H. (1998). "Modeling of copper (II), cadmium (II), and lead (II) adsorption on red mud." *Journal of Colloid and Interface Science*, 203, 122-130

ASTM C593 (2011). "Standard specification for fly ash and other pozzolans for use with lime for soil stabilization." *ASTM International*, West Conshohocken, PA, USA.

ASTM D 1883-16 (2016). "Standard test method for unconfined compressive strength of cohesive soil." *ASTM International*, West Conshohocken, PA, USA.

ASTM D 2166-16 (2016). "Standard test method for California bearing ratio (CBR) of laboratory compacted soils." *ASTM International,* West Conshohocken, PA, USA.

ASTM D 5333-03 (2003). "Standard test method for measurement of collapse potential of soil ." *ASTM International*, West Conshohocken, PA, USA.

ASTM D1193 (2011). "Standard specification for reagent water." *ASTM International*, West Conshohocken, PA, USA.

ASTM D2487 (2011). "Standard specification for classification of soil for engineering purposes (Unified soil classification system)." *ASTM International*, West Conshohocken, PA, USA.

ASTM D3080/D3080M (2011). "Standard test methods for direct shear test of soils under consolidated drained conditions." *ASTM International*, West Conshohocken, PA, USA.

ASTM D4253 (2016). "Standard test methods for maximum index density and unit weight of soil using a vibratory table." *ASTM International*, West Conshohocken, PA, USA.

ASTM D4644 (2016). "Standard test method for slake durability of shales and other similar weak rocks." *ASTM International*, West Conshohocken, PA, USA.

ASTM D4647-13 (2013). "Standard test method for identification and classification of dispersive clay soil by the pinhole test." *ASTM International*, West Conshohocken, PA, USA.

ASTM D4793 (2009). "Standard test method for sequential batch extraction of waste with water." ASTM International, *West Conshohocken*, PA, USA.

ASTM D5334 (2014). "Standard test methods for determination of thermal conductivity of soil and soft rock by thermal needle probe procedure." *ASTM International*, West Conshohocken, PA, USA.

ASTM D559 (2015). "Standard test methods for wetting and drying compacted of soil-cement mixtures." *ASTM International*, West Conshohocken, PA, USA.

ASTM D6913 (2017). "Standard test methods for particle size distribution (gradation) of soils using sieve analysis." *ASTM International*, West Conshohocken, PA, USA.

ASTM D698 (2007). "Standard test methods for laboratory compaction characteristics of soil using standard effort." *ASTM International*, West Conshohocken, PA, USA.

ASTM D7928 (2017). "Standard test method for particle size distribution (gradation) of fine grained soils using the sedimentation (hydrometer) analysis." *ASTM International*, West Conshohocken, PA, USA.

ASTM D854 (2003). "Standard test methods for specific gravity of soil solids by water pycnometer." *ASTM International*, West Conshohocken, PA, USA.

Atasoy, A. (2005). "An investigation on characterization and thermal analysis of the aughinish red mud." *Journal of Thermal Analysis and Calorimetry*, 81, 357-361

Atkinson, J. H., Charles, J. A., and Mhach, H. K. (1990). "Examination of erosion resistance of clay in embankment dams." *Journal of Engineering Geology,* 23, 103-108.

Bain, J. A. (1971). "A plasticity chart as an aid to the identification and assessment of industrial clay." *Clay Minerals*, 9 (1), 1-17.

Barksdale, R. D., Kemp, M. A., Sheffield, W. J., and Hubbard, J. L. (1991). "Measurement of aggregate shape, surface area, and roughness." *Transportation Research Record*, 1301, 107-116.

Barrow, N. J. (1982). "Possibility of using caustic residue from bauxite for improving chemical and physical properties of sandy soil." *Australian Journal of Agriculture*

Research, 33, 275-285.

Bernal, S. A., Rodríguez, E. D.,Gutiérrez, R. M. de, Provis, J. L., and Delvasto, S. (2012). "Activation of metakaolin/slag blends using alkaline solutions based on chemically modified silica fume and rice husk ash." *Waste Biomass Valorization*, 3 (1), 99-108.

Bertocchi, A. F., Ghiani, M., Peretti, R., and Zucca, A. (2006). "Red mud and fly ash for remediation of mine sites contaminated with As, Cd, Cu, Pb and Zn." *Journal of Hazardous Materials*, B134, 112-119.

Brooks, R. H. and Corey, A. T. (1964). "Hydraulic property of pours media." *Hydrology Papers*, Colorado State University, Colorado.

Burke, I. T., Mayes, W. M., Peacock, C. L., Brown, A. P., Jarvis, A. P., and Gruiz, K. (2012). "Speciation of Arsenic, Chromium, and Vanadium in red mud samples from the Ajka spill site, Hungary." *Environmental Science and Technology*, 46, 3085-3092.

Cablik, V. (2007). "Characterization and applications of red mud from bauxite processing." *Gospodarka Surowcami Mineralnymi*, 27-38.

Campbell, G. S., Smith, D. M., and Teare, B. L. (2007). "Application of a dew point method to obtain the soil water characteristic." In: *Schanz T. (eds) Experimental Unsaturated Soil Mechanics. Springer Proceedings in Physics*, 112, Springer, Berlin, Heidelberg.

Castaldi, P., Silvetti, M., Enzo, S., and Deiana, S. (2011). "XRD and thermal analysisof bauxite ore-processing waste (red mud) exchanged with arsenate and phosphate." *Clay and Clay Minerals*, 59 (2), 189-199.

Castaldi, P., Silvetti, M., Enzo, S., and Melis, P. (2010). "Study of sorption processes and FT-IR analysis of arsenate sorbed onto red muds (a bauxite ore processing waste)." *Journal of Hazardous Materials*, 175, 172-178.

Castaldi, P., Silvetti, M., Santona, L., Enzo, S., and Melis, P. (2008). "XRD, FTIR, and thermal analysis of bauxite ore-processing waste (red mud) exchanged with heavy matels." *Clay and Clay Minerals*, 56 (4), 461-469.

Cengeloglu, Y., Kir, E., and Ersoz, M. (2002). "Removal of fluoride from aqueous solution by using red mud." *Separation and Purification Technology*, 28, 81-86.

Cengeloglu, Y., Tor, A., Arslan, G., Ersoz, M., and Gezgin, S. (2007). "Removal of boron from aqueous solution by using neutralized red mud." *Journal of Hazardous Materials*, 142, 412-417.

Cerato, A. B., and Lutenegger, A. J. (2002). "Determination of surface area of fine-grained soils by the ethylene glycol monoethyl ether (EGME) method." *Geotechnical Testing Journal,* 25(3), 315-321.

Chaabane, L., Moussaceb, K., and Ait-Mokhtar, A. (2016). "Factors affecting the leaching of heavy metals (Ni^{+2}, Pb^{+2}, Cr^{+3}) contained in sludge waste stabilization/solidification by hydraulic benders, Part:1 Water/cement and waste/cement ratio in S/S mortar." *Environmental Progress & Sustainable Energy*, 36 (1), 93-103.

Chauhan, S., and Silori, C. S. (2011). "An evaluation of successful reclamation of bauxite residue through afforestation activities in south India." *Journal of Horticulture and Forestry*, 3 (7), 214-221.

Chen, R., Zhang, L., and Budhu, M. (2013). "Biopolymer stabilization of mine tailings." *J. Geotech. Geoenviron. Eng.*, 139 (10), 1802-1807.

Cho, G. C., Dodds, J., and Santamarina, J. C. (2006). "Particle shape effect on packing density, stiffness, and strength: natural and crushed sand." *Journal of Geotechnical and Geoenvironmental Engineering,* 132(5), 591-602.

Cortes, D. D., Kim, H. K., Palomino, A. M., and Santamarina, J. C. (2008). "Rheological and mechanical properties of mortars prepared with natural and manufactured sands." *Cement and Concrete Research,* 38, 1142-1147.

Courtney, R. G., and Timpson, J. P. (2004). "Nutrient status of vegetation growth in alkaline bauxite processing residue amended with gypsum and thermally dried sewage sludge- A two year field study." *Plant and Soil*, 266, 187-194.

Courtney, R. G., and Timpson, J. P. (2005). "Reclamation of fine fraction bauxite processing residue (red mud) amended with coarse fraction residue and gypsum." *Water, Air, and Soil Pollution*, 164, 91-102.

Cristelo, N., Glendinning, S., Fernandes, L., and Pinto, A. T. (2012). "Effect of calcium content on soil stabilisation with alkaline activation." *Construction and Building Materials*, 29, 167-174.

Dalinaidu, A., Das, B. B., and Singh, D. N. (2007). "Methodology for rapid determination of pozzolanic activity of materials." *Journal of ASTM International*, 4 (6), 1-11.

Cristelo, N., Glendinning, S., Miranda, T., Oliveria, D., and Silva, R. (2012). "Soil stabilisation using alkaline activation of fly ash for self-compacting rammed earth

Das, S. K., and Yudhbir (2006). "A simplified model for prediction of pozzolanic characteristics of fly ash, based on chemical composition." *Cement and Concrete Research*, 36, 1827-1832.

Das, S. K., and Yudhbir (2005). "Geotechnical characterization of some Indian fly ashes." *Journal of Materials in Civil Engineering*, 17 (5), 544-552.

Dass, A., and Malhotra, S. K. (1990). "Lime-stabilized red mud bricks." *Materials and Structures,* 23(4), 252-255.

Desai, V. G. M, and Herkal, R. N. (2010). "Red mud bricks –an alternative low cost building material." *6th International Congress on Environmental Geotechnics*, New Delhi, India, 1049-1052.

Diamond, P. (1983). "On the glass present in low-calcium and in high-calciumflyashes." *Cement and Concrete Research*, 13 (4), 459-464.

Dijkstra, J. J., Meeussen, J. C. L., and Comans, R. N. J. (2004). "Leaching of heavy metals from contaminated soil: An experimental and modeling study." *Environmental Science & Technology*, 38 (16), 4390-4395.

Dodoo-Arhin, D., Konadu, D. S., Annan, E., Buabeng, F. P., Yaya, A., Agyei-Tuffour, B. (2013). "Fabrication and characterization of Ghanaian bauxite red mud-clay composite bricks for construction application." *American Journal of Materials Science*, 3 (5), 110-119.

Droppo, I. G., and Ongley, E. D. (1989). "Flocculation of suspended solids in southern Ontario river." *Sedimentation and Environment, Proc., Baltimote Symp.,* The International Association of Hydrological Science,Wallingford, Oxfordshire, U.K., Publication No. 184.

Dubey, K., and Dubey, K. P. (2011). "A study of the effect of red mud amendments on the growth of cyanobacterial species." *Bioremediation Journal*, 15 (3), 133-139.

Duchesne, J., and Doye, I. (2005). "Effectiveness of covers and liners made of red mud bauxite and/or cement kiln dust for limiting acid mine drainage." *J. Environ. Eng.*, 131 (8), 1230-1235.

Duman, O., and Tunc, S. (2009). "Electrokinetic and rheological properties of Na-bentonite in some electrolyte solutions." *Microporous and Mesoporous Materials*, 117, 331-338.

Dumbleton, M. J., and West, G. (1966). "Some factor affecting the relation between the clay minerals in soils and their plasticity." *Clay Minerals*, 6, 179-193.

Fahey, M., Newson, T. A., and Fujiyasu, Y. (2002). "Engineering with tailing." Invited Lecture, *Proc., 4th Int. Conf. On Environmental Geotechnics*, Rio de Janeiro, Brazil, 947-973.

Fahey, M., Newson, T. A., and Fujiyasu, Y. (2002). "Engineering with tailing." *Invited Lecture, Proc., 4th Int. Conf. On Environmental Geotechnics*, Riode janeiro, Brazil, 2, 947-973, Balkema, Lisse.

Farouki, O. T. (1981). "Thermal property of soil. United States Army Corps of Engineers." *Cold regions research and engineering laboratory*, Hanover, New Hampshire, U.S.A.

Fois, E., Lallai, A., and Mura, G. (2007). "Sulfur dioxide absorption in a bubbling reactor with suspensions of Bayer red mud." *Industrial and Engineering Chemistry Research*, 46, 6770-6776.

Fredlund , M. D., Fredlund, D. G., Wilson, G. W. (1998). "Estimation of unsaturated soil properties using a knowledge-based system." *Proc., 2nd Int. Conf. on Unsaturated Soils*, UNSAT '98, 1, 479–484.

Fredlund, D. G., and Xing, A. (1994). "Equation for the soil-water characteristic curve." *Canadian Geotechnical Journal*, 31 (3), 521-532.

Galvao, T. V. B., Viana, C. N., and Kaya, A. (2003). "Physical and zeta potential characteristics of erodible lateritic soils." *Nat Hazards Rev.*, 4(2), 95-110.

Gherardi, M. J., and Rengel, Z. (2001). "Bauxite residue sand has the capacity to rapidly decrease availability of added manganese." *Plant and Soil*, 234, 143-151.

Gidley, J. S., and Sack, W. A. (1983). "environmental aspects of waste utilization in construction." *Journal of Environmental Engineering*, 110 (6), 1117-1133.

Glenister, D. J., Thornber, M. R. (1985). "Alkalinity of red mud and its application for management of acid waste. Chemeca 85: Innovation in the process and resource industry: *The Thirteenth Australian Chemical Engineering Conference*, Perth.

Gok, A., Omastova, M., and Prokes, J. (2007). "Synthesis and characterization of red mud/polyaniline composites: Electrical properties and thermal stability." *European Polymer Journal*, 43, 2471-2480.

Goncalves, J. P., Tavares, L. M., Filho, R. D. T., Fairbairn, E. M. R., and Cunha, E. R. (2007). "Comparison of natural and manufactured fine aggregates in cement mortars." *Cement and Concrete Research*, 37, 924-932.

Goodman, R. E. (1989). "Introduction to rock mechanics." Wiley, New York.

Gordon, J. N., Pinnock, W. R., and Moore, M. M. (1996). "A preliminary investigation of strength development in Jamaican red mud composites." *Cement and Concrete*, 18, 371-379.

Grafe, M., Power, G., and Klauber, C. (2011). "Bauxite residue issues: III. Alkalinity and associated chemistry." *Hydrometallurgy*, 108, 60-79.

Gu, H., Wang, N., and Liu, S. (2012). "Radiological restrictions of using red mud as building material additive." *Waste Management & Research*, 30 (9), 961-965.

Guideline for drinking water quality, 4th Edition, *World Health Organization*, 2011.

Gupta, V. K., Ali, I., and Saini, V. K. (2004). "Removel of chlorophenols from wastewater using red mud: an aluminum industry waste." *Environmental Science and Technology*, 38 (14), 4012-4018.

Gupta, V. K., Gupta, M., and Sharma, S. (2001). "Process development for the removal of lead and chromium from aqueous solutions using red mud - an aluminium industry waste." *Water Research*, 35 (5), 1125-1134.

Gwiazda, E. S. (2014). "Potential effect of pH on the leaching of heavy metals from sediments of the Carpathian dam reservoirs." *Geology, Geophysics and Environment*, 40 (4), 349-358.

Hai, L. D., Khai, N. M., Quy, T. V., and Huan, N. X. (2014). "Material composition and

properties of red mud coming from alumina processing plant Tanrai, Lamdong, Vietnam." *International Journal of Research in Earth & Environmental Science*, 1 (6), 1-7.

Hanahan, C., McConchie, D., Pohl, J., Creelman, R., Clark, M., and Stocksiek, C. (2004). "Chemistry of sea water neutralization of bauxite refinery residue (red mud)." *Environmental Engineering Science*, 21 (2), 125-138.

He, J., Chu, J., Tan, S. K., and Vu, T. T. (2017). "Sedimentation behaviour of flocculent-treated soil slurry." *Marine Georesources & Geotechnology*, 35 (5), 593-602.

He, J., Jie, Y., Zhang, J., Yu, Y, and Zhang, G. (2013). "Synthesis and characterization of red mud and rice husk ash-based geopolymer composites." *Cement & Concrete Composites*, 37, 108-118.

Hildebrando, E. A., Souza, J. A., Angelica, R. S., and Neves, R. (2013). "Application of Bauxite Waste from Amazon Region in the Heavy Clay Industry." *Materials Research*.

Hirosue, H., Yamada, N., Abe, E., and Tateyama, H. (1988). "Coagulation of red mud suspension with an inorganic coagulant." *Powder Technology*, 54, 27-30.

Ho, G. E., Mathew, K., and Newman, P. W. G. (1989). "Leachate quality from gypsum neutralize red mud applied to sandy soil." *Water, Air, and Soil Pollution*, 47, 1-18.

Holubec, I., and Appolonia, E. D. (1973). "Effect of particle shape on engineering property of granular soil." *Evaluation of Relative Density and Its Role in Geotechnical Projects Involving Cohesionless Soils*, ASTM STP 523, 304-318.

Huang, W., Wang, S., Zhu, Z., Li, L., Yao, X., Rudolph, V., and Haghseresht, F. (2008). "Phosphate removal from wastewater using red mud." *Journal of Hazardous Materials*, 158, 35-42.

Imai, G. (1980). "Settling behavior of clay suspension." *Soils and Foundations*, 20 (2), 61-77.

Imai, G. (1981). "Experimental studies on sedimentation mechanism and sediment formation of clay materials." *Soils and Foundations*, 21 (1), 7-20.

Introduction to hazardous waste identification (2005), *Environmental Protection Agency*, 40 CFR, 261, United States.

Ippolito, , J. A., Redente, E. F., and Barbarick, K. A. (2005). "Amendment effects on pH

and salt content of bauxite residue. *Soil Science*, 170 (10), 832-841.

IRC 37 (2001). "Guidelines for the design of flexible pavements (second revision)." *The Insian Road Congress*, New Delhi.

IS 10500 (2012). "Indian standard for drinking water specification." *Bureau of Indian Standard*. New Delhi.

IS 1498 (1970). "Classification and identification of soils for general engineering purposes." *Bureau of Indian Standards*, New Delhi.

IS 383 (1970). "Specification for coarse and fine aggregates from natural sources for concrete." *Bureau of Indian Standard,* New Delhi.

IS 650 (1991). "Specification for standard sand for testing of cement." *Bureau of Indian Standards,* New Delhi.

Jaditager, M., and Sivakugan, N. (2017). "Influence of fly ash-based geopolymer binder on the sedimentation behavior of dredged mud." *Journal of Waterway, Port, Coastal, and Ocean Engineering*, 143 (5): 04017012.

Janoo, V. C. (1998). "Quantification of shape, angularity, and surface texture of base course materials." *CRREL Special Report No. 98-1,* Cold Regions Research and Engineering Laboratory, USA.

Jerves, A. X., Kawamoto., R. Y., and Andrade., J. E. (2016). "Effect of grain morphology on critical state: a computational analysis." *Acta Geotechnica*, 11, 493-503.

Johnston, M., Clark, M. W., McMahon, P., and Ward, N. (2010). "Alkalinity conversion of bauxite refinery residues by neutralization." *Journal of Hazardous Materials*, 182, 710-715.

Joshi, R. C., and Lohtia, R. P. (1997). "Fly ash in concrete, production, properties and uses." *Gordon and Breach Science*, Vol. 2, Amsterdam, The Netherlands.

Kalkan, E. (2006). "Utilization of red mud as a stabilization material for the preparation of clay liners." *Engineering Geology*, 87, 220-229.

Kani, E. N., Allahverdi, A., and Provis, J. L. (2012). "Efflorescence control in geopolymer binders based on natural pozzolan." *Cement and Concrete Composites*, 34, 25-33.

Kaya, K., and Soyer-Uzun, S. (2016). "Evolution of structural characteristics and compressive strength in red mud- metakaolin based geopolymer systems." *Ceramics International*, 42 (6), 7406-7413.

Kehagia, F. (2008). "An innovative geotechnical application of bauxite residue." *EJGE*, 13, 1-10.

Kehagia, F. (2014). "Construction of an unpaved road using industrial by-products (bauxite residue)." *WSEAS Transactions on Environment and Development*, 10, 160-168.

Khan, J., Amritphale, S. S., Chandra, N., and Patel, M. (2012). "A noble binder free and energy efficient process for making ceramic tiles using red mud and sericitic pyrophyllite." *Indian Journal of Chemical Technology*, 19, 420-426.

Klauber, C., Grafe, M., and Power, G. (2009). "Review of bauxite residue "Re-use" options." *CSIRO document DMR-3609*, Department of resources, energy and tourism, Australia.

Koloski, J. W., Schwarz, S. D., and Tubbs, D. W. (1989). "Geotechnical properties of geologic materials." *Engineering Geology in Washington*, Volume 1, Washington Division of Geology and Earth Resources Bulletin 78.

Komonweeraket, K., Cetin, B., Aydilek, A. H., Benson, C. H., and Edil, T. B. (2015). "Effect of pH on the leaching mechanisms of elements from fly ash mixed soils." *Fuel*, 140, 788-802.

Kosmulski, M., Gustafsson, J., and Rosenholm, J. B. (1999). "Correlation between the zeta potential and rheological property of anatas dispersions." *Journal of Colloid and Interface Science*, 209 (1), 200-206.

Kosugi, K. (1996). "Lognormal distribution model for unsaturated soil hydraulic properties." *Water Resource Research*, 32 (9), 2697-2703.

Koulikourdis, A., Paspatis, E., and Grigoropoulou, H. (2005). "Red mud residue application to soil." *Proceedings of the 9th International Conference on Environmental Science and Technology*, Rhodes Island, Greece.

Krishnaiah, S., and Singh, D. N. (2004). "A device for determination of thermal property." *Journal of Testing and Evaluation,* 32 (2), 1-6.

Krivenko, P., Kovalchuk, O., Pasko, A., Croymans, T., Hult, M., Lutter, G., Vandevenne, N., Schreurs, S., and Schroeyers, W. (2017). "Development of alkali activated cements and concrete mixture design with high volumes of red mud." *Construction and Building Materials*, 151, 819-826.

Kumar, A., and Kumar, S. (2013). "Development of paving blocks from synergistic use of red mud and fly ash using geopolymerization." *Construction and Building Materials*, 38, 865-871.

Kumar, R., Srivastave, J. P., and Premchand (1998). "Utilization of iron value of red mud for metallurgical application." *Environmental and Waste Management*, ISSN: 0971-9407, 108-119

Kynch, G.J. (1952). "A theory of sedimentation." *Transactions of the Faraday Society*, 48, 166-176.

Lemougna, P. N., Wang, K. T., Tang, Q, and Cui, X. M. (2017). "Study on the development of inorganic polymers from red mud and slag system: Application in mortar and lightweight materials" *Construction and Building Materials*, 156 (15), 486-495.

Li, G., and Zhao, X. (2003). "Properties of concrete incorporating fly ash and ground granulated blast-furnace slag." *Cement and Concrete Composites*, 25, 293-299.

Li, L. Y. (2001). "A study of iron mineral transformation to reduce red mud tailings." *Waste Management*, 21, 525-534.

Li, Y. (1998). "Properties of red mud tailings produced under varying process conditions." *Journal of Environmental Engineering*, 124 (3), 254-264.

Lindqvist, M. (2008). "Energy considerations in compressive and impact crushing of rock." *Minerals Engineering*, 21, 631-641.

Liu, D. Y., and Wu, C. S. (2012). "Stockpiling and comprehensive utilization of red mud research progress." *Materials*, 5, 1232-1246.

Liu, R. X., and Poon, C. S. (2016). "Effects of red mud on properties of self-compacting mortar." *Journal of Cleaner Production*, 135, (1), 1170-1178.

Liu, R. X., and Poon, C. S. (2016). "Utilization of red mud derived from bauxite in self-compacting concrete." *Journal of Cleaner Production,* 112 (1), 384-391.

Liu, W., Chen, X., Li, W., Yu, Y., and Yan, K. (2014). "Environmental assessment, management and utilization of red mud in China." *Journal of Cleaner Production*, 84, 606-610.

Liu, X., Zhang, N., Sun, H., Zhang, J., and Li, L. (2011). "Structural investigation relating to the cementitious activity of bauxite residue — Red mud." *Cement and Concrete Research*, 41, 847–853.

Liu, Y., Lin, C., and Wu, Y. (2007). "Characterization of red mud derived from a combined Bayer process and bauxite calcination method." *Journal of Hazardous Materials*, 146, 255-261.

Liu, Z., Cai, C. S., Liu, F., and Fan, F. (2016). "Feasibility study of loess stabilization with fly ash–based geopolymer." *Journal of Materials in Civil Engineering*, 28 (5), 04016003.

Lohr, S. L. (1999). Sampling: Dasign and analysis, Second ed., Cengage, Boston, USA.

Lombi, E., Hamon, R. E., Mcgrath, S. P., and ughlin, M. J. (2003). Lability of Cd, Cu, and Zn in polluted soils treated with lime, beringite, and red mud and identification of a non-labile colloidal fraction of metals using isotopic techniques." *Environmental Science and Technology*, 37, 979-984.

Lopez, E., Soto, B., Arias, M., Nunez, A., Rubinos, D., and Barral, M. T. (1998). "Adsorbent properties of red mud and its use for waste water treatment." *Water Research*, 32 (4), 1314-1322.

Luo, P., Zhao, Y., Zhang, B., Liu, J., Yang, Y., and Liu, J. (2010). "Study on the adsorption of Neutral Red from aqueous solution onto halloysite nanotubes." *Water Research*, 44, 1489-1497.

Manfroi, E. P., Cheriaf, M., and Rocha, J. C. (2014). "Microstructure, minerology and environmental evaluation of cementitious composites produced with red mud waste." *Construction and Building Materials*, 67, 29-36.

Marsalek, R. (2012). "Zeta potential – Application." *2nd International Conference on Environment and Industrial Innovation*, 35. IACSIT Press, Singapor.

Martinez, E. L. (2012). "Investigation of sedimentation behaviour of micro crystalline cellulose." *Master's Thesis*, Chalmers University of Technology, Sweden.

Mayes, W. M., Burke, I. T., Gomes, H. I., Anton, A. D., Molnar, M., Feigl, V., and Ujaczki, E. (2016). "Advance in understanding environmental risks of red mud after the Ajka spill, Hungary." *Journal of Sustainable Metallurgy*, 2, 332-343.

Mayes, W. M., Jarvis, A. P., Burke, I. T., Walton, M., and Gruiz, K. (2011). "Trace and rare earth element dispersal downstream of the Ajka red mud spill, Hungary." *Mine Water – Managing the Challenges*, IMWA 2011, Aachen, Germany, 29-34.

Mayes, W. M., Jarvis, A. P., Burke, I. T., Walton, M., Feigl, V., Klebercz, O., and Gruiz, K. (2011). "Dispersal and attenuation of trace contaminants downstream of the Ajka bauxite residue (red mud) depository failure, Hungary." *Environmental Science and Technology*, 45, 5147-5155.

McRoberts, E. C., and Nixon, J. F. (1976). "A theory of soil sedimentation." *Canadian Geotechnical Journal*, 13 (3), 294-310.

Meher, S. N. (2014). "Thermal analysis of NALCO red mud." *International Journal of Chemical Studied*, 1 (5), 1-9.

Menzies, N. W., Fulton, I. M., and Morrell, W. J. (2004). "Seawater neutralization of alkaline bauxite residue and implications for revegetation." *Journal of Environmental Quality*, 33 (5), 1877-1884.

Miao, S., Shen, Z., Wang, X., Luo, F., Huang, X., and Wei, C. (2017). "Stabilization of highly expansive black cotton soils by means of geopolymerization." *Journal of Materials in Civil Engineering*, 29 (10): 04017170.

Miners, K. (1973). "Alcan's experience of the disposal of red mud from the Bayer ore process, *Proc., 1st Int. Tailings Symposium,* San Francisco, 553–562.

Mirzababaei, M., Yasrobi, S., and Al-Rawas, A. (2009). "Effect of polymers on swelling potential of expensive soil." *Ground Improvement*, 162 (3), 111-119.

Mishra, B., Staley, A., and Kirkipatrick, D. (2002). "Recovery of value added products from red mud." *Minerals and Metallurgical Processing,* 19 (2), 87-94.

Mishra, P. N., Suman, S., and Das, S. K. (2016). "Experimental investigation and prediction models for thermal conductivity of biomodified buffer materials for hazardous waste disposal." *Journal of Hazardous, Toxic, and Radioactive Waste,* 21 (2): 04016011

Mitchell, J. K. (1956), "The fabric of natural clays and its relation to engineering properties." *Highway Research Board*, Washington, DC, Publication No. 426, 35, 693-713.

Molineux, C. J., Newport, D. J., Ayati, B., Wang, C., Connop, S. P., and Green, J. E. (2016). "Bauxite residue (red mud) as a pulverised fuel ash substitute in the manufacture of lightweight aggregate." *Journal of Cleaner Production*, 112 (1), 401-408.

Mora, C. F., and Kwan, A. K. H. (2000). "Sphericity, shape factor and convexity measurement of coarse aggregate for concrete using digital image processing." *Cement and Concrete Research*, 30 (3), 351-358.

Mymrin, V. A., and Vazauez-Vaamonde, A. J. (2001). "Red mud of aluminium production waste as basic component of new construction materials." *Waste Management & Research*, 19, 465-469.

Nadaroglu, H., Kalkan, E., Demir, N. (2010). "Removal of copper from aqueous solution using red mud." *Desalination*, 251, 90-95.

Nagela, E., and Schneider, U. (1989). "The zeta potential of blast furnace salg and fly ash." *Cement and Concrete Research,* 19 (5), 811-820.

Naidu, A. D., and Singh, D.N. (2004). "A generalized procedure for determining thermal resistivity of soils." *Int J Therm Sci.*, 43(1), 43–51.

Nanthagopalan, P., and Santhanam, M. (2011). "Fresh and hardened properties of self-compacting concrete produced with manufactured sand." *Cement and Concrete Composites,* 33, 353-358.

Nath, H., Sahoo, P. and Sahoo, A. (2015). "Characterization of red mud treated under high temperature fluidization." *Powder Technology*, 269, 233-239.

Negussey, D., Wijewickreme, W.K.D., Vaid, Y.P. (1988). "Contact volume friction angle of granular materials." *Canadian Geotechnical Journal,* 25(1), 50-55.

Newson, T., Dyer, T., Adam, C., and Sharp, S. (2006). "Effect of structure on geotechnical properties of bauxite residue." *Journal of Geotechnical and Geoenvironmental Engineering*, 132 (2), 143-151.

Nikbin, I. M., Aliaghazadeh, M., Charkhtab, S, and Fathollahpour, A. (2018). "Environmental impacts and mechanical properties of lightweight concrete containing bauxite residue (red mud)." *Journal of Cleaner Production*, 172, (20), 2683-2694.

Nikraz, H. R., Bodley, A. J., Cooling, D. J., Kong, P. Y. L., and Soomro, M. (2007). "Comparison of physical properties between treated and untreated bauxite residue mud." *J. Mater. Civ. Eng.*, 19 (1), 2-9.

Ouhadi, V. R., and Goodarzi, A. R. (2006). "Assessment of the stability of a dispersive soil treated by alum." *Engineering Geology*, 85, 91-101.

Padmakumar, G.P., Sriniva, K., Uday, K.V., Iyer, K.R., Pathak, P., Keshava, S.M., Singh, D.N. (2012). "Characterization of aeolian sand from Indian desert." *Engineering Geology*, 139-140, 38-49.

Palmer, S. J., and Frost, R. L. (2009). "Characterization of bauxite and seawater neutralized bauxite residue using XRD and vibrational spectroscopic techniques." *Journal of Materials Science*, 44 (1), 55-63.

Panda, I., Jain, S., Das, S. K., and Jayabalan, R. (2017). "Characterization of red mud as a structural fill and embankment material using bioremediation." *International Biodeterioration & Biodegradation*, 119, 368-376.

Paradis, M., Duchesne, J., Lamontagne, A., and Isabel, D. (2007). "Long-term neutralisation potential of red mud bauxite with brine amendment for the neutralisation of acidic minetailings." *Applied Geochemistry*, 22, 2326-2333.

Paramguru, R. K., Rath, P. C., and Misra, V. N. (2005). "Trends inredmudutilization - a review." *Mineral Processing and Extractive Metallurgy Review*, 26, 1-29.

Park, S. J., Seo, D. I., and Nah, C. (2002). "Effect of acidic surface treatment of red mud on mechanical interfacial properties of epoxy/red mud nanocomposites." *Journal of Colloid and Interface Science*, 251, 225-229.

Pera, J., Boumaza, R., Ambroise, J. (1997). "Development of a pozzolanic pigment from red mud." *Cement and Concrete Research,* 27(10), 1513-1522.

Persson, A. L. (1998). "Image analysis of shape and size of fine aggregates." *Engineering Geology*, 50, 177-186.

Phanikumar, B. R., and Sharma, R. S. (2007). "Volume change behavior of fly ash-stabilized clays." *Journal of Materials in Civil Engineering*, 19 (1), 67-74.

Pinnock, W.R., and Gordon, J.N. (1992), "Assessment of strength development in bayer process residues." *Journal of Materials Science,* 27, 692-696.

Pontikes, Y., and Angelopoulos, G. N. (2013). "Bauxite residue in cement and cementitious applications: Current status and a possible way forward." *Resources, Conservation and Recycling,* 73, 53-63.

Pontikes, Y., Nikolopoulos, P., and Angelopoulos, G. N. (2007). "Thermal behaviour of clay mixtures with bauxite residue for the production of heavy-clay ceramics." *Journal of the European Ceramic Society*, 27, 1645-1649.

Power, G., Grafe, M., and Klauber, C. (2009). "Review of current bauxite residue management, disposal and storage: Practices, engineering and science." *CSIRO Document,* DMR-3608, Australia.

Power, G., Grafe, M., Klauber, C. (2011). "Bauxite residue issues: I. current management, disposal and storage practices." *Hydrometallurgy,* 108(1), 33-45.

Pradhan, J., Das, J., Das, S., and Thakur, R. S. (1998). "Adsorption of phosphate from aqueous solution using activated red mud." *Journal of Colloid and Interface Science*, 204, 169-172.

Pratt, K. C., and Christoverson, V. (1981). "Hydrogenation of a model hydrogen-donor system using activated red mud catalyst." *Fuel*, 61,460-462.

Quina, M. J., Bordado, J. C. M., and Quinta-Ferreira, R. M. (2009). "The influence of pH on the leaching behavior of inorganic components from municipal solid waste APC residues." *Waste Management*, 29, 2483-2493.

Rai, S., Lataye, D. H., Chaddha, M. J., Mishra, R. S., Mahendiran, P., Mukhopadhayay, J., Yoo. C., and Wasewar, K. L. (2013). "An alternative to clay in building materials: red mud sintering using fly ash via Taguchi's methodology." *Advances in Materials Science and Engineering*, 2013, 1-7.

Rai, S., Wasewar, K. L., and Agnihotri, A. (2017). "Treatment of alumina refinery waste (red mud) through neutralization techniques-a review." *Waste management and Research*, 35 (6), 563-580.

Ribeiro, D. V., Labrincha, J. A., and Morelli, M. R. (2010). "Potential use of natural red mud as pozzolan in Portland cement." *Materials Research*, 14 (1), 60-66.

Ribeiro, D. V., Labrincha, J. A., and Morelli, M. R. (2010). "Use of red mud as addition for Portland cement mortars." *Journal of Materials Science and Engineering,* 4 (8), 1-8.

Rout, S. K., Sahoo, T., and Das, S. K. (2012). "Utility of red mud as an embankment material." *International Journal of Earth Science and Engineering*, 5 (6), 1645-1651.

Rout, S. K., Sahoo, T., and Das, S. K. (2013). "Design of tailing dam using red mud." *Central European Journal of Engineering*, 3 (2), 316-328.

Ruan, H. D., Frost, R. L., and Kloprogge, J. T. (2001). "The behavior of units of synthetic goethite and its dehydroxylated product hematite." *Spectrochimica Acta: Part A*, 57, 2575-2586.

Rubinos, D., Spagnoli, G., and Barral, M. T. (2013). "Assessment of bauxite refining residue (red mud) as a liner for waste disposal facilities." *International Journal of Mining, Reclamation and Environment*, 29 (6), 433-452.

Rubinos, D., Spagnoli, G., and Barral, M. T. (2016). "Chemical and environmental compatibility of red mud liners for hazardous waste containment." *International Journal of Environmental Science and Technology*, 13 (3), 773-792.

Sahu, R. C., Patel, R., and Ray, B. C. (2001). "Removal of hydrogen sulfide using red mud at ambient conditions." *Fuel Processing Technology*, 92, 1587-1592.

Sahu, R. C., Patel, R., and Ray, B. C. (2011). "Adsorption of Zn(II) on activated red mud: neutralized by CO_2." *Desalination*, 266, 93-97.

Sahu, R. C., Patel, R., Ray, B. C. (2010). "Neutralization of red mud using CO_2 sequestration cycle." *Journal of Hazardous Materials,* 179, 28–34.

Salehi, M. (2009). "Lime-clay modification and its application in the construction of man-made islands." *M. Sc. Thesis*, James Cook University, Townsville, QLD, Australia.

Samal, S., Ray, A. K., and Bandopadhyay, A. (2013). "Proposal for resources, utilization and processes of red mud in India — a review." *International Journal of Mineral Processing*, 118, 43-55.

Satayanarayana, P. V. V., Naidu, P. G., Adiseshu, S., and Rao, C. V. H. (2012). "Characterization of lime stabilized red mud mix for feasibility in road construction."

International Journal of Engineering Research and Development, 3 (7), 20-26.

Sglavo, V. M., Campostrini, R., Maurina, S., Carturan, G., Monagheddu, M., Budroni, G., and Cocco, G. (2000). "Bauxite 'red mud' in the ceramic industry. Part 1: Thermal behavior." *Journal of European Ceramic Society*, 20, 235-244.

Sglavo, V. M., Maurina, S., Conci, A., Salviati, A., and Cocco, G. (2000). "Bauxite `red mud' in the ceramic industry Part 2: production of clay-based ceramic." *Journal of the European Ceramic Society*, 20, 245-252.

Sharma, P. K., and Singh, T. N. (2008). "A correlation between P-wave velocity, impact strength index, slake durability index and uniaxial compressive strength." *Bulletin of Engineering Geology and the Environment*, 67, 17-22.

Shi, C., Xu, J., Beckman, E., and Enick, R. (2000). "Carbon dioxide sequestration via pH reduction of red mud using liquid CO_2." *ACS Division of Fuel Chemistry*, 45 (4), 703-705.

Singh, A.P., Singh, P.C., Singh, V.N. (1993"). "Cyclohexanethiol separation from kerosene oil by red mud." *J Chem Technol Biotechnology,* 56(2), 167-174.

Smiljanic, S., Smiciklas, I., Peric-Grujic, A., Loncar, B., and Mitric, M. (2010). "Rinsed and thermally treated red mud sorbents for aqueous Ni^{2+} ions." *Chemical Engineering Journal*, 162, 75-83.

Somogyi, F., and Gray, D. (1977). "Engineering properties affecting disposal of red mud." *Proc. Conf. on Geotechnical Practice for Disposal of Solid Waste Materials*, ACSE, 1-22.

SP 36 - Part 1 (1987). "Compendium of Indian standards on soil engineering." *Bureau of Indian Standards*, New Delhi.

Spagnoli, G., Rubinos, D., Stanjek, H., Fernandez-Steeger, T., Feinendegen, M., and Azzam, R., (2012). "Undrained shear strength of clays as modified by pH variations." *Bulletin of Engineering Geology and the Environment*, 71, 135–148.

Srikanth, S., Ray. A. K., Bandopadhyay, A., and Ravikumar, B. (2005). "Phase constitution during sintering of red mud and red mud–fly ash mixtures." *Journal of the American Ceramic Society*, 88 (9), 2396-2401.

Stark, N., Hay, A.E., Cheel, R., Lake, C.B. (2014). "The impact of particle shape on the angle of internal friction and the implications for sediment dynamics at a steep, mixed sand–gravel beach." *Earth Surf Dynam*, 2(2), 469-480.

Su, O., Toroglu, I, and Akcin, N. A. (2010). "An evaluation of the impact strength index as a criterion of grindability." *Energy Sources: Part A*, 32, 1671-1678.

Sundaram, R., and Gupta, S. (2010). "Constructing foundation on red mud." *Pro. of 6th International Congress on Environmental Geotechnics*, New Delhi, India.

Sutar, H., Mishra, S. C., Sahoo, S. K., Chakraverty, A. P., and Maharana, H. S. (2014). "Progress of red mud utilization: an overview." *American Chemical Science Journal*, 4 (3), 255-279.

Tong, L., Wang, Y.H. (2015). "DEM simulation of shear modulus and damping ratio of sand with emphasis on the effect of particle number, particle shape and aging." *Acta Geotechnica*, 10, 117-130.

Toraman, O. Y., Kahraman, S., and Cayirli, S. (2010). "Predicting the crushability of rocks from the impact strength index." *Minerals Engineering*, 23, 752-754.

Toth, P. S., Chan, H. T., and Cragg, C. B. (1988). "Coal ash as a structural fill with specific reference to Ontario experience." *Can. Geotech. Journal*, 25(4), 694-704.

Tsakiridis, P. E., Agatzini-Leonardou, S., and Oustadakis, P. (2004). "Red mud addition in the raw meal for the production of Portland cement clinker." *Journal of Hazardous Materials B*, 116, 103-110.

Tsamo, C., Parfait, Z. A., Kamga, R., Belibi, B. P. D., and Bikie-Mbah, J. B. (2014). "Preparation and characterization of red mud derived from Minim-Martap (Cameroon) bauxite." *International Journal of Research in Chemistry and Environment*, 4 (2), 153-160.

Vachon, P., Tyagi, R. D., Auclalr, J. C., Wllklnson, K. J. (1994). "Chemical and biological leaching of aluminum from red mud." *Environmental Science and Technology*, 28 (1), 26-30.

Vakili, A. H., Selamat, M. R., Aziz, H. B. A., Mojiri, A., Ahmad, Z., and Safarzadeh, M. (2017). "Treatment of dispersive clay soil by ZELIAC." *Geoderma*, 285, 270-279.

Vakili, A. H., Selamat, M. R., Moayedi, H., and Amani, H. (2013). "Stabilization of dispersive soils by pozzolan." *Sixth Congress on Forensic Engineering*, San Francisco, California, United States. 726-735.

van Genuchten, M. T. (1980). "A close-form equation for prediction of hydraulic conductivity of unsaturated soil." *Soil Science Society of America*, 44 (5), 892-898.

Vick, S. G. (1990). *Planning, design and analysis of tailings dams*, Wiley, New York.

Vogt, M. F. (1974). "Development studies on dewatering of red mud." *103rd Annual Meeting of AIME*, Dallas, Tex., 73-91.

Wadell, H. (1932). "Volume, shape and roundness of rock particles." *The Journal of Geology,* 40(5), 443-451.

Wang, P., and Liu, D. Y. (2012). "Physical and chemical properties of sintering red mud and Bayer red mud and the implications for beneficial utilization." *Materials*, 5, 1800-1810.

Wang, S., Ang, H. M., and Tade, M. O. (2008). "Novel applications of red mud as coagulant, adsorbent and catalyst for environmentally benign processes." *Chemosphere*, 72, 1621-1635.

Wang, S., Boyjoo, Y., Choueib, A., and Zhu, Z. H. (2005). "Removal of dyes from aqueous solution using fly ash and red mud." *Water Research*, 39, 129-138.

Westerholm, M., Lagerblad, B., Silfwerbrand, J., Forssberg, E. (2008). Influence of fine aggregate characteristics on the rheological properties of mortars. *Cement and Concrete Composites*, 30, 274-282.

Wnek, W. J. (1977). "An analysis of the dependence of the zeta potential and surface charge on surfactant concentration, ionic strength, and pH." *Journal of Colloid and Interface Science*, 60 (2), 361-375.

Wong, J. W. C., and Ho, G. E. (1991). "Effect of gypsum and sewage sludge amendment on physical property of fine bauxite refining residue." *Soil Science*, 152 (5). 326-332.

Wong, J. W. C., and Ho, G. E. (1993). "Use of waste gypsum in the revegetation on red mud deposits: a greenhouse study." *Waste Management and Research*, 11 (3). 249-256.

Woodard, H. J., Hossner, L., and Bush, J. (2008). "Ameliorating caustic properties of aluminum extraction residue to establish a vegetative cover." *Journal of Environment Science and Health*: *Part A*, 43 (10), 1157-1166.

Xenidis, A., Harokopou, A. D., Mylona, E., and Brofas, G. (2005). "Modifying alumina red mud to support a revegetation cover." *JOM*, 57 (2), 42-46.

Xue, S., Zhu, F., Kong, X., Wu, C., Huang, L., Huang, N., and Hartley, W. (2016). "A review of the characterization and revegetation of bauxite residues (Red mud)." *Environmental Science and Pollution Research*, 23 (2), 1120-1132.

Xue, S., Zhu, F., Kong, X., Wu, C., Huang, L., Huang, N., and Hartley, W. (2015). "A review of the characterization and revegetation of bauxite residues (red mud)." *Environmental Science and Pollution Research*, 23 (2), 1120-1132.

Yadav, V. S., Prasad, M., Khan, J., Amritphale, S. S., and Raju, C. B. (2010). "Sequestration of carbon dioxide (CO_2) using red mud." *Journal of Hazardous Materials*, 176, 1044-1050

Yalcin, N., and Sevinc, V. (2000). "Utilization of bauxite waste in ceramic glazes." *Ceramic International*, 26, 485-493.

Yang, J., and Xiao, B. (2008). "Development of unsintered construction materials from red mud wastes produced in the sintering alumina process." *Construction and Building Materials*, 22, 2299-2307.

Yang, J., and Xiao, B. (2008). "Development of unsintered construction materials from red mud wastes produced in the sintering alumina process." *Construction and Building Materials*, 22, 2299-2307.

Yang, X., Zhao, J., Li, H., Zhao, P., and Chen, Q. (2017). "Recycling red mud from the production of aluminium as a red cement-based mortar." *Waste Management & Research*, 35 (5), 500-507.

Yang, Y., Wen, Q., and Hu, L. (2012). "Experimental study on application of industrial waste in landfill liner." *GeoCongress 2012*, ASCE, 3881-3890.

Yao, Y., Li, Y., Liu, X., Jiang, S., Feng, C., and Rafanan, E. (2013). "Characterization on a cementitious material composed of red mud and coal industry byproducts." *Construction and Building Materials,* 47, 496-501.

Ye, N., Yang, J., Liang, S., Hu, Y., Hu, J., Xiao, B., and Huang, Q. (2016). "Synthesis and strength optimization of one-part geopolymer based on red mud." *Construction and Building Materials*, 111, 317-325.

Yi, Y., Li, C., and Liu, S. (2015). "Alkali-activated ground-granulated blast furnace slag for stabilization of marine soft clay." *Journal of Materials in Civil Engineering*, 27 (4), 04014146.

Yousuf, M., Mollah, A., Vempati, R. K., Lin, T. C., Cocke, D. L. (1995). "The interfacial chemistry of solidification/stabilization of materials in cement and pozzolanic material systems." *Waste Management*, 15 (2), 137-148.

Yudhbir, Rahim, A. (1991). "Quantification of particle shape and angularity using the image analyser." *Geotechnical Testing Journal*, GTJODJ, 14(3), 296-308.

Yue, Q., Zhao, Y., Li, Q., Li, W., Gao, B., Han, S., Qi, Y., and Yu, H. (2010). "Research on the characteristics of red mud granular adsorbents (RMGA) for phosphate removal." *Journal of Hazardous Materials*, 176, 741-748.

Yukselen, Y., and Kaya, A. (2003). "Zeta potential of kaolinite in the presence of alkali, alkaline earth and hydrolysable metal ions." *Water, Air and Soil Pollution*, 145, 155-168.

Zhang, K., Hu, H., Zhang, L., and Chen, Q. (2008). "Surface charge properties of red mud particles generated from Chinese diaspore bauxite." *Transaction of Nonferrous Metals Society of China*, 18, 1285-1289.

Zhang, M., Zhao, M., Zhang, G., Mann, D., Lumsden, K., and Tao, M. (2016) "Durability of red mud-fly ash based geopolymer and leaching behavior of heavy metals in sulfuric acid solutions and deionized water." *Construction and Building Materials*, 124, 373-382.

Zhang, N., Sun, H., Liu, X., and Zhang, J. (2009). "Early-age characteristics of red mud–coal gangue cementitious material." *Journal of Hazardous Materials*, 167, 927-932.

Zhao, Y., Wang, J., Luan, Z., Peng, X., Liang, Z., and Shi, L. (2009). "Removal of phosphate from aqueous solution by red mud using a factorial design." *Journal of Hazardous Materials*, 165, 1193-1199.

Zhihua, P., Dongxu, L., Jian, Y., and Nanru, Y. (2003). "Properties and microstructure of the hardened alkali-activated red mud–slag cementitious material." *Cement and Concrete Research*, 33, 1437-1441.

Zhuang, L., Nakata, Y., Kim, U.G., and Kim, D. (2014). "Influence of relative density, particle shape, and stress path on the plane strain compression behaviour of granular materials." *Acta Geotechnica*. 9, 241-255.

Dissemination

Peer Reviewed Journals:

1. **Shamshad Alam**, Sarat Kumar Das, and B. Hanumantha Rao (2017). "Characterization of coarse fraction of red mud as a civil engineering construction material." *Journal of Cleaner Production*, 168, 679-691. **SCI- IF 5.715**

2. **Shamshad Alam,** Bijaya Kumar Das, and Sarat Kumar Das (2018). "Dispersion and Sedimentation Characteristics of Red Mud" *Journal of Hazardous, Toxic, and Radioactive Waste*, ASCE, 22(4). doi:10.1061/(ASCE)HZ.2153-5515.0000420

3. Sarat Kumar Das, Subrat Kumar Rout, and **Shamshad Alam** (2015). "NITR Compactor – A laboratory vibratory compactor for compaction of granular soil." *Journal of Indian Highway*, 43 (10), 27-31.

4. **Shamshad Alam**, Sarat Kumar Das, and B. Hanumantha Rao. "Strength and durability characteristic of alkali activated GGBS stabilized red mud as geo-material." *Construction and Building Materials*. (Under Review).

5. Anshumali Mishra, **Shamshad Alam**, and Sarat Das. "Sulphate resistant mortar using coarse fraction of red mud." *Advances in Civil Engineering Materials*. (Under Review).

6. **Shamshad Alam**, Sarat Kumar Das, and B. Hanumantha Rao. "Geotechnical Characterization of Two Indian Red Mud." (Under preparation)

Conference Papers:

1. **Shamshad Alam**, Sarat Kumar Das, B. Hanumantha Rao, "Stabilization of Red Mud Using Low Ash Coal Fly Ash", Indian Geotechnical Conference, December 2017, Guwahati, India.

2. **Shamshad Alam**, Sarat Kumar Das, B. Hanumantha Rao, "Hydraulic Characteristics of Red Mud", Indian Young Geotechnical Engineering Conference 2017, NIT Trichy, India.

3. **Shamshad Alam**, Sarat Kumar Das, B. Hanumantha Rao, "Particle Shape Analysis of Coarse Fraction of Red Mud as Construction Materials", Compendium of TRB Annual Meeting, January 8-12, 2017, US.

4. Sarat Kumar Das, Subrat Rout, **Shamshad Alam**, "Characterization of Red Mud as a Subgrade Construction Materials", 3rd CTRG, 2015, Kolkata, India.